Characterization of the *Legionella pneumophila* GDSL hydrolases PlaA and PlaD regarding enzymatic activity and modulation of host cell signaling

Von der Fakultät für Lebenswissenschaften

der Technischen Universität Carolo-Wilhelmina zu Braunschweig

zur Erlangung des Grades einer

Doktorin der Naturwissenschaften

(Dr. rer. nat.)

genehmigte

D i s s e r t a t i o n

von Miriam Hiller

aus Göttingen

1. Referentin: Prof. Dr. Antje Flieger
2. Referent: Prof. Dr. Michael Steinert
eingereicht am: 25.09.2019
mündliche Prüfung (Disputation) am: 17.04.2020

Druckjahr 2021

Vorveröffentlichungen der Dissertation

Teilergebnisse aus dieser Arbeit wurden mit Genehmigung der Fakultät für Lebenswissenschaften, vertreten durch die Mentorin der Arbeit, in folgenden Beiträgen vorab veröffentlicht:

Publikationen

Lang, C.*, Hiller, M.*, Flieger, A., 2017. Disulfide loop cleavage of Legionella pneumophila PlaA boosts lysophospholipase A activity. Sci. Rep. 7, 16313.
** equal contribution*

Hiller, M., Lang, C., Michel, W., Flieger, A., 2018. Secreted phospholipases of the lung pathogen Legionella pneumophila. Int. J. Med. Microbiol. 308, 168-175

Tagungsbeiträge

Hiller, M., Lang, C., Flieger, A., 2017. Characterization of the Legionella pneumophila GDSL hydrolases and their impact on host pathogen interaction. Vortrag 3. Diplomanden- und Doktorandentreffen des Robert Koch-Instituts, Wernigerode.

Hiller, M., Lang, C., Flieger, A., 2018. Impact of the L. pneumophila GDSL hydrolases on host pathogen interaction. Vortrag 20. Tagung der Fachgruppen Mikrobielle Pathogenität und Gastrointestinale Infektionen, Bad Urach.

Posterbeiträge

Hiller, M., Lang, C., Becher, D., Hilbi, H., Flieger, A., 2015. Impact of *Legionella pneumophila* phospholipases A on modification of phagosomal membranes. Poster 13. Diplomanden- und Doktorandentreffen des Robert Koch-Instituts, Wernigerode.

Hiller, M., Lang, C., Flieger, A., 2016. Impact of Legionella pneumophila phospholipases A on modification of phagosomal membranes. Poster 25. 68. Jahrestagung der Deutschen Gesellschaft für Hygiene und Mikrobiologie, Ulm.

Hiller, M., Lang, C., Flieger, A., 2016. Impact of Legionella pneumophila phospholipases A on modification of phagosomal membranes. Poster. International Symposium on Legionella, Braunschweig.

Hiller, M., Lang, C., Flieger, A., 2016. Impact of *Legionella* phospholipases A on modification of phagosomal membranes. Poster 10. Diplomanden- und Doktorandentreffen des Robert Koch-Instituts, Berlin.

Hiller, M., Lang, C., Hilbi, H., Flieger, A., 2017. Characterization of phospholipase activity and secretion pathway of Legionella pneumophila GDSL hydrolases and their impact on LCV lipids. Poster 16. International Conference on Intracellular Niches of Pathogens, Glashütten.

Hiller, M., Lang, C., Flieger, A., 2017. Disulfide loop cleavage of Legionella pneumophila PlaA boosts lysophospholipase A but diminishes glycerophospholipid cholesterol acyltransferase activity. Poster 3. The 9th International Conference on Legionella, Rom.

Hiller, M., Lang, C., Flieger, A., 2017. The GDSL hydrolase PlaD is a Dot/Icm secreted effector of Legionella pneumophila and confers high toxicity to eukaryotic cells. Poster 12. The 9th International Conference on Legionella, Rom.

Hiller, M., Lang, C., Döllinger, J., Flieger, A., 2018. The Legionella pneumophila GDSL hydrolase PlaD: a novel T4SS-secreted effector with anti-apoptotic characteristics? Poster 5. Diplomanden- und Doktorandentreffen des Robert Koch-Instituts, Berlin.

Hiller, M., Lang, C., Döllinger, J., Flieger, A., 2019. Characterization of the Legionella pneumophila GDSL hydrolase PlaD. Poster 79. 71. Jahrestagung der Deutschen Gesellschaft für Hygiene und Mikrobiologie, Göttingen.

Summary

The facultative intracellular bacterium *Legionella pneumophila* is the causative agent for Legionnaires' disease, a potentially fatal pneumonia. The bacterium is ubiquitous in aqueous habitats where it exists as planktonic form, as part of multispecies biofilms or inside protozoa which are the natural host for *L. pneumophila*. Infections of humans occur in response to the inhalation of contaminated aerosols. Then, *L. pneumophila* replicates mainly inside alveolar macrophages. *L. pneumophila* avoids degradation inside the host cell and instead replicates in a specialized phagosome termed *Legionella* containing vacuole. During infection, *L. pneumophila* secretes a multitude of proteins via its type II and type IVB secretion systems (T4BSS). Among others, multiple phospholipases are secreted. In total, *L. pneumophila* possesses 19 phospholipases which are divided into 15 phospholipases A, 3 phospholipases C and 1 phospholipase D. The phospholipases A are further divided into the patatin-like proteins, the PlaB-like proteins and the GDSL hydrolases.

The aim of this thesis was the characterization of two *L. pneumophila* GDSL hydrolases, namely PlaA and PlaD, with regard to their enzymatic activity and activation mechanisms as well as the analysis of the interactions of PlaD with host cell proteins and signaling. To this end, *L. pneumophila plaA*$^{-}$ and *plaD*$^{-}$ mutants were analyzed in infection assays and purified recombinant proteins were used for investigation of lipolytic enzyme activity and determination of protein structure. Moreover, translocation assays and interaction studies were performed for the characterization of PlaD.

It was demonstrated that PlaA exhibits strong lysophospholipase A activity and is processed by the *L. pneumophila* zinc metalloproteinase ProA within a disulfide loop in the C-terminal half of the protein which even increases the lysophospholipase A activity of PlaA. Additionally, unprocessed PlaA shows glycerophospholipid:cholesterol acyltransferase activity which is diminished upon processing by ProA. In contrast, only minor activity was detected for PlaD. Instead, it was shown that, during infection, PlaD is Dot/Icm-dependently injected into the host cell cytoplasm where it interacts with the regulatory 14-3-3 proteins. Thus, PlaD was described as a novel T4BSS dependent effector protein of *L. pneumophila*. Moreover, it was found that PlaD is involved in the inhibition of host cell apoptosis upon *L. pneumophila* infection.

The generated data lead to the hypothesis that the lysophospholipase A activity of PlaA might be directed towards the membrane of the *Legionella* containing vacuole and might thus be important for the exit from the host cell. It is suspected that PlaD would have to be activated by a so far unidentified activator to develop its full activity. Additionally, it is assumed that PlaD functions to modulate the host immune response during infection.

Zusammenfassung

Legionella pneumophila ist ein fakultativ intrazelluläres Bakterium und Ursache der Legionärskrankheit, einer potentiell tödlichen Pneumonie. Der Erreger kommt ubiquitär in wässrigen Habitaten vor und existiert als planktonische Form, als Teil von Biofilmen oder intrazellulär in Protozoen, dem natürlichen Wirt für *L. pneumophila*. Menschen können durch das Inhalieren kontaminierter Aerosole infiziert werden. In dem Fall repliziert *L. pneumophila* hauptsächlich in Alveolarmakrophagen. *L. pneumophila* entgeht der Degradation innerhalb der Wirtszelle und repliziert stattdessen innerhalb eines spezialisierten Phagosoms, welches „*Legionella* containing vacuole“ genannt wird. Während der Infektion sekretiert *L. pneumophila* eine Vielzahl an Proteinen über Typ II und Typ IVB Sekretionssystem (T4BSS). Unter anderem werden auch Phospholipasen sekretiert. Insgesamt besitzt *L. pneumophila* 19 Phospholipasen, welche sich in 15 Phospholipasen A, 3 Phospholipasen C und 1 Phospholipase D untergliedern. Die Phospholipasen A werden zusätzlich in die „Patatin-like proteins“, „die PlaB-like proteins“ und die „GDSL Hydrolasen“ eingeteilt.

Das Ziel dieser Arbeit war die Charakterisierung der beiden GDSL Hydrolasen PlaA und PlaD hinsichtlich ihrer enzymatischen Aktivitäten und Aktivierungsmechanismen sowie die Untersuchung von PlaD hinsichtlich Interaktionen mit Proteinen und der Immunantwort des Wirts. Hierzu wurden Infektionsassays mit *L. pneumophila plaA*$^{-}$ und *plaD*$^{-}$ Mutanten durchgeführt und aufgereinigtes rekombinantes Protein auf lipolytische Aktivität analysiert sowie zur Bestimmung der Proteinstruktur verwendet. Außerdem wurden für PlaD Translokationsassays und Interaktionsstudien durchgeführt.

Es wurde gezeigt, dass PlaA starke Lysophospholipase A (LPLA) Aktivität aufweist und innerhalb eines Disulfidloops in der C-terminalen Hälfte des Proteins durch die *L. pneumophila* Zink Metalloproteinase ProA prozessiert wird, was die LPLA Aktivität zusätzlich steigert. Unprozessiertes PlaA zeigt zudem Glycerophospholipid:Cholesterol Acyltransferase Aktivität, welche durch die Prozessierung verschwindet. Im Gegensatz dazu konnte für PlaD nur sehr geringe Aktivität detektiert werden. Stattdessen wurde gezeigt, dass PlaD Dot/Icm-abhängig in das Zytoplasma der Wirtszelle injiziert wird und mit den regulatorischen 14-3-3 Proteinen interagiert. PlaD konnte somit als neuer T4BSS abhängiger Effektor von *L. pneumophila* beschrieben werden. Darüber hinaus wurde gezeigt, dass PlaD, während einer *L. pneumophila* Infektion, die Apoptose der Wirtszelle inhibiert.

Die Daten haben zu der Hypothese geführt, dass die Lysophospholipase A Aktivität von PlaA gegen die Membran der „*Legionella* containing vacuole“ gerichtet und somit wichtig für das Verlassen der Wirtszelle sein könnte. Es wird vermutet, dass ein bisher nicht identifizierter Aktivator notwendig ist, um die volle Aktivität von PlaD zu entwickeln. Außerdem wird angenommen, dass die Funktion von PlaD währen einer *L. pneumophila* Infektion in der Modulation der Immunantwort des Wirts liegt.

Index

Index of tables

Index of figures

Abbreviations

°C	Degree Celsius
µM	Micromolar
Amp^R	Ampicillin resistance
APS	Ammonium peroxodisulfate
CFU	Colony forming units
Cm^R	Chloramphenicol resistance
CR1	Complement receptor 1
CR3	Complement receptor 3
DAG	Diacylglycerol
DNA	Deoxyribonucleic acid
Dot	Defective in organelle trafficking
ER	Endoplasmic reticulum
FCS	Fetal calf serum
FFA	Free fatty acids
FRET	Förster resonance energy transfer
GCAT	Glycerophospholipid:cholesterol acyltransferase
$Gent^R$	Gentamicin resistance
h	Hours
Hyg^R	Hygromycin resistance
Icm	Intracellular multiplication
IL	Interleukin
kDa	kilo Dalton
Km^R	Kanamycin resistance
LCV	*Legionella* containing vacuole
LPC	Lysophosphatidylcholine
LPG	Lysophosphatidylglycerol
LPLA	Lysophospholipase A
LPS	Lipopolysaccharide
M	Molar
min	Minutes
Mip	Macrophage infectivity potentiator
mM	Millimolar
MOI	Multiplicity of infection

MOMP	Major outer membrane protein
MPG	1-monoacylglycerol
PA	Phosphatidic acid
PAMP	Pathogen associated molecular pattern
PC	Phosphatidylcholine
PCR	Polymerase chain reaction
PG	Phosphatidylglycerol
PI	Phosphatidylinositol
PI(3)P	Phosphatidylinositol 3-phosphate
$PI(3,4)P_2$	Phosphatidylinositol 3,4-bisphosphate
$PI(3,4,5)P_3$	Phosphatidylinositol 3,4,5-trisphosphate
$PI(3,5)P_2$	Phosphatidylinositol 3,5-bisphosphate
PI(4)P	Phosphatidylinositol 4-phosphate
$PI(4,5)P_2$	Phosphatidylinositol 4,5-bisphosphate
PI(5)P	Phosphatidylinositol 5-phosphate
PI4KIIIβ	Phosphatidylinositol 4 kinase III β
PIPs	Phosphatidylinositol phosphates
PKB	Protein kinase B
PLA	Phospholipase A
PLB	Phospholipase B
PLC	Phospholipase C
PLD	Phospholipase D
PS	Phosphatidylserine
rcf	Relative centrifugal force
s	Seconds
SDS	Sodium dodecyl sulfate
SDS-PAGE	Sodium dodecyl sulfate polyacrylamide gel electrophoresis
T2SS	Type II secretion system
T3SS	Type III secretion system
T4BSS	Type IVB secretion system

1 Introduction

1.1 *Legionella pneumophila* – the causative agent of Legionnaires' disease

1.1.1 Epidemiology of Legionnaires' disease

Legionella pneumophila is a gram negative, facultative intracellular bacterium that is responsible for a severe and potentially fatal pneumonia termed Legionnaires' disease (Hilbi et al., 2010). Legionnaires' disease is characterized by high fever, cough, shortness of breath, muscle aches and headaches and has an incubation period of 2-10 days with mortality rates ranging from 7 to 24 % in industrialized countries (Beauté et al., 2013; Cunha et al., 2016; Fields et al., 2002; Marion et al., 2016). Additionally, infection with *L. pneumophila* can result in Pontiac fever which has similar but milder, more flu-like symptoms and a shorter incubation period (Ambrose et al., 2014). In rare cases, an infection with Legionellae can manifest outside of the respiratory tract and cause meningoencephalitis, rhabdomyolysis, acute renal failure and endocarditis (Grun et al., 2019; Laivier et al., 2019; Tompkins et al., 1988; Young et al., 2019). However, *L. pneumophila* is an opportunistic pathogen that is adapted to protozoan hosts and does not have mechanisms to efficiently avoid the immune response in healthy individuals. Thus, the susceptible population for infection with *L. pneumophila* consists of immunocompromised, elderly and patients with chronic lung disease. Additionally, male gender, heavy smoking and alcohol abuse have been reported as risk factors (Abu Khweek and Amer, 2010; Cunha et al., 2016). Humans usually are dead-end hosts for *L. pneumophila* and so far only one case of human-to-human transmission has been described (Correia et al., 2016).

L. pneumophila was first discovered after a large outbreak following the 58th Annual Convention of the American Legion in Philadelphia in 1976. At that time, 182 persons attending the convention fell ill with pneumonia leading to 147 cases of hospitalization and 29 deaths (Fraser et al., 1977). Since then, control measures and monitoring of water sources have been implemented. In Germany, the "German drinking water ordinance" defines a technical measures trigger value of 100 colony forming units (CFU) per 100 ml for the presence of Legionellae in water. Surpassing of this threshold has to be notified to the local health authorities (TrinkwV, 2018). However, in spite of the effort, sporadic cases and outbreaks of Legionnaires' disease occur. Up to now, the largest outbreak of Legionnaires' disease in Germany was in the summer of 2013 in Warstein with 78 confirmed cases (RKI, 2013). In Germany, cases of Legionnaires' disease need to be notified to the Robert Koch-Institut and in 2017 and 2018 the numbers of reported cases were 1282 and 1444 respectively (RKI, 2018, 2019a). The corresponding incidence for 2017 was 1.6 per 100000 inhabitants in Germany. For the whole of Europe, incidences varied between 1 and 3 per 100000 inhabitants per country. Overall, an increase

in the number of reported Legionnaires' disease cases from almost 6000 in 2013 to more than 9000 in 2017 is observed in Europe (ECDC, 2019; RKI, 2019b). Moreover, in the United States, *Legionella spp.* is described as the most common cause for outbreaks of waterborne diseases (Hamilton et al., 2019).

1.1.2 *Legionella pneumophila* thrives in aqueous habitats and uses amino acids as main carbon source

More than 58 *Legionella* species with at least 79 serogroups have been described and all of them should be classified as potentially pathogenic to humans. However, only 20 *Legionella* species have been shown to be associated with human disease (Cunha et al., 2016; Oliva et al., 2018). Among those, *L. pneumophila* serogroup 1 is responsible for approximately 85 % of Legionnaires' disease cases worldwide (Bangsborg, 1997; RKI, 2019b).

L. pneumophila occurs in freshwater environments or human-made water systems where it exists as planktonic form, as part of multispecies biofilms or inside amoebae and other protozoa which are the natural host for this bacterium (Figure 1A) (Hilbi et al., 2011a; Steinert et al., 2002). Existence inside host cells protects *L. pneumophila* from environmental stress factors such as temperature and climate changes or disinfection measures. Moreover, amoebae serve as vectors which facilitate the spread of *L. pneumophila* and even increase its virulence and invasiveness due to the increased expression of virulence factors (Cirillo et al., 1994). Additionally, amoebae present a nutrient-rich environment for the replication of *L. pneumophila* which requires amino acids as main carbon source (Newton et al., 2010). Under laboratory conditions *L. pneumophila* is grown in broth containing yeast extract which serves as source for amino acids. Agar plates for cultivation of *L. pneumophila* are additionally supplemented with activated charcoal due to the bacterium's sensitivity towards reactive oxygen species (Feeley et al., 1979; Warren and Miller, 1979). *L. pneumophila* tolerates temperatures ranging from 25 to 42 °C but replication is most efficient at approximately 35 °C. Apart from amoebae, *L. pneumophila* may infect humans when contaminated aerosols are inhaled. *L. pneumophila* then replicates mainly in alveolar macrophages (Horwitz and Silverstein, 1980; Rowbotham, 1986). Both amoebae and human cell lines are applied for *in vitro* infection experiments. A common animal model for infection with *L. pneumophila* is the guinea pig. The guinea pig is characterized by susceptibility to *L. pneumophila* and a pathology that is comparable to that observed during human infections (Padilla-Carlin et al., 2008). In contrast, most, but not all, mouse strains restrict intracellular replication of *L. pneumophila* (Abu Khweek and Amer, 2010; Horwitz and Silverstein, 1980). Nevertheless, mouse models for *L. pneumophila* infection exist. For example the

mouse strains BALBc and A/J have been found to be susceptible towards *L. pneumophila* infection (Brieland et al., 1994; Losick et al., 2009).

1.1.3 *Legionella pneumophila* replicates in a specialized phagosome termed *Legionella* containing vacuole

Being a facultative intracellular bacterium *L. pneumophila* does exist as planktonic form. However, replication occurs exclusively inside host cells (Horwitz and Silverstein, 1980; Oliva et al., 2018; Rowbotham, 1986). Thus, *L. pneumophila* exerts a biphasic life cycle (Molofsky and Swanson, 2004). Planktonic bacteria represent the transmissive form of *L. pneumophila* which is flagellated and appears as rod-shaped cells. Transmissive *L. pneumophila* is characterized by motility, increased cytotoxicity, invasiveness and acid resistance. The switch to the replicative form is triggered by invasion of host cells and is accompanied by morphogenic and metabolic changes. Intracellular, replicative *L. pneumophila* is non-motile due to the absence of flagella and appears as long filamentous rods (Albert-Weissenberger et al., 2007; Allombert et al., 2013; Aurass et al., 2016; Bruggemann et al., 2006; Weissenmayer et al., 2011). Depletion of nutrients at late stages of replication triggers a stringent response in *L. pneumophila* resulting in the generation of the second messenger ppGpp which induces the transition to the transmissive form (Dalebroux et al., 2010; Hammer and Swanson, 1999). This is accompanied by an increased expression of virulence traits associated with motility, cytotoxicity, resistance to osmotic shock and sensitivity towards sodium (Byrne and Swanson, 1998). That way the exit of *L. pneumophila* from the host cell is triggered resulting in the initiation of a new infection cycle. This biphasic life cycle can also be observed in broth cultures of *L. pneumophila* (Figure 1B). There, the replicative phase can be observed during exponential growth while the transmissive phase corresponds to the post-exponential growth phase (Albert-Weissenberger et al., 2007; Allombert et al., 2013; Bruggemann et al., 2006).

The intracellular replication process of *L. pneumophila* in protozoa and human cells is very similar (Figure 1A). Bacteria attach to the surface of host cells and are internalized by conventional or coiling phagocytosis (Bozue and Johnson, 1996; Escoll et al., 2013; Kwaik, 1996). This is mediated by attachment via proteins located in the outer membrane of *L. pneumophila* and by complement receptors 1 (CR1) and 3 (CR3) in human cells (Payne and Horwitz, 1987; Shevchuk et al., 2011; Vogel and Isberg, 1999). Subsequently, *L. pneumophila* blocks maturation of the phagosome by avoiding acidification as well as interactions with endosomes and lysosomes (Horwitz and Maxfield, 1984). Instead, the recruitment of ER-derived vesicles, ribosomes and mitochondria to the phagosome is induced during the first four hours of infection. This process is mainly triggered by the secretion of effector proteins via the Dot/Icm type IV B secretion system (T4BSS) into the host cell cytoplasm

(Allombert et al., 2013). Moreover, an accumulation of phosphatidylinositol 4-phosphate (PI(4)P) on the cytoplasmic side of the phagosome is observed (Weber et al., 2018; Weber et al., 2014; Weber et al., 2006). Thus, a nutrient-rich replicative niche for *L. pneumophila* is established which is designated as *Legionella* containing vacuole (LCV) (Allombert et al., 2013). New data suggest that the LCV membrane becomes semipermeable approximately 6 h post infection. Notably, this was only observed in amoebae and human but not in murine cells (Truchan et al., 2017). Usually a 50-100 fold replication of *L. pneumophila* is observed after 24 h of infection followed by exit from the host cell and the start of a new infection cycle (Molmeret and Kwaik, 2002). It was shown that *L. pneumophila* exits host cells either via non-lytic exocytosis or via a pore-forming activity (Flieger et al., 2018).

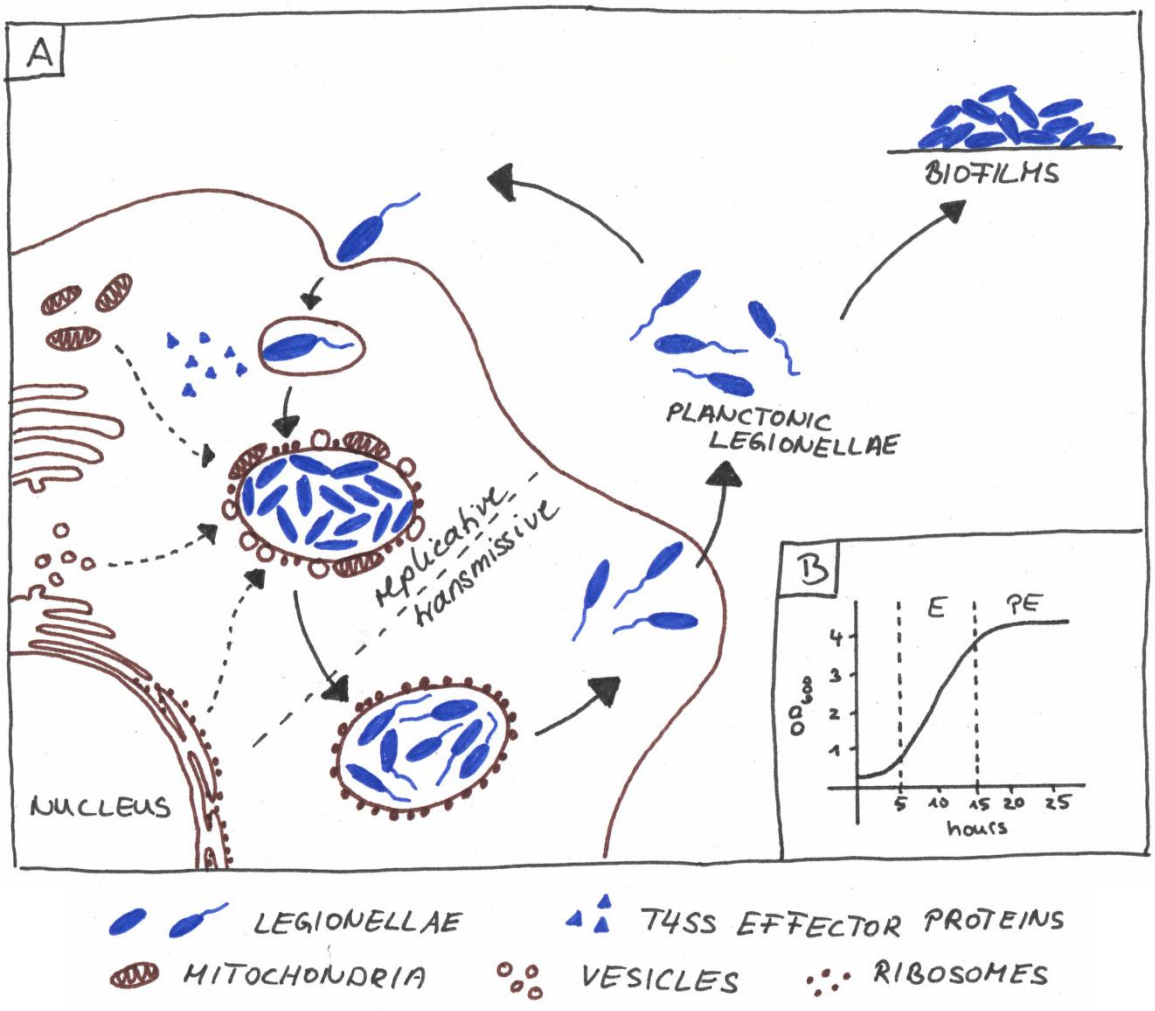

Figure 1: Schematic illustration of the biphasic life cycle of *L. pneumophila*.
(A) *L. pneumophila* occurs as planktonic form, in multispecies biofilms or inside host cells where it switches between replicative and transmissive phase. Legionellae and T4BSS effector proteins are depicted in blue while organelles of the host cell are depicted in brown. Continuous arrows indicate the transition between *L. pneumophila* morphological states during the biphasic life cycle. Dashed arrows indicate the recruitment of host cell organelles to the LCV. The biphasic life cycle of *L. pneumophila* during host infections ***(A)*** corresponds to the exponential (E) and post-exponential (PE) growth phases in liquid cultures of *L. pneumophila* ***(B)***.

1.1.4 *Legionella pneumophila* virulence factors and secretion systems

L. pneumophila expresses a multitude of virulence factors that contribute to infection of amoebae and mammalian cells. These include enzymes and toxins which are amongst others involved in adherence, motility, nutrient acquisition and evasion of host immune responses. A key feature of many *L. pneumophila* virulence factors is molecular mimicry. On the one hand *L. pneumophila* proteins may contain individual domains that are mostly found in eukaryotic proteins. On the other hand *L. pneumophila* expresses so-called eukaryotic like factors that resemble eukaryotic proteins. These proteins are secreted virulence factors of *L. pneumophila* and enable the subversion of host cell pathways to the benefit of the pathogen (Allombert et al., 2013; Gomez-Valero et al., 2011). Due to the huge number of virulence factors, a lot of redundancy is observed. Thus, the knock-out of single virulence factors often does not result in a phenotype. This redundancy might actually be accounted for by the adaptation to the various hosts of *L. pneumophila* (Ghosh and O'Connor, 2017). Moreover, a study by D'Auria et al. from 2010 revealed that some virulence factors of *L. pneumophila* are strain specific and are in part encoded in the accessory genome (D'Auria et al., 2010). As virulence factors need to interact directly with the host cell they are either surface-exposed or secreted. In the following, *L. pneumophila* virulence factors that are surface-exposed, secreted via the type II secretion system (T2SS) or the T4BSS will be discussed. Among others, phospholipases are important virulence factors of *L. pneumophila*. A total of 19 phospholipases has been described for *L. pneumophila* (Hiller et al., 2018). Due to the focus of this thesis, the phospholipases of *L. pneumophila* will be discussed in detail in a separate chapter.

1.1.4.1 Surface-exposed virulence factors mediate attachment and uptake of *Legionella pneumophila*

Virulence factors exposed on the surface of *L. pneumophila* may be implicated in attachment and adherence and trigger uptake by the host cell. The 25 kDa major outer membrane protein (MOMP), a porin, interacts with components of the complement system and thus mediates the uptake of *L. pneumophila* via CR1 and CR3 (Bellinger-Kawahara and Horwitz, 1990). Moreover, MOMP was shown to be essential for virulence of *L. pneumophila* (Krinos et al., 1999). Proteins of the T4BSS are also found in the outer membrane of *L. pneumophila* and contribute to virulence. The type IV pili composed of PilD and PilE proteins are involved in attachment to host cells and mediate natural competence (Stone and Abu Kwaik, 1998; Stone and Kwaik, 1999). Moreover, they promote biofilm formation. Lack of PilD has been associated with impaired intracellular replication. The macrophage infectivity potentiator (Mip), a peptidyl-prolyl *cis/trans* isomerase, is necessary for intracellular survival of *L. pneumophila*. It was shown that mutation of the mip gene attenuates virulence of

L. pneumophila (Cianciotto et al., 1990). Additionally, the PLA PlaB is attached to the outer membrane of *L. pneumophila* but its role in infection has not yet been elucidated completely (Hiller et al., 2018).

1.1.4.2 The Lsp type II secretion system and secreted virulence factors

The T2SS of *L. pneumophila* is considered a major virulence factor as T2SS-mutants show a defect in intracellular replication in both amoebae and mammalian cells (Cianciotto, 2005). In contrast, the T2SS does not affect invasion of host cells or avoidance of lysosomal degradation. However, secretion via the T2SS contributes to evasion of the host immune response (Hales and Shuman, 1999).

Only recently, the *in situ* structure of the *L. pneumophila* Lsp T2SS was published (Ghosal et al., 2019). The Lsp T2SS of *L. pneumophila* is encoded by 12 genes which are located on five different genomic regions. These 12 core components are assembled into an inner membrane platform (LspCFLM) which recruits an ATPase (LspE), an inner membrane prepilin-peptidase/methyltransferase (LspO/PilD), a periplasmic pilus-like structure (LspG and LspHIJK) and the outer membrane-spanning secretin (LspD). The pre-pseudopilins (LspG and LspHIJK) are processed by LspO/PilD prior to assembly of the pilus-like structure in the periplasm. Apart from type II secretion LspO/PilD is also involved in formation of type IV pili. Secretion via the T2SS occurs in two steps and requires an N-terminal signal sequence for translocation across the inner membrane via Tat or Sec. Within the periplasm, secreted proteins are processed, recognized by the T2SS and pushed through the secretin LspD in the outer membrane with the help of the pilus-like structure. The energy required for this process is generated at the inner membrane by the ATPase LspE (Cianciotto, 2009).

The biochemical activities that are exported by T2SS in *L. pneumophila* comprise phosphatase, phospho- and lysophospholipase, lipase, protease, RNase and chitinase activity. At least 27 proteins are secreted via the T2SS of *L. pneumophila* but not all of them have been fully characterized yet (Cianciotto, 2009). Commonly it was acknowledged that proteins secreted via the T2SS are located inside the LCV lumen. However, as mentioned above, a permeabliziation of the LCV membrane starting approximately 6 h post infection was shown. This enables the release of T2SS proteins into the host cell cytoplasm (Truchan et al., 2017). One of the most abundant proteins secreted via the T2SS is the zinc metalloproteinase ProA which is, due to its abundance, sometimes also referred to as major secretory protein Msp (Szeto and Shuman, 1990). This 38 kDa protein mediates the extracellular proteolytic activity of *L. pneumophila*. The main targets of ProA are casein, gelatin,

collagen and human serum proteins. Additionally, it was shown that ProA processes the equally T2SS secreted *L. pneumophila* PLAs PlaA and PlaC (Lang et al., 2017; Lang et al., 2012). Apart from the PLAs the phospholipases C (PLC) PlcA and PlcB are also secreted from *L. pneumophila* via the T2SS (Aragon et al., 2002; Aurass et al., 2013; Rossier and Cianciotto, 2005). Moreover, at least two phosphatases are found in the culture supernatant of *L. pneumophila*. The most abundant is the major acid phosphatase (Map) which confers the main phosphatase activity. However, activity of Map is not essential for intracellular replication within amoebae or mammalian cells. It is speculated that lack of Map may be compensated by other secreted phosphatases with minor activities (Aragon et al., 2001).

1.1.4.3 The Dot/Icm type IVB secretion system and injected effector proteins

The T4BSS of *L. pneumophila* was discovered by the Isberg and the Shuman laboratories in parallel and its components were designated as “defective in organelle trafficking” (Dot) and “intracellular multiplication” (Icm) respectively. Thus, the T4BSS is commonly designated Dot/Icm. Mutants of *L. pneumophila* with an impaired T4BSS are unable to interfere with the endocytic pathway of the host cell and intracellular replication is restricted (Segal et al., 1998; Vogel et al., 1998).

The highly conserved T4BSS is encoded by 27 genes which are located on two genomic regions. These 27 components are divided into 22 structural proteins and 5 chaperones. The main pore of the T4BSS is formed by DotC, DotD, DotF, DotG and DotH. DotC, DotD and DotH are located in the outer bacterial membrane while DotF and DotG form a stalk in the periplasmic space (Voth et al., 2012). The location of the T4BSS is restricted to the poles of *L. pneumophila* (Jeong et al., 2017). In 2017 the *in situ* structure of the T4BSS was resolved which confirmed its localization near the bacterial poles (Ghosal et al., 2017).

L. pneumophila secretes a multitude of more than 300 effector proteins via the T4BSS (Ensminger and Isberg, 2009). It was found that many effector proteins contain a translocation signal containing hydrophobic amino acids and such with small side chains close to the proteins C-terminus (Kubori et al., 2008; Nagai et al., 2005b). Due to the nature of the secretion system these effector proteins are directly injected into the host cell cytoplasm. However, some effector proteins are anchored to the cytoplasmic side of the LCV membrane via binding to PI(4)P (Ragaz et al., 2008). Moreover, many effector proteins show homology to or interact with host proteins. That way *L. pneumophila* is able to modify host metabolism and signaling pathways (Hayek et al., 2019; Weber and Faris, 2018). For example, the effector proteins SdcA, SidC and SidJ are anchored to the LCV membrane and are involved in the recruitment of ER-dervied vesicles to the LCV. The protein SdhA is essential for

intracellular replication of *L. pneumophila* and maintenance of LCV integrity. Moreover, several phospholipases are injected into the host cell cytoplasm via the T4BSS. These are primarily involved in the modulation of host phospholipids (Hiller et al., 2018). The huge number of effector proteins results in redundancy and thus complicates the identification of their functions. However, this diversity may also account for the adaptation of *L. pneumophila* to its various hosts (Ghosh and O'Connor, 2017).

1.2 Phospholipases are important virulence factors

1.2.1 Phospholipids are a major constituent of lipid membranes

Cell membranes are dynamic structures that represent the barrier of and between cells and are essential for compartmentalization within individual cells. The main structural components of pro- and eukaryotic cell membranes are phospholipids. These are composed of a glycerol backbone to which generally two fatty acids and a polar head group are attached. The combination of the hydrophobic diacylglycerol (DAG) and the polar head group is the cause for the amphipathic nature of phospholipids. This results in the spontaneous organization into lipid bilayers. Moreover, phospholipids may assemble into monolayers leading to the formation of micelles. The formation of micelles is among others utilized during *in vitro* assays for the determination of lipolytic enzyme activity. The attached fatty acids may be either saturated or unsaturated and vary in length. Common head groups of phospholipids are choline, ethanolamine, serine and inositol. The majority of phospholipids in eukaryotic membranes contain choline as a head group (Lordan et al., 2017; van Meer et al., 2008) which occurs also in the membranes of a subset of intracellular bacteria, among others *L. pneumophila* (Sohlenkamp and Geiger, 2016). Apart from phospholipids, eukaryotic cell membranes contain sphingolipids and cholesterol which are especially enriched in plasma membranes. They contribute to stability and help resist mechanical stresses (Lordan et al., 2017). Moreover, sphingolipids and sterols often cluster together forming lipid rafts which in cooperation with attached proteins are thought to act as platforms for signal transduction (Levental and Veatch, 2016; Simons and Van Meer, 1988).

1.2.2 Phospholipases and their activities divide into four classes according to their activities

Phospholipases and their respective activities are classified into the four categories PLA, phospholipases B (PLB), PLC and phospholipases D (PLD) (Schmiel and Miller, 1999).

PLAs are further subclassified as PLA_1 and PLA_2 which hydrolyze phospholipids either at the sn-1 or sn-2 position of the glycerol backbone respectively. Cleavage by PLAs results in the release of single free fatty acids (FFA). The remaining lipid is designated as lysophospholipid. For example, cleavage of phosphatidylcholine (PC) by a PLA results in the generation of lysophosphatidylcholine (LPC) and one FFA (Schmiel and Miller, 1999). LPC may cause permeabilization of cell membranes and loss of endothelial barrier function. Moreover, the induction of oxidant and chemokine production, such as monocyte chemoattractant protein-1 and Interleukin (IL) -8, was shown (Hollie et al., 2014; Leung et al., 1998; Mehta, 2005; Murugesan et al., 2003; Takeshita et al., 2000). The remaining acyl chain of LPC may then be cleaved off by a lysophospholipase A (LPLA) producing an FFA and glycerophosphocholine (Schmiel and Miller, 1999). Depending on the nature of the acyl chain, the released FFA may act as second messenger in signaling pathways. Arachidonic acid, for example, is an important inflammatory intermediate which is ultimately converted into eicosanoids, leukotrienes and prostaglandins (Funk, 2001; Saliba et al., 2005).

PLBs cleave off both acyl chains of a phospholipid simultaneously releasing two FFA at the same time. In fact, the cleavage products of PLBs are the same as those of PLAs except for the intermediate lysophospholipid (Schmiel and Miller, 1999).

PLCs and PLDs both hydrolyze the phosphodiester bond of a phospholipid and are thus also termed phosphodiesterases. Cleavage of phospholipids, e.g. phosphatidylinositol (PI), by PLCs results in the release of the second messengers 1,2-diacylglycerol and inositol trisphosphate which activate protein kinase C and induce the opening of Ca^{2+} channels respectively (Schmiel and Miller, 1999).

Cleavage by PLDs releases the polar head group of the phospholipid and generates phosphatidic acid (PA) or lysophosphatidic acid (LPA) which are both important signaling molecules and involved in modulation of membrane curvature promoting fusion and fission of membrane vesicles (Schmiel and Miller, 1999). Moreover, LPA has high affinity towards G-protein coupled receptors and stimulates cell proliferation (Lin et al., 2010).

In addition to the described activities some phospholipases are able to transfer fatty acids from phospholipids to cholesterol or ergosterol which is designated as glycerophospholipid:cholesterol acyltransferase (GCAT) activity and results in the formation of cholesterol or ergosterol esters (Akoh et al., 2004; MacIntyre et al., 1979; Upton and Buckley, 1995).

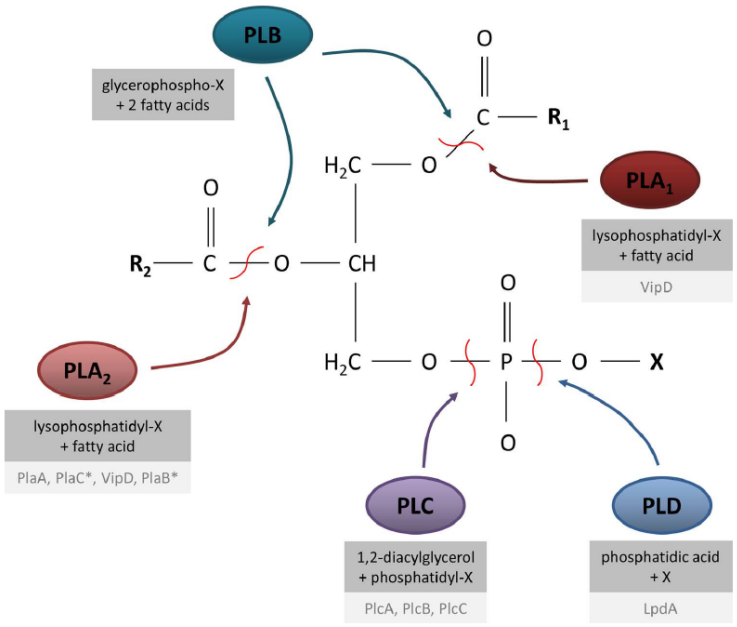

Figure 2: Schematic overview of phospholipase cleavage sites within phospholipids. Depicted is a phospholipid backbone where R_1 and R_2 denote long chain fatty acid residues and X denotes the phospholipid head group. Dark grey boxes show the reaction products of the respective phospholipases and light grey boxes show *L. pneumophila* phospholipases that comprise the respective activity. * PlaB and PlaC may also be classified as PLB as they show both PLA and LPLA activity (Hiller et al., 2018).

1.2.3 Examples for bacterial virulence-associated phospholipases A

Many pathogenic bacteria express a variety of phospholipase genes that contribute to their virulence (Flores-Diaz et al., 2016). Mostly, these phospholipases are secreted or injected into the host cell or are presented on the surface of the pathogen to maximize their impact on the host cell. Examples for secreted phospholipases are SseJ from *Salmonella enterica* spp. *enterica* serovar Typhimurium and ExoU from *Pseudomonas aeruginosa* (Miao and Miller, 2000). A surface-attached phospholipase is the *L. pneumophila* PLA PlaB (Schunder et al., 2010).

SseJ is one of many virulence factors of *S. enterica* spp. *enterica* serovar Typhimurium that is injected into the host cell cytoplasm via a type III secretion system (Miao and Miller, 2000). The protein belongs to the family of GDSL hydrolases, which will be discussed in more detail below, and shows deacetylase, phospholipase and GCAT activity (Lossi et al., 2008; Upton and Buckley, 1995). SseJ is involved in the modification of the *Salmonella* containing vacuole membrane and promotes its destabilization in the absence of the stabilizing factor SifA (Ruiz-Albert et al., 2002). Moreover, impaired replication in macrophages and attenuated virulence in mice was described for *sseJ*-deficient mutants (Freeman et al., 2003; Lawley et al., 2006; Ohlson et al., 2005).

The *P. aeruginosa* cytotoxin ExoU is also secreted via a type III secretion system and is injected into the cytoplasm of inflammatory cells which enables *P. aeruginosa* to persist and replicate (Diaz and Hauser, 2010; Diaz et al., 2008). The protein belongs to the patatin-like proteins and shows PLA and LPLA activities (Rahme et al., 2000; Sato and Frank, 2004). Mutants lacking ExoU are characterized by

diminished virulence and are cleared faster in experimental models of acute pneumonia (Allewelt et al., 2000; Diaz et al., 2008; Machado et al., 2010).

The only described surface-exposed phospholipase of *L. pneumophila* is the PLA PlaB. Although it was shown that PlaB is attached to the outer membrane of *L. pneumophila,* the transport mechanism was not established yet (Schunder et al., 2010). This enzyme comprises a unique embedding of the active center and is highly active towards phospho- and lysophospholipids including strong hemolytic activity. Importantly, its activity is approximately 100-fold higher than that of other secreted *L. pneumophila* phospholipases (Flieger et al., 2004; Schunder et al., 2010). Additionally, PlaB promotes virulence in the guinea pig infection model (Schunder et al., 2010). Interestingly it was shown that the activity of PlaB is inhibited by multimerization (Kuhle et al., 2014).

1.2.4 *Legionella pneumophila* possesses a multitude of phospholipases

So far, 19 phospholipases divided into 15 PLAs, three PLCs, and one PLD have been identified within the genome *L. pneumophila* (Figure 3) (Hiller et al., 2018). Many, but not all of them have been characterized by now.

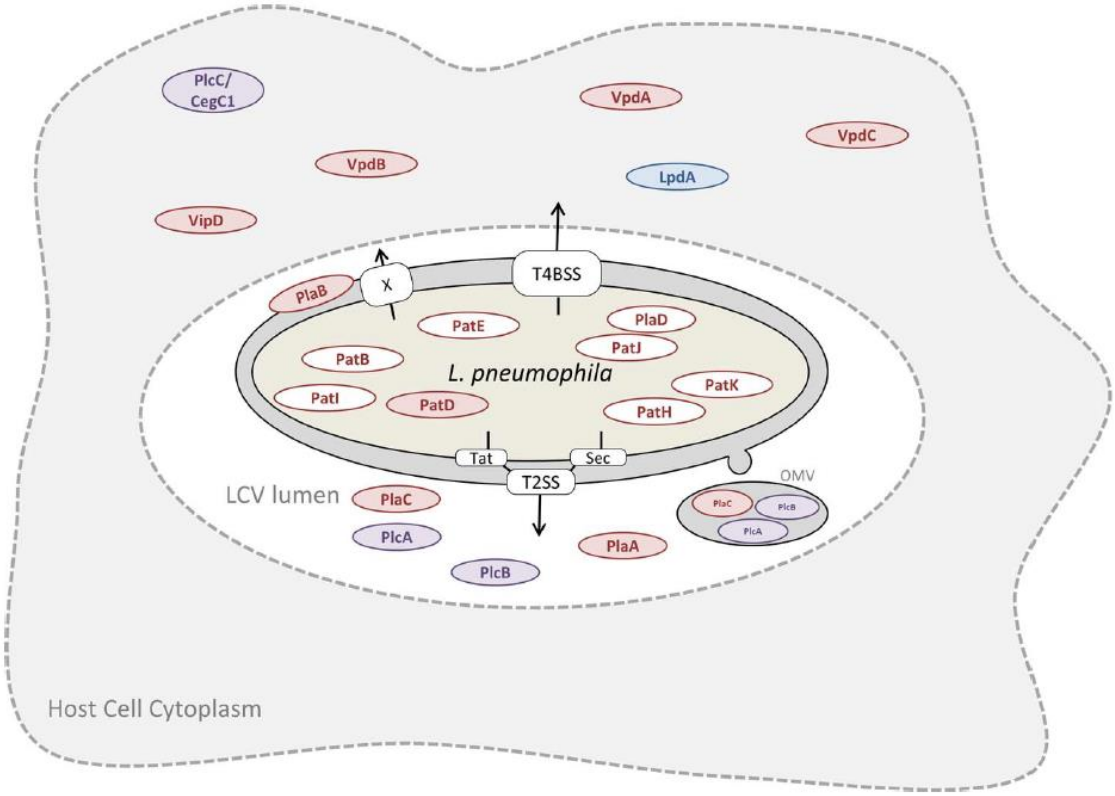

Figure 3: Schematic overview of the *L. pneumophila* phospholipases and their mode of secretion.
Proteins are colorcoded according to the phospholipase classes to which they belong. PLAs are shown in red, PLCs ind purple and the PLD in blue. Unfilled circles represent uncharacterized enzymes (Hiller et al., 2018).

The phospholipases A additionally divide into three families namely the GDSL hydrolases, the PlaB-like phospholipases and the patatin-like proteins. The family of GDSL hydrolases contains three members, namely PlaA, PlaC and PlaD and will be described in detail in the next chapter as the characterization of PlaA and PlaD was the aim of this thesis. The only member of the family of PlaB-like phospholipases is the above described virulence factor PlaB (Flieger et al., 2004). The patatin-like proteins contain mostly 11 different proteins which are named PatA/VipD, PatB, PatC/VpdA, PatD, PatE, PatF/VpdC, PatG/VpdB and PatH to PatK (Aurass et al., 2013; Shohdy et al., 2005; VanRheenen et al., 2006). Interestingly, the strains *L. pneumophila* Corby and Lens encode only for ten patatin-like proteins and lack PatA/VipD. PatA/VipD, as well as its homologues (PatC/VpdA, PatF/VpdC and PatG/VpdB), is injected into the host cell cytoplasm via the T4BSS (Ku et al., 2012; Shohdy et al., 2005; VanRheenen et al., 2006). There, PatA/VipD interferes with the endosomal trafficking. Interestingly, this process is independent of the N-terminal half of the protein which contains the catalytic patatin domain (Shohdy et al., 2005). Interestingly, neither PatA/VipD nor its paralogs PatC/VpdA, PatF/VpdC and PatG/VpdB seem to be essential for infection with *L. pneumophila* but their deletion increases replication inside *Dictyostelium discoideum* (VanRheenen et al., 2006).

The three members of the *L. pneumophila* PLCs are PlcA, PlcB and PlcC/CegC1. PlcA and PlcB are secreted via the T2SS and are thus present in the supernatant of liquid cultures as well as inside the LCV during infection with *L. pneumophila* (Aragon et al., 2002; Aurass et al., 2013; Rossier and Cianciotto, 2005). Recombinant PlcA shows weak PLC activity while none has been described for PlcB. However, the enzymatic activity is increased or activated by the addition of supernatant from *L. pneumophila* liquid cultures (Aragon et al., 2002; Aurass et al., 2013; Flieger et al., 2000c; Rossier and Cianciotto, 2005). In contrast, PlcC is injected into the host cell cytoplasm via the T4BSS and ectopic expression in yeast cells was shown to cause growth defects. Recombinant PlcC exhibits PLC activity which is further increased by the addition of Zn^{2+} (Aurass et al., 2013). Although neither of the described PLCs is essential for intracellular replication of *L. pneumophila* in *Acanthamoeba castellanii* or U937 macrophages the three enzymes together are indispensable for killing of *G. mellonella* larvae (Aurass et al., 2013).

The only described PLD of Legionellae is LpdA which is found exclusively in *L. pneumophila* (Gomez-Valero et al., 2011; Viner et al., 2012; Zhu et al., 2011). LpdA is post-translationally palmitoylated and injected into the host cell cytoplasm where it attaches to the surface of the LCV as well as to Rab4 and Rab14 positive vesicles. LpdA has been shown to contribute to virulence of *L. pneumophila* in A/J mice. It is involved in the interruption of the Golgi apparatus and hydrolyzes PI, phosphatidylinositol 3-phosphate (PI(3)P), PI(4)P and phosphatidylglycerol (PG) (Schroeder et al., 2015; Viner et al., 2012).

1.2.4.1 GDSL hydrolases

The GDSL hydrolases have been first described by Upton and Buckley as a new family of lipolytic enzymes in 1995 (Upton and Buckley, 1995). The activities described for GDSL hydrolases range from protease to arylesterase to PLA/LPLA and GCAT activity. Generally, GDSL hydrolases are characterized by a flexible active site that adapts its conformation to the presented substrates which results in a broad substrate specificity of these enzymes (Akoh et al., 2004; Upton and Buckley, 1995). Most lipases contain a catalytic active site that consists of Ser, His and Asp/Glu. Such a catalytic triad is also found in the GDSL hydrolases but the consensus sequences and the localization within the protein are different from other lipases. Commonly, the active site Ser is present in a Gly-X-Ser-X-Gly motif which is located in the middle of the protein sequence at the turn between a β-sheet and an α-helix thus creating a nucleophilic elbow (Rubin, 1994). In contrast, the active site Ser of the GDSL hydrolases is present in a Gly-Asp-Ser-Leu motif that is located closer to the N-terminus of the protein. Moreover, no nucleophilic elbow is formed in the GDSL hydrolases. In sum, the GDSL hydrolases contain five highly conserved amino acid sequence blocks that are distributed over the complete protein sequence. The GDSL motif with the active site Ser is located within the first block while His and Asp are located in block five (Akoh et al., 2004; Upton and Buckley, 1995).

The family of GDSL hydrolases can be found both in bacteria and plants. A typical example of a bacterial GDSL hydrolase is the LPS-activated GCAT lipase SatA of *Aeromonas salmonicida* which in addition to GCAT shows PLA, LPLA and lipase activities. SatA is an important virulence factor and is T2SS secreted (Buckley et al., 1982; Salte et al., 1992; Vanden Bergh and Frey, 2014). Other examples are SseJ from *Salmonella enterica* spp. *enterica* serovar Typhimurium which has been described above and the esterase EstA from *Pseudomonas aeruginosa*. The latter is autotransported into the bacterial outer membrane where it is involved in production of rhamnolipids and biofilm formation (Tielen et al., 2010; Wilhelm et al., 2007). In 2010 the crystal structure of EstA has been published (van den Berg, 2010).

1.2.4.2 What was known about PlaA, PlaC and PlaD before this thesis?

L. pneumophila possesses three GDSL hydrolases which are designated PlaA, PlaC and PlaD. PlaA was originally discovered as the protein responsible for a secreted PLA/LPLA activity of *L. pneumophila* by fractionation via anion exchange chromatography and biochemical characterization of *L. pneumophila* culture supernatants (Flieger et al., 2001b; Flieger et al., 2002). That activity was detected from mid-exponential phase on and is most prominent in late-logarithmic phase (Flieger et

al., 2001a). It was shown that the secreted PLA destroys phospholipids from alveolar surfactant resulting in the generation of FFA and highly cytotoxic LPC indicating that the *L. pneumophila* PLA might contribute to pathogenesis during pneumonia. However, it was also found that the generated LPC was detoxified by the *L. pneumophila* PLA (Flieger et al., 2000b; Flieger et al., 2002).

Early studies indicated already that *L. pneumophila* expresses multiple enzymes with PLA activities as independent protein peaks showed activity towards phospholipids after fractionation of culture supernatant (Flieger et al., 2001b). Later, BLAST analyses revealed two homologues of PlaA within *L. pneumophila* which were designated as PlaC and PlaD (Banerji et al., 2008; Banerji et al., 2005). Sequence analyses of all three proteins revealed that they contain the five conserved sequence blocks that are typical for the GDSL hydrolases (Figure 4A) (Lang et al., 2012). Moreover it was obvious that the three enzymes had distinct sizes. The calculated molecular weights for PlaA, PlaC and PlaD were 34.4, 49.7 and 59.6 kDa respectively. For both PlaA and PlaC a disulfide loop within the C-terminal part of the protein was predicted which was absent in PlaD. Moreover, for PlaA and PlaC, an N-terminal signal peptide for secretion via the Sec-system was predicted indicating secretion over the T2SS. No signal peptide was predicted for PlaD. In contrast, the sequence of PlaD contains an approximately 170 amino acids long extension of the C-terminus after the homology block five (Lang et al., 2017; Lang et al., 2012).

A

organism	name		block I		block II		block III		block IV		block V	
Aeromonas salmonicida	SatA	27	IVMF**GDSL**SDTG	37	LTIANEAEGGAT	37	VILWVGANDYL	26	NGAKQILLFNLPD	128	FW**D**QV**H**PT	24
Legionella pneumophila	PlaA	23	IVVF**GDSL**SDNG	41	SHLLDYAFGGAG	34	FVIWIGANNYL	26	KGAKHILVLNLPD	104	FF**D**LV**H**PT	25
Legionella pneumophila	PlaC	30	IVVF**GDSL**SDNG	108	EVYLNKAFGGSW	53	YFIYSGSNDYI	34	AGARRFVIMGIPH	123	FW**D**EI**H**PT	30
Legionella pneumophila	PlaD	10	LVVL**GDSL**SDRG	98	RFARFYCEGGLT	49	VVEWSGANDLI	78	KYKELGIPVNLSV	53	FW**D**DV**H**PT	170

B

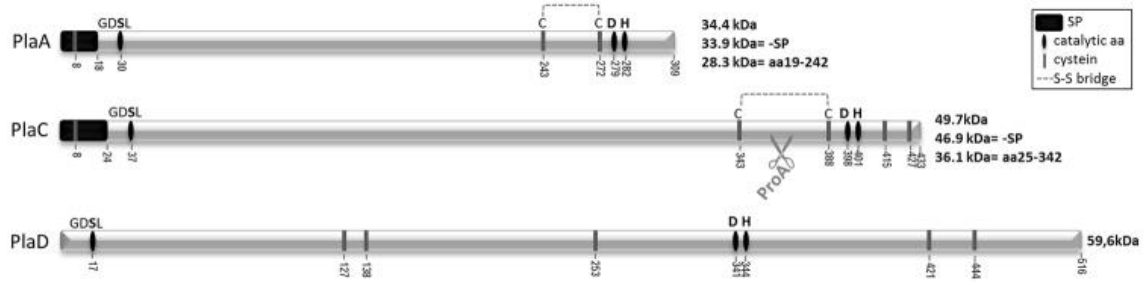

Figure 4: The *L. pneumophila* GDSL hydrolases PlaA, PlaC and PlaD.
Schematic overview of conserved amino acid sequences (A) and 1D protein structures (B) of *L. pneumophila* GDSL hydrolases. Numbers denote amino acid positions (Lang et al., 2017; Lang et al., 2012).

1.2.4.2.1 PlaA

PlaA is detected in the culture supernatant of *L. pneumophila*. In contrast, the protein is absent in the culture supernatant of an *lspDE*$^{-}$ mutant which has an impaired T2SS demonstrating the secretion of PlaA via the T2SS. PlaA is detected as a 25 kDa protein band in Western blots of *L. pneumophila*

culture supernatants although its predicted molecular weight is 34.4 kDa. However, in Western blots of culture supernatants from an *L. pneumophila proA*$^-$ mutant PlaA is detected at the predicted molecular weight of approximately 35 kDa. Thus, a proteolytic processing of PlaA by the zinc metalloproteinase ProA was assumed (Flieger et al., 2001b; Flieger et al., 2002; Lang et al., 2017). However, the mechanism and effect of ProA processing of PlaA have not been elucidated in detail yet.

As described above, PlaA is the major secreted LPLA of *L. pneumophila* and is thus responsible for the major portion of the LPLA activity detected in culture supernatants of *L. pneumophila* (Flieger et al., 2000a; Flieger et al., 2002). Accordingly, LPLA activity of culture supernatants obtained from an *L. pneumophila plaA*$^-$ mutant was reduced considerably. However, the deletion of PlaA had no effect on the PLA activity of *L. pneumophila* culture supernatant. Interestingly, GCAT activity towards LPC was only detected in *L. pneumophila plaA*$^-$ but not in the wild type strain (Lang et al., 2017).

The *L. pneumophila plaA*$^-$ mutant did not show any defects in intracellular replication in U937 macrophages and *Hartmanella vermiformis* amoebae. Thus it was assumed that PlaA is dispensable for intracellular infections (Flieger et al., 2002). However, most interestingly, during intracellular infections with *L. pneumophila*, PlaA induces destabilization of the LCV membrane in the absence of the T4BSS secreted effector SdhA (Creasey and Isberg, 2012).

1.2.4.2.2 PlaC

Similar to PlaA, its paralog PlaC was shown to be secreted via the T2SS of *L. pneumophila* as it can be detected via Western blot in the culture supernatants of *L. pneumophila* wild type but not in the T2SS-deficient *lspDE*$^-$ mutant (Banerji et al., 2005; Lang et al., 2012). Additionally, the size of the protein band detected in Western blots is approximately 10 kDa smaller than the predicted molecular weight of 49.7 kDa. Comparable to PlaA, a protein band of the size of the predicted molecular weight was detected in Western blots performed with culture supernatants from an *L. pneumophila proA*$^-$ mutant. Taken together, PlaC is secreted into the culture supernatant via the T2SS and proteolytically processed by the zinc metalloproteinase ProA (Lang et al., 2017; Lang et al., 2012).

PlaC was detected as homologue of PlaA (Banerji et al., 2005). However, only minor LPLA activity has been described for PlaC. In contrast, PlaC showed PLA and GCAT activity. Experiments with recombinant PlaC expressed ectopically in *E. coli* confirmed its PLA and GCAT activity towards the phospholipids PG and PC. GCAT activity was detected only towards PG and PC in the presence of

cholesterol but not ergosterol. Interestingly, PLA and GCAT activity in the presence of cholesterol were increased by the addition of the zinc metalloproteinase ProA. Moreover, ProA induced the GCAT activity of PlaC in the presence of ergosterol. From that it was assumed that PlaC needs to be processed proteolytically by ProA in order to display its complete activity (Banerji et al., 2005; Lang et al., 2012). This was supported by the fact that elimination of the disulfide bond essential for the disulfide loop diminished PlaC activity. In contrast, deletion of the stretch of amino acids inside the disulfide loop resulted in increased PLA and GCAT activity which was comparable to ProA-activated PlaC. Further investigations revealed that ProA indeed cleaves PlaC within the disulfide loop in the C-terminal part of the protein. Importantly, no unique cleavage site for ProA was identified. Instead it was assumed that ProA might recognize the loop structure within the C-terminal part of PlaC (Lang et al., 2012).

In 2006 Brüggemann et al. pointed out that expression of *plaC* was not altered significantly between replicative and transmissive growth phase. These data were obtained from *A. castellanii* amoebae that were infected with *L. pneumophila* strain Paris, Lens or Philadelphia for 14 h (Bruggemann et al., 2006). Moreover, it was shown that PlaC is dispensable for intracellular replication within *A. castellanii* and U937 macrophages during infections (Banerji et al., 2005). However, new data, obtained using *L. pneumophila* strain 130b, indicate that the expression level of *plaC* is elevated after infection of *A. castellanii* for 44 h (White et al., 2018). Interestingly, deletion of *plaC* resulted in increased expression levels of the amino peptidases *lapA* and *lapB* while deletion of *lapA* and *lapB* resulted in enhanced expression of *plaC*. This indicated that the enzymatic activities of these proteins might counterbalance each other during infections. Indeed, *lapA*$^{-}$*/plaC*$^{-}$ double mutants showed a severe replication defect during infection of *A. castellanii* (White et al., 2018).

1.2.4.2.3 PlaD

The *L. pneumophila* GDSL hydrolase PlaD has been identified as homologue of PlaA but has not been characterized extensively so far. It was shown that the protein is not secreted into the culture supernatant of *L. pneumophila* and no signal peptide for secretion via the Sec-system was predicted (Lang et al., 2017). Weak activities towards phospho- and lysophospholipids as well as weak GCAT activity were proposed for the protein but have not been confirmed yet. Comparable to PlaA and PlaC, PlaD seemed to be dispensable during intracellular infections (Banerji et al., 2008). Overall, PlaD is the least characterized of the *L. pneumophila* GDSL hydrolases. Neither the activity of PlaD nor whether it is secreted from *L. pneumophila* has been elucidated yet. Moreover, the function of PlaD during infections is not understood.

1.3 Host cell death in response to infection with *Legionella pneumophila*

1.3.1 Common forms of host cell death are apoptosis, necrosis and pyroptosis

Three forms of host cell death in response to infection with intracellular pathogens are generally acknowledged. These are apoptosis, necrosis and pyroptosis (Lamkanfi and Dixit, 2010) (Figure 5). Occurrence of apoptosis and pyroptosis, but not necrosis, in response to infection with *L. pneumophila* has been described (Abdelaziz et al., 2011; Gao and Abu Kwaik, 1999b).

Apoptosis is a non-inflammatory form of programmed cell death that is important for homeostasis, during embryonic development and also in host-pathogen interactions (Savill et al., 2002). The process of apoptosis is highly regulated by signal transduction cascades. Briefly, apoptosis is induced after binding of ligands to death receptors (extrinsic pathway) or by genotoxic stress and other stimuli that result in the activation of pro-apoptotic Bcl-2 proteins such as Bax and Bak (intrinsic pathway) (Hengartner, 2000; Nafis et al., 2015). These stimuli may be, for example, pathogen associated molecular patterns (PAMPs). Both pathways result in the activation of caspase cascades that lead to the activation of the executioner caspases 3 and 7 which finally execute apoptosis (Nafis et al., 2015). The pro-apoptotic Bcl-2 proteins are regulated by their phosphorylation status. Phosphorylated Bax and Bak are sequestered and thus inactivated by regulatory proteins termed 14-3-3 proteins (Datta et al., 2000; Nomura et al., 2003). Characteristics of apoptosis are cell shrinkage, condensation and fragmentation of chromatin and nuclei, selective translocation of phosphatidylserine (PS) to the outer leaflet of the plasma membrane and membrane blebbing resulting in the formation of apoptotic bodies (Elmore, 2007). Membranes of apoptotic cells do not lyse and thus no pro-inflammatory immune response is induced (Savill et al., 2002).

Necrosis is a caspase-independent form of cell death that results in a pro-inflammatory immune response due to the release of intracellular contents into the extracellular milieu. Some hallmarks of necrosis are, in contrast to apoptosis, cell swelling, chromatin degradation and loss of membrane integrity which results in the release of cellular contents (Lamkanfi and Dixit, 2010).

Pyroptosis is characterized by a mixture of apoptotic and necrotic features. It is, like apoptosis, a form of controlled cell death but the characteristics are more comparable to necrosis and similarly result in the activation of pro-inflammatory immune responses. Pyroptosis is initiated by the detection of PAMPs which induces the assembly of so called inflammasomes and results in the activation of caspase-1. Active caspase-1 then stimulates permeabilization of plasma membranes,

release of the pro-inflammatory cytokines IL-18 and IL-1β and activation of caspase-7 (Bergsbaken et al., 2009; Labbe and Saleh, 2008).

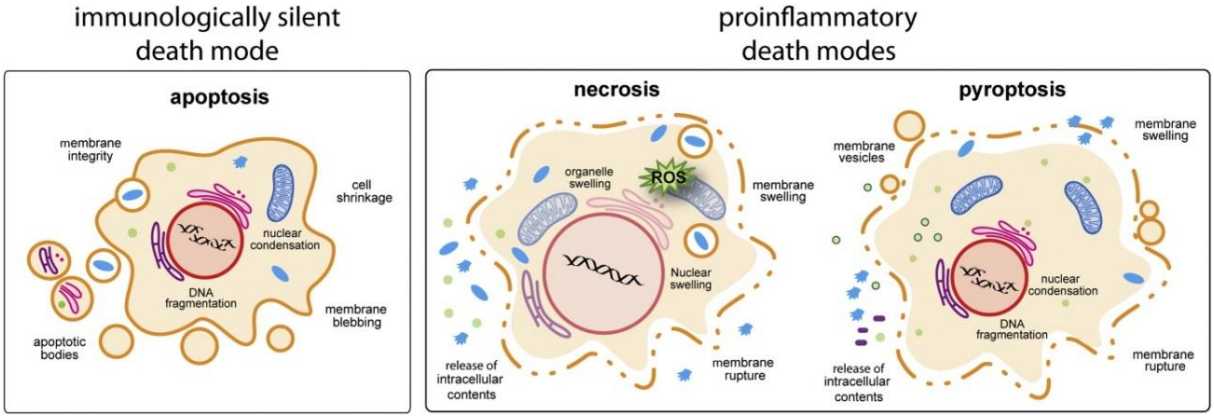

Figure 5: Illustration of forms of programmed host cell death.
(Lamkanfi and Dixit, 2010).

1.3.2 *Legionella pneumophila* induces apoptosis in human and pyroptosis in murine cells

The induction of caspase-3 dependent apoptosis by multiple Dot/Icm effectors of *L. pneumophila* has been described for human macrophages, monocytes, dendritic cells and lung epithelial cells (Furugen et al., 2008; Gao and Abu Kwaik, 1999b; Nogueira et al., 2009; Zink et al., 2002) and is executed via the intrinsic pathway (Fischer et al., 2006; Neumeister et al., 2002). Among others, induction of caspase-3 activity by the patatin-like protein VipD was shown (Zhu et al., 2013). However, at the same time, it was demonstrated that apoptosis is not executed until late stages of infection when replication is finished (Abu-Zant et al., 2005; Santic et al., 2007). Moreover, the secretion of Dot/Icm effectors increasing resistance of infected cells towards exogenous apoptosis stimuli is described. These target especially pro-apoptotic Bcl-2 proteins (Abu-Zant et al., 2007; Banga et al., 2007). Interestingly, the induction of caspase-3 has been described only for human but not for murine or protozoan cells (Abu Khweek and Amer, 2010; Akhter et al., 2009; Hagele et al., 1998; Santic et al., 2007).

In contrast, for infection of murine but not human cells with *L. pneumophila*, the induction of caspase-1 triggering pyroptosis has been described (Abdelaziz et al., 2011). This is triggered by the detection of bacterial flagellin by murine Naip5 which induces the formation of the Nlrc4 inflammasome (Cerqueira et al., 2015; Ren et al., 2006). It is assumed that induction of pyroptosis may be the reason for *L. pneumophila* growth restriction in many mouse strains. Interestingly, expression levels of Naip5 differ between mouse strains which may affect susceptibility towards *L. pneumophila* infection. As described above, BALBc mice, and the derived RAW264.7 mouse

macrophages, are permissive for infections with *L. pneumophila* and do not show significant caspase-1 induction following infection (Losick et al., 2009; Wright Jr et al., 2003). A study of Katagiri et al. showed that human NAIP, similar to the murine Naip5, inhibits apoptosis and promotes pyroptotic cell death. However, this could only be demonstrated in experimental settings where human NAIP was ectopically overexpressed in murine or human cells. In contrast, human NAIP does not activate caspase-1 in human macrophages infected with *L. pneumophila*. It is hypothesized that this might be due to low NAIP expression levels in human macrophages (Katagiri et al., 2012).

1.4 Aim of the study

This thesis primarily aimed to characterize the two GDSL hydrolases PlaA and PlaD of *L. pneumophila* with regard to their importance during infection, their enzymatic activities and their 3D structure. To this end, *L. pneumophila* wild type and isogenic *plaA*$^{-}$ and *plaD*$^{-}$ mutants were applied for single and competitive infections of *A. castellanii* amoebae and RAW264.7 mouse macrophages. Moreover, both enzymes were purified as recombinant protein and subjected to biochemical activity assays and crystallization in cooperation with the Helmholtz Centre for Infection research (HZI) in Braunschweig.

For the characterization of PlaD, an additional focus was set on its mode of secretion and possible interactions with host proteins. This was investigated by translocation assay, proximity ligation and pull down assays.

2 Material and Methods

2.1 Material

2.1.1 Equipment

Table 1: List of used devices.

Device	Name	Company
Chemiluminescence imager	Fusion FX Spectra	Vilber
Centrifuge	Centrifuge 5427 R	Eppendorf
Centrifuge	Centrifuge 5424	Eppendorf
Centrifuge	Centrifuge 5810 R	Eppendorf
Centrifuge	MyFUGE Mini Microcentrifuge	Biozym
Centrifuge	Heraeus Megafuge 16	Thermo Fisher Scientific
Chromatography system	ÄKTA prime	GE Healthcare
Colony counter	Acolyte	Synbiosis
Electroporator	Gene Pulser XCell Electroporation System	BioRad
French Press	Emulsiflex C3	Avestin
Incubation shaker	Innova 42	New Brunswick Scientific
Incubation shaker	Innova 43	New Brunswick Scientific
Incubator	Function Line	HERAEUS
Incubator	HERAcell 240	HERAEUS
Microscope	Eclipse Ti	Nikon
pH electrode	pHenomenal pH1100L	VWR
Photometer	DU 720	Beckman Coulter
Nanophotometer	Nanophotometer	Implen
Protein blotter	Semi-Dry-Blotter, kuroGEL	VWR
Shaker	Microplate Shaker	VWR
Shaker	Polymax 2040	Heidolph

Device	Name	Company
Ultrasonic homogenizer	Sonoplus	Bandelin
Ultrasonic homogenizer	Digital Sonifier	Branson
Absorbance microplate reader	Tecan Sunrise	Tecan
Fluorescence microplate reader	Tecan Infinite M1000	Tecan
Thermocycler	FlexCycler²	Analytik Jena
Thermomixer	Thermomixer compact	Eppendorf
Tissue lyser	Tissue Lyser II	Qiagen
UV-transluminator	Gel Doc 2000	BioRad
Thermo shaker	Thermo shaker	bioSan
Water bath	Precision GP 02	Thermo Fisher Scientific
Speedvac	Centrivap Concentrator	LABCONCO

2.1.2 Special materials

Table 2: special material

Name	Company	Order-Nr
Agar	Merck	1.01615.1000
Agarose, universal	VWR	35-1020
Amicon Ultra-15 Centrifugal Filter Units, 10 kDa	Merck	UFC901024
Azocasein	Sigma-Aldrich	A-2765
Blotting Papers, Grade GB003	GE Healthcare Life Sciences	10426892
Bovine serum albumine	VWA	0332-100G
BugBuster® Protein Extraction Reagent	Merck	70584
C18 sorbent material		
cOmplete EDTA-free Protease Inhibitor	Roche	05056489001
Cryo-vials with inner thread	Roth	E309.1

Name	Company	Order-Nr
Desthiobiotin	Iba	2-1000-002
dNTP Mix 40 mM	Bioline	BIO-39043
Ethidium bromide solution 0,5 % in dropper bottle	Roth	HP46.1
filter 10000 MWCO	Merck	UFC501096
GeneRuler 1 kb DNA Ladder	Thermo Fisher Scientific	SM0312
Glass beads, 0.1 mm	Roth	N033.1
HiTrap Q HP anion exchange chromatography column	GE Healthcare	17115301
IPTG	Bioline	BIO-37036
Legionella BCYE medium	Oxoid	PO5072A
Legionella BCYE-Supplement	Oxoid	SR0110C
Membrane lipid strips	Echelon Biosciences	P-6002
METAFECTENE® PRO	Biontex	T040-1.0
Micropipettes	Blaubrand	708709
PageRuler prestained protein ladder	Thermo Fisher Scientific	26616
Pierce™ NeutrAvidin™ Agarose	Thermo Fisher Scientific	29200
Poly-Prep® Chromatography Columns	BioRad	7311550
ProLong Gold Antifade Reagent	Thermo Fisher Scientific	P36935
PVDF membrane, Immobilon P transfer membranes	Merck	IPVH00010
Roti®-Blue	Carl Roth	A152.1
Roti®-Nanoquant	Carl Roth	K880.3
Rotiphorese® 10x SDS-PAGE	Roth	3060.2
Rotiphorese® Gel 30 (37,5:1)	Carl Roth	3029.1
Rotipuran water	Roth	T172.2
Strep-Tactin® Superflow® high capacity 50% suspension	Iba	2-1208-010
TLC Silica Gel 60	Merck	1.05553.0001

Name	Company	Order-Nr
Trypsin Gold, mass spectrometry grade	Promega	V5280
Trypsin-EDTA (0.05 %) in DPBS (1x)	Capricorn	TRY-1B

2.1.3 Chemicals and lipids

Table 3: List of applied chemicals.

chemical	Company	Order-Nr
2-Mercaptoethanol	Sigma-Aldrich	TW78.13
2-Propanol	Roth	CP41.3
Acetic acid	Roth	3738.4
Acetone	Roth	5025.1
Acetonitrile	Sigma-Aldrich	271004
Ammonium peroxodisulfate (APS)	Applichem	A1142,0250
Biotin	Sigma-Aldrich	B4501
Bromphenolblue	Serva	15375
Calcium chloride dihydrate	Merck	1.02382.0250
Chloroform	Roth	Y015.1
Diethyl ether	Roth	8810.1
EDTA	Sigma-Aldrich	E51354-500G
EGTA	Calbiochem	324626
Ethanol	Roth	9065.4
Etoposide	Sigma-Aldrich	E1383-25MG
Formic acid	Sigma-Aldrich	F0507-500ML
Glycerol	Roth	7533.3
Glycin	Roth	3908.2
Hydrochloric acid, 37 %	Roth	4625.1
Iodoacetamide	Merck	I1149
IPTG	VWR	N679-10G

chemical	Company	Order-Nr
Mangan(II) chloride	Roth	T881.3
Methanol	Roth	4627.5
NAD^+	AppliChem	A1124,0001
Naphtol blue black	Sigma-Aldrich	195243-100G
Natriumhydroxide	Roth	6771.3
Paraformaldehyde	Merck	8.18715.0100
Perchloric acid, 70 %	Riedel de Häen	30755
Petroleumether	Merck	1.01769.1000
p-Nitrophenyl phosphate	Sigma	N4645-1G
Probenecid	Sigma-Aldrich	P8761-25G
Saponin	Roth	4185.1
SDS Pellets	Roth	CN30.2
Skim Milk	Sigma-Aldrich	70166-500G
Sodium azide	Merck	1.06688.0100
Sodium chloride	Roth	9265.3
Staurosporin	Merck	S5921-.1MG
Sucrose	Roth	9097.2
Temed	Roth	2367.3
Trichloracetic acid	Roth	3744.1
Tris Base	Roth	54292
Tris HCl	Roth	9090.3
Triton X-100	Sigma-Aldrich	T8787-50ML
Trypan blue solution	Sigma-Aldrich	T8154-100ML
Tween20	Merck	8.22184.1000
Urea	Roth	2317.3
Zinc chloride	Roth	T887.1

Table 4: List of applied lipid substrates.
All lipids were solved in 40 mM Tris HCl, pH7.5 supplemented with 1 % Triton X-100 and 6 mM NaN_3. All lipids contain two residues of palmitic acid (di-C16). Lipids were suspended in a concentration of 13.4 mM. However, phosphatidylinositol and phosphatidylinositol phosphates (PIPs) were suspended in a concentration of 500 µM.

Lipid	Molar mass [g/mol]	Company	Order-Nr
Phosphatidylcholine [PC]	744.96	Avanti	850355
Phosphatidylglycerol [PG]	734.05	Avanti	840455
Phosphatidylserine [PS]	757.96	Avanti	830037
1-monoacylglycerol [MPG]	330.5	Sigma	M1640-1G
Lysophosphatidylcholine [LPC]	495.64	Avanti	855675
Lysophosphatidylglycerol [LPG]	506.55	Avanti	858122
Phosphatidylinositol [PI]	833.01	Echelon Biosciences	P-0016
Phosphatidylinositol 3-phosphate [PI(3)P]	956.96	Echelon Biosciences	P-3016
Phosphatidylinositol 4-phosphate [PI(4)P]	956.96	Echelon Biosciences	P-4016
Phosphatidylinositol 5-phosphate [PI(5)P]	956.96	Echelon Biosciences	P-5016
Phosphatidylinositol 3,4-bisphosphate [$PI(3,4)P_2$]	1080.90	Echelon Biosciences	P-3416
Phosphatidylinositol 3,5-bisphosphate [$PI(3,5)P_2$]	1080.90	Echelon Biosciences	P-3516
Phosphatidylinositol 4,5-bisphosphate [$PI(4,5)P_2$]	1080.90	Echelon Biosciences	P-4516
Phosphatidylinositol 3,4,5-trisphosphate [$PI(3,4,5)P_3$]	1204.84	Echelon Biosciences	P-3916

2.1.4 Antibodies

Table 5: List of applied antibodies.

antigen	isotype	conjugate	dilution (diluent (in TBS-T))	company (order number)
14-3-3 (pan) [a]	rabbit IgG	none	1/1000 (5 % BSA)	Cell Signaling Technology
Beta-Lactamase [b]	mouse IgG	none	1/200 (5 % Skim Milk)	QED Bioscience Inc., (15720)
Strep-tag [b]	mouse IgG	HRP	1/10000 (5 % Skim Milk)	iba, (2-1509-001)
PlaA [b]	rabbit IgG	none	1/1000 (5 % Skim Milk)	(Lang et al., 2017)
PlaD [b]	rabbit IgG	none	1/1000 (5 % Skim Milk)	(Lang et al., 2017)
rabbit IgG [b]	-	HRP	1/10000 (5 % Skim Milk)	Sigma, (A9044)
mouse IgG [b]	-	HRP	1/10000 (5 % Skim Milk)	Sigma, (A0545)

[a] Incubation overnight at 4 °C
[b] Incubation for 1 h at room temperature

2.1.5 Kits

Table 6: kits

Kit name	Company	Order-Nr
BigDye Terminator v3.1 Cycle Sequencing Kit	Thermo Fisher Scientific	4337456
CellEvent Caspase-3/7 Green Detection Reagent	Thermo Fisher Scientific	C10723
GenElute™ Bacterial Genomic DNA Kit	Sigma-Aldrich	NA2110
HDAC Activity Colorimetric Assay Kit	BioVision	K331
LiveBLAzer™ FRET-B/G Loading Kit with CCF4-AM	Thermo Fisher Scientific	K1095
NEFA-HR(2) (Reagent 1, Reagent 2 and standard)	Fujifilm	434-91795, 436-91995, 270-77000
NucleoSpin® Gel and PCR Clean-up	Macherey-Nagel	740609.50
QIAprep Spin Miniprep Kit	Qiagen	27106
QIAquick Gel Extraction Kit	Qiagen	28706
QIAquick PCR Purification Kit	Qiagen	28106
SuperSignal™ West Dura Extended Duration Substrate	Thermo Fisher Scientific	34075

2.1.6 Buffers and solutions

Table 7: List and composition of applied buffers.

Name	Composition
40 mM Tris HCl	40 mM Tris HCl → solved in ddH_2O → adjusted to pH 7.5
4x Laemmli Buffer	10 % 2-Mercaptoethanol 4 % SDS 0.01 % Bromphenolblue 20 % Glycerol 125 mM Tris HCl → solved in ddH_2O → adjusted to pH 6.8
50 mM Ammonium Bicarbonate Buffer	50 mM Ammonium bicarbonate → solved in ddH_2O → adjusted to pH 8.0

Name	Composition
AEC Buffer A	20 mM Tris HCl → solved in ddH_2O → adjusted to pH 9.0
AEC Buffer B	20 mM Tris HCl 1 M NaCl → diluted in ddH_2O → adjusted to pH 9.0
Blocking Buffer	5 % Skim Milk → solved in TBS-T
HBSS-HP	20 mM HEPES 3 mM Probenecid → diluted in HBSS → pH not adjusted
Osmotic Shock Buffer	30 mM Tris HCl 1 mM EDTA 20 % Sucrose → solved in ddH_2O → adjusted to pH 8.0
PBS	137 mM NaCl 2.7 mM KCl 10 mM Na_2HPO_4 1.8 mM KH_2PO_4 → solved in ddH_2O → adjusted to pH 7.4
Protein Purification Buffer	100 mM Tris HCl 150 mM NaCl → solved in ddH_2O → adjusted to pH 8.0
RIPA	50 mM Tris HCl 150 mM NaCl 1 % Triton X-100 5 mM EDTA 1 mM EGTA 0.1 % SDS 0.5 % Sodiumdeoxychalate → solved in ddH_2O → adjusted to pH 8.0 → 10 % HALT protease inhibitor added immediately before use

Name	Composition
TAE	40 µM Tris Base 20 µM Acetic acid 2 µM Na_2EDTA → solved in ddH_2O → adjusted to pH 8.0
TBS	100 mM Tris HCl 150 mM NaCl → solved in ddH_2O → adjusted to pH 8.0
TBS-T	0.1 % Tween-20 → diluted in TBS
Western Blot Transfer Buffer	25 mM Tris Base 200 mM Glycine 10 % MeOH → solved in ddH_2O → pH not adjusted

2.1.7 Culture media

Table 8: List of purchased media.

Name	Company	Order-Nr
DMEM	Capricorn	DMEM-HA
RPMI	Capricorn	RPMI-A
HBSS	Gibco	14025-092

Table 9: List of selfmade media.

Name	Composition
A. castellanii infection medium	40 mM $MgSO_4$ 40 mM CaCl2 25 mM Na_2HPO_4 25 mM KH_2HPO_4 0.5 mM $Fe(NH_4)_2(SO_4)_2$ 3 mM NaCitrate → solved in ddH_2O and autoclaved

Peptone Yeast Extract Glucose (PYG)	2 % Proteose peptone 0.1 % Yeast extract 40 mM $MgSO_4$ 40 mM CaCl2 25 mM Na_2HPO_4 25 mM KH_2HPO_4 0.5 mM $Fe(NH_4)_2(SO_4)_2$ 3 mM NaCitrate → solved in ddH_2O and autoclaved → 0.1 M filter sterilized glucose added after autoclaving
Luria-Bertani broth (LB)	5 g Yeast extract 5 g NaCl → solved in 1000 ml ddH_2O and autoclaved
Buffered yeast extract (BYE)	10 g Yeast extract 2 bottles of Legionella BCYE-Supplement (Oxoid) → solved in 1000 ml ddH_2O and filter sterilized
SOC medium	20 g Tryptone 5 g Yeast extract 0.584 g NaCl 0.186 g KCl → solved in 1000 ml ddH_2O → adjusted to pH 7.0 and autoclaved → addition of 10 ml 2 M Mg^{2+} stock solution → addition of 10 ml 2 M glucose stock solution

2.1.8 Antibiotics

Table 10: List of applied antibiotics.

Product	Company	Order-Nr	Final concentration [µg/ml]	
			E. coli	*L. pneumophila*
Kanamycin	Sigma-Aldrich	K4000-5G	50	25
Ampicillin	Sigma-Aldrich	A9518-25G	100	-
Chloramphenicol	Sigma-Aldrich	C1919-5G	30	6

2.1.9 Enzymes

Table 11: List of applied restriction enzymes.

Restriction Enzyme	Company	Order-Nr
KpnI	New England Biolabs	R0142S
XbaI	New England Biolabs	R0145S
SalI	New England Biolabs	R0138S
DpnI	New England Biolabs	R0176S

Table 12: List of applied DNA polymerases.

Product	Company	Order-Nr
Phusion® High-Fidelity DNA Polymerase	New England Biolabs	M0530L
Taq DNA Polymerase with ThermoPol® Buffer	New England Biolabs	M0267L
PfuTurbo DNA Polymerase	Agilent	600252

Table 13: List of other applied enzymes.

Product	Company	Order-Nr
T4 DNA ligase	New England Biolabs	M0202L
Antarctica phosphatase	New England Biolabs	M02859S
Bacillus polymyxa protease	Sigma	P6141

2.1.10 Primers

Table 14: List of applied primers.
Primers that were used for generation of new plasmids are referred to in Table 15. All other primers were used for Sanger sequencing of the generated plasmids.

Primer #	Name	Sequence	Tm [°C]
48	gdsl3_s2_f	CTCCAAAAGGTCGATTCACTAA	56.1
50	gdsl3_s3_f	TTGGGAGGAAAACGGACTCAA	59.5
52	gdsl3_s4_f	TAATCAACAACTGCAGACAAAA	54.8
53	gdsl3_s4_r	GCCATATTGTTCGGGATTACTG	57.3
55	gdsl3_s5_r	CGCCTGACCACTCCACAAC	61

Primer #	Name	Sequence	Tm [°C]
253	pMMB_a1_f	AATTAATCATCGGCTCGTATAATG	55.3
254	pMMB_b1_r	CTCTCATCCGCCAAAACAG	56.3
289	T7Promo	TAATACGACTCACTATAGGG	50.3
290	T7Terminat	GCTAGTTATTGCTCAGCGG	56.2
434	PlaD_H344f	TGGGATGATGTTAACCCGACTGCAACAAT	66.8
435	PlaD_H344r	ATTGTTGCAGTCGGGTTAACATCATCCCA	66.8
452	PlaD_S17f	GTATTAGGAGATAATTTATCCGATAGAG	55.2
491	PlaD_S17_R	CTCTATCGGATAAATTATCTCCTAATAC	55.2
692	ProA_BamHI_fw	CggATCCgAAAAAgTTCAAgCAAAAggg	65.3
693	ProA_XhoI_rv	ACTCgAgTTAATCgACATAACAAgATTg	60
1233	pCMV3Flag_rv	TGGGGAGGGGTCACAGG	59.8
2103	PlaD_SacI_fw	ATG AGC TCA ATG GCC CAA AAA	58.7
2104	PlaD_BamHI_rv	ATg gat ccT CAG GTA AAT TTA AC	54.1
2462	plaA-SP_SacI_fw	taG AGC TCT ATG ACA CCA CTT AAT AAC ATA G	60.5
2463	plaA_BamHI_rv	taG GAT CCT TAA TTC TCG GCG AA	59.1
2500	PlaA_S30N_fw	GTATTTGGTGATAATTTGTCGGATAACGG	61.2
2501	PlaA_S30N_rv	CCGTTATCCGACAAATTATCACCAAATAC	61.2
2502	PlaA_D279N_fw	GGTTATTTGTTTTTTAATTTGGTTCATCCGACA	62.5
2503	PlaA_D279N_rv	TGTCGGATGAACCAAATTAAAAAACAAATAACC	62.5
2504	PlaA_H282N_fw	TTTGATTTGGTTAATCCGACAGCGTTG	63
2505	PlaA_H282N_rv	CAACGCTGTCGGATTAACCAAATCAAA	63
2506	PlaA_Del247_rv	TATCGAAAAGGAGCAAGTACCTGT	59.8
2507	PlaA_Del268_fw	ACAGAAAGCGCATGTGATGGT	60.9
2505	PlaA_H282N_rv	CAACGCTGTCGGATTAACCAAATCAAA	63
2710	PlaDß_KpnI_fw	ATGGTACCATGGCCCAAAAACCAACTAAAATCA	67.2
2711	PlaDß_XbaI_rv	ATTCTAGATCAGGTAAATTTAACGAGATGTTCAT	61.6

Primer #	Name	Sequence	Tm [°C]
2726	pBirA_rep_r	TCCATCCTGCTCAAGTAATAAAGCC	60.9
2749	BirA-int252-fw	GCCAGTGATTGACTCCAC	55.4
2750	BirA-int747-fw	TTCGAACAAGAAGGATTG	49.8
2752	BirA-147_168-rv	TTTACCCGGAACGGTAAAG	54.8
2808	fabI(C)_KpnI_f	ATGGTACCGTGGGATTTTTAACTGGAAAAAAAGCAC	67.9
2809	fabI(C)_Xba_r	ATTCTAGACTAACCTAGTTCGCTCATCGCTGATACT	67.4
2817	LPC_1331F	ATGGTACCATGACAGATACTCCAAAAGCT	64.1
2818	LPC_1331R	ATTCTAGACTAACCTGTGAGAGTTTGAGTTG	62.7
2835	plaD1126_XbaI_r	ATTCTAGAGCTACTTTGCCTGAAGCGGTGGTTCAA	70.3
2876	PlaD-Trunk_fw	CTTCAGGCAAAGTAGTAGGCACAAAGAAACTGC	67.7
2877	PlaD-Trunk_rv	GTTTCTTTGTGCCTACTACTTTGCCTGAAGCGG	69.2
2930	plD486stp_Xba_r	ACCTTAAACCCTGATCATTCAAAATGATCTAGAAT	63.3
2931	plD418stp_Xba_r	TGCTATCCATTCAAGAGCATGATCTAGAAT	62.4
3028	plaA_E266N_L267N_fw	TCTGTGAAGCCAAATAATACAGAAAGCGCA	65.5
3029	plaA_E266N_L267N_rv	TGCGCTTTCTGTATTATTTGGCTTCACAGA	65.5
3033	BirA-PlaD_SalI_fw	ATTGTCGACATGAAGGATAACACCGTGCCA	68.2
3035	pBirA*_XbaI_rv	ATTCTAGATTATTTTTCTGCACTACGC	58.4
3326	plaD_S45A_fw	TTAAGAAGCAAAGCTCCAAAAGGTCGA	63.4
3327	plaD_S45A_rv	TCGACCTTTTGGAGCTTTGCTTCTTAA	63.4
3328	plaD_S108A_fw	GAAAACTCTTTTGCCTTAAATGAAGAC	58.2
3329	plaD_S108A_rv	GTCTTCATTTAAGGCAAAAGAGTTTTC	58.2
3330	plaD_T141A_fw	TCTTGTAGCTTTGCCTTTAACCTGGTT	63.2
3331	plaD_T141A_rv	AACCAGGTTAAAGGCAAAGCTACAAGA	63.2
3332	plaD_T180A_fw	GAAAAATCTGAAGCATTAGTTGTGGAG	59.5
3333	plaD_T180A_rv	CTCCACAACTAATGCTTCAGATTTTTC	59.5
3334	plaD_S251A_fw	CAGCGTAATGCAGCCGATTGTACTGAA	65.8

Primer #	Name	Sequence	Tm [°C]
3335	plaD_S251A_rv	TTCAGTACAATCGGCTGCATTACGCTG	65.8
3336	plaD_S265A_fw	CTGCAGACAAAAGCTCTTGAATTAATC	59.7
3337	plaD_S265A_rv	GATTAATTCAAGAGCTTTTGTCTGCAG	59.7
3338	plaD_T460A_fw	ATCTCCGCATTTGCCTTAAACCCTGAT	65
3339	plaD_T460A_rv	ATCAGGGTTTAAGGCAAATGCGGAGAT	65

2.1.11 Plasmids

Table 15: List of plasmids generated and used during this study.

Name	Construct	Insert [kb]	Selection marker	Cloning strategy
pCL15	pet28a(x) + *proA*		Km^R	Amplification with primers #692/#963. Restriction cloning with BamHI and XhoI. This plasmid was constructed by Dr. Christina Lang.
pCL119	pGP172 + $plaA^{(-SP)}$		Amp^R	Amplification with primers #2462/#2463. Restriction cloning with SacI and BamHI. This plasmid was constructed by Dr. Christina Lang.
pCL121	pGP172 + $plaA^{S30N\ (-SP)}$		Amp^R	QuickChange mutagenesis of plasmid pCL119 with primers #2500/#2501. This plasmid was generated by Dr. Christina Lang.
pCL122	pGP172 + $plaA^{D279N\ (-SP)}$		Amp^R	QuickChange mutagenesis of plasmid pCL119 with primers #2502/#2503. This plasmid was generated by Dr. Christina Lang.
pCL123	pGP172 + $plaA^{H282N\ (-SP)}$		Amp^R	QuickChange mutagenesis of plasmid pCL119 with primers #2504/#2505. This plasmid was generated by Dr. Christina Lang.
pCL126	pGP172 + $plaA^{\Delta AA248\text{-}67}$ (-SP)		Amp^R	QuickChange mutagenesis of plasmid pCL119 with primers #2506/#2507. This plasmid was generated by Dr. Christina Lang.

Name	Construct	Insert [kb]	Selection marker	Cloning strategy
pCL127	pGP172 + *plaA*^{S30N} ΔAA248-67 (-SP)		Amp^{R}	QuickChange mutagenesis of plasmid pCL126 with primers #2500/#2501. This plasmid was generated by Dr. Christina Lang.
pMH01	pXDC61 + *plaD*		Cm^{R}	Amplification with primers #2710/#2711. Restriction cloning with KpnI and XbaI.
pMH09	pXDC61 + *fabI*		Cm^{R}	Amplification with primers #2808/#2809. Restriction cloning with KpnI and XbaI.
pMH10	pXDC61 + *lpc1331*		Cm^{R}	Amplification with primers #2817/#2818. Restriction cloning with KpnI and XbaI.
pMH22	pXDC61 + *plaD*$^{ΔAA469-516}$		Cm^{R}	Amplification with primers #2710/#2930. Restriction cloning with KpnI and XbaI.
pMH29	pXDC61 + *plaD*^{S17N} H344N		Cm^{R}	QuickChange mutagenesis of plasmid pMH19 with primers #434/#435.
pMH41	pGP172 + *plaA* ^{E266N} L267N (-SP)		Amp^{R}	QuickChange mutagenesis of plasmid pCL119 with primers #3028/#3029.
pMH42	pGP172 + *plaA*$^{S30N\ E266N}$ L267N (-SP)		Amp^{R}	QuickChange mutagenesis of plasmid pCL121 with primers #3028/#3029.
pMH45	p3xFLAG-*Myc*-CMV-24 + *birA** + *plaD*		Amp^{R}	Amplification with primers #3033/#2711. Restriction cloning with SalI and XbaI.
pMH46	p3xFLAG-*Myc*-CMV-24 + *birA**		Amp^{R}	Amplification with primers #3033/#3035. Restriction cloning with SalI and XbaI.
pMH61	pGP172 + *plaD*^{S45A}		Amp^{R}	QuickChange mutagenesis of plasmid pSB2 with primers #3326/#3327.
pMH62	pGP172 + *plaD*^{S108A}		Amp^{R}	QuickChange mutagenesis of plasmid pSB2 with primers #3328/#3329.
pMH63	pGP172 + *plaD*^{T141A}		Amp^{R}	QuickChange mutagenesis of plasmid pSB2 with primers #3330/#3331.
pMH64	pGP172 + *plaD*^{T180A}		Amp^{R}	QuickChange mutagenesis of plasmid pSB2 with primers #3332/#3333.
pMH65	pGP172 + *plaD*^{S251A}		Amp^{R}	QuickChange mutagenesis of plasmid pSB2 with primers #3334/#3335.
pMH66	pGP172 + *plaD*^{S265A}		Amp^{R}	QuickChange mutagenesis of plasmid pSB2 with primers #3336/#3337.

Name	Construct	Insert [kb]	Selection marker	Cloning strategy
pMH67	pGP172 + *plaD*^{T460A}		Amp^R	QuickChange mutagenesis of plasmid pSB2 with primers #3338/#3339.
pMH68	pGP172 + *plaD*$^{S45A\ S251A}$		Amp^R	QuickChange mutagenesis of plasmid pMH61 with primers #3334/#3335.
pMH69	pGP172 + *plaD*$^{S45A\ S251A\ T180A}$		Amp^R	QuickChange mutagenesis of plasmid pMH68 with primers #3332/#3333.
pMH70	pGP172 + *plaD*$^{S45A\ S251A\ T180A\ S108A}$		Amp^R	QuickChange mutagenesis of plasmid pMH69 with primers #3328/#3329.
pMH71	pGP172 + *plaD*$^{S45A\ S251A\ T180A\ S108A\ T460A}$		Amp^R	QuickChange mutagenesis of plasmid pMH70 with primers #3338/#3339.
pMH72	pGP172 + *plaD*$^{S45A\ S251A\ T180A\ S108A\ T460A\ T141A}$		Amp^R	QuickChange mutagenesis of plasmid pMH71 with primers #3330/#3331.
pMH73	pGP172 + *plaD*$^{S45A\ S251A\ T180A\ S108A\ T460A\ T141AS265A}$		Amp^R	QuickChange mutagenesis of plasmid pMH72 with primers #3336/#3337.
pSB2	pGP172 + *plaD*		Amp^R	Amplification with primers #2103/#2104. Restriction cloning with SacI and BamHI. This plasmid was constructed by Simone Brandt.
pSB4	pGP172 + *plaD*^{S17N}		Amp^R	QuickChange mutagenesis of plasmid pSB2 with primers #452/#491. This plasmid was constructed by Simone Brandt.

2.1.12 Bacterial strains

Table 16: *E. coli* strains used for molecular cloning and gene expression.

Organism	Company	Order Number
E. coli Top10	Invitrogen	C66455
E. coli BL21	Sigma Aldrich	69450-3

Table 17: *L. pneumophila* Corby wild type and knockout mutants used in this study.

Organism	Selection marker	Reference
L. pneumophila	-	(Jepras et al., 1985)
L. pneumophila plaA^{-}	Km^R	(Lang et al., 2012)
L. pneumophila plaD^{-}	Km^R	(Lang et al., 2012)
L. pneumophila plaACD^{-}	Km^R, Hyg^R, $Gent^R$	(Lang et al., 2017)
L. pneumophila dotA^{-}	Km^R	(Lang et al., 2017)

Table 18: Genetically modified *E. coli* Top10 created during this study.

GMO	Plasmid	Selection marker
E. coli Top10 (pMH01)	pMH01 = pXDC61 + *plaD*	Cm^R
E. coli Top10 (pMH09)	pMH09 = pXDC61 + *fabI*	Cm^R
E. coli Top10 (pMH10)	pMH10 = pXDC61 + *lpc1331*	Cm^R
E. coli Top10 (pMH22)	pMH22 = pXDC61 + $plaD^{\Delta AA469-516}$	Cm^R
E. coli Top10 (pMH29)	pMH29 = pXDC61 + $plaD^{S17N\ H344N}$	Cm^R
E. coli Top10 (pMH41)	pMH41 = pGP172 + $plaA^{E266N\ L267N\ (-SP)}$	Amp^R
E. coli Top10 (pMH42)	pMH42 = pGP172 + $plaA^{S30N\ E266N\ L267N\ (-SP)}$	Amp^R
E. coli Top10 (pMH45)	pMH45 = p3xFLAG-*Myc*-CMV-24 + *birA** + *plaD*	Amp^R
E. coli Top10 (pMH46)	pMH46 = p3xFLAG-*Myc*-CMV-24 + *birA**	Amp^R
E. coli Top10 (pMH61)	pMH61 = pGP172 + $plaD^{S45A}$	Amp^R
E. coli Top10 (pMH62)	pMH62 = pGP172 + $plaD^{S108A}$	Amp^R
E. coli Top10 (pMH63)	pMH63 = pGP172 + $plaD^{T141A}$	Amp^R

GMO	Plasmid	Selection marker
E. coli Top10 (pMH64)	pMH64 = pGP172 + *plaD*^{T180A}	Amp^{R}
E. coli Top10 (pMH65)	pMH65 = pGP172 + *plaD*^{S251A}	Amp^{R}
E. coli Top10 (pMH66)	pMH66 = pGP172 + *plaD*^{S265A}	Amp^{R}
E. coli Top10 (pMH67)	pMH67 = pGP172 + *plaD*^{T460A}	Amp^{R}
E. coli Top10 (pMH68)	pMH68 = pGP172 + *plaD*$^{S45A\ S251A}$	Amp^{R}
E. coli Top10 (pMH69)	pMH69 = pGP172 + *plaD*$^{S45A\ S251A\ T180A}$	Amp^{R}
E. coli Top10 (pMH70)	pMH70 = pGP172 + *plaD*$^{S45A\ S251A\ T180A\ S108A}$	Amp^{R}
E. coli Top10 (pMH71)	pMH71 = pGP172 + *plaD*$^{S45A\ S251A\ T180A\ S108A\ T460A}$	Amp^{R}
E. coli Top10 (pMH72)	pMH72 = pGP172 + *plaD*$^{S45A\ S251A\ T180A\ S108A\ T460A\ T141A}$	Amp^{R}
E. coli Top10 (pMH73)	pMH73 = pGP172 + *plaD*$^{S45A\ S251A\ T180A\ S108A\ T460A\ T141AS265A}$	Amp^{R}

Table 19: Genetically modified *E. coli* BL21 used and created during this study.

GMO	Plasmid	Selection marker
E. coli BL21 (pCL119)	pCL119 = pGP172 + *plaA*$^{(-SP)}$	Amp^{R}
E. coli BL21 (pCL121)	pCL121 = pGP172 + *plaA*$^{S30N\ (-SP)}$	Amp^{R}
E. coli BL21 (pCL122)	pCL122 = pGP172 + *plaA*$^{D279N\ (-SP)}$	Amp^{R}
E. coli BL21 (pCL123)	pCL123 = pGP172 + *plaA*$^{H282N\ (-SP)}$	Amp^{R}
E. coli BL21 (pCL126)	pCL126 = pGP172 + *plaA*$^{\Delta AA248-67\ (-SP)}$	Amp^{R}
E. coli BL21	pCL127 = pGP172 + *plaA*$^{S30N\ \Delta AA248-67\ (-SP)}$	Amp^{R}

GMO	Plasmid	Selection marker
(pCL127)		
E. coli BL21 (pCL15)	pCL15 = pet28a(x) + *proA*	Km^R
E. coli BL21 (pMH41)	pMH41 = pGP172 + *plaA*$^{E266N\ L267N\ (-SP)}$	Amp^R
E. coli BL21 (pMH42)	pMH42 = pGP172 + *plaA*$^{S30N\ E266N\ L267N\ (-SP)}$	Amp^R
E. coli BL21 (pMH61)	pMH61 = pGP172 + *plaD*^{S45A}	Amp^R
E. coli BL21 (pMH62)	pMH62 = pGP172 + *plaD*^{S108A}	Amp^R
E. coli BL21 (pMH63)	pMH63 = pGP172 + *plaD*^{T141A}	Amp^R
E. coli BL21 (pMH64)	pMH64 = pGP172 + *plaD*^{T180A}	Amp^R
E. coli BL21 (pMH65)	pMH65 = pGP172 + *plaD*^{S251A}	Amp^R
E. coli BL21 (pMH66)	pMH66 = pGP172 + *plaD*^{S265A}	Amp^R
E. coli BL21 (pMH67)	pMH67 = pGP172 + *plaD*^{T460A}	Amp^R
E. coli BL21 (pMH68)	pMH68 = pGP172 + *plaD*$^{S45A\ S251A}$	Amp^R
E. coli BL21 (pMH69)	pMH69 = pGP172 + *plaD*$^{S45A\ S251A\ T180A}$	Amp^R
E. coli BL21 (pMH70)	pMH70 = pGP172 + *plaD*$^{S45A\ S251A\ T180A\ S108A}$	Amp^R
E. coli BL21 (pMH71)	pMH71 = pGP172 + *plaD*$^{S45A\ S251A\ T180A\ S108A\ T460A}$	Amp^R
E. coli BL21 (pMH72)	pMH72 = pGP172 + *plaD*$^{S45A\ S251A\ T180A\ S108A\ T460A\ T141A}$	Amp^R
E. coli BL21 (pMH73)	pMH73 = pGP172 + *plaD*$^{S45A\ S251A\ T180A\ S108A\ T460A\ T141AS265A}$	Amp^R
E. coli BL21 (pSB2)	pSB2 = pGP172 + *plaD*	Amp^R

GMO	Plasmid	Selection marker
E. coli BL21 (pSB4)	pSB4 = pGP172 + *plaD*^{S17N}	Amp^{R}

Table 20: Genetically modified *L. pneumophila* Corby created during this study.

Organism	Plasmid	Selection marker
L. pneumophila	pMH01 = pXDC61 + *plaD*	Cm^{R}
L. pneumophila plaD^{-}	pMH01 = pXDC61 + *plaD*	Km^{R}, Cm^{R}
L. pneumophila dotA^{-}	pMH01 = pXDC61 + *plaD*	Km^{R}, Cm^{R}
L. pneumophila	pMH09 = pXDC61 + *fabI*	Cm^{R}
L. pneumophila	pMH10 = pXDC61 + *lpc1331*	Cm^{R}
L. pneumophila	pMH22 = pXDC61 + *plaD*$^{\Delta AA469-516}$	Cm^{R}
L. pneumophila plaD^{-}	pMH22 = pXDC61 + *plaD*$^{\Delta AA469-516}$	Km^{R}, Cm^{R}
L. pneumophila dotA^{-}	pMH22 = pXDC61 + *plaD*$^{\Delta AA469-516}$	Km^{R}, Cm^{R}
L. pneumophila	pMH29 = pXDC61 + *plaD*$^{S17N\ H344N}$	Cm^{R}
L. pneumophila plaD^{-}	pMH29 = pXDC61 + *plaD*$^{S17N\ H344N}$	Km^{R}, Cm^{R}
L. pneumophila dotA^{-}	pMH29 = pXDC61 + *plaD*$^{S17N\ H344N}$	Km^{R}, Cm^{R}

2.1.13 Software

Table 21: Software

Software	Company
Geneious 11.1.5	Biomatters Ltd.
Adobe Photoshop Version 13	Adobe Systems Incorporated
Microsoft Office Standard 2010	Microsoft Corporation
14-3-3-Pred	http://www.compbio.dundee.ac.uk/1433pred (Madeira et al., 2015)
Protein Homology/analogY Recognition Engine V 2.0 (PHYRE2)	http://www.sbg.bio.ic.ac.uk/~phyre2/html/page.cgi?id=index (Kelley et al., 2015)

2.2 Methods

2.2.1 Bacterial culture

All bacterial strains used during this work were stored as glycerol stocks at -80 °C. Glycerol stocks were generated from overnight cultures which were supplemented in a ratio of 1:2 with 86 % glycerol. The applied strains are listed in (Table 16-Table 20).

2.2.1.1 *Escherichia coli*

E. coli strains were grown on LB agar supplemented with the appropriate antibiotics (Table 10, Table 16, Table 18 and Table 19) for 1 day at 37 °C and stored at 4 °C for up to 4 weeks. *E. coli* overnight cultures were used for further experiments. Therefore, LB broth supplemented with the appropriate antibiotics (Table 10) was inoculated with single colonies from the *E. coli* LB agar plates and grown overnight at 37 °C and 250 rpm.

2.2.1.2 *Legionella pneumophila*

L. pneumophila strains were grown on BCYE agar supplemented with the appropriate antibiotics (Table 10, Table 17 and Table 20 and) for 2-3 days at 37 °C and stored for up to 4 weeks at 4 °C as "mother plates". These were used to inoculate fresh BCYE agar plates which were incubated at 37 °C for 1-2 days to generate fresh "daughter plates". For all experiments, liquid cultures of *L. pneumophila* grown in BYE broth were used. These were inoculated from "daughter plates" to an OD_{600} of 0.3 and grown to late exponential phase (OD_{600} ~ 3.5) if not stated otherwise. Appropriate antibiotics were added to all "mother plates". Additionally, "daughter plates" and liquid cultures of plasmid-carrying strains were supplemented with the appropriate antibiotics. In contrast, strains with chromosomal integration of resistance cassettes were cultured on "daughter plates" and in liquid cultures without the addition of antibiotics.

2.2.2 DNA and plasmid preparation

2.2.2.1 Isolation of genomic DNA from *L. pneumophila*

The isolation of genomic DNA from *L. pneumophila* was performed with the "GenElute™ Bacterial Genomic DNA Kit" (Qiagen) according to the manufacturer's instructions. Genomic DNA was isolated from 3 ml overnight cultures and eluted in 200 µl ddH_2O. Concentration and purity were determined with a nanophotometer (Implen). Isolated genomic DNA was stored at -20 °C.

2.2.2.2 Plasmid preparation

Plasmids were purified with the "QIAprep Spin Miniprep Kit" (Qiagen) according to the manufacturer's instructions. Plasmid DNA was prepared from 3 ml overnight culture and eluted in 50 µl ddH_2O. Concentration and purity of the plasmid DNA were determined with a nanophotometer (Implen). Plasmids were stored at -20 °C.

2.2.3 Polymerase chain reaction

2.2.3.1 Standard PCR reactions

DNA amplification from purified genomic or plasmid DNA was performed with the "phusion polymerase" (New England Biolabs) according to the protocols below (Table 22 and Table 23). The reaction was followed by a DpnI digest to remove the parental DNA and the PCR products were evaluated by agarose gel electrophoresis prior to purification.

Table 22: Composition of standard PCR reactions.

Component	Volume
Phusion HF Buffer (5x)	10 µl
dNTP Mix (40 mM)	1 µl
Primer, forward (50 µM)	0.4 µl
Primer, reverse (50 µM)	0.4 µl
Template DNA	*a*
Phusion polymerase (2 U/µl)	0.25 µl
ddH_2O	ad 50 µl

[a] volume equal to 200 ng genomic DNA or 50 ng plasmid DNA

Table 23: Cycling parameters for standard PCR reactions.

Reaction	Cycles	Time	Temp.
Initial denaturation	1	3 min	98 °C
Denaturation	35	10 s	98 °C
Annealing	35	30 s	*a*
Elongation	35	*b*	72 °C
Final elongation	1	10 min	72 °C
Storage	1	∞	4 °C

[a] Annealing temperature = Primer T_m – 5 °C
[b] Elongation time = 30 s /kb

2.2.3.2 Colony PCR

Colony PCR was performed to check for positive clones after transformation of *E. coli* or to verify mutations inserted into the genome of *L. pneumophila*. For *E. coli,* single colonies were suspended in 10 µl ddH_2O and denatured for 10 min at 95 °C. The complete suspension was used for the subsequent PCR. For *L. pneumophila,* single colonies were suspended in 50 µl ddH_2O, frozen at -20 °C and denatured for 10 min at 95 °C. Here, 5 µl of the suspension were subjected to subsequent PCR. Colony PCR was performed with the "taq polymerase" (New England Biolabs) according to the

protocols below (Table 24 and Table 25). Evaluation of the colony PCR was done by agarose gel electrophoresis.

Table 24: Composition of colony PCR reactions.

Component	Volume
Thermo Pol. Buffer (10x)	2.5 µl
dNTP Mix (40 mM)	0.5 µl
Primer, forward (50 µM)	0.2 µl
Primer, reverse (50 µM)	0.2 µl
Template DNA	*a*
Taq polymerase (5 U/µl)	0.125 µl
ddH_2O	ad 25 µl

[a] 10 µl of *E. coli* or 5 µl of *L. pneumophila* colony suspension

Table 25: Cycling parameters for colony PCR reactions.

Reaction	Cycles	Time	Temp.
Initial denaturation	1	5 min	95 °C
Denaturation	35	30 s	95 °C
Annealing	35	30 s	*a*
Elongation	35	*b*	68 °C
Final elongation	1	10 min	68 °C
Storage	1	∞	4 °C

[a] Annealing temperature = Primer T_m – 5 °C
[b] Elongation time = 1 min /kb

2.2.3.3 Quick change PCR

Introduction of site-specific mutations into existing vectors was performed by Quick Change PCR. Forward and reverse primer annealed to the same sequence but on opposite strands of the plasmid with the desired mutation present in both primers. Quick Change PCR was performed with the "Pfu Turbo polymerase" (Agilent) according to the protocols below (Table 26 and Table 27). The reaction was followed by a DpnI digest to remove the parental plasmid DNA and 1 µl of the reaction was directly transformed into *E. coli* Top10.

Table 26: Composition of Quick Change PCR reactions.

Component	Volume
Pfu reaction buffer (10x)	5 µl
dNTP Mix (40 mM)	1 µl
Primer, forward (50 µM)	0.2 µl
Primer, reverse (50 µM)	0.2 µl
Template DNA	*a*
Pfu Turbo polymerase (2.5 U/µl)	1 µl
ddH_2O	ad 50 µl

[a] volume equal to 50 ng plasmid DNA

Table 27: Cycling parameters for Quick Change PCR reactions.

Reaction	Cycles	Time	Temp.
Initial denaturation	1	30 s	95 °C
Denaturation	*a*	30 s	95 °C
Annealing	*a*	30 s	*b*
Elongation	*a*	*c*	68 °C
Storage	1	∞	4 °C

[a] 12 for point mutations, 16 for amino acid exchange
[b] Annealing temperature = Primer T_m – 5 °C
[c] Elongation time = 1 min /kb

2.2.3.4 PCR reactions for Sanger sequencing

New plasmids were verified by Sanger sequencing with the "BigDye™ Terminator v3.1 Cycle Sequencing Kit" (Thermo Fisher Scientific). The PCR reactions were performed according to the protocols below (Table 28 and Table 29) and samples were stored at -20 °C until further analysis at the sequencing facility (MF2) of the Robert Koch-Institut. Evaluation of the sequences was performed with the software "Geneious".

Table 28: Composition of PCR reactions for Sanger sequencing.

Component	Volume
ABI Buffer (5x)	2 µl
Primer (50 µM)	0.1 µl
Template DNA	*a*
BigDye 3.1	0.5 µl
ddH_2O	ad 10 µl

[a] volume equal to 150-300 ng plasmid DNA

Table 29: Cycling parameters for PCR reactions for Sanger sequencing.

Reaction	Cycles	Time	Temp.
Initial denaturation	1	1.5 min	96 °C
Denaturation	25	10 s	96 °C
Annealing	25	5 s	*a*
Elongation	25	4 min	60 °C
Storage	1	∞	4 °C

[a] Annealing temperature = Primer T_m – 5 °C

2.2.3.5 Agarose gel electrophoresis

Agarose gel electrophoresis was used for evaluation of PCR reactions and restriction digests as well as purification via gel extraction. Samples were mixed with "6x loading dye", loaded onto 1 % agarose gels and run in TAE buffer at 150 V for 30-45 min. The "GeneRuler 1 kb DNA Ladder" (Thermo Fisher Scientific) was used as marker. Subsequently, agarose gels were incubated for 5 min in an ethidiumbromide bath consisting of 400 ml TAE buffer supplemented with 2 drops of a 0.5 % Ethidium bromide solution (Roth). Then, DNA was visualized with a "GelDoc 2000" gel documentation system (BioRad).

2.2.3.6 Purification of PCR products

PCR products were usually purified with the "QIAquick PCR Purification Kit" (Qiagen) according to the manufacturer's instructions. For constructs that could not be purified with this kit gel extraction was applied. This was performed with the "QIAquick Gel Extraction Kit" (Qiagen) or the "NucleoSpin® Gel and PCR Clean-up kit" (Macherey-Nagel) according to the manufacturer's instructions. In both cases the DNA was eluted in 30 µl ddH_2O. Concentration and purity of purified PCR products was determined with a nanophotometer (Implen). Purification of restriction digests was performed equally. Purified PCR products and restriction digests were stored at -20 °C.

2.2.4 Molecular cloning

Vectors and PCR amplified inserts were digested with restriction enzymes and ligated for molecular cloning of new plasmids. Subsequently, *E. coli* Top10 were transformed with the ligation reaction.

2.2.4.1 Restriction digest

Restriction digests were set up according to Table 30 and incubated for 3 h at 37 °C. All restriction enzymes were purchased from New England Biolabs and are listed in Table 11. The reaction buffers for the applied restriction enzymes and enzyme combinations were chosen according to the manufacturer's recommendation. Digestion was followed by PCR purification or gel extraction.

Table 30: Protocol for restriction digest.

Component	Volume
NEB Buffer (10x)	3 µl
DNA [a]	25 µl
Enzyme 1	1 µl
Enzyme 2 (optional)	1 µl

[a] vector or PCR amplified insert

PCR reactions were digested with the methylation-sensitive restriction enzyme DpnI for removal of parental DNA. To this end, 1 µl DpnI was added directly to the PCR reaction and incubated at 37 °C for 1 h prior to PCR purification or gel extraction.

2.2.4.2 Vector dephosphorylation

Digested vectors were dephosphorylated prior to ligation to prevent religation without insert. Dephosphorylation was performed with the "Antarctica phosphatase" (New England Biolabs) for 1 h at 37 °C according to the protocol in Table 31.

Table 31: Protocol for vector dephosphorylation.

Component	Volume
Antarctica phosphatase buffer (10x)	3 µl
Antarctica phosphatase (5 U/µl)	1 µl
Digested vector	26 µl

2.2.4.3 Ligation

Ligation reactions were set up according to Table 32 and incubated for 1 h at room temperature or overnight at 16 °C. The applied volumes of vector and insert varied dependent on their concentration. In general, an excess of the insert was used to improve ligation efficiency.

Table 32: Protocol for ligation.

Component	Volume
T4 DNA Ligase Buffer (10x)	1 µl
T4 DNA Ligase (400 U/µl)	1 µl
Insert	5-7 µl
Vector	1-3 µl
ddH_2O	ad 10 µl

2.2.4.4 Transformation

Ligation reactions were transformed into *E. coli* Top10 or DH5α. Finished plasmids were transformed into *E. coli* BL21 for protein production or into *L. pneumophila* Corby.

Transformation into *E. coli* was done via chemical competence. To this end, *E. coli* were inoculated 1:100 from overnight cultures in LB medium and grown for approximately 2 h. Then, cultures were centrifuged for 5 min at 5000 rcf and 4 °C, resuspended in ice-cold 0.1 M $CaCl_2$ and incubated on ice for 30 min. Cultures were centrifuged again for 5 min at 5000 rcf and 4 °C and resuspended in ice-cold 0.1 M $CaCl_2$ in 1/25 of the original culture volume. The chemically competent cells were used directly or supplemented with 10 % glycerol and stored in 50 µl aliquots at -80 °C. The complete ligation reaction or 1-2 µl of a finished plasmid were added to 50 µl fresh or frozen chemically competent *E. coli* and incubated on ice for 30 min. Subsequently, the reaction tubes were moved to a 42 °C water bath for 1 min. Then, 500 µl of prewarmed SOC medium were added to the cells and they were incubated at 37 °C and 250 rpm for 1 h followed by plating on selective LB agar plates.

Transformation into *L. pneumophila* was done by electroporation. Therefore, *L. pneumophila* from one fresh daughter plate was washed three times in 5 ml ice-cold ddH_2O with 10 % glycerol and finally resuspended in 500 µl ice-cold ddH_2O with 10 % glycerol. For each reaction, 50 µl of electrocompetent *L. pneumophila* was incubated with 1-2 µl of plasmid DNA on ice for 30 min. Electroporation was performed in the "Gene Pulser Xcell™ Electroporation System" (BioRad) and sterile electroporation cuvettes with 2 mm gap (VWR). The electroporation parameters were set to 25 µF, 200 Ω and 3000 V with exponential decay. Electroporated *L. pneumophila* was transferred into

2 ml prewarmed BYE medium and incubated for 4 h at 37 °C and 250 rpm followed by plating on selective BCYE agar plates.

2.2.5 Production and purification of recombinant proteins

2.2.5.1 Production and purification of recombinant *L. pneumophila* GDSL hydrolases via Strep-tactin affinity chromatography

Overnight cultures of *E. coli* BL21 carrying pGP172-derived plasmids for production of recombinant Strep-tagged proteins (Table 19) were diluted 1:100 in 500 ml LB broth with ampicillin and grown at 37 °C and 250 rpm to an OD_{600} of 0.8. Then, protein production was induced by the addition of 0.1 mM IPTG and cultures were further incubated overnight at 18 °C and 250 rpm. Bacteria were pelleted by centrifugation for 5 min at 10000 rcf and resuspended in 25 ml "Protein Purification Buffer" supplemented with "cOmplete EDTA-free Protease Inhibitor Cocktail" (Roche). Afterwards, samples were homogenized for 3 min in the high pressure homogenizer "EmulsiFlex-C3" (Avestin) with a pressure of 2.7 bar. Before, after and between homogenization of samples, the device was rinsed with ddH_2O. Centrifugation for 30 min at 10000 rcf and 4 °C yielded the soluble fractions which were loaded onto "Poly-Prep® Chromatography Columns" (BioRad) containing 500 µl "Strep-Tactin® Superflow® high capacity resin" (IBA) that had previously been equilibrated with 1 ml "Protein Purification Buffer". Afterwards the columns were washed with 2.5 ml "Protein Purification Buffer" and eluted in 6 fractions à 250 µl "Protein Purification Buffer" containing 2.5 mM D-desthiobiotin. Protein concentration and purity of the eluates were determined as described below (2.2.6) and Coomassie-staining of SDS-Gels (2.2.7.2) respectively.

Protein intended for crystallization was produced in 2000 ml cultures and purified with 2 ml "Strep-Tactin® Superflow® high capacity resin" (IBA). The elution fractions were pooled and concentrated to 500 µl with "Amicon Ultra-15 Centrifugal Filter Units" (Merck) with a nominal molecular weight limit of 10 kDa. Crystallization was performed by cooperation partners Maurice Diwo and Prof. Wulf Blankenfeldt at the Helmholtz Centre for Infection Research in Braunschweig.

2.2.5.2 Production and purification of recombinant *L. pneumophila* zinc metalloproteinase ProA via anion exchange chromatography

E. coli BL21 (pCL15) was diluted 1:100 in 500 ml LB broth with kanamycin from an overnight culture and grown at 37 °C and 250 rpm to an OD_{600} of 0.8. Then, protein production was induced by addition of 0.5 mM IPTG and further incubation overnight at 24 °C and 250 rpm. Bacteria were pelleted by centrifugation for 10 min at 10000 rcf and resuspended in 25 ml "osmotic shock buffer"

followed by incubation for 10 min at 25 °C and 200 rpm. Centrifugation for 10 min at 10000 rcf and 4 °C yielded the periplasmic fraction containing recombinant ProA. The supernatant was discarded.

The periplasmic fraction was subjected to anion exchange chromatography (AEC) for purification of recombinant ProA. Therefore, the periplasmic fraction was diluted 1:10 in "AEC buffer A" and loaded onto a 1 ml "HiTrap Q HP anion exchange chromatography column" (GE Healthcare) using the "ÄKTA prime" (Amersham Pharmacia Biotech) with a flow velocity of 0.5 ml/min. Proteins were eluted with a continuous NaCl gradient ranging from 0 to 1 M NaCl with a flow velocity of 1 ml/min. 1 ml eluate fractions were collected and subjected to SDS-PAGE with subsequent Coomassie-staining (2.2.7.2). Protein bands with a size of 38 kDa indicated the presence of recombinant ProA. These fractions were tested for activity in an azocasein assay (2.2.9). Finally, fractions containing active rProA were pooled and concentrated to 500 µl with "Amicon Ultra-15 Centrifugal Filter Units" (Merck) with a nominal molecular weight limit of 10 kDa.

2.2.6 Determination of protein concentration with Roti-Nanoquant

For determination of protein concentration 5 µl of protein samples were mixed with 195 µl of 1:5-diluted "Roti-Nanoquant" (Roth) in clear 96-well plates and absorbance at 595 nm was measured in a "Sunrise" microplate reader (TECAN). The absorbance at 595 nm was proportional to the protein amount in the sample. Therefore, a standard curve ranging from 0.25 to 2 mg/ml BSA was used for calculation of the protein concentration of samples. Highly concentrated proteins were diluted with ddH_2O prior to measurement.

2.2.7 Protein analysis

2.2.7.1 Preparation of protein samples

Purified proteins were directly diluted with "4x Laemmli buffer" and denatured for 10 min at 95 °C. For preparation of protein samples from bacterial cultures, these were adjusted to an OD_{600} of 1 and centrifuged for 5 min at 5000 rcf. Pellets were resuspended in "BugBuster® Protein Extraction Reagent" (Merck) in 1/10 of the original culture volume and incubated rotating for 30 min at room temperature before denaturation with "4x Laemmli buffer" for 10 min at 95 °C. Supernatants were precipitated with 10 % TCA overnight at 4 °C, centrifuged for 30 min at 16000 rcf and 4 °C, resuspended in 8 M urea in 40 mM Tris HCl (pH 7.5) and denatured with "4x Laemmli" buffer as described above.

2.2.7.2 SDS-PAGE

SDS-PAGE was used for the separation of protein samples according to their molecular weight. Samples were prepared as described above (2.2.7.1) before loading onto 12.5 % SDS-polyacrylamide gels (Table 33 and Table 34). Usually, 20 µl of protein samples were loaded. SDS-PAGEs were run in 1x "Rotiphorese® SDS-PAGE buffer" (Roth) at 150 V for 75 min. Subsequently, the gels were either stained with "Roti-Blue" (Roth) Coomassie staining according to the manufacturer's instructions or subjected to Western blot analysis.

Table 33: Composition of 12.5 % SDS-polyacrylamide separation gels.

Component	Volume
Rotiphorese 30	4.2 ml
1.5 MTris HCl (pH 8.8)	2.5 ml
H_2O	3.1 ml
10 % SDS	100 µl
10 % APS	100 µl
TEMED	10 µl

Table 34: Composition of 5 % SDS-polyacrylamide stacking gels.

Component	Volume
Rotiphorese 30	530 µl
0.5 MTris HCl (pH 6.8)	1 ml
H_2O	2.4 ml
10 % SDS	40 µl
10 % APS	50 µl
TEMED	10 µl

2.2.7.3 Semidry Western blot and immunodetection of proteins

During Western blot the separated proteins were transferred from SDS-polyacrylamide gels to PVDF membranes. Therefore, PVDF membranes were activated in 100 % methanol and equilibrated in "Western blot transfer buffer". The SDS-polyacrylamide gels and "Blotting Papers" (GE Healtcare Life Sciences) were also equilibrated in that buffer. Three layers of "Blotting Papers" (GE Healtcare Life Sciences) were assembled on the anode of the semidry blotter. The PVDF membranes were placed on top of the "Blotting Papers" (GE Healtcare Life Sciences) followed by the SDS-polyacrylamide gels. Three layers of "Blotting Papers" (GE Healtcare Life Sciences) were placed on top of the SDS-polyacrylamide gels before the blotter was closed with the cathode. Western blots were run with a current of 100 mA per membrane for 1 h.

After blotting, the PVDF membranes were blocked for 1 h in 5 % Skim Milk in TBS-T. The PVDF membranes were washed once in "TBS-T" before application of the primary antibodies. Incubation with the primary antibodies was done on a shaker either for 1 h at room temperature or overnight at 4 °C. Then, the membranes were washed 3x 5 min with "TBS-T" and the horseradish peroxidase (HRP)-conjugated secondary antibodies were applied. Incubation with the secondary antibodies was performed on a shaker for 1 h at room temperature. Afterwards, the PVDF membranes were washed again 3x 5 min with "TBS-T". Detection was performed with the "SuperSignal™ West Dura Extended

Duration Substrate" (Thermo Fisher Scientific) according to the manufacturer's instructions using the "Fusion FX Spectra" imaging platform (Vilber). The applied antibodies including information on their dilution and incubation conditions are listed in Table 5.

2.2.8 Protein-Lipid overlay assay

The binding of *L. pneumophila* GDSL hydrolases to biologically important membrane lipids was analyzed with recombinant Strep-tagged proteins which had been purified as described above (2.2.5.1) and commercially available "membrane lipid strips" (Echelon Biosciences). These are spotted with 100 pmol each of the following lipids: triglyceride, phosphatidylinositol (PI), phosphatidylinositol (4)-phosphate (PI4P), phosphatidylinositol (4,5)-bisphosphate ($PI(4,5)P_2$), phosphatidylinositol (3,4,5)-triphosphate ($PI3,4,5P_3$), phosphatidylserine (PS), phosphatidylethanolamine (PE), phosphatidic acid (PA), DAG, cholesterol, phosphatidylcholine (PC), sphingomyelin, phosphatidylglycerol (PG), 3-sulfogalactosylceramide (Sulfatide) and cardiolipin. The membranes were blocked for 1 h in 3 % BSA in "TBS-T". Then, membranes were incubated for 1 h at room temperature with 5 µg of protein which had been diluted in 3 % BSA in "TBS-T". Afterwards, the membrane lipid strips were treated like Western blots (2.2.7.3) and antibodies directed against the Strep-tag of the recombinant proteins were applied.

2.2.9 Determination of rProA activity

50 µl of 1:10-diluted fractions obtained from anion exchange chromatography (2.2.5.2) were incubated with 100 µl of 2 % azocasein in 40 mM Tris HCl (pH 7.5) for 1 h at 37 °C in 1.5 ml reaction tubes. Additionally, a standard curve of *Bacillus polymyxa* protease (Sigma) ranging from 0.1 to 0.5 U/ml was incubated with azocasein as described above. Then, 200 µl of 7 % perchloric acid were added and samples were centrifuged for 5 min at 5000 rcf. 150 µl of the supernatant were carefully transferred to clear 96-well plates and 50 µl of 10 N NaOH were added. Evaluation was done by measuring the absorbance at 430 nm in a "Sunrise" microplate reader (TECAN). The standard curve was used for calculation of protease activity in the tested chromatography fractions.

2.2.10 Analysis of phospholipase activities

2.2.10.1 Preparation of lipid substrates

Lipids were suspended in a concentration of 13.4 mM and 1 % triton X-100 and 6 mM NaN_3 were added. However, phosphatidylinositol and phosphatidylinositol phosphates (PIPs) were suspended in

a concentration of 500 µM. Lipids were vortexed and subsequently incubated for 30 min at 37 °C and 250 rpm. Then, lipids were sonicated three times for 15 s at cycle 4 and 65 % intensity in a "Sonopuls" ultrasonic homogenizer (Bandelin). The applied lipid substrates are listed in Table 16.

2.2.10.2 Lipid hydrolysis assay

Recombinant proteins were incubated with 6.7 mM lipid substrates at 37 °C and 150 rpm for 1-24 h in a total reaction volume of 50 µl Tris HCl (pH 7.5). For rPlaA and rPlaA variants usually 25 ng protein were applied. For rPlaD and rPlaD variants protein amounts varied from 1-100 µg. To assess activation of enzyme activity, the reactions were performed in the presence of 50 % culture supernatant from *L. pneumophila plaACD*$^{-}$ or 3.5 mU rProA. Lipolytic activities were determined by the amount of generated FFA during incubation of recombinant proteins with lipid substrates. These were quantified with the "NEFA-HR (2) Kit" (Fujifilm) according to the manufacturer's instructions. Briefly, the presence of FFA resulted in the enzymatic conversion of a colorimetric substrate leading to the formation of a purple pigment which was measured in a plate reader at 550 nm wavelength. Importantly, the absorption at 550 nm is proportional to the amount of FFA. Thus, the "NEFA standard" (Fujifilm) was diluted to reach a concentration curve ranging from 0 to 1 mM oleic acid. This standard curve was measured with the samples and used as basis for the calculation of FFA in the samples.

2.2.10.3 Lipid extraction and thin layer chromatography

2.2.10.3.1 Analysis of GCAT activity

For analysis of GCAT activity the reactions described for lipid hydrolysis assay were doubled and 0.25 mg/ml cholesterol was added. Incubations were performed for 24 h if not stated otherwise.

Subsequently, lipids were extracted with chloroform/methanol extraction adapted from (Bligh and Dyer, 1959). Samples were mixed with 400 µl methanol and 200 µl chloroform and incubated for 30 min at 37 °C. Then, 280 µl water and 200 µl chloroform were added and samples were incubated for 10 min rotating at room temperature and subsequently centrifuged at 2000 rcf for phase separation. The upper aqueous phase was removed and the lower chloroform phase, containing the lipids, was evaporated in a speedvac for 45 min at 30 °C. The extracted lipids were resuspended in 20 µl chloroform:methanol (2:1) and used for thin layer chromatography (TLC). 10 µl of each sample were spotted onto "TLC Silica gel 60" plates (Merck) with disposable "BLAUBRAND® micropipettes" (Brand). Additionally, 10 µg of FFA, cholesterol, cholesterolproprionate, cholesterolbutyrate and cholesterolpalmitate solved in chloroform:methanol (2:1) were spotted on the "TLC Silica gel 60"

plates (Merck) as standards. Chromatograms were developed with petroleum ether:diethyl ether:glacial acetic acid (90:10:1) in a closed TLC chamber until the solvent front reached the top of the "TLC Silica gel 60" plates (Merck). The average running time was 45 min. Subsequently, the plates were dried at room temperature under a fume hood and shortly soaked in ddH_2O. Then, plates were stained with 0.2 % Napthol Blue Black in 1 M NaCl, washed in 1 M NaCl and photographed.

2.2.10.3.2 Analysis of phosphoinositide conversion

For analysis of dephosphorylation of PIPs by rPlaD, PIPs were incubated without or with 50 µg of rPlaD at 37 °C and 150 rpm for 24 h in 40 mM Tris HCl in a total reaction volume of 100 µl. Subsequently, lipids were extracted and analyzed via thin layer chromatography. For extraction of PIPs samples were mixed with 375 µl of chloroform:methanol:12 N HCl (2:4:0.1). Then 125 µl of chloroform and subsequently 125 µl of water were added. After thorough mixing the samples were centrifuged for 10 min at 2000 rcf for phase separation. The upper aqueous phase was removed and the lower chloroform phase, containing the lipids, was evaporated in a speedvac for 45 min at 30 °C. The extracted lipids were resuspended in 20 µl chloroform and used for TLC. 10 µl of each sample were spotted onto "TLC Silica gel 60" plates (Merck) with disposable "BLAUBRAND® micropipettes" (Brand). Chromatograms were developed with chloroform:methanol:25 % NH_4OH:H_2O (90:70:4:16) in a closed TLC chamber until the solvent front reached the top of the "TLC Silica gel 60" plates (Merck). The average running time was 60 min. Subsequently, the plates were dried at room temperature under a fume hood and shortly soaked in ddH_2O. Then, plates were stained with 0.2 % Napthol Blue Black in 1 M NaCl, washed in 1 M NaCl and photographed.

2.2.10.3.3 Phosphatase activity assay

The phosphatase activity of rPlaD was assayed by measuring conversion of the substrate pNP-phosphate. To this end, 50 µg rPlaD or rPlaD variants were incubated for 24 h at 37 °C with 10 mM pNP-phosphate diluted in 40 mM Tris HCl buffer containing 10 µl/ml Triton X-100, 6 mM NaN_3 and 20 mM $MnCl_2$. Substrate conversion was observed by measuring absorption at 405 nm.

2.2.11 Histone deacetylase activity assay

The histone deacetylase activity of rPlaD was assayed with the "HDAC Activity Colorimetric Assay Kit" (BioVision) according to the manufacturer's instructions in clear 96-well plates. 50 µg of rPlaD or $rPlaD^{S17N}$ diluted in 40 mM Tris HCl (pH 7.5) were applied for the assay. Further, the influence of

addition of 1 mM $ZnCl_2$ or 1 mM NAD^+ was tested in the assay. Evaluation was done by measuring the absorbance at 400 nm in a "Sunrise" microplate reader (TECAN).

2.2.12 Analysis of processing of PlaA by ProA

2.2.12.1 Processing of rPlaA by rProA *in vitro*

For *in vitro* analysis of rPlaA cleavage by rProA, 250 ng rPlaA or rPlaA variants were incubated with 0.5 mU rProA for 5 h. Samples for Western blot were prepared after 10 min, 1 h, 3 h and 5 h. Western blots were performed with primary antibodies directed against the N-terminal Strep-tag of rPlaA (2.2.5).

For determination of the rProA cleavage site within rPlaA via mass spectrometry 5 µg of rPlaA were incubated with 5 mU rProA for 5, 10 and 30 min. Then, samples were prepared for mass spectrometry analysis as described below (2.2.18).

2.2.12.2 Processing of PlaA in liquid culture

Additionally, the processing status of PlaA secreted from *L. pneumophila* liquid cultures was assessed via Western blotting. To this end, *L. pneumophila* was adjusted to an OD_{600} of 0.3 from overnight cultures and washed once with warm BYE broth to remove secreted proteins. Then, cultures were incubated for 8 h at 37 °C and 250 rpm. OD_{600} was measured and samples were prepared every hour. For preparation of protein samples, aliquots of the cultures were adjusted to an OD_{600} of 0.1 and supernatants were precipitated with TCA as described above (2.2.7.1). Importantly, the samples were concentrated 100-fold for Western blot analysis with primary antibodies directed against PlaA and ProA.

2.2.13 Mammalian and amoebal cell culture

The eukaryotic cell lines used during this work were maintained at 37 °C and 5 % CO_2 and passaged twice a week. Cell lines were used for up to 30 passages before new cells were taken into culture from storage in liquid nitrogen.

RAW264.7 mouse macrophages were cultivated in DMEM with 10 % fetal calf serum (FCS). For passaging the old medium was drained off cells. Then, cells were scraped into fresh medium, gently resuspended and diluted in ratios of 1:10 to 1:12 before seeding into new cell culture flasks.

A549 human lung type II epithelial cells were cultivated in RPMI1640 medium with 10 % FCS. For passaging the old medium was drained off cells which were then washed twice with PBS. Then, cells were detached from cell culture flasks with "0.05 % Trypsin-EDTA" (Capricorn) at 37 °C and 5 % CO_2 for 5-10 min. Afterwards, cells were gently resuspended in fresh medium and centrifuged at 1000 rcf for 5 min. The pellet was again resuspended in fresh medium and diluted in ratios of 1:10 to 1:12 before seeding into new cell culture flasks.

A. castellanii amoebae were cultivated in PYG medium. For passaging the old medium was drained off cells. Then, cells were scraped into fresh medium, gently resuspended and diluted in ratios of 1:10 to 1:12 before seeding into new cell culture flasks.

2.2.14 Infection experiments

2.2.14.1 Infection of RAW264.7 mouse macrophages and A549 human lung type II epithelial cells

Infection of RAW264.7 mouse macrophages with *L. pneumophila* was used for analysis of PlaD translocation via β-lactamase translocation assay and for apoptosis assays. Infection of A549 human lung type II epithelial cells with *L. pneumophila* was used for the identification of PlaD interaction partners via BioID assay. In both cases, cells were adjusted to a density of $5x10^5$ ml^{-1} in cell culture medium with 10 % FCS and incubated in appropriate cell culture vessels for 24 h at 37 °C and 5 % CO_2 prior to infection. Immediately before infection the culture medium was replaced by fresh medium without FCS. The infections were performed with overnight liquid cultures of *L. pneumophila* which were grown to an OD_{600} of approximately 3.5. These were diluted in cell culture medium without FCS to an OD_{600} of 0.3 to reach a concentration of approximately $5x10^8$ CFU/ml. These were diluted in cell culture medium without FCS in multiple steps of 1:10-dilutions to reach the desired multiplicity of infection (MOI). Infections were performed by adding the Legionellae to the cells with the last of the required 1:10-dilution steps. Subsequently, cells were centrifuged for 10 min at 800 rcf for synchronization of the infection followed by incubation at 37 °C and 5 % CO_2 for 1-8 h until further analyses. The specific parameters used for infections in distinct assays are listed in Table 35. The *L. pneumophila* strains used for infections are listed in Table 17.

Table 35: Overview of specific parameters for infections.
Cells were always adjusted to a density of $5x10^5$ ml^{-1}.

Assay	Cell type	Cell culture format	Volume of cells	Total cell number per well/flask	MOI
Beta-lactamase translocation assay	RAW264.7 mouse macrophages	96-well, half area plates	100 µl in DMEM	$5x10^4$	100
BioID assay	A549 human lung type II epithelial cells	T75 cell culture flask	10 ml in RPMI	$5x10^6$	100
Detection of caspase-3 activity	RAW264.7 mouse macrophages	96-well, half area plates	100 µl in DMEM	$5x10^4$	1
Detection of nuclear fragmentation	RAW264.7 mouse macrophages	24-well plates	1 ml in DMEM	$5x10^5$	1

2.2.14.2 Analysis of *L. pneumophila* intracellular replication over 72 h

The intracellular replication of *L. pneumophila* was analyzed in *A. castellanii* amoebae and RAW264.7 macrophages over a period of 72 h. These infections were performed as single infections or as competitions between *L. pneumophila* wild type and mutant.

A. castellanii amoebae were seeded directly before infection in "Ac infection medium" in a cell density of $1x10^5$ ml^{-1} in 1 ml per well in 24-well plates. *L. pneumophila* was diluted in "Ac infection medium" as described above and infection was performed with an MOI of 0.1. Here, 1 ml of diluted *L. pneumophila* was added directly to the cells. For competitions, *L. pneumophila* wild type and mutant were diluted as described above and mixed in a 1:1 ratio for infection.

Single infections of RAW264.7 mouse macrophages were performed with an MOI of 1 in 24-well plates as described before (2.2.14.1). For competitions, *L. pneumophila* wild type and mutant were diluted as described above (2.2.14.1) and mixed in a 1:1 ratio for infection at an MOI of 1. Subsequently, the infected cells were centrifuged for 10 min at 800 rcf for synchronization of the infection. Infected RAW264.7 mouse macrophages were incubated at 37 °C and 5 % CO_2 for 4 h. Then, the *L. pneumophila*-containing medium was aspirated and the cells were washed once with warm PBS before fresh culture medium without FCS was added.

Infections of *A. castellanii* amoebae and RAW264.7 mouse macrophages were incubated at 37 °C and 5 % CO_2 for 72 h. Replication of *L. pneumophila* was analyzed by CFU determination every 24 h starting at 0 h for infections of *A. castellanii* amoebae and at 4 h post infection for infections of RAW264.7 macrophages. To this end, infected *A. castellanii* amoebae were resuspended thoroughly and diluted to an estimated CFU of 10^3 ml^{-1} in PBS. Infected RAW264.7 macrophages were lysed by the addition of 0.1 % saponin, resuspended thoroughly and also diluted to an estimated CFU of 10^3 ml^{-1} in PBS. For single infections, the diluted cell suspensions were plated onto BCYE agar. For

competitions, the diluted cell suspensions were plated onto BCYE agar and BCYE agar containing an appropriate concentration of kanamycin to allow discrimination between *L. pneumophila* wild type and mutant. The plates were incubated for 3 days at 37 °C. Then, CFU were calculated from colony counts. Importantly, in competitions the total CFU was determined from BCYE agar plates and the CFU of the mutant was determined from kanamycin-containing BCYE agar plates. The CFU of the wild type was calculated by subtracting the CFU of the mutant from the total CFU. Finally, the ratio of wild type CFU to mutant CFU was calculated.

2.2.15 Transfection of eukaryotic cell lines

2.2.15.1 Transfection of A549 epithelial cells with Metafectene

Transfection of A549 epithelial cells was achieved with the "METAFECTENE® PRO transfection reagent" (Biontex). Cells were adjusted to a density of $2x10^5$ ml^{-1} and seeded into 24-well cell culture plates or T75 cell culture flasks followed by incubation for 2-3 h at 37 °C and 5 % CO_2 for adhesion. Then, "METAFECTENE® PRO transfection reagent" (Biontex) and the plasmid DNA were each diluted in PBS. All concentrations can be found below in Table 36. After incubation at room temperature for 15 min the plasmid solution was added to the METAFECTENE® PRO solution and mixed gently by pipetting. This transfection mix was added to the cells drop by drop. The cells were further incubated at 37 °C and 5 % CO_2 without change of medium. Analysis of expression and further experiments were performed 24-72 h post transfection.

Table 36: Overview of parameters for transfection.

Cell Culture format	Volume of cells	Amount of	
		plasmid DNA	METAFECTENE® PRO
24-well plate	1 ml	0.5 µg in 30 µl PBS	2 µl in 30 µl PBS
T75 cell culture flask	10 ml	12 µg in 700 µl PBS	42 µl in 700 µl PBS

2.2.16 Beta-Lactamase Translocation Assay

The translocation of PlaD via the Dot/Icm T4BSS was analyzed in RAW264.7 mouse macrophages infected with *L. pneumophila* with a beta-lactamase translocation assay adapted from the protocol described by Felipe et al. (de Felipe et al., 2008) using the "LiveBLAzer FRET – B/G Loading Kit with CCF4-AM" (Thermo Fisher Scientific). The assay is based on Förster Resonance Energy Transfer (FRET) and relies on the fluorescent CCF4 beta-lactamase substrate which is trapped in the cytosol of eukaryotic cells. This substrate is labeled with coumarin and fluorescein which form a FRET pair.

Without presence of beta-lactamase activity, excitation of the coumarin at 410 nm results in FRET to the fluorescein resulting in emission of green fluorescence at 520 nm. With presence of beta-lactamase activity, however, the CCF4 substrate is cleaved resulting in disruption of FRET. Then, excitation of the coumarin at 410 nm results in emission of blue fluorescence at 450 nm. Hence, translocation of a beta-lactamase fused protein produced in *L. pneumophila* into the host cell cytoplasm can be detected during infection.

Proteins were fused to the TEM-1 beta-Lactamase for analysis in the assay. Controls were selected according to the results of de Felipe et al. (de Felipe et al., 2008). The putative microtubule binding protein LPC_1331 was chosen as positive control for the assay as it showed the highest translocation rate in the above mentioned study. The enoyl-reductase FabI, which was not translocated in the above mentioned study, was selected as negative control. Both controls were produced only in *L. pneumophila* wild type.

Cells were seeded in 96-well half area plates with black walls and clear bottoms and infected as described in 2.2.14.1. Infections were performed with *L. pneumophila* strain Corby wild type, *plaD*$^-$ mutant or *dotA*$^-$ mutant producing various TEM1-fusion proteins from pXDC61-derived plasmids (Table 20). Strains were inoculated to an $OD_{600} = 0.1$ in BYE broth containing 6 µg/ml chloramphenicol and 0.5 mM IPTG and grown at 37 °C and 250 rpm for 21 h. Infections were performed with an MOI of 100 as described before (2.2.14.1) and the infected cells were incubated at 37 °C and 5 % CO_2 for 1 h. Afterwards the supernatant was replaced by 50 µl "HBSS-HP" and 10 µl freshly prepared CCF4-AM beta-lactamase substrate were added. The cells were incubated for 2 h at room temperature in the dark. Then, fluorescence emission at 450 nm (blue fluorescence) and 520 nm (green fluorescence) in response to excitation at 410 nm was quantified on an "Infinite M1000" microplate reader (TECAN). The translocation rate was calculated as recommended in the "LiveBLAzer FRET-B/G Loading Kit" manual. Briefly, emission values were first corrected by subtraction of the average background signals recorded for empty wells. Then, the 450-nm/520-nm emission ratio was calculated for each well. The translocation rate was expressed as "Response Ratio" which describes the fold increase of the 450-nm/520-nm emission ratio of infected cells relative to the 450-nm/520-nm emission ratio of uninfected cells. Additionally, cells were inspected microscopically and pictures were taken. Importantly, in the microscopic images green fluorescence only indicates the uptake of the CCF4 dye by the cells as the fluorescein part of the dye was excited directly instead of visualizing the FRET signal. However, blue fluorescence of cells indicates cleavage of CCF4 and thus translocation of the β-lactamase-fusion protein. The presented data are mean values and standard deviations of technical triplicates and are representative for at least three replications of the same experiment.

2.2.17 Analysis of protein-protein interactions

The identification of putative PlaD interaction partners was analyzed via proximity ligation with a BioID assay followed by mass spectrometry analysis. Verification of hits from the BioID assay was achieved by pull-down assay.

2.2.17.1 BioID assay

The BioID assay relies on promiscuous biotinylation of interacting proteins by BirA* which is derived from the *E. coli* biotin ligase BirA by insertion of a R118G mutation and was adapted from the protocol described by Lambert et al. (Lambert et al., 2015). BirA* was fused N-terminally to PlaD and ectopically expressed in A549 human lung type II epithelial cells that had been passaged twice in the presence of 50 µM biotin in the cell culture medium. As controls, BirA* alone was expressed ectopically or cells were left untransfected. For each condition, two T75 flasks were prepared from which one was infected with *L. pneumophila* wild type at an MOI of 100 for 3 h. Afterwards, cells were washed three times with warm PBS and scraped into 1 ml ice-cold PBS with "cOmplete EDTA-free Protease Inhibitor Cocktail" (Roche) and centrifuged for 5 min at 16000 rcf and 4 °C. Pellets were resuspended in 1.5 ml "RIPA buffer" with "cOmplete EDTA-free Protease Inhibitor Cocktail" (Roche) and frozen for 1 h at -80 °C. Then, 100 mU benzonase (Merck) and 0.1 % saponin in ddH_2O were added to each sample followed by rotating incubation for 1 h at 4 °C for cell lysis. The cell lysats were cleared by centrifugation for 30 min at 16000 rcf and 4 °C and incubated rotating overnight at 4 °C with 60 µl "Pierce™ NeutrAvidin™ Agarose" (Thermo Fisher Scientific) that had previously been washed three times with 1 ml RIPA buffer. Afterwards, samples were washed twice with 1 ml "RIPA buffer" and subsequently twice with 1 ml "50 mM ammonium bicarbonate buffer". Finally, samples were centrifuged for 1 min at 2000 rcf and supernatants were discarded. The beads were denatured directly in 50 µl "4x Laemmli buffer" for Western blot analysis or prepared for mass spectrometry analysis by after bead digest and peptide purification 2.2.18.

2.2.17.2 Pull-down assay

Proteins for pull-down assays were produced in *E.* coli strain BL21 as described before (2.2.5) but in 3 ml culture volume. Bacteria were pelleted by centrifugation at 5000 rcf for 5 min, resuspended in 1 ml „Protein Purification Buffer" containing "cOmplete EDTA-free Protease Inhibitor Cocktail" (Roche) and lysed with 250 mg 0.1 mm glass beads (Roth) in a "TissueLyser II" (Qiagen). The bacterial lysates were cleared by centrifugation at 16000 rcf for 10 min and incubated rotating for 2 h at room temperature with 200 µl "Strep-Tactin® Superflow® high capacity resin" (IBA) that had previously

been washed with 1 ml „Protein Purification Buffer“. Subsequently, samples were centrifuged for 1 min at 1000 rcf and supernatants were discarded. The samples were washed once with 1 ml “Protein Purification Buffer” for 10 min rotating at room temperature. Afterwards, 1 ml of eukaryotic cell lysate was added to each sample for incubation overnight rotating at 4 °C. These eukaryotic cell lysates had been generated from A549 human lung type II epithelial cells, RAW264.7 mouse macrophages or *A. castellanii* amoebae that had been grown to confluency. The cell cultures were washed once with warm PBS and scraped into „Protein Purification Buffer“ containing “cOmplete EDTA-free Protease Inhibitor Cocktail” (Roche), 0.1 % saponin and 100 mU/ml benzonase in 1/10 of the original culture volume. The eukaryotic cell lysates were incubated for 1 h rotating at 4 °C and then sonified for 5 min with 30 % amplitude in a Digital Sonifier (Branson). The eukaryotic cell lysates were cleared by centrifugation at 16000 rcf for 30 min before usage in the pull-down assay. Afterwards, samples were washed once with 1 ml „Protein Purification Buffer“ for 10 min rotating at room temperature and eluted by incubation with 100 µl „Protein Purification Buffer“ containing 2.5 mM D-desthiobiotin for 30 min rotating at room temperature. Finally, samples were centrifuged for 1 min at 2000 rcf and supernatants were stored at 4 °C. The eluted proteins were analyzed via Western blotting (2.2.7) and mass spectrometry (2.2.18).

2.2.18 Preparation of protein samples for mass spectrometry analysis

For analysis of rProA-processed rPlaA protein samples were precipitated with 4 volumes of cold acetone for 1 h at -20 °C and centrifuged for 10 min at 16000 rcf and 4 °C. Supernatants were removed and pellets were resuspended in 1 M urea in 100 mM Tris HCl (pH 8.5). Samples were digested with 100 ng trypsin gold (Promega) overnight at 37 °C. Subsequently, samples were shipped to the proteomics service (ZBS6) of the Robert Koch-Institut for peptide purification and mass spectrometry analysis.

Proteins from BioID and pull-down assay intended for mass spectrometry analysis were purified with “Pierce™ NeutrAvidin™ Agarose” (Thermo Fisher Scientific) and “Strep-Tactin® Superflow® high capacity resin” (IBA) respectively. Beads were subsequently incubated with 100 µl 8 M urea and 5 mM DTT in 50 mM Tris HCl (pH 8) for 1 h at 37 °C for elution of proteins. Supernatants were transferred to new reaction tubes and iodoacetamide was added in a final concentration of 15 mM. Samples were incubated for 30 min at room temperature in the dark. Then, samples were diluted 1:8 to reach a concentration of 1 M urea and 100 ng trypsin gold were added prior to incubation overnight with gentle mixing at 37 °C. For peptide purification samples were adjusted with 1 % TFA to a pH of 2 and desalted with C18-stage tips using centrifugation steps at 2000 rcf for 1 min. For preparation of C18-stage tips, 200 µl pipette tips were each loaded with 4 µm³ of C18 sorbent

material. Then, the C18-stage tips were activated with 100 µl methanol. This was followed by equilibration with 100 µl 60 % acetonitrile in 0.1 % formic acid and subsequently 100 µl of 0.2 % formic acid. Then, samples were loaded and washed with 200 µl 0.2 % TFA. Proteins were eluted in 50 µl 60 % acetonitrile in 0.1 % formic acid. Afterwards, samples were dried in a speed vac for 30 min at 30 °C and stored at -80 °C until shipping to the proteomics service (ZBS6) of the Robert Koch-Institut for analysis.

2.2.19 Analysis of apoptosis in RAW264.7 macrophages

The apoptotic status of RAW264.7 macrophages was assessed by detection of caspase-3 activity 2.2.19.1 as well as chromatin condensation and nuclear fragmentation 2.2.19.2.

2.2.19.1 Detection of caspase-3 activity

Caspase-3 activity was analyzed with the "CellEvent™ Caspase-3/7 Green Detection Reagent" (Thermo Fisher Scientific). This fluorogenic dye binds to nucleic acids after cleavage of the conjugated DEVD-peptide by active caspase-3 resulting in fluorescence emission at 530 nm in response to excitation at 502 nm. The assay was conducted in RAW264.7 mouse macrophages which were seeded in 96-well half area plates with black walls and clear bottoms as described in (2.2.13). Prior to infection, the medium was replaced by DMEM supplemented with 2 µM "CellEvent™ Caspase-3/7 Green Detection Reagent" (Thermo Fisher Scientific) and incubated for 30 min at 37 °C and 5 % CO_2. Infections with *L. pneumophila* wild type and *plaD*$^-$ mutant were performed with an MOI of 1 as described before (2.2.14.1). As positive control 200 µM etoposide was added to uninfected cells. Untreated cells were used as negative control. Fluorescence emission at 530 nm in response to excitation at 502 nm was quantified on an "Infinite M1000" microplate reader (TECAN) every 24 h. Additionally, cells were inspected microscopically and pictures were taken.

2.2.19.2 Detection of chromatin condensation and nuclear fragmentation

For experiments designed to analyze the apoptosis inhibitory activity of PlaD it was analyzed whether infection with *L. pneumophila* wild type or *plaD*$^-$ mutant protects cells from staurosporine-induced apoptosis. To this end, RAW264.7 mouse macrophages were grown on coverslips in 24-well cell culture plates and infected with *L. pneumophila* wild type or *plaD*$^-$ mutant at an MOI of 1 for 8 h as described above (2.2.14.1). Uninfected cells were used as control. Subsequently, medium was exchanged and apoptosis was induced by addition of 0-1 µM staurosporine in cell culture medium. After 4 h of incubation, cells were washed once with warm PBS and fixated by incubation with 4 %

PFA in PBS for 20 min at room temperature. Cells were washed again with PBS and mounted on microscope slides using “ProLong™ Gold Antifade Mountant with DAPI” (Thermo Fisher Scientific). Samples were cured overnight at room temperature and subsequently imaged followed by quantification of apoptotic nuclei. To this end, the apoptotic status of 100 nuclei per condition was determined and converted into percentages.

3 Results

3.1 Characterization of the *L. pneumophila* GDSL hydrolase PlaA

3.1.1 Importance of PlaA for replication of *L. pneumophila* in infections

As a start, the importance of PlaA for replication of *L. pneumophila* in intracellular infections of *A. castellanii* amoebae was assessed. To this end, *L. pneumophila* wild type was compared with an isogenic *plaA*$^-$ strain. The replication of *L. pneumophila* wild type and *plaA*$^-$ mutant was analyzed in single (Figure 6A) and competitive (Figure 6B) infections of *A. castellanii* amoebae. For both single and competitive infections, 1x10^5 *A. castellanii* amoebae were infected with 1x10^4 *L. pneumophila* corresponding to an MOI of 0.1. Intracellular replication was monitored over a period of 72 h by CFU determination. In single infections, replication of *L. pneumophila* wild type and *plaA*$^-$ was very similar which had already been described previously (Flieger et al., 2002). Approximately 8x10^3 *L. pneumophila* were recovered immediately after infection. At 24 h and 48 h post infection approximately 2-log and 3-log increases in CFU were detected respectively. From 48 h to 72 h post infection only minor replication was observed. At 72 h post infection the number of CFU reached approximately 2x10^7 for both *L. pneumophila* wild type and *plaA*$^-$ mutant. Overall, no significant differences were observed between replication of *L. pneumophila* wild type and *plaA*$^-$ mutant in single infections (Figure 6A and B). In competitive infections of *A. castellanii* amoebae with *L. pneumophila* wild type and *plaA*$^-$ the mutant strain was outcompeted by the wild type (Figure 6B). Infection was started with an excess of the *plaA*$^-$ mutant resulting in the recovery of *L. pneumophila* wild type and *plaA*$^-$ in a ratio of 40 % to 60 % immediately after infection. After 24 h of infection this ratio was inversed. After 48 h the recovered Legionellae consisted of approximately 75 % wild type and 25 % *plaA*$^-$ mutant.

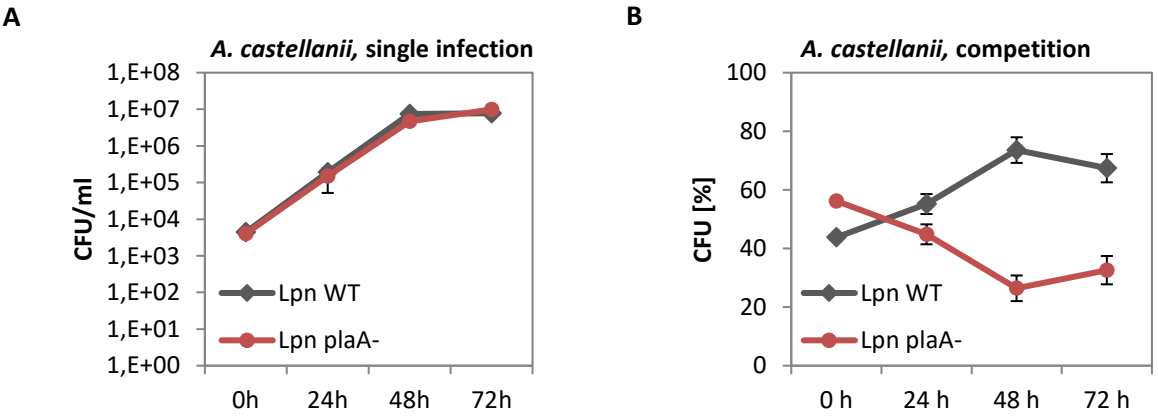

Figure 6: *L. pneumophila plaA*$^-$ is outcompeted by the wild type strain in competitive infections.
Intracellular replication of *L. pneumophila* wild type and *plaA*$^-$ mutant in *A. castellanii* amoebae was monitored over 72 h by CFU determination from single ***(A)*** and competitive ***(B)*** infections. Infections were performed at an MOI of 0.1. Representative for 2 additional experiments.

In sum, it was demonstrated that *L. pneumophila* wild type and *plaA*$^{-}$ show comparable replication in standard intracellular infections. In contrast, in competitive infections the *plaA*$^{-}$ mutant is outcompeted by the wild type which indicates that PlaA might be important during infections under competitive conditions. Thus, the protein was investigated with regard to its biochemical activity.

3.1.2 PlaA shows LPLA and GCAT activities which depend on all members of the predicted catalytic triad

3.1.2.1 Cell lysates of rPlaA producing *E. coli* show strong LPLA and GCAT activity

The *L. pneumophila* GDSL hydrolase PlaA and PlaA variants with site directed mutations of the predicted catalytic triad were recombinantly produced in *E. coli* BL21 and analyzed for their lipolytic activities (Figure 7). Incubation of *E. coli* BL21 lysates producing rPlaA with the lysophospholipids LPG and LPC, but not with the phospholipids PG and PC, for 1 h at 37 °C resulted in the generation of 1.7 mM FFA (Figure 7A). In contrast, generation of FFA was reduced to background level when the lipids were incubated with lysates from *E. coli* BL21 producing rPlaA variants with site directed mutations of the predicted catalytic triad. Thus, rPlaA possesses LPLA activity which depends on the individual members of the predicted catalytic triad. Additionally, the formation of cholesterolpalmitate and cholesterolproprionate was detected when lysates from *E. coli* BL21 producing rPlaA were incubated with LPG or LPC for 16 h in the presence of cholesterol (Figure 7B). This indicated GCAT activity of rPlaA towards lysophospholipids. In contrast, no GCAT activity was detected after incubation with the phospholipids PG and PC or when lysates from *E. coli* BL21 producing rPlaA variants with site directed mutations of the predicted catalytic triad were applied.

Taken together, rPlaA produced in *E. coli* BL21 showed LPLA and lysophospholipid dependent GCAT activity which required all members of the predicted catalytic triad. Next, it was assessed whether these activities would also be detected with purified, recombinant protein (3.1.2.2).

3.1.2.2 Purified rPlaA shows broad range LPLA, GCAT and lipase activity

For activity analysis of purified recombinant proteins, rPlaA was purified via an N-terminal Strep-tag after recombinant production in *E. coli* BL21. Additionally, the inactive variant rPlaA^{S30N} was purified as a representative for the inactive catalytic site directed mutants determined before (3.1.2.1). Importantly, the proteins were produced and purified without the amino acids 1-18 which had been predicted as signal peptide for secretion via the Sec system. For ease of reading, the purified recombinant proteins are denoted as Strep-rPlaA and Strep-rPlaA variants only in the figure legends

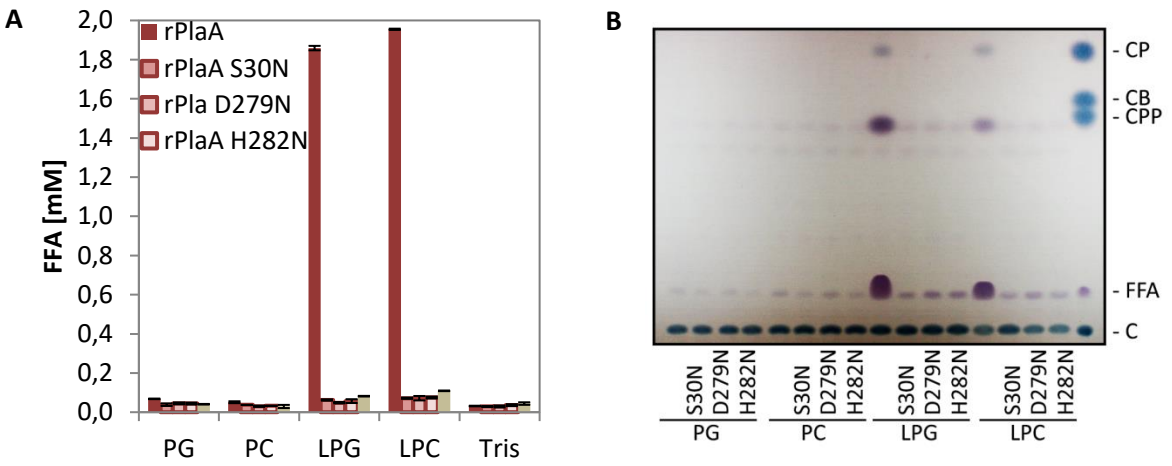

Figure 7: Lysates generated from *E. coli* BL21 producing Strep-rPlaA show strong LPLA and GCAT activity which depend on the individual members of the predicted catalytic triad.
Quantification of FFA was performed after incubation of *E. coli* cell lysates with the indicated lipids for 3 h at 37 °C for determination of PLA and LPLA activity ***(A)***. GCAT activity was analyzed via detection of cholesterol ester formation after incubation of *E. coli* cell lysates for 16 h at 37 °C with the indicated lipids, followed by lipid extraction and TLC ***(B)***. Reactions were performed with cell lysates of *E. coli* clones producing rPlaA, rPlaA^{S30N}, rPlaA^{D279N}, or rPlaA^{H282N} [BL21 (pGP172 *plaA* = pCL119), BL21 (pGP172 *plaA*^{S30N} = pCL121), BL21 (pGP172 *plaA*^{D279N} = pCL122) and BL21 (pGP172 *plaA*^{H282N} = pCL123)]. The results represent the means and standard deviations of duplicate reactions. All results shown are representative for two additional experiments. Published in (Lang et al., 2017).

while they are denoted as rPlaA and rPlaA variants in the main text. Figure 8 shows representative Coomassie-stained SDS-PAGEs of eluted rPlaA (Figure 8A) and rPlaA^{S30N} (Figure 8B). The bands were visible at approximately 35 kDa which corresponds to the size of unprocessed rPlaA. The proteins appeared to be stable except for minor degradation detected in fraction 3. However, this might be accounted to the high protein concentration in this fraction. The highest protein concentrations with up to 2 mg/ml were achieved in the elution fractions 3 and 4.

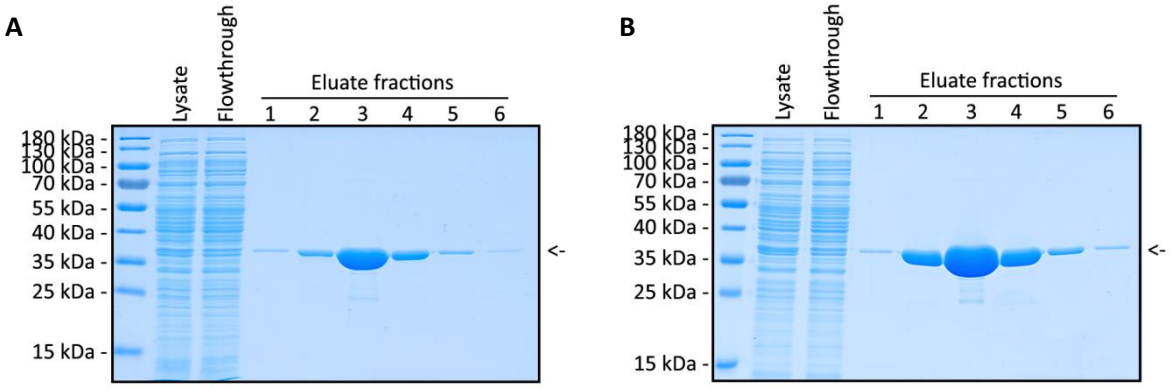

Figure 8: Strep-rPlaA and Strep-rPlaA^{S30N} are purified as highly concentrated and stable proteins.
10 µl of *E. coli* lysate, the flow through collected during purification and all eluate fractions were subjected to SDS-PAGE with subsequent Coomassie-staining. Proteins were purified after production in *E. coli* clones BL21 (pGP172-*plaA* = pCL119) ***(A)*** and BL21 (pGP172 *plaA*^{S30N} = pCL121) ***(B)***. Representative of at least two additional experiments. Arrows denote the size of Strep-rPlaA ***(A)*** and Strep-rPlaA^{S30N} ***(B)*** respectively.

The activity of purified rPlaA and rPlaA^{S30N} was tested against a broader substrate range (Figure 9) as compared to the assays performed with cell lysates from *E. coli* BL21 producing rPlaA or inactive variants (3.1.2.1). Here, 25 ng of recombinant protein were applied for the assays. It was observed that rPlaA possessed broad spectrum LPLA activity as well as lipase activity. The strongest LPLA activity was detected after incubation with the lysophospholipids LPG and LPC and was more than twice as high as the activity against LPE and MPG. The highest concentration of FFA was 0.8 mM and was obtained after incubation of 25 ng rPlaA with 6.7 mM LPC for 3 h. In contrast, no FFA were generated after incubation of rPlaA with the phospholipids PG, PC and PS (Figure 9A). Furthermore, GCAT activity transferring short and long chain fatty acids to cholesterol, resulting in the generation of cholesterolpropionate and cholesterolpalmitate respectively, was detected for purified rPlaA when incubated with MPG or lysophospholipids (Figure 9B). This activity was strongest for the incubation of rPlaA with LPC. In concordance with the results gained from the experiments with *E. coli* cell lysates (3.1.2.1), LPLA, GCAT and lipase activity of purified rPlaA^{S30N} were reduced to background level.

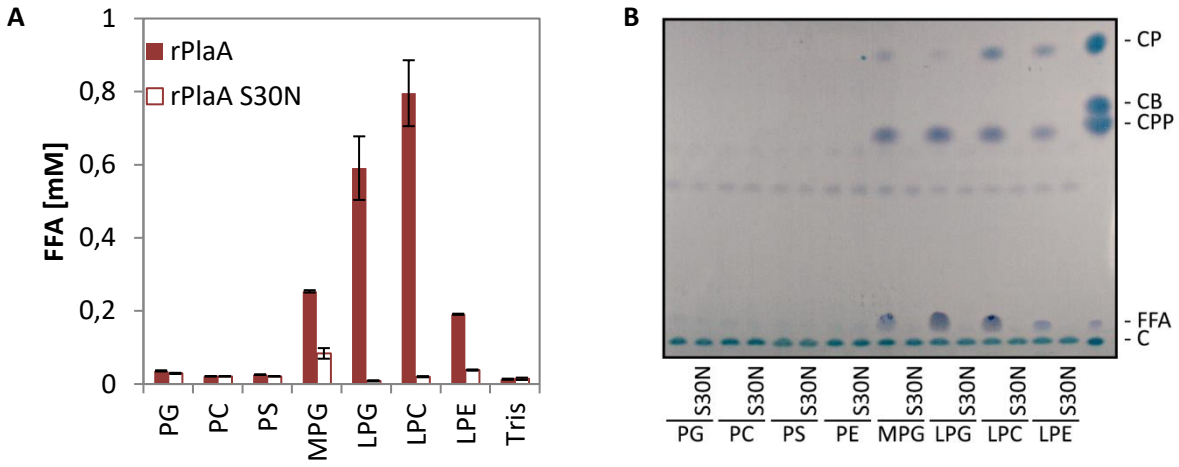

Figure 9: Strep-rPlaA shows strong LPLA, GCAT and lipase activity with broad substrate range.
Quantification of FFA was performed after incubation of 25 ng Strep-rPlaA or Strep-rPlaA^{S30N} with the indicated lipids for 3 h at 37 °C for determination of PLA and LPLA activity ***(A)***. GCAT activity was analyzed via detection of cholesterol ester formation after incubation of 50 ng Strep-rPlaA or Strep-rPlaA^{S30N} with the indicated lipids for 16 h at 37 °C, followed by lipid extraction and TLC ***(B)***. The results represent the means and standard deviations of duplicate reactions ***(A)***. All results shown are representative for at least two additional experiments. Published in (Lang et al., 2017).

In sum, the LPLA and lysophospholipid dependent GCAT activity of rPlaA and the importance of the predicted catalytic serine S30 were confirmed with purified, recombinant protein. Additionally, it was shown that rPlaA is active against MPG and a broader range of lysophospholipids.

3.1.3 rPlaA has a compact alpha/beta hydrolase fold

In addition to the activity analyses, purified rPlaA was also used for determination of the three-dimensional protein structure via protein crystallization by cooperation partners Maurice Diwo and Prof. Wulf Blankenfeld at the Helmholtz Centre for Infection Research in Braunschweig. The structure of *L. pneumophila* rPlaA without the N-terminal signal peptide was solved at a resolution of 1.4 Å.

The recombinant protein subjected to crystallization comprised the amino acids 19-309 as the N-terminal signal peptide was not present in the recombinant protein. Additionally, the protein contained an N-terminal Strep-tag. However, the presented protein structure (Figure 10) comprises the amino acids 20-309 of PlaA and no Strep-tag. The N-terminal Strep-tag used for purification and the amino acid Thr19 were cleaved off spontaneously during the incubation procedure for crystallization. rPlaA comprises an alpha/beta hydrolase fold consisting of twelve alpha helices and five beta sheets. The overall structure is very compact. The color coding in Figure 10A shows that the N-terminus (blue) and the C-terminus (red) of rPlaA are located in close proximity to each other. Moreover, crystallization was only possible in the presence of polyethylenglycol (PEG). A fragment of the PEG was present in close proximity to the predicted catalytic triad of rPlaA in the crystal structure. The PEG-fragment and the side chains of the predicted catalytic triad are highlighted in light grey and black, respectively in Figure 10A. Additionally, a disulfide bond between C243 and C272 was detected. This is highlighted in grey in Figure 10A. The amino acids in between form a loop structure which is colored in orange in Figure 10A and Figure 10C. Removal of this disulfide loop from the illustrated crystal structure revealed that it forms a lid which is shielding the predicted catalytic triad (Figure 10D). The predicted catalytic triad is highlighted in white in Figure 10D. Database searches identified EstA from *Pseudomonas aeruginosa* (PDB code 3kvn) and a putative lipolytic protein of GDSL family from *Desulfitobacterium hafniense* DCB-2 (PDB code 4rsh) as structurally similar to PlaA.

3.1.4 rProA increases the LPLA activity of rPlaA but diminishes its GCAT activity

As described before (1.2.4.2.2), PLA and GCAT activity of the *L. pneumophila* GDSL hydrolase rPlaC increase in response to incubation with culture supernatant from an *L. pneumophila plaACD*$^-$ mutant which exhibited almost no secreted PLA, LPLA and GCAT activity itself. The same is observed after processing of rPlaC with the T2SS secreted zinc metalloproteinase ProA of *L. pneumophila* (Lang et al., 2012). A processing of PlaA by ProA had been observed previously as well in reducing SDS-PAGEs of *L. pneumophila* culture supernatants (Flieger et al., 2001b; Lang et al., 2017). Thus, it was tested whether the addition of culture supernatant from an *L. pneumophila plaACD*$^-$ mutant or recombinant ProA would similarly increase the activity of rPlaA.

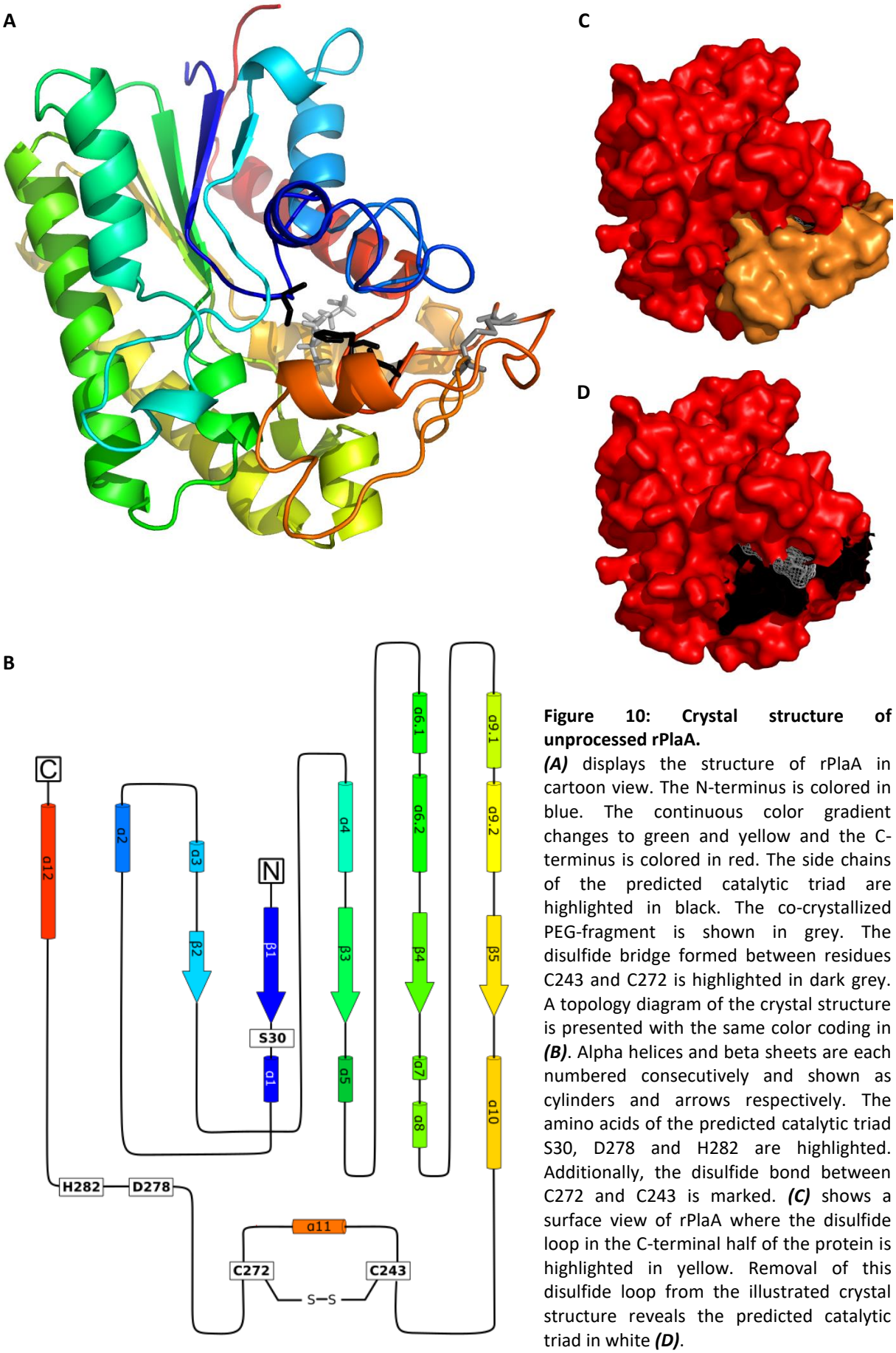

Figure 10: Crystal structure of unprocessed rPlaA.
(A) displays the structure of rPlaA in cartoon view. The N-terminus is colored in blue. The continuous color gradient changes to green and yellow and the C-terminus is colored in red. The side chains of the predicted catalytic triad are highlighted in black. The co-crystallized PEG-fragment is shown in grey. The disulfide bridge formed between residues C243 and C272 is highlighted in dark grey. A topology diagram of the crystal structure is presented with the same color coding in ***(B)***. Alpha helices and beta sheets are each numbered consecutively and shown as cylinders and arrows respectively. The amino acids of the predicted catalytic triad S30, D278 and H282 are highlighted. Additionally, the disulfide bond between C272 and C243 is marked. ***(C)*** shows a surface view of rPlaA where the disulfide loop in the C-terminal half of the protein is highlighted in yellow. Removal of this disulfide loop from the illustrated crystal structure reveals the predicted catalytic triad in white ***(D)***.

To this end, filter sterilized supernatant generated from overnight cultures of an *L. pneumophila plaACD*$^-$ mutant was prepared for activity assays with rPlaA. Additionally, the zinc metalloproteinase ProA was purified from recombinant production in *E. coli* BL21 via anion exchange chromatography (Figure 11). A coomassie-stained SDS-PAGE of the chromatography fractions showed protein bands at 38 kDa in the chromatography fractions 15 to 18 indicating the presence of rProA (Figure 11A). Importantly, fraction 15 showed a very pure band at 38 kDa. In contrast, additional proteins bands were visible at 70 kDa and 30 kDa for fractions 16 to 18. These fractions were pooled for subsequent determination of activity. Next, the protease activity of the rProA chromatography fractions was assessed via azocasein assay (Figure 11B). The activity of the rProA fraction 15 was 3.5 mU/µl while the pooled fractions 16-18 showed an activity of 5.6 mU/µl. The rProA fraction 15 was used for all further experiments due to its superior purity.

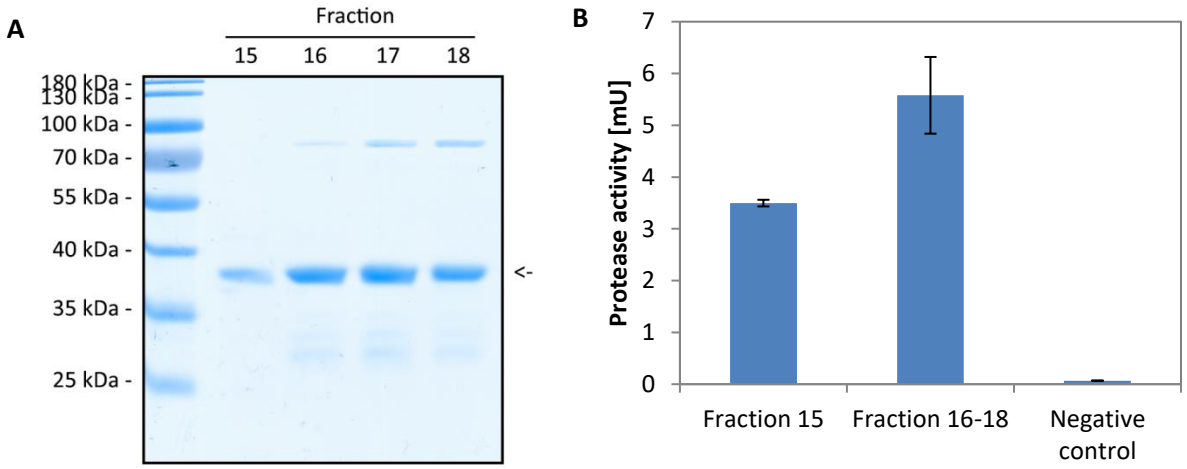

Figure 11: rProA was purified as active protein.
10 µl of protein containing fractions obtained from anion exchange chromatography were subjected to SDS-PAGE with subsequent Coomassie-staining. The arrow denotes the size of rProA ***(A)***. rProA was purified from production in *E. coli* BL21 (pet28a(x) *proA*$_{Corby}$ = pCL15). Protease activity of rProA-containing fractions was assessed via azocasein assay. 40 mM Tris HCl, pH 7.5 was used as negative control ***(B)***. The purification of rProA was performed only once as the protein obtained in fraction 15 was sufficient for all conducted experiments.

Activity analyses of rPlaA performed with the addition of *L. pneumophila plaACD*$^-$ culture supernatant or 3.5 mU purified rProA have indeed shown a change in rPlaA activity. In both cases the LPLA activity of rPlaA was markedly increased (Figure 12). Comparable to the previous assay, incubation of rPlaA with the lysophospholipids LPG and LPC for 3 h resulted in the generation of 0.6 and 0.8 mM FFA respectively (Figure 12A). Addition of *L. pneumophila plaACD*$^-$ culture supernatant raised the LPLA activity about 4-fold to approximately 2.5 and 2.7 mM FFA for incubation with LPG and LPC respectively (Figure 12B). Addition of 3.5 mU rProA lead to a 2-fold rise in activity resulting in the generation of 1.8 and 1.6 mM FFA for incubation with LPG and LPC (Figure 12C). In contrast, weak

PLA activity was only detected when rPlaA was incubated with PG in the presence of *L. pneumophila plaACD*$^{-}$ culture supernatant. Here, 0.4 mM FFA were generated after incubation for 3 h (Figure 12B). Importantly, no PLA or LPLA activity was detected for rPlaA^{S30N} unless *L. pneumophila plaACD*$^{-}$ culture supernatant was added (Figure 12A-C). Incubation of rPlaA^{S30N} with PG, LPG and LPC in the presence of *pneumophila plaACD*$^{-}$ culture supernatant resulted in the generation of 0.2, 0.3 and 0.2 mM FFA respectively (Figure 12B). However, these FFA concentrations were considerably lower than that obtained with active rPlaA. Interestingly, the addition of 3.5 mU rProA diminished the GCAT activity of rPlaA (Figure 12D).

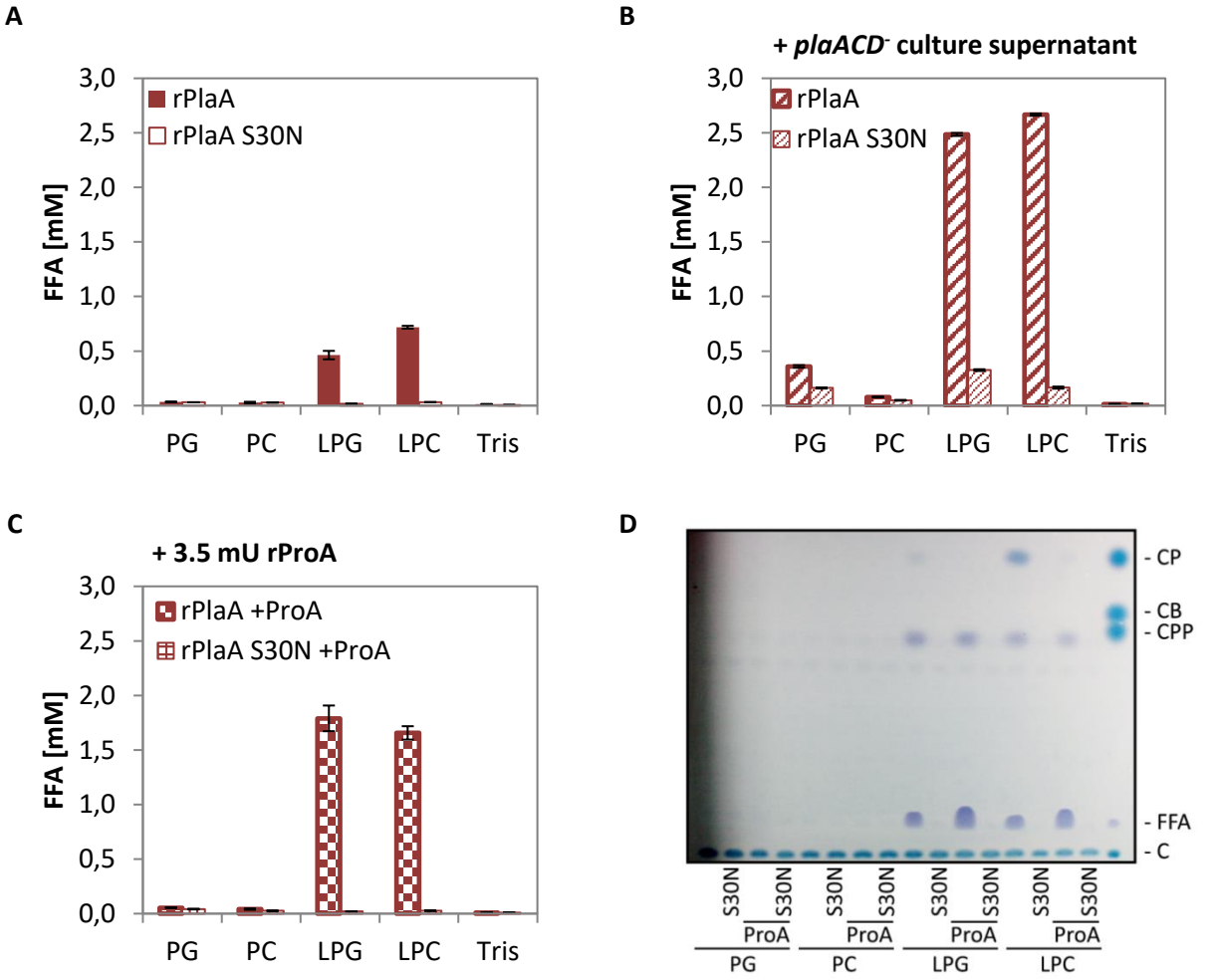

Figure 12: Culture supernatant of *L. pneumophila plaACD*$^{-}$ and rProA increase the LPLA activity of Strep-rPlaA but diminish its GCAT activity.
Quantification of FFA was performed after incubation of 25 ng Strep-rPlaA or Strep-rPlaA^{S30N} without ***(A)*** or with addition of culture supernatant from *L. pneumophila plaACD*$^{-}$ ***(B)*** or 3.5 mU rProA ***(C)***. Incubation was performed with the indicated lipids for 3 h at 37 °C for determination of PLA and LPLA activity ***(A-C)***. GCAT activity was analyzed via detection of cholesterol ester formation after incubation of 50 ng Strep-rPlaA or Strep-rPlaA^{S30N} without or with addition of 3.5 mU rProA ***(D)***. Incubation was performed with the indicated lipids for 16 h at 37 °C, followed by lipid extraction and TLC ***(D)***. The results represent the means and standard deviations of duplicate reactions ***(A-C)***. All results shown are representative for at least two additional experiments. *CP - cholesterol palmitate, CB - cholesterol butyrate, CPP - cholesterol proprionate, FFA - free fatty acids, C - cholesterol.* Published in (Lang et al., 2017).

However, only the transfer of long chain fatty acids to cholesterol resulting in the generation of cholesterol palmitate was blocked. The transfer of short chain fatty acids to cholesterol generating cholesterol propionate was independent of the addition of rProA. Comparable to the previous experiments, no GCAT activity was detected for incubation of rPlaA with the phospholipids PG and PC in any of the tested conditions. Additionally, no GCAT activity was detected for rPlaA^{S30N} in any conditions.

Taken together, the LPLA activity of rPlaA is distinctly increased after incubation with rProA. In contrast to rPlaC, however, the GCAT activity of rPlaA is diminished by incubation with rProA. Next, it was analyzed how rPlaA is processed by rProA.

3.1.5 rPlaA is processed by rProA within a disulfide loop in the C-terminal half of the protein

3.1.5.1 N-terminal sequencing identified the rProA cleavage site within rPlaA

It is known that rPlaC is processed by rProA within a disulfide loop (Lang et al., 2012). A disulfide loop is also present in the C-terminal half of rPlaA which had been predicted from the amino acid sequence (1.2.4.2) and was confirmed via protein crystallization (3.1.3). Thus, it was hypothesized that rProA might cleave rPlaA within this disulfide loop.

The processing of rPlaA by rProA was shown *in vitro* via Western blot. To this end, rPlaA was incubated alone or in the presence of rProA at 37 °C for up to five hours and subsequently analyzed by Western blot for rPlaA protein size as indicator of the processing status (Figure 13). It was observed that rPlaA alone remained stable over time with only minor decrease in protein size after 5 h of incubation. In contrast, when rPlaA was incubated in the presence of rProA a decrease in protein size by approximately 10 kDa was observed as early as 10 min after start of the incubation. At later time points a secondary processing was detected resulting in double bands at approximately 25 kDa. This seemed to correspond to the minor processing observed for rPlaA that was incubated without rProA.

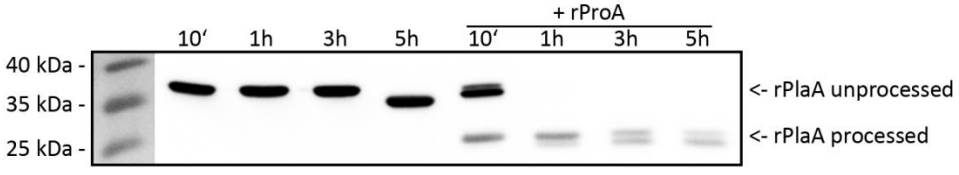

Figure 13: Strep-rPlaA is processed by rProA *in vitro.*
Processing of Strep-rPlaA by rProA was analyzed by Western blot with an antibody directed against PlaA after incubation of 250 ng Strep-rPlaA without or with 0.5 mU rProA for up to 5 h at 37 °C. A molecular weight standard is shown on the left of the Western blot. The blot was trimmed from all sides. Representative for at least three replications. Published in (Lang et al., 2017).

In cooperation with Dr. Jörg Döllinger from the proteomics service of the Robert Koch-Institut the site of ProA-processing within PlaA was determined via N-terminal sequencing of rProA-processed rPlaA. Mass spectrometry analysis of rProA-processed rPlaA revealed that cleavage occurred within the disulfide loop between C243 and C272 in the C-terminal half of rPlaA (Figure 14). Seven distinct cleavage sites were detected between P265 and A271. The by far most prominently detected cleavage site was located between E266 and L267.

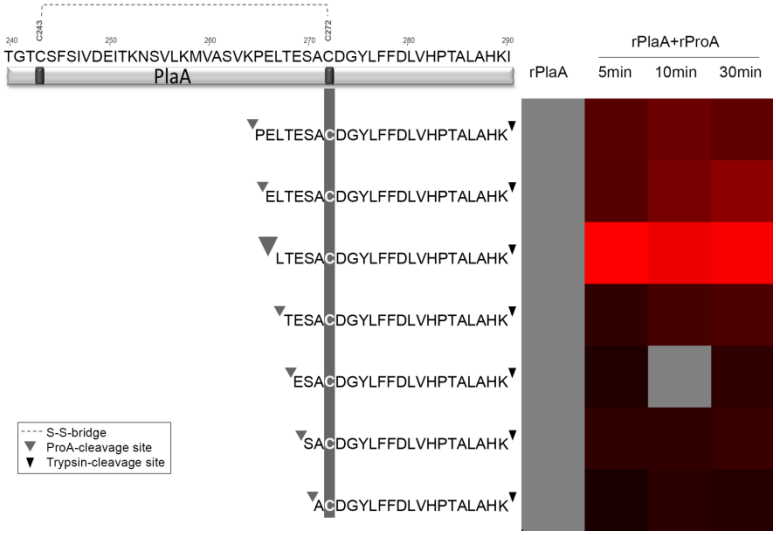

Figure 14: N-terminal sequencing of rProA-processed Strep-rPlaA reveals cleavage site within disulfide loop in the C-terminal half of Strep-rPlaA.
Presentation of semi-tryptic peptides of ProA-processed Strep-rPlaA identified by mass spectrometry. Above, a fragment of the PlaA protein sequence from amino acids 240 to 290 is displayed. The heat map on the right visualizes the intensity values of the detected peptides where brighter red indicates higher intensity. All detected cleavage sites were present within the PlaA disulfide loop region between C243 and C272. The highest intensity was found for the cleavage site in front of L267 which is highlighted by the big grey arrow. Cleavage sites with smaller intensities are marked with smaller grey arrows. Trypsin cleavage sites are highlighted by small black arrows. N-terminal sequencing was performed once. Published in (Lang et al., 2017).

3.1.5.1.1 Mutation of the most prominent rProA-cleavage site in rPlaA does not prevent processing

Next, it was assessed whether mutation of the main rProA-cleavage site within rPlaA from E266/L267 to N266/N267 would prevent the processing of rPlaA by rProA. However, this was not the case as can be seen in Figure 15. Therefore, the protein size of rPlaA E266N L267N that had been incubated without or with presence of 0.5 mU rProA for 10 min and 1 h was examined via Western blotting with an antibody directed against PlaA (Figure 15A). It can be seen that rPlaA$^{E266N\ L267N}$ without addition of rProA remained stable over time. However, incubation of rPlaA$^{E266N\ L267N}$ in the presence of 0.5 mU rProA resulted in a decrease in protein size indicating processing. Moreover, similar to wildtype rPlaA, the mutant protein showed strong LPLA activities which were even increased by

addition of rProA (Figure 15B). Overall, it seems that mutation of the main rProA cleavage site within rPlaA was not sufficient to prevent processing by rProA.

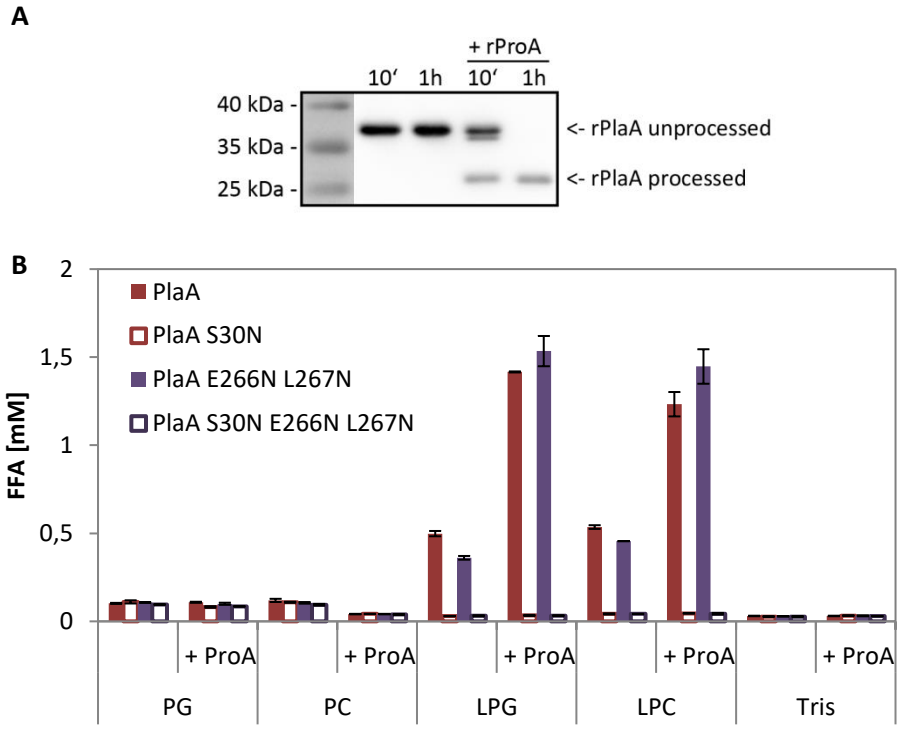

Figure 15: Strep-rPlaA$^{E266N\ L267N}$ is processed by rProA *in vitro* resulting in increased LPLA activity.
Processing of Strep-rPlaA$^{E266N\ L267N}$ by rProA was analyzed by Western blot with an antibody directed against PlaA after incubation of 250 ng rPlaA$^{E266N\ L267N}$ without or with 0.5 mU rProA for 10 min and 1 h at 37 °C. A molecular weight standard is shown on the left of the Western blot ***(A)***. Quantification of FFA was performed after incubation of 25 ng Strep-rPlaA$^{E266N\ L267N}$ or Strep-rPlaA$^{S30N\ E266N\ L267N}$ with the indicated lipids for 3 h at 37 °C for determination of PLA and LPLA activity. The results represent the means and standard deviations of duplicate reactions ***(B)***. The blot was trimmed from all sides. The results are representative for one additional experiment.

3.1.5.2 PlaA is secreted as full length protein and subsequently processed by ProA

Moreover, the state of PlaA processing was examined in liquid cultures of *L. pneumophila*. Therefore, *L. pneumophila* growth was monitored over a period of seven hours (Figure 16A) and supernatant samples were collected every hour for analysis of the presence and processing status of PlaA and ProA (Figure 16B and C). The Western blots in Figure 16 (B and C) show that PlaA was secreted as full length protein during early growth phases. The first time a band for processed PlaA was visible was after 4 h of growth. From 5 h of incubation on, only processed PlaA was detected in the culture supernatant. Interestingly, ProA was detected in the culture supernatant already in the first sample taken after 1 h of growth. Overall, it was shown that ProA proteolytically processes PlaA both *in vitro* and in cultures of *L. pneumophila.*

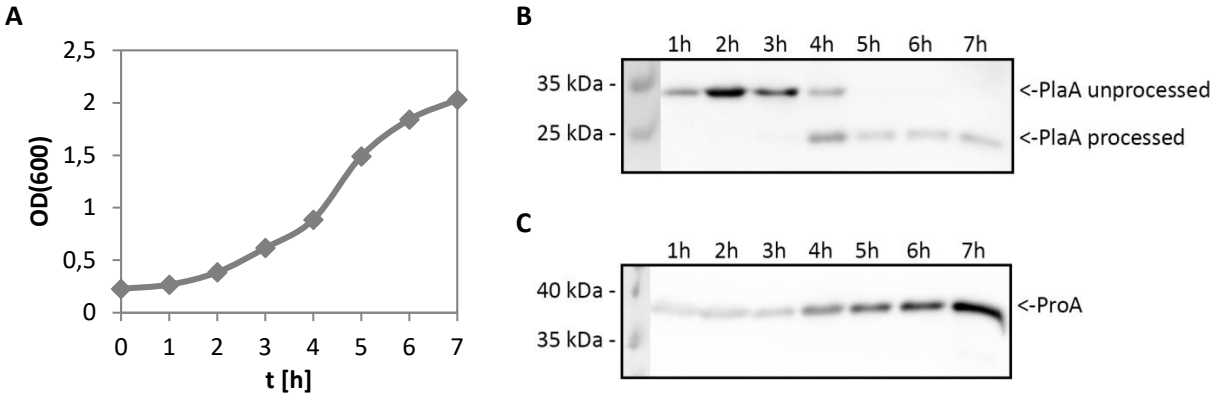

Figure 16: Processing of PlaA in culture depends on the amount of secreted ProA.
The growth of *L. pneumophila* wild type was monitored over a period of 7 h ***(A)*** and samples of culture supernatant were analyzed for the presence and processing status of PlaA ***(B)*** and presence of ProA ***(C)*** by Western blotting with PlaA- and ProA-directed antibodies. Molecular weight standards are shown on the left of the Western blots. The blots were trimmed from all sides. Representative for one additional experiment.

3.1.5.3 Deletion of the disulfide loop from rPlaA reflects activation by rProA

It was shown that the activity of rPlaA is increased by the addition of rProA and that rProA cleaves the disulfide loop in the C-terminal half of rPlaA. Thus, it was assumed that the processing of the disulfide loop causes the change in activity. As a next step, it was analyzed whether the complete removal of the disulfide loop from rPlaA would result in increased lipolytic activity. To this end, the deletion mutant rPlaA$^{del248\text{-}267}$ was analyzed for its PLA, LPLA and GCAT activity.

Activity assays with the loop deletion mutant rPlaA$^{del248\text{-}267}$ showed the same substrate range as observed for rPlaA. However, a steep increase in LPLA activity in comparison to the full length rPlaA was observed (Figure 17A). The loop deletion mutant showed at least a 4-fold increase in activity against MPG, LPG and LPE resulting in the generation of 2.5, 1.9 and 0.7 mM FFA respectively (Figure 17A). However, the LPLA activity towards LPC was not increased as much. Additionally, no effect on PLA activity was observed for the deletion mutant. Importantly, rPlaA$^{S30N\ del248\text{-}267}$ only generated 0.1 mM FFA after incubation with LPC and LPE. Under all other conditions, the activity of rPlaA$^{S30N\ del248\text{-}267}$ remained at background level. Moreover, no GCAT activity transferring long chain fatty acids to cholesterol was observed for rPlaA$^{del248\text{-}267}$ (Figure 17B). However, the generation of cholesterol propionate was still detected. Overall, the activities observed for the deletion mutant rPlaA$^{del248\text{-}267}$ resembled the phenotype of rPlaA that was incubated in the presence of *L. pneumophila plaACD*$^{-}$ culture supernatant or 3.5 mU rProA.

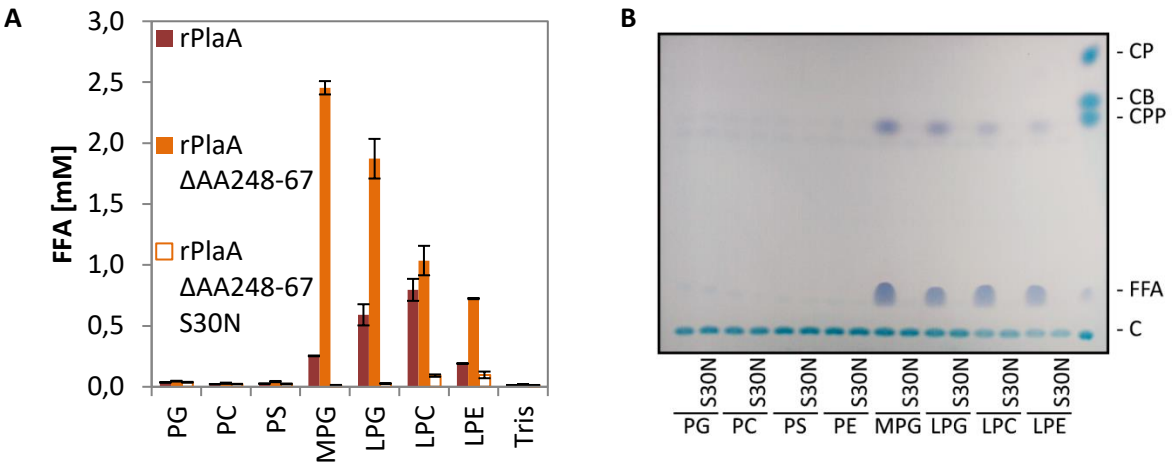

Figure 17: Deletion of a C-terminal disulfide loop from Strep-rPlaA results in increased LPLA and diminished GCAT activity.
Quantification of FFA was performed after incubation of 25 ng Strep-rPlaA, Strep-rPlaA$^{\Delta AA248-67}$ or Strep-rPlaA$^{S30N\ \Delta AA248-67}$ with the indicated lipids for 3 h at 37 °C for determination of PLA and LPLA activity ***(A)***. GCAT activity was analyzed via detection of cholesterol ester formation after incubation of 50 ng Strep-rPlaA$^{\Delta AA248-67}$ or Strep-rPlaA$^{S30N\ \Delta AA248-67}$ with the indicated lipids for 16 h at 37 °C, followed by lipid extraction and TLC ***(B)***. The results represent the means and standard deviations of duplicate reactions ***(A)***. All results shown are representative for at least two additional experiments. Published in (Lang et al., 2017).

Interestingly, addition of *L. pneumophila plaACD*$^{-}$ culture supernatant or 3.5 mU rProA only slightly increased the LPLA activity of rPlaA$^{del248-267}$ (Figure 18). This effect was more pronounced after 1 h (Figure 18A-C) of incubation than after 3 h (Figure 18D-E). Moreover, after 1 h of incubation, addition of *L. pneumophila plaACD*$^{-}$ culture supernatant (Figure 18B) resulted in a stronger increase in LPLA activity than addition of 3.5 mU rProA (Figure 18C). Incubation of rPlaA$^{del248-267}$ with LPG and LPC resulted in the generation of 1 and 0.8 mM FFA respectively. Presence of *L. pneumophila plaACD*$^{-}$ culture supernatant increased the amount of generated FFA to 1.8 and 1.5 mM. In contrast, addition of 3.5 mU rProA only slightly increased the amount of generated FFA to 1.2 and 0.9 mM. After 3 h of incubation 2-2.5 mM FFA were detected in all conditions except for incubation of rPlaA$^{del248-267}$ with LPC in the presence of *L. pneumophila plaACD*$^{-}$ culture supernatant (Figure 18D-F). This resulted in the generation of 2.8 mM FFA. Importantly, generation of FFA by rPlaA$^{S30N\ del248-267}$ remained at background levels in all tested conditions.

In summary, it was demonstrated that the deletion of the disulfide loop from the C-terminal half of PlaA results in the same phenotype as processing by ProA.

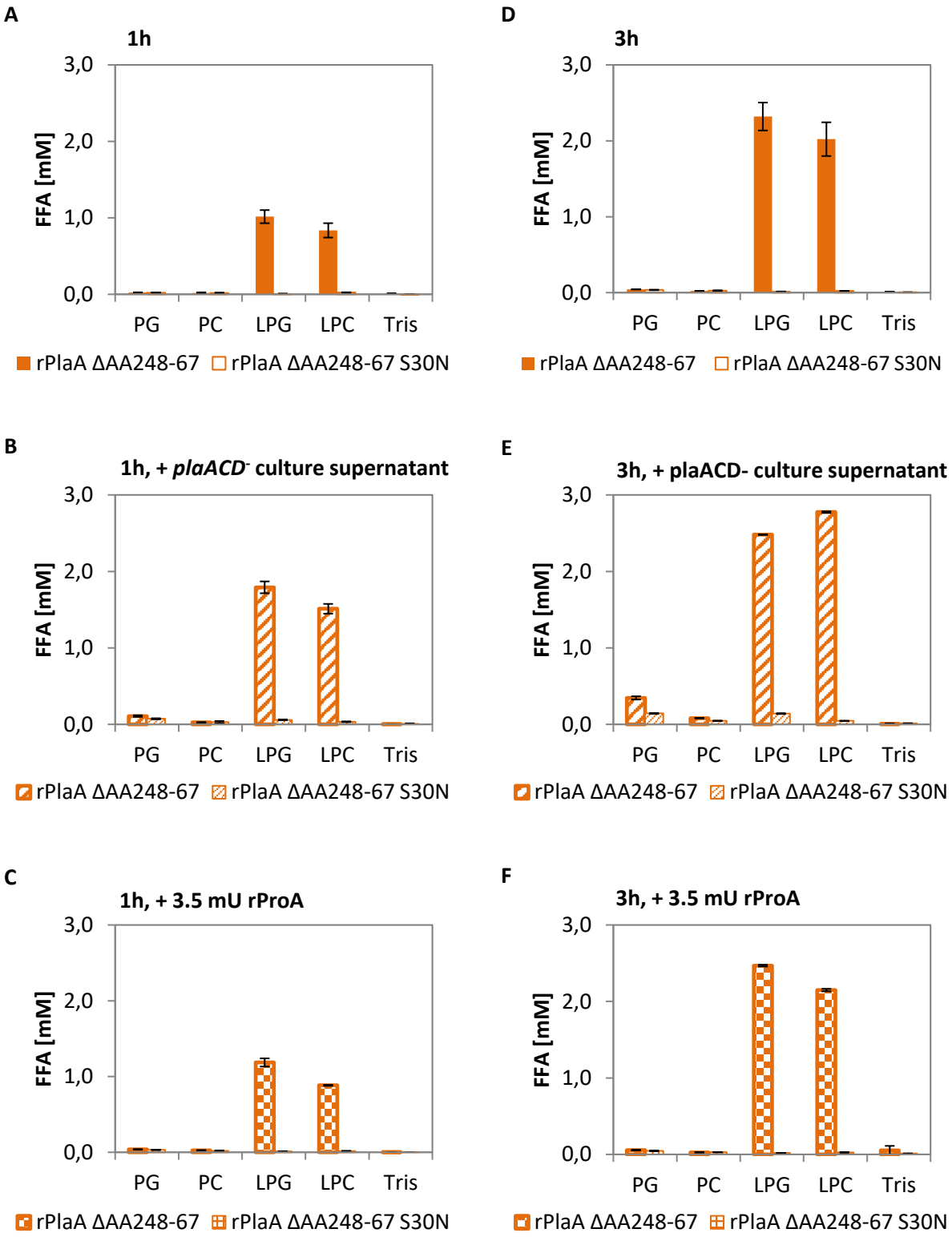

Figure 18: *L. pneumophila plaACD*⁻ culture supernatant and rProA do not lead to a strong increase in LPLA activity of Strep-rPlaA$^{del248-267}$.
Quantification of FFA was performed after incubation of 25 ng Strep-rPlaA$^{del248-267}$ or Strep-rPlaA$^{S30N\ del248-267}$ without ***(A, D)*** or with addition of culture supernatant from *L. pneumophila plaACD*⁻ ***(B, E)*** or 3.5 mU rProA ***(C, F)***. Incubation was performed with the indicated lipids for 1 h ***(A-C)*** or 3 h ***(D- F)*** at 37 °C for determination of PLA and LPLA activity. The results represent the means and standard deviations of duplicate reactions and are representative for at least two additional experiments. Published in (Lang et al., 2017).

3.2 Characterization of the *L. pneumophila* GDSL hydrolase PlaD

3.2.1 Importance of PlaD for replication of *L. pneumophila* in infections

The analysis of the *L. pneumophila* GDSL hydrolase PlaD was started by determining its importance for infections of *A. castellanii* amoebae and RAW264.7 mouse macrophages. Therefore, replication of *L. pneumophila* wild type and an isogenic *plaD*$^-$ mutant was analyzed in single and competitive infections. Infections in *A. castellanii* amoebae were performed with an MOI of 0.1 while RAW264.7 mouse macrophages were infected with an MOI of 1. Intracellular replication was monitored over a period of 72 h by CFU determination.

Intracellular replication of *L. pneumophila* wild type and *plaD*$^-$ mutant was very similar in single infections of both *A. castellanii* amoebae (Figure 19A) and RAW264.7 mouse macrophages (Figure 19B). Approximately 5x10^3 and 5x10^5 CFU of *L. pneumophila* wild type and *plaD*$^-$ were recovered 0 or 4 h post infection of *A. castellanii* amoebae and RAW264.7 mouse macrophages respectively. CFU numbers of both strains increased by approximately 4 log-units over the first 48 h of infection. Interestingly, the *plaD*$^-$ mutant seemed to replicate slightly faster over the first 24 h. From 48 to 72 h post infection no further replication was observed. At 72 h post infection the number of CFU detected in infected *A. castellanii* amoebae and RAW264.7 mouse macrophages reached approximately 2x10^7 and 2x10^9 respectively for both *L. pneumophila* wild type and *plaD*$^-$ mutant.

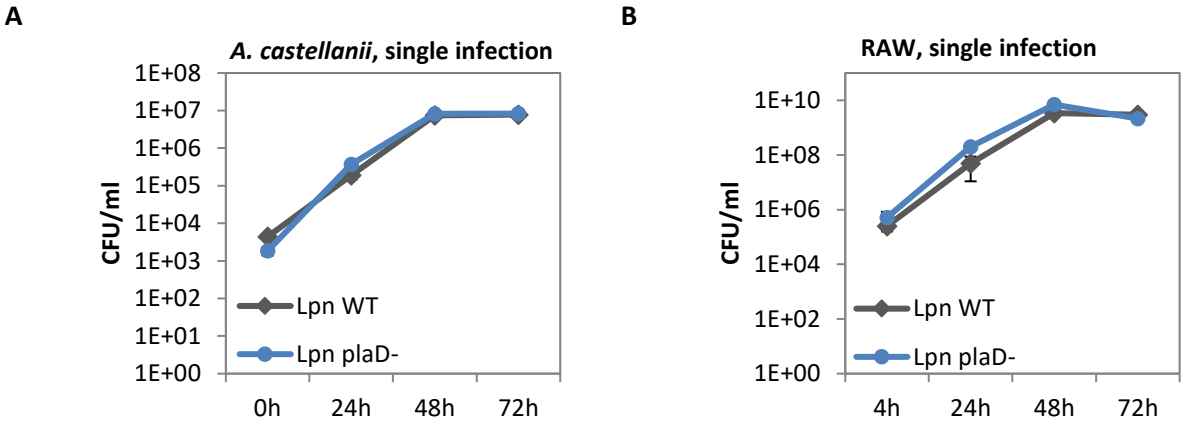

Figure 19: *L. pneumophila* wild type and *plaD*$^-$ mutant replicate similarly in single infections of *A. castellanii* amoebae and RAW264.7 mouse macrophages.
Intracellular replication of *L. pneumophila* wild type and *plaD*$^-$ mutant in *A. castellanii* amoebae ***(A)*** and RAW264.7 mouse macrophages ***(B)*** was monitored over 72 h by CFU determination. Infections were performed at an MOI of 0.1 in *A. castellanii* amoebae and at an MOI of 1 in RAW264.7 mouse macrophages. Results are displayed as mean and standard deviation of technical triplicates and are representative for two additional experiments.

In competitive infections of both *A. castellanii* amoebae and RAW264.7 mouse macrophages with *L. pneumophila* the *plaD*$^-$ mutant outcompeted the wild type strain. Infection was started with an

excess of *L. pneumophila* wild type. Immediately after infection of *A. castellanii* amoebae and 4 h post infection of RAW264.7 mouse macrophages, the recovered Legionellae were composed of approximately 60 % wild type and 40 % *plaD*$^{-}$ mutant. Already 24 h post infection the relation of *L. pneumophila* wild type to *plaD*$^{-}$ mutant was inversed. Then, the recovered Legionellae consisted of approximately 30 % wild type and 70 % *plaD*$^{-}$ mutant. This ratio was maintained over the rest of the infection with only minor variations. In infections of *A. castellanii* amoebae an additional increase in the amount of the *plaD*$^{-}$ mutant to approximately 80 % of the recovered Legionellae was observed 72 h post infection.

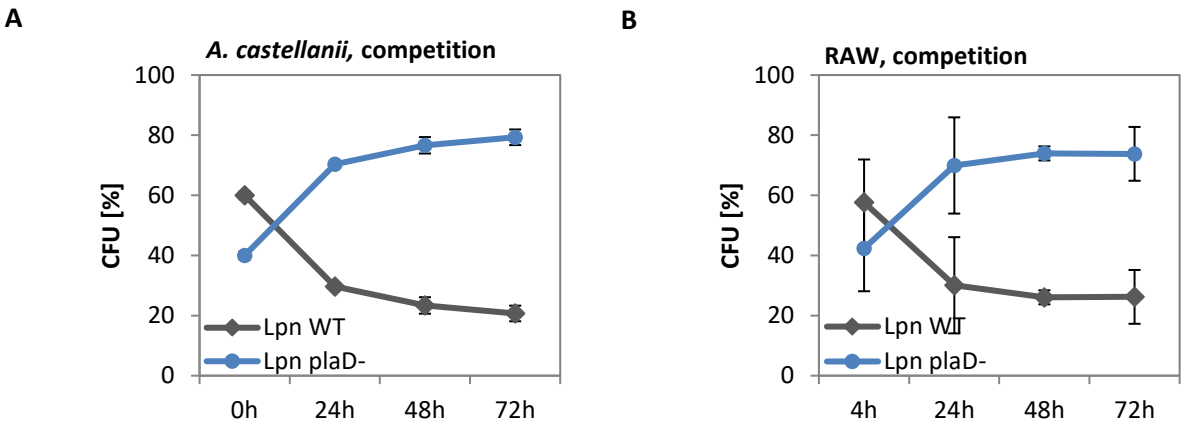

Figure 20: *L. pneumophila plaD*$^{-}$ mutant prevails in competitive infections with the wild type strain.
Intracellular replication of *L. pneumophila* wild type and *plaD*$^{-}$ mutant in competitive infections of *A. castellanii* amoebae ***(A)*** and RAW264.7 mouse macrophages ***(B)*** was monitored over 72 h by CFU determination. Infections were performed at an MOI of 0.1 in *A. castellanii* amoebae and at an MOI of 1 in RAW264.7 mouse macrophages. Results are displayed as mean and standard deviation of technical triplicates and are representative for two additional experiments.

In sum, both *L. pneumophila* wild type and *plaD*$^{-}$ mutant replicated intracellularly in *A. castellanii* amoebae and RAW264.7 mouse macrophages with a slight advantage of the *plaD*$^{-}$ mutant in the beginning of the single infections of *A. castellanii* amoebae. In coinfections, the *L. pneumophila plaD*$^{-}$ mutant outcompeted the wild type strain within 24 h.

3.2.2 Purification of recombinant PlaD and activity analyses

3.2.2.1 Purified rPlaD is not very stable

For further biochemical characterization and determination of its 3D-structure rPlaD was purified via an N-terminal Strep-tag after recombinant production in *E. coli* BL21. Additionally, rPlaD^{S17N}, a variant with site-directed mutation of the predicted catalytic serine, was purified. For ease of reading, the purified recombinant proteins are denoted as Strep-rPlaD and Strep-rPlaD variants only in the figure legends while they are denoted as rPlaD and rPlaD variants in the main text. Figure 21 shows

representative Coomassie-stained SDS-PAGEs of rPlaD (Figure 21A) and rPlaD^{S17N} (Figure 21B). Protein was eluted in fractions 2 to 5 with protein concentrations of up to 5 mg/ml. Intensive protein bands were visible at approximately 60 kDa which corresponds to the size of PlaD. However, additional distinct protein bands were visible at approximately 38 kDa in each protein containing fraction. Western blot analysis of the eluted rPlaD with an antibody directed against the N-terminal Strep-tag resulted in a similar band pattern as observed in the Coomassie-stained SDS-PAGEs (Figure 21C). A very strong band was detected at approximately 60 kDa and a weak protein band at approximately 38 kDa was observed as well.

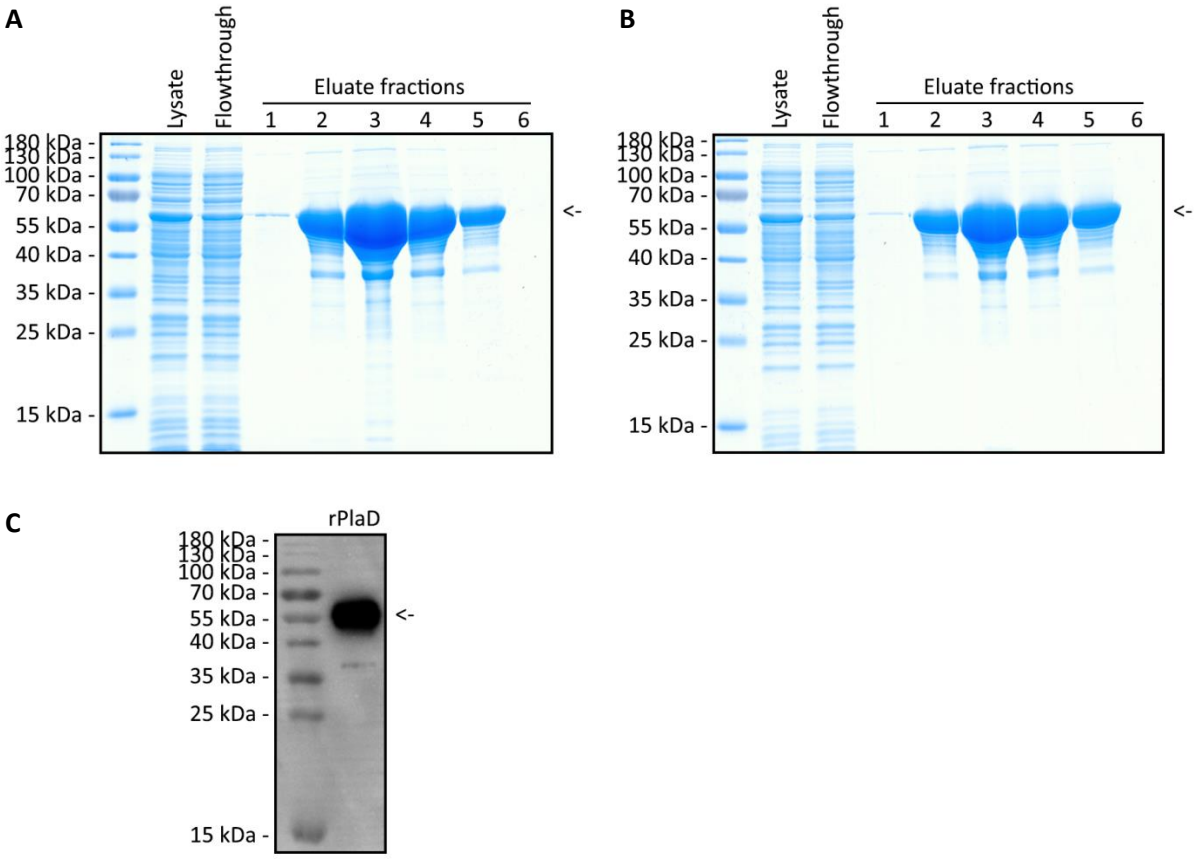

Figure 21: Strep-rPlaD and Strep-rPlaD^{S17N} are purified as highly concentrated but unstable proteins.
10 µl of *E. coli* lysate, the flowthrough collected during purification and each eluate fraction were subjected to SDS-PAGE with subsequent Coomassie-staining. Proteins were purified from production in *E. coli* clones BL21 (pGP172 *plaD* = pSB2) ***(A)*** and BL21 (pGP172 *plaD*^{S17N} = pSB4) ***(B)***. Additionally, 100 ng of Strep-rPlaD were subjected to Western blot analysis with an antibody directed against the N-terminal Strep-tag ***(C)***. Arrows denote the size of full length PlaD. The blot was trimmed from all sides. Representative of at least three replications.

Thus, it was shown that no major quantities of contaminating proteins were co-purified. Instead, rPlaD was purified as 60 kDa full length protein with an additional rPlaD protein fragment with lower molecular weight

3.2.2.2 Purified rPlaD shows weak LPLA and GCAT activity *in vitro*

As PlaD belongs to the family of GDSL hydrolases which are characterized by lipolytic enzyme activity, purified rPlaD was tested for lipase and GCAT activity towards the phospholipids PG and PC as well as the lysophospholipids LPG and LPC (Figure 22A and B). The results shown in Figure 22A were obtained after incubation of 50 µg rPlaD with LPG and LPC for 24 h which resulted in the generation of 1.2 and 0.8 mM FFA respectively. Application of rPlaD^{S17N} resulted in the generation of 0.3 mM FFA which was distinctly lower than observed for rPlaD but still elevated in comparison to the buffer control. In contrast, the level of FFA remained at background level after incubation of rPlaD or rPlaD^{S17N} with PG and PC (Figure 22A). Additionally, the generation of cholesterolpalmitate was detected after incubation of 100 µg rPlaD but not rPlaD^{S17N} with LPC in the presence of cholesterol (Figure 22B). In contrast, no transfer of long chain fatty acids was detected after incubation of rPlaD or rPlaD^{S17N} with any of the other tested lipids. Moreover, the transfer of short chain fatty acids to cholesterol resulting in the generation of chlolesterolpropionate was detected under all tested conditions. However, the intensity of the spots was strongest for incubation of rPlaD with LPG and LPC (Figure 22B). This indicates a weak LPLA and lysophospholipid-dependent GCAT activity of PlaD.

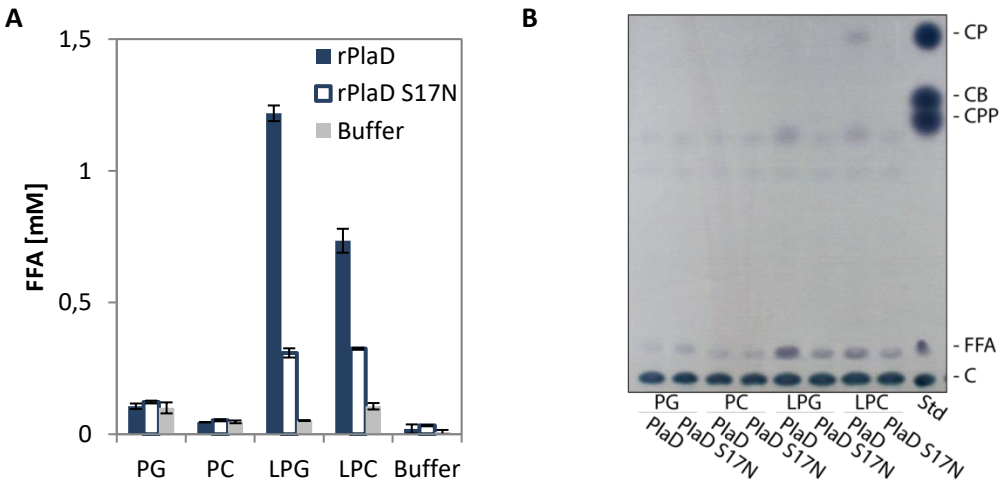

Figure 22: Strep-rPlaD shows weak LPLA and lysophospholipid-dependet GCAT activity.
Quantification of FFA was performed after incubation of 50 µg Strep-rPlaD or Strep-rPlaD^{S17N} with the indicated lipids for 16 h at 37 °C for determination of PLA and LPLA activity. The results represent the means and standard deviations of duplicate reactions ***(A)***. GCAT activity was analyzed via detection of cholesterol ester formation after incubation of 100 µg of Strep-rPlaD or Strep-rPlaD^{S17N} with the indicated lipids for 16 h at 37 °C, followed by lipid extraction and TLC ***(B)***. All results shown are representative for at least two additional experiments.

3.2.2.3 Purified rPlaD binds to PIPs but does not show activity towards them *in vitro*

As the above described enzyme activities of rPlaD were rather weak it was tested whether rPlaD would interact with other than the previously applied lipids. To this end, protein-lipid overlay assays were performed with rPlaD and rPlaD variants (Figure 23). These showed the binding of rPlaD and

rPlaD^{S17N} to PI, PI(4)P and PI(3,4,5)P_3. In contrast, an rPlaD version with truncation of the C-terminus from amino acids 376-516 (rPlaD$^{\Delta AA376-516)}$) did not interact with these lipids indicating that the binding is mediated by the C-terminal part of PlaD (Figure 23).

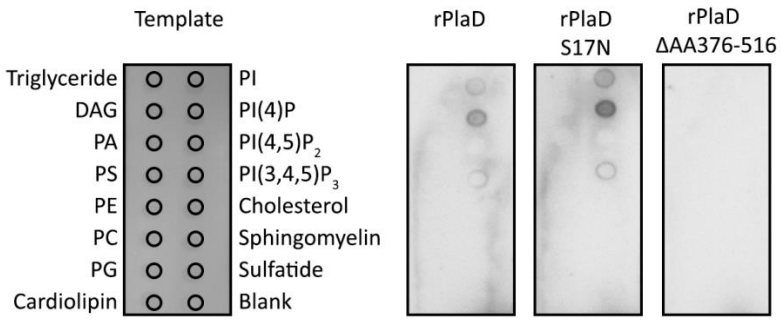

Figure 23: Strep-rPlaD and Strep-rPlaD^{S17N} bind to PI, PI(4)P and PI(3,4,5)P_3 in protein-lipid-overlay assays. Lipid strips which were loaded as shown for the template on the left side were incubated with 5 µg of Strep-rPlaD, Strep-rPlaD^{S17N} or Strep-rPlaD$^{\Delta AA376-516}$ for 1 h and subsequently probed with an antibody directed against the N-terminal Strep-tag of the recombinant proteins. The displayed results are representative for two additional experiments.

On that basis, it was analyzed whether rPlaD would hydrolyze different PI species (Figure 24A). However, under the tested conditions, the amount of FFA generated by rPlaD was only slightly increased in contrast to the buffer control and no differences between rPlaD and catalytic mutant rPlaD^{S17N} were observed. Additionally, it was tested whether PlaD might be involved in the dephosphorylation of PIPs. Therefore, the exhibition of phosphatase activity by rPlaD and rPlaD variants was tested with the substrate pNP-phosphate. Interestingly, all tested rPlaD variants resulted in substrate conversion and thus increased absorbance at 405 nm by the pNP-substrate. Some of the mutants exhibited even stronger activity towards the substrate than rPlaD itself (Figure 24B). Finally, it was tested whether rPlaD could directly dephosphorylate PIP species. To this end, PIPs were incubated without or with addition of rPlaD and subsequently analyzed by TLC. However, incubation with rPlaD did not affect the phosphorylation of the tested PIPs (Figure 24C).

3.2.2.4 Purified rPlaD shows very weak deacetylase activity *in vitro*

Additionally, it was analyzed whether rPlaD would recognize short fatty acids as substrate. Therefore, rPlaD was subjected to a deacetylase activity assay (Figure 25). HeLa cell lysate, provided with the assay, was used as positive control and caused an increase in the absorption at 405 nm to 0.3 as compared to the buffer control for which an absorption of 0.06 was measured. Incubation with 50 µg rPlaD only slightly increased the absorption at 405 nm to approximately 0.09. In contrast, the

absorption remained at background level when rPlaD^{S17N} was subjected to the assay. Addition of 1 mM $ZnCl_2$ or 1 mM NAD^+ to the assay did not affect the results.

Taken together, the biochemical activity assays performed with rPlaD showed that rPlaD exhibits weak LPLA and GCAT activity and binds to but does not react with PI(4)P. Moreover, a phosphatase activity that is independent of the predicted catalytic triad and the C-terminus of the protein was indicated. Lastly, rPlaD induced a very weak deacetylase activity that depended on the predicted catalytic serine S17. However, importantly, all descirbed activities could only be detected when at least 50 µg of recombinant protein were applied.

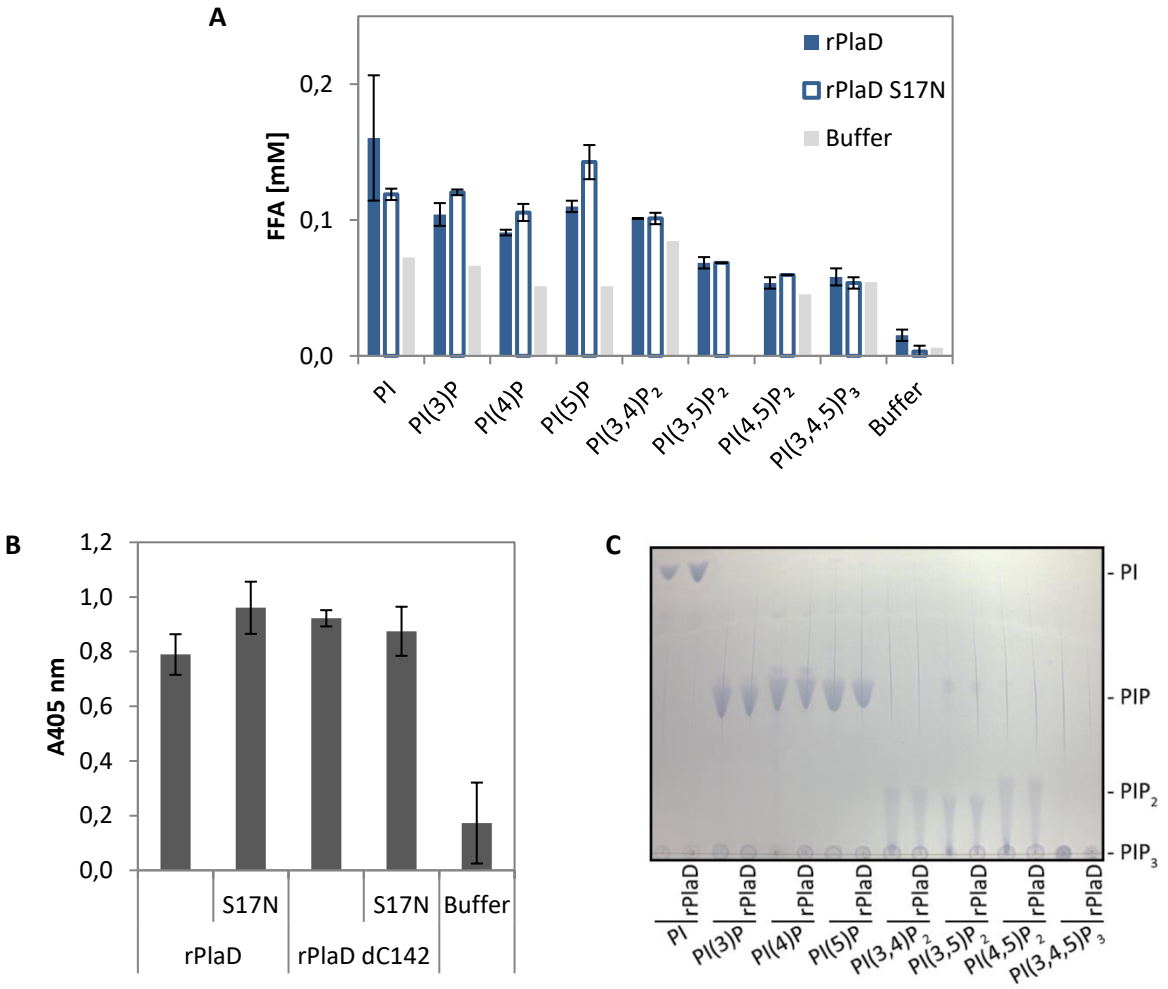

Figure 24: Strep-rPlaD shows weak posphatase activity independent of the predicted catalytic serin. Quantification of FFA was performed after incubation 50 µg Strep-rPlaD or Strep-rPlaD^{S17N} with the indicated PIP species for 16 h at 37 °C ***(A)***. 50 µg of Strep-rPlaD, Strep-rPlaD^{S17N}, Strep-rPlaD$^{\Delta AA376-516}$ and Strep-rPlaD$^{S17N\ \Delta AA376-516}$ were incubated with pNP-phosphate for 24 h at 37 °C and substrate conversion was measured via absorption at 405 nm ***(B)***. The phosphorylation status of PIPs after incubation without or with Strep-rPlaD for 24 h at 37 °C was analyzed via thin layer chromatography after lipid extraction ***(C)***.The results are displayed as means and standard deviation of technical duplicates ***(A, B)*** and are representative for one additional experiment.

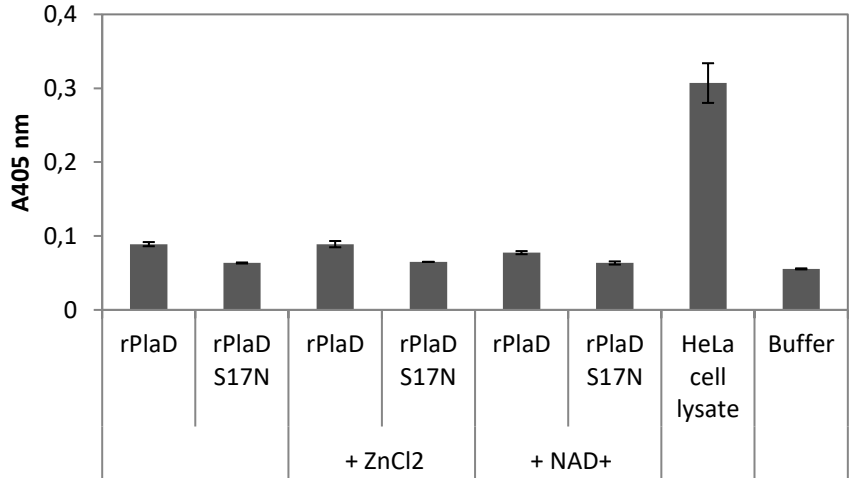

Figure 25: Strep-rPlaD shows minor deacetylase activity.
50 µg of Strep-rPlaD or Strep-rPlaD^{S17N} without or with addition of 1 mM $ZnCl_2$ or 1 mM NAD^+ were applied for analysis of deacetylase activity with the HDAC Activity Colorimetric Assay Kit. Incubation was performed for 1 h at 37 °C. HeLa cell lysate was supplied in the kit as positive control. The results are displayed as mean and standard deviation of duplicate reactions and are representative for one additional experiment.

3.2.3 An alpha/beta hydrolase fold is predicted for PlaD

Purified rPlaD was sent for crystallization to cooperation partners Maurice Diwo and Prof. Wulf Blankenfeld at the Helmholtz Centre for Infection Research in Braunschweig. However, due to the instability of the protein, crystallization was not possible. Instead, the "Phyre 2 server" (Kelley et al., 2015) was used to predict a 3D model for PlaD (Figure 26). The program was run on intensive mode and produced a final model where 66 % of the protein was modeled with > 90 % confidence. This corresponds to the N-terminal domain ranging from the N-terminus of the protein to helix a11 which is colored with a continuous gradient from blue to red in the topology diagram in Figure 26A. The crystal structures of a GDSL hydrolase of *Photobacterium sp.* J15 (PDB code 5xtu) and of EstA from *Pseudomonas aeruginosa* (PDB code 3kvn) were used as templates for this domain. The C-terminal domain of the protein ranging from helix a12 to the C-terminus was modeled *ab initio* without template and is depicted completely in red in the topology diagram (Figure 26A).Figure 26B shows the predicted 3D model of PlaD in cartoon view with the N-terminal domain in blue and the C-terminal domain in light blue. The predicted catalytic triad of PlaD is shown as sticks and highlighted in yellow. The model for PlaD has a compact shape and consists of 19 alpha helices and 7 beta sheets indicating a classical alpha/beta hydrolase fold. Superposition of the model for PlaD with the crystal structure of rPlaA revealed high similarity. Even the predicted catalytic triads of both proteins are present in the same location as can be seen in Figure 26C. However, while the predicted

catalytic triad of rPlaA, highlighted in red, is covered by a disulfide loop no such structure is present in the 3D model of PlaD.

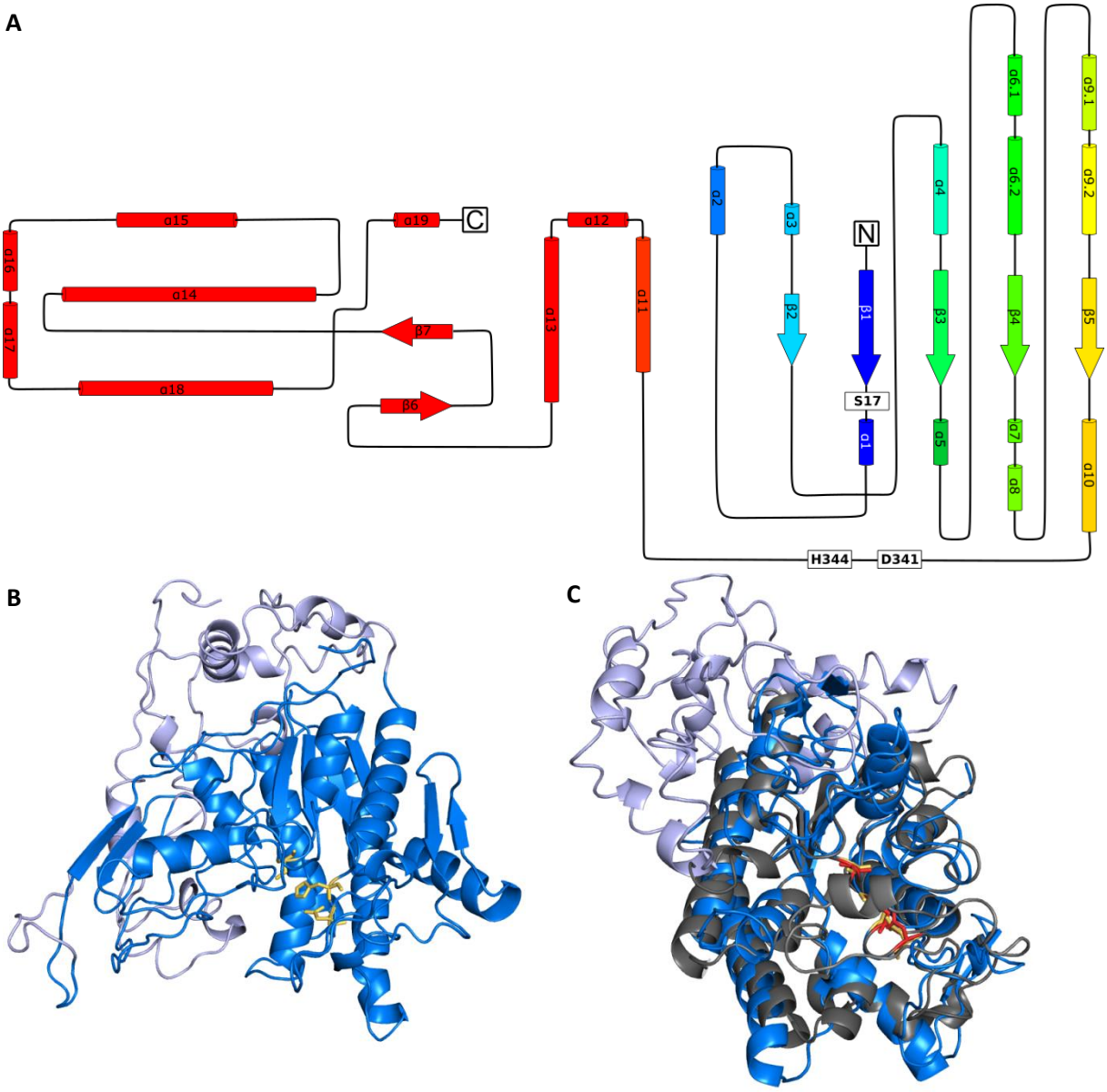

Figure 26: Predicted model for the 3D structure of PlaD.
The 3D structure of PlaD was predicted using the "Phyre 2 server" (Kelley et al., 2015). The topology diagram ***(A)*** illustrates the division of PlaD into an N-terminal and a C-terminal domain. Alpha helices and beta sheets are each numbered consecutively and shown as cylinders and arrows respectively. The N-terminal domain ranges domain from the N-terminus to helix a11 and is colored in a continuous gradient from blue to red. The amino acids of the predicted catalytic triad S17, D341 and H344 are highlighted. The predicted 3D structure of PlaD is additionally displayed in cartoon view where parts modeled with 100 % confidence are shown in blue and *ab initio* modeled parts in light blue ***(B)***. Superposition with the crystal structure of PlaA, shown in grey, is displayed in ***(C)***. The side chains of the predicted catalytic triad of PlaD are highlighted in yellow ***(A, B)*** and those of PlaA are highlighted in red ***(B)***.

3.2.4 PlaD interacts with the host cell

3.2.4.1 PlaD is injected into the host cell cytoplasm in a Dot/Icm dependent manner

As described previously (1.2.4.2.3) the *L. pneumophila* GDSL hydrolase PlaD, in contrast to PlaA and PlaC, is not type II-secreted (Lang et al., 2017). The protein possesses a stretch of approximately 170 amino acids in the C-terminal part of the protein after the predicted catalytic triad which is typical for type IVB-secreted phospholipases such as the *L. pneumophila* phospholipase PlcC/CegC1 (Altman and Segal, 2008; Heidtman et al., 2009). Moreover, an ortholog of PlaD in *L. longbeachae* had been predicted to be T4BSS secreted (Lifshitz et al., 2013). Thus, the suspected type IVB-secretion of PlaD was analyzed with a TEM1 beta-lactamase translocation assay (2.2.16, Figure 27). The assay was performed in RAW264.7 mouse macrophages that were infected with *L. pneumophila* wild type, *plaD*$^{-}$ or *dotA*$^{-}$ producing TEM1-fusion proteins.

The results obtained from the assay (Figure 27A) were normalized to uninfected cells resulting in a "Response Ratio" of 1 for this sample. As expected, the "Response Ratio" remained at background level after infection of RAW264.7 mouse macrophages with the negative control (Lpn WT (TEM1-FabI)). In contrast, infection with the positive control (Lpn WT (TEM1-LPC1331)) resulted in an increase of the "Response Ratio" to a value of approximately 3.5. Infection of RAW264.7 mouse macrophages with *L. pneumophila* wild type or *plaD*$^{-}$ mutant producing TEM1-PlaD resulted in an increase of the "Response Ratio" to 2.1 and 2.8 respectively. In contrast, no increase of the "Response Ratio" was detected after infection with the TEM1-PlaD producing *dotA*$^{-}$ mutant which has a defective T4BSS. Additionally, the translocation of PlaD variants with site directed mutation of the predicted catalytic triad (TEM1-PlaD$^{S17N\ H344N}$) or truncation of the C-terminus (TEM1-PlaD$^{\Delta AA468-516}$) was analyzed. That length of truncation was chosen because translocation signals are usually found in the distal C-terminus. Production of TEM1-PlaD with site directed mutation of the predicted catalytic triad in *L. pneumophila* wild type and *plaD*$^{-}$ did result in an increased "Response Ratio" with values of 1.7 and 3.1 respectively while production in the *dotA*$^{-}$ mutant did not result in increase of the "Response Ratio". Interestingly, the production of the C-terminally truncated version TEM1-PlaD$^{\Delta AA468-516}$ did not lead to an increase of the "Response Ratio" in any of the tested *L. pneumophila* strains. All above described results were reflected in the epifluorescence images (Figure 27). Green fluorescence of cells was visible after direct emission of the fluorescein part of the dye under all conditions. In contrast, blue fluorescence of the coumarin part of the dye was only observed after loss of FRET. This was only the case after infection of cells with the positive control (Lpn WT (TEM1-LPC1331)) and *L. pneumophila* wild type and *plaD*$^{-}$ producing TEM1-PlaD or TEM1-PlaD$^{S17N\ H344N}$.

Overall, it was shown that PlaD is injected into the host cell cytoplasm which is independent of the predicted catalytic triad but depends on the distal C-terminus of the protein.

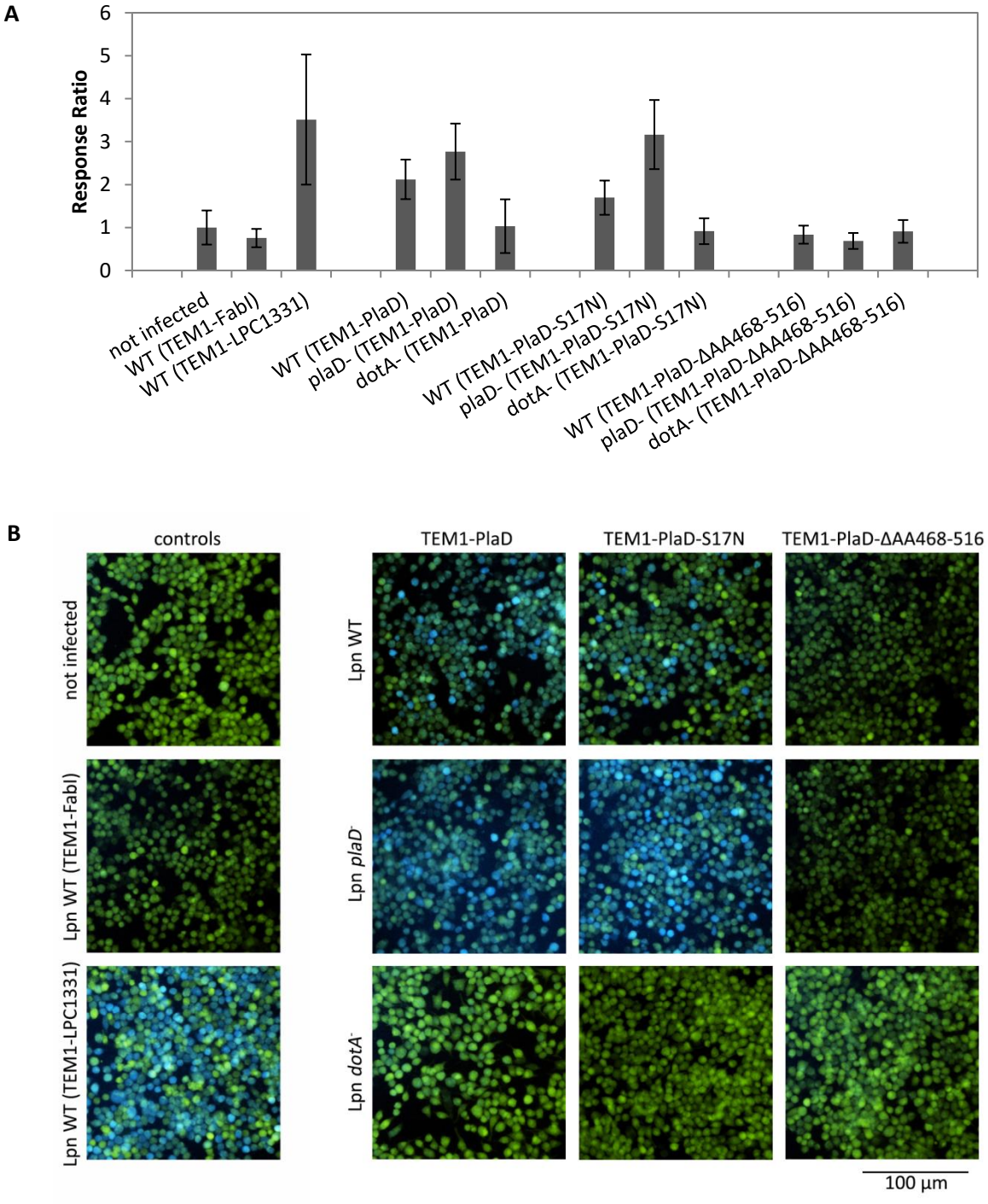

Figure 27: Dot/Icm dependent translocation of PlaD into the cytoplasm of RAW264.7 mouse macrophages. RAW264.7 macrophages were infected with *L. pneumophila* wild type, *plaD*$^-$ or *dotA*$^-$ producing TEM1-fusion proteins at an MOI of 100 for 1 h. Cells were loaded with CCF4/AM and translocation of the TEM1-fusions was determined by measuring the ratio of cleaved (450 nm) to uncleaved (520 nm) CCF4/AM. These are given as "Response Ratio" in arbitrary fluorescence units where a ratio > 1 indicates translocation ***(A)***. Representative epifluorescence images of the assay are shown in ***(B)***. The results represent the means and standard deviation of technical triplicates and are representative for at least three additional experiments.

3.2.4.2 PlaD specifically interacts with eukaryotic 14-3-3 proteins

As it has been shown that PlaD is injected into the host cell cytoplasm, interactions with host cell proteins were expected. This was analyzed via BioID assay (2.2.17.1) in cooperation with Dr. Jörg Döllinger from the proteomics service (ZBS6) of the Robert Koch-Institut. Hits were then verified via pull-down assays (2.2.17.2).

Biotinylated proteins were purified from uninfected and infected A549 epithelial cells without or with ectopic expression of BirA*-PlaD or BirA* and analyzed via mass spectrometry (Figure 28). Analysis was performed separately for proteins purified from uninfected cells and cells infected with *L. pneumophila* wild type. In both cases, BirA*-PlaD-expressing cells were compared to non-transfected and to BirA*-expressing cells individually. This created four categories for the evaluation of the BioID assay. The first category compared uninfected, BirA*-PlaD-expressing with uninfected, non-transfected cells. There, 7 significantly enriched proteins were detected. The second category compared uninfected, BirA*-PlaD-expressing with uninfected, BirA*-expressing cells. 11 significantly enriched proteins were detected in that category. The third category compared infected, BirA*-PlaD-expressing with infected, non-transfected cells and contained 8 significantly enriched proteins. The fourth category compared infected, BirA*-PlaD-expressing with infected, BirA*-expressing cells. There, 293 significantly enriched proteins were detected. Overall, the fold changes ranged from 1.2 to 14.7. A complete list of all significantly upregulated proteins can be found in the supplement (Table 37-Table 40). Figure 28 displays the numbers of proteins that were significantly increased in the BirA*-PlaD-expressing cells in each category as well as the overlap of the categories.

Interestingly, 6 proteins were identified as significantly increased in all four categories. Moreover, these were the proteins with the highest detected fold changes. These were 6 isoforms of the 14-3-3 protein family. This protein family consists of 7 isoforms in total. The isoform 14-3-3 sigma was detected only in the fourth category and was enriched with a fold change of 2. Overall, the results clearly indicated an interaction of PlaD with eukaryotic 14-3-3 proteins.

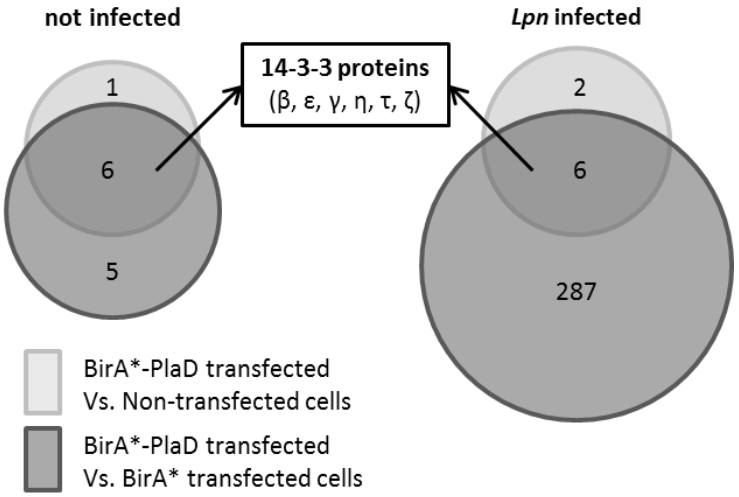

Figure 28: BioID assay identifies eukaryotic 14-3-3 proteins as interaction partner of PlaD.
Biotinylated proteins were purified from A549 human lung type II epithelial cells without or with ectopic expression of the promiscuous biotin ligase BirA* or BirA*-PlaD and analyzed via mass spectrometry by Dr. Jörg Döllinger the proteomics service of the Robert Koch-Institut. This was performed with uninfected cells and cells that had been infected with *L. pneumophila* wild type. The displayed venn diagram shows the number of proteins that were detected as significantly enriched in a false discovery rate controlled t-test in BirA*-PlaD expressing cells as compared to BirA* expressing (dark grey) or untransfected cells (light grey) without or with additional infection with *L. pneumophila* wild type. The BioID assay was performed once with technical triplicates.

The interaction of PlaD with 14-3-3 proteins was confirmed with pull-down assays (Figure 29). Here, N-terminally Strep-tagged rPlaD was immobilized onto Strep-Tactin beads as bait and cell lysates generated from A549 human lung type II epithelial cells, RAW264.7 mouse macrophages and *A. castellanii* amoebae were used as prey. Strep-Tactin without immobilized rPlaD was used as control. The Western blot in Figure 29A shows that the 14-3-3 proteins were detected only in samples that contained both rPlaD as bait and the eukaryotic cell lysates as prey but not in those samples that lacked the eukaryotic cell lysates or rPlaD. This confirmed the interaction of rPlaD with eukaryotic 14-3-3 proteins. The protein band for the 14-3-3 proteins from *A. castellanii* amoebae is considerably weaker than those of 14-3-3 proteins from A549 human lung type II epithelial cells or RAW264.7 mouse macrophages. However, this might be explained by the species specificity of the applied antibody which is directed against human and mouse but seems to cross-react with the 14-3-3 protein from amoeba. Moreover, it was shown that not only rPlaD but also the variant with site-directed mutagenesis of the predicted catalytic serine (rPlaD^{S17N}) interacted with the 14-3-3 proteins from RAW264.7 mouse macrophages (Figure 29B). In contrast, no interaction was observed when rPlaA was used as bait (Figure 29C). Additionally, eluates obtained from pull-down assays performed with rPlaD as bait and cell lysates of A549 human lung type II epithelial cells as prey were analyzed via mass spectrometry in cooperation with Dr. Jörg Döllinger the proteomics service (ZBS6) of the Robert Koch-Institut. A list of all detected proteins can be found in the supplement (Table 41).

This analysis also confirmed the interaction of rPlaD with the 14-3-3 proteins. Interestingly, no other interacting proteins were detected in that assay.

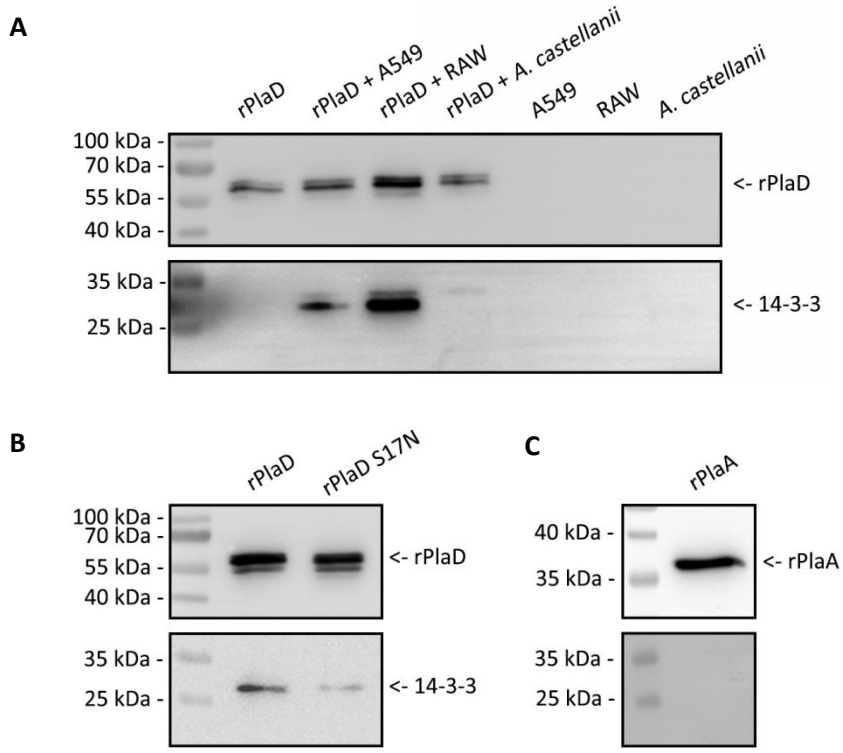

Figure 29: Strep-rPlaD interacts with 14-3-3 proteins from multiple eukaryotic host cells.
Purified Strep-rPlaD ***(A, B)***, Strep-rPlaD^{S17N} ***(B)*** and Strep-rPlaA ***(C)*** were immobilized onto Strep-Tactin beads as bait for a pull-down assay and cell lysates prepared from A549 human lung type II epithelial cells, RAW264.7 mouse macrophages or *A. castellanii* amoebae were used prey. The eluted proteins were analyzed by Western blot with antibodies directed against the N-terminal Strep-tag of the recombinant proteins and against 14-3-3 proteins. The blots were trimmed from all sides. The displayed results are representative for one ***(A, C)*** or two ***(B)*** additional experiments.

Next, candidate 14-3-3-binding sites within the sequence of PlaD were predicted using the webserver 14-3-3-Pred (Madeira et al., 2015) (Figure 30A). Seven binding sites were predicted which are distributed over the entire sequence of PlaD. Scores of the individual candidate 14-3-3-binding sites ranged from 0.279 to 0.631 and are given in Figure 30A. Importantly, higher scores indicate a higher certainty of the predicted binding site. On that basis, PlaD variants with site directed mutations of the candidate 14-3-3-binding sites were generated. These were produced as single and multiplex mutants. In the multiplex mutants, mutations were inserted in order of the scores of the predicted binding sites. Application of rPlaD variants with site directed mutations of individual candidate 14-3-3-binding sites as bait for the pull-down assay still resulted in the co-purification of 14-3-3 proteins from RAW264.7 mouse macrophages (Figure 30B). Importantly, all rPlaD variants were purified to similar extents (Figure 30B). However, the efficiency of 14-3-3 protein co-purification varied. Particularly the application of rPlaD^{T141A} as bait resulted in a noticeable reduction of 14-3-3 protein

co-purification (Figure 30B). Interestingly, a rather low score of 0.361 was predicted for this candidate 14-3-3-binding site (Figure 30A). Additionally, multiplex mutants with site-directed mutations of 2 to 7 of the predicted 14-3-3-binding sites were tested in the pull-down assay (Figure 30C). Interestingly, only the double and triple mutants were purified properly. The other applied multiplex mutants were either not purified at all or to a very small extent. The rPlaD double mutant, with S45A- and S251A-mutations, did interact with the 14-3-3 proteins from RAW264.7 macrophages. In contrast, co-purification of the 14-3-3 proteins failed when the rPlaD triple mutant, with an additional T180A-mutation, was applied as bait for the pull-down assay (Figure 30C).

A

#	motif	score
#1	SGLRSK[S_{45}]PKGR	0,631
#2	DEQRNA[S_{251}]DCTE	0,508
#3	NLEKSE[T_{180}]LVVE	0,467
#4	ENENSF[S_{108}]LNED	0,452
#5	GLISAF[T_{460}]LNPD	0,426
#6	DYSCSF[T_{141}]FNLV	0,361
#7	QQLQTK[S_{265}]LELI	0,279

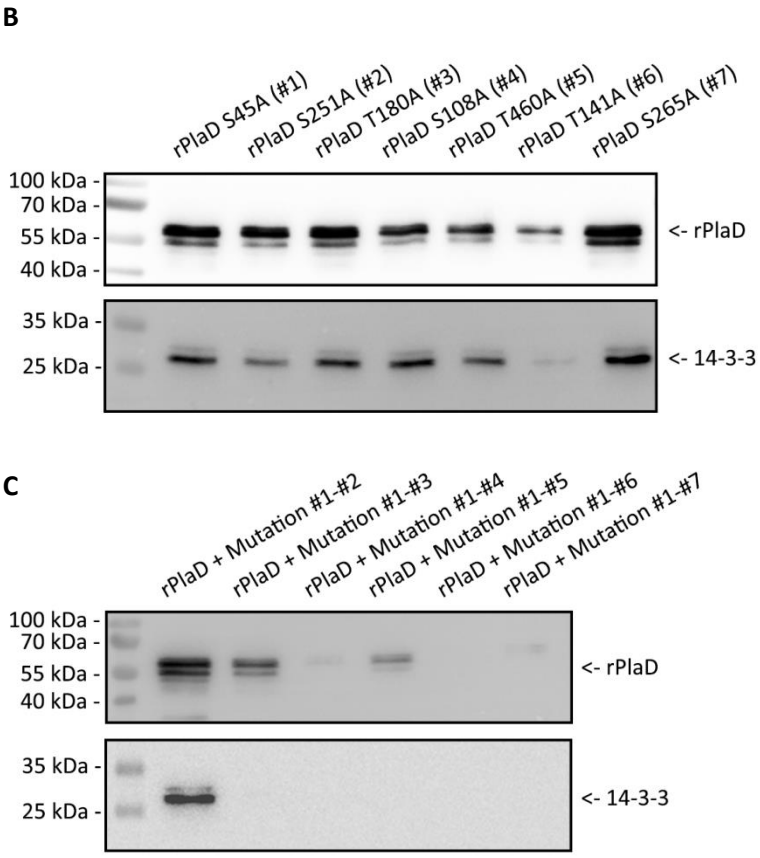

Figure 30: Binding of Strep-rPlaD to 14-3-3 proteins is prevented by mutation of three predicted binding sites.
Seven putative binding sites for 14-3-3 proteins were predicted within the sequence of PlaD using the webserver 14-3-3-Pred (Madeira et al., 2015). These are listed in ***(A)*** according to their score. The predicted binding sites were mutated individually ***(B)*** or in combinations ***(C)*** in Strep-rPlaD and these Strep-rPlaD variants were then used as bait for pull-down assays with lysates prepared from RAW264.7 mouse macrophages as prey. Samples were analyzed via Western blotting with specific antibodies directed against the N-terminal Strep-tag of the recombinant proteins as well as the 14-3-3 proteins. The blots were trimmed from all sides. The displayed results are representative for two additional experiments.

3.2.4.3 PlaD is involved in inhibition of host cell apoptosis

As shown above, PlaD interacts with eukaryotic 14-3-3 proteins which are implicated in multiple cellular functions including inhibition of apoptosis (Pennington et al., 2018b). Additionally, it was described that infection with *L. pneumophila* protects host cells from exogenous cell death stimuli

(Banga et al., 2007). On that basis, it was investigated whether presence or absence of PlaD has an influence on host cell apoptosis.

To this end, caspase-3 activity in RAW264.7 mouse macrophages was monitored as hallmark for induction of apoptosis (2.2.19.1). Here, cells infected with *L. pneumophila* wild type or *plaD*$^-$ were compared to untreated and etoposide-treated cells over a period of 55 h (Figure 31A and B). Treatment with topoisomerase II inhibitor etoposide was used as positive control for induction of apoptosis. Already 8 h after etoposide-treatment of cells an increase in fluorescence emission was observed. The fluorescence emission in etoposide-treated cells was further increased after 22 and 28 h and dropped to the level of untreated cells after 48 h. The strongest fluorescence emission with a 5-fold increase in comparison to untreated cells was detected 22 h after treatment. Fluorescence emission from cells infected with *L. pneumophila* wild type remained at the level of untreated cells for 48 h and was increased 1.5-fold in comparison to untreated cells after 55 h. In contrast, the fluorescence emission from cells infected with *L. pneumophila plaD*$^-$ was increased by a factor of 2.2 in comparison to untreated cells already 22 h post infection. From 28 h onwards fluorescence emission in these cells remained elevated by a factor of 1.7. In addition to the evaluation of fluorescence emission, cells were inspected microscopically 24 h after treatment (Figure 31B). There, the above described differences in fluorescence emission were confirmed. Only a minor portion of untreated and *L. pneumophila* wild type infected cells showed fluorescence of the cleaved caspase-3 substrate. In contrast, a noticeably larger portion of fluorescent cells was observed in response to treatment with etoposide or infection with *L. pneumophila plaD*$^-$.

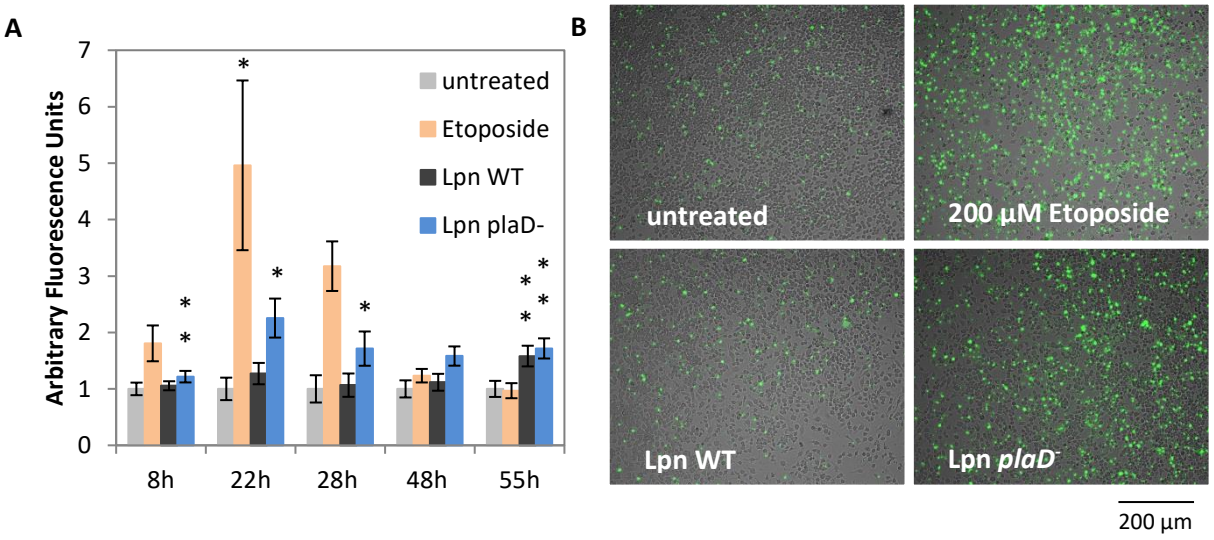

Figure 31: Infection with *L. pneumophila plaD*$^-$ causes increases host cell apoptosis.
Caspase-3 activity was monitored over a period of 55 h in untreated RAW264.7 mouse macrophages and in response to apoptosis induction with 200 µM etoposide or infection with *L. pneumophila* wild type or *plaD*$^-$ at an MOI of 1. Fluorescence intensities are given in arbitrary fluorescence units and are normalized to untreated cells. Statistical evaluation was done via two-sided, paired t-test comparing treated to untreated cells for each time point (* p-value < 0.05, ** p-value < 0.01, n=2) ***(A)***. Representative epifluorescence images of cells that had been treated for 24 h are depicted in ***(B)***. Results are representative for two additional experiments.

Additionally it was analyzed whether the *plaD*$^{-}$ mutant, like *L. pneumophila* wild type, would be able to protect host cells from staurosporine-induced apoptosis (2.2.19.2). This was achieved by assessing chromatin condensation and nuclear fragmentation of RAW264.7 mouse macrophages that were either uninfected or infected with *L. pneumophila* wild type or *plaD*$^{-}$ prior to induction of apoptosis with 1 µM staurosporine (Figure 32A and B). In this assay, the protein kinase inhibitor staurosporine instead of etoposide was used for induction of apoptosis. However, the change of the apoptosis inductor was only due to easier handling. Control cells were either uninfected or infected like the samples but not treated with staurosporine. Importantly, no chromatin condensation or nuclear fragmentation was detected in uninfected or *L. pneumophila* wild type infected cells without addition of staurosporine. However, some apoptotic nuclei were detected after infection with *L. pneumophila plaD*$^{-}$ without addition of staurosporine. In uninfected cells treatment with staurosporine for 4 h resulted in apoptosis in approximately 30 % of the cells (Figure 32B). In cells that had been infected with *L. pneumophila* wild type prior to treatment with staurosporine only very few apoptotic nuclei were observed. Approximately 10 % of cells were apoptotic (Figure 32B). In contrast, infection with *L. pneumophila plaD*$^{-}$ prior to treatment with staurosporine resulted in approximately 45 % of apoptotic cells (Figure 32B). This was an even larger portion than observed in uninfected and staurosporine-treated cells.

Overall it was shown that, in contrast to *L. pneumophila* wild type, the *plaD*$^{-}$ mutant induced stronger apoptosis in host cells and was unable to protect host cells from staurosporine-induced apoptosis. Thus, it was concluded that PlaD is involved in inhibition of host cell apoptosis.

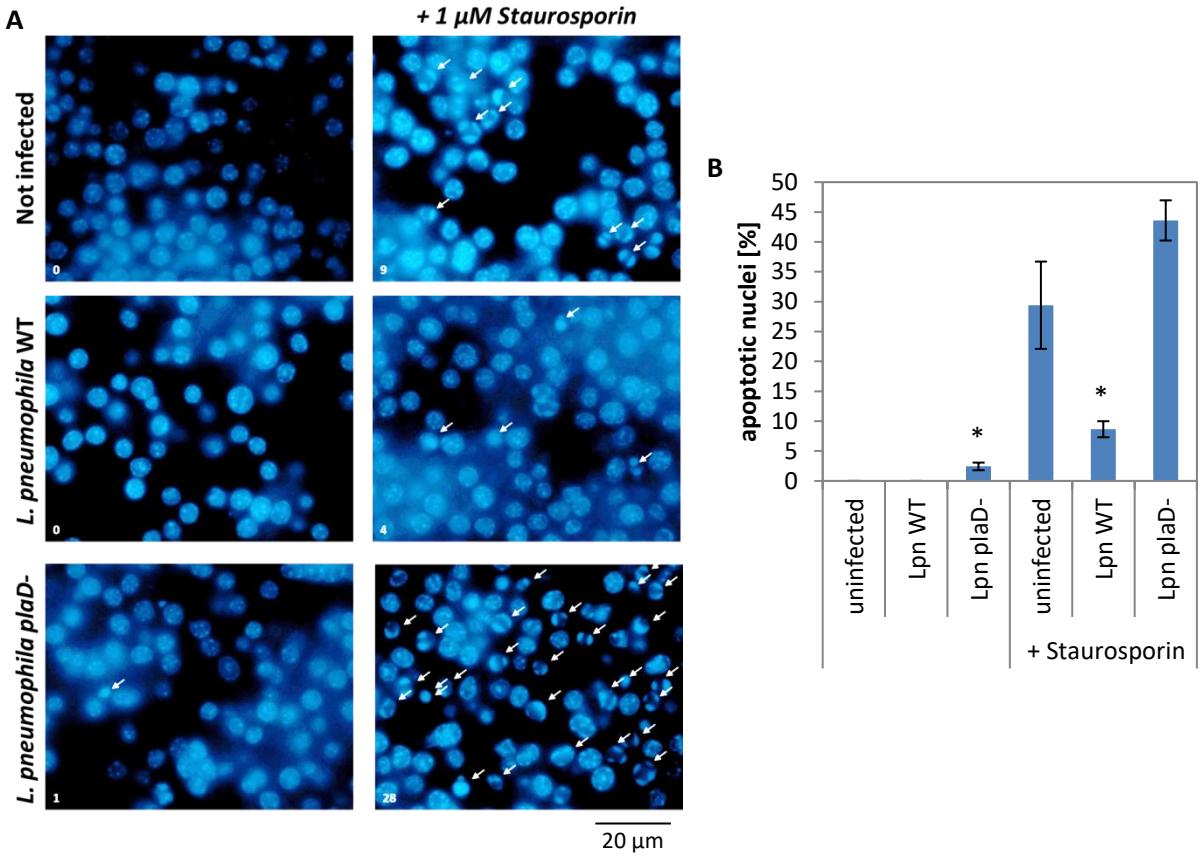

Figure 32: Infection with *L. pneumophila* wild type but not *plaD*$^-$ prevents staurosporine-induced apoptosis. RAW264.7 mouse macrophages or cells that had been infected with *L. pneumophila* wild type or *plaD*$^-$ at an MOI of 1 for 8 h were further incubated without or with addition of 1 µM staurosporin for 4 h followed by PFA fixation and DAPI staining of nuclei ***(A)***. Apoptotic nuclei are marked by white arrows and quantified ***(A, B)***. Statistical evaluation was done via two-sided, paired t-test comparing Lpn infected to uninfected cells for untreated and staurosporin-treated cells (* p-value < 0.05, n=2) ***(B)***. The displayed data are representative for two additional experiments.

4 Discussion

4.1 Characterization of PlaA

4.1.1 All three amino acids of the predicted catalytic triad of PlaA are required for activity

As described before, the family of GDSL hydrolases is characterized by a conserved amino acid motif (Upton and Buckley, 1995). This allowed the prediction of the amino acid residues S30, D279 and H282 as the catalytic triad of PlaA. The predicted catalytic serine S30 is located near the N-terminus of the protein while the residues D279 and H282 are located closer to the C-terminus. It was assumed that the three amino acids of the predicted catalytic triad would be located in close proximity in the folded protein. This was confirmed by the crystal structure of rPlaA (Figure 10).

Moreover, during this thesis, it was shown that PlaA is processed by ProA and the disulfide loop within the C-terminal half of PlaA was determined as the site of processing (Figure 13, Figure 14). Importantly, one main and six minor cleavage positions were detected and mutation of the main cleavage site was not sufficient to prevent processing by rProA (Lang et al., 2017). Thus, it can be concluded that ProA recognizes the structure of the disulfide loop rather than a specific amino acid sequence. This is comparable to the mechanism proposed for the processing of rPlaC by rProA (Lang et al., 2012).

In previous studies it had been shown that PlaA contains an LPLA activity (Flieger et al., 2001a; Flieger et al., 2001b; Flieger et al., 2002). This phenotype was confirmed with rPlaA during this thesis (Lang et al., 2017) (Figure 7, Figure 9). The LPLA activity of rPlaA was reduced to background level when individual residues of the predicted catalytic triad were mutated (Figure 7). This indicated that all three amino acids of the predicted catalytic triad are essential for activity of PlaA (Lang et al., 2017). Interestingly, the activity of the PlaA^{S30N} mutant was not rescued by the serine residue S32 which is located directly adjacent to the GDSL motif. Thus, it may be assumed that the exact orientation of the amino acids within the active center is important for execution of activity. Moreover, presence of rProA in the activity assays increased the LPLA activity of rPlaA (Figure 12). A similar behavior was already shown for rPlaC which exhibits increased PLA and GCAT activity in the presence of rProA (Lang et al., 2012). In contrast, previous studies also described a weak PLA activity for PlaA (Flieger et al., 2001b) which was not observed in activity assays performed with rPlaA during this thesis. It may be assumed that the weak PLA activity observed in previous studies might have been caused by another enzyme. In addition, a lysophospholipid-dependent GCAT activity was detected for rPlaA which had not been described in previous studies (Figure 9). The lipids applied in the assays contained palmitic acids. Thus, the generation of cholesterolpalmitate was observed. However, the

transfer of the short chain fatty acid propionic acid to cholesterol was observed in addition (Lang et al., 2017) (Figure 9). So far, the source of the propionic acid has not been elucidated. Although the applied lipid substrates are >99 % pure there might be a contamination with traces of propionic acid. Interestingly, the transfer of palmitic acid to cholesterol was diminished after ProA-processing of PlaA while the transfer of propionic acid was unaffected (Figure 12). This might point towards distinct mechanisms for the generation of cholesterolpalmitate and cholesterolpropionate. Similarly, it has been described for various enzymes, that they show distinct specificities towards substrates with different fatty acid chain lengths (Gjellesvik, 1991; Souza et al., 2014). For example the secreted lipase LAB01 of *Aspergillus japonicus* showed a preference towards substrates with long chain fatty acids and the activity decreased with decreasing length of the fatty acid chains (Souza et al., 2014). Similarly, it may be possible that PlaA also shows distinct preferences towards different fatty acid chain lengths.

4.1.2 Model for the secretion and activation of PlaA

The data generated by comparing *L. pneumophila* wild type with an isogenic *plaA*$^-$ mutant strain and by use of recombinant PlaA resulted in the following model for the secretion and activation mechanism of PlaA (Figure 33) (Lang et al., 2017).

PlaA is present in the cytoplasm of *L. pneumophila* as preproform with an N-terminal signal peptide for the Sec-dependent secretion. This signal peptide is cleaved off in the periplasm. There, a disulfide loop within the C-terminal half of PlaA is formed and the protein obtains its tertiary structure. This PlaA proform is secreted across the outer membrane of *L. pneumophila* via the T2SS and contains LPLA and lysophospholipid-dependent GCAT activity. Finally, the PlaA proform is processed within the disulfide loop by the T2SS secreted zinc metalloproteinase ProA. This generates the mature form of PlaA which is characterized by increased LPLA activity but does not show GCAT activity anymore. PlaA is present in the culture supernatant of *L. pneumophila* while it is expected to be present inside the lumen of the LCV during *L. pneumophila* infections of host cells. However, with regard to recent data which propose a permeabilization of the LCV membrane approximately 6 h post infection (Truchan et al., 2017) it may be speculated that PlaA could get access to the host cell cytoplasm at later time points during infection. Thus, it might be interesting to investigate whether and when PlaA can be detected in the host cell cytoplasm. This could be analyzed with the beta-Lactamase translocation assay that has been applied for the analysis of PlaD translocation during this thesis.

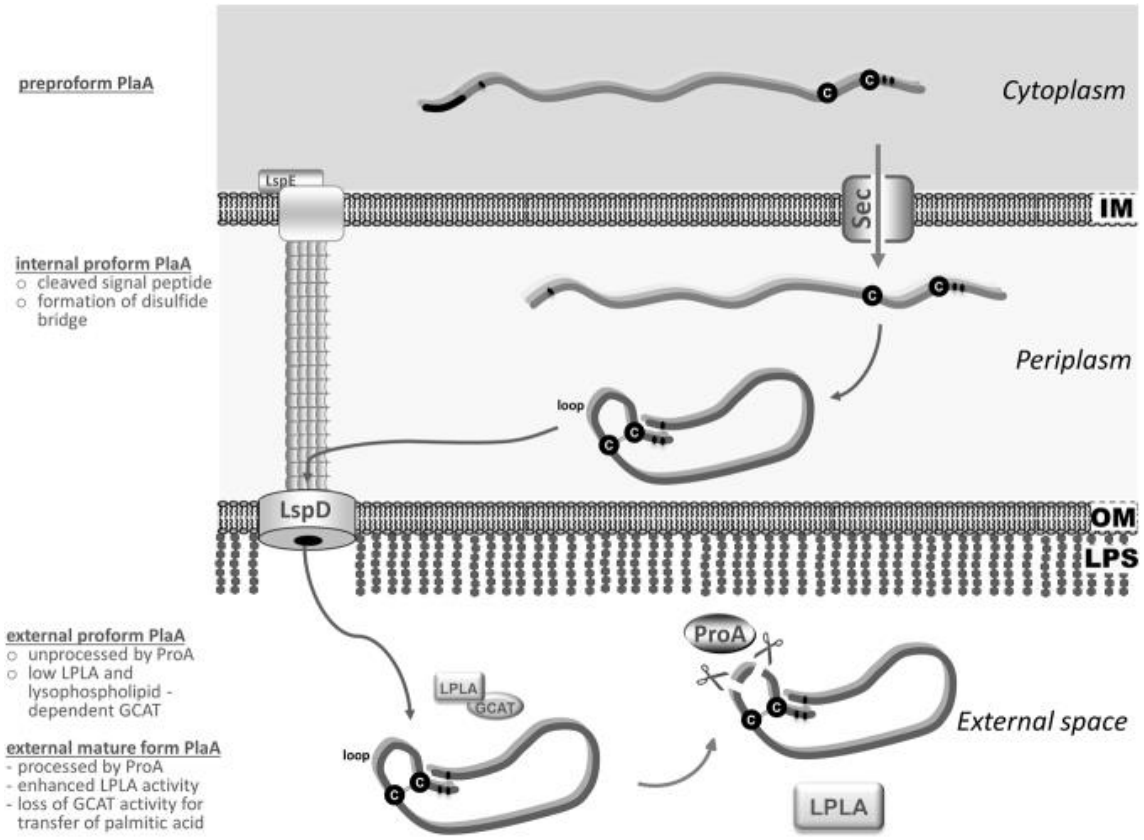

Figure 33: Model of the secretion and activation of PlaA.
PlaA and ProA are produced in the cytoplasm as preproforms and transported into the periplasmic space via the Sec system. Cleavages of the N-terminal signal peptides and formation of a disulfide bond within the C-terminal half of PlaA generates the internal proforms. Subsequently, both proteins are secreted via the T2SS into the extracellular space where ProA acquires its mature form via autoactivation. The external proform of PlaA exhibits LPLA and GCAT activity. Processing of PlaA by ProA within the disulfide loop then produces the mature form of PlaA which exhibits increased LPLA but no GCAT activity (Lang et al., 2017).

4.1.3 Altered PlaA activity may be related to conformational changes induced by ProA processing

The GCAT activity of rPlaA was only shown for the full-length protein. In contrast, rProA-processed rPlaA or the rPlaA variant with complete deletion of the disulfide loop rPlaA$^{\Delta AA248\text{-}67}$ both showed increased LPLA activity while no GCAT activity transferring palmitic acid was detected. In contrast, the transfer of propionic acid was still observed (Figure 12, Figure 17) (Lang et al., 2017). These results suggest the assumption that the intact disulfide loop is required for the transfer of palmitic acid to cholesterol while it reduces the LPLA activity of rPlaA.

Analysis of the rPlaA crystal structure revealed that the disulfide loop in the C-terminal half of the protein forms a lid which blocks the substrate entrance to the active site channel (Figure 10). Such lid structures are very common with lipases and are important for substrate specificity and control of enzymatic activity (Khan et al., 2017). Moreover, the crystal structure of rPlaA revealed several surface-exposed amino acid residues near the entrance to the active site channel which possibly are substrate contact sites. This potential binding domain is unstructured and located in close proximity

to the disulfide loop of full length rPlaA. It can be assumed that processing of the rPlaA disulfide loop by rProA might completely remove the lid or increase its flexibility. This might affect the conformation of the active site or the potential substrate-binding domain or both. Proteolytic processing is a common mechanism in many bacteria for activation of enzymes that have been produced as inactive zymogens (Vanaman and Bradshaw, 1999). Among others, the induction of enzymatic activity after processing within a disulfide loop has been shown for *Pseudomonas* exotoxin A and Shiga toxin from enterohemorrhagic *Escherichia coli* (Gordon and Leppla, 1994; Kurmanova et al., 2007; Ogata et al., 1992; van Deurs and Sandvig, 1995). Although full length rPlaA is not completely inactive it can be assumed that the rationale of rProA processing of rPlaA is to increase the enzymatic activity. It is conceivable that the access of lipid substrates to the active site channel of rPlaA is facilitated by the structural alterations induced by rProA processing which might explain the increased LPLA activity of processed rPlaA. Moreover, it could be speculated that conformational changes of the potential substrate-binding domain might reduce the binding affinity towards cholesterol. On the other hand, it is rather unlikely that binding of cholesterol is blocked completely as the transfer of propionic acid to cholesterol is still observed. Instead, it might be assumed that the lid is responsible for retaining the lipid substrates in the active site channel. Removal of the lid might then result in shorter length of stay of the lipid substrates in the active site channel which may be too short for the transfer of palmitic acid to cholesterol.

To verify the proposed conformational changes and changes of substrate binding affinities of rPlaA in response to disulfide loop cleavage it would be important to obtain crystal structures from rProA-processed rPlaA or from the loop deletion mutant rPlaA$^{\Delta AA248\text{-}67}$. Both approaches have been attempted during this thesis but have not been successful (data not shown). Processing of rPlaA with rProA during the purification step always resulted in a mixture of unprocessed and processed protein which impaired crystallization. Likewise, the crystallization of the loop deletion mutant rPlaA$^{\Delta AA248\text{-}67}$ was not possible under the tested conditions. Here, it might be beneficial to adjust the crystallization conditions. Moreover, a co-crystallization of rPlaA with cholesterolpalmitate, the reaction product of the GCAT activity, was attempted but was not successful either (data not shown). This might be due to steric hindrance as the amino acid residues that are suspected to be involved in substrate binding also form important crystal contacts. Additionally, it would be interesting to analyze binding affinities of rPlaA and rPlaA variants towards lysophospholipids and cholesterol. Here, it could be tested whether and how mutations of the suspected substrate binding sites affect binding affinities.

4.1.4 ProA processing of PlaA might allow for regulation of activity as a function of cell density

The above described model for PlaA secretion and activation raises the question of how *L. pneumophila* would benefit from the regulation of PlaA activity.

Approximately 10 % of all sequenced bacteria contain genes for the synthesis of hopanoids which are analogs of eukaryotic cholesterol (Gomez-Valero et al., 2014; Ourisson et al., 1979). Thus, it could be hypothesized that the GCAT activity of PlaA might be directed towards *L. pneumophila* itself. However, genes encoding for the biosysnthesis of hopanoids have not been detected in any *Legionella* species except for the apathogenic *L. fallonii* which does not contain the *plaA* gene (Gomez-Valero et al., 2014). Therefore it would be rather unlikely that the GCAT activity of PlaA is directed towards *L. pneumophila* itself. As described above, proteolytic processing of enzymes resulting in their activation is very common among bacteria and also viruses. This allows for the temporal and spatial control of enzyme activity (Vanaman and Bradshaw, 1999). It may be possible that the processing of PlaA by ProA serves a similar purpose. The processing might act as a molecular switch for the temporal regulation of PlaA activity.

Importantly, the kinetics of PlaA processing and activity *in vivo* are so far unknown. However, analyses of culture supernatants at multiple time points during *L. pneumophila* growth revealed that PlaA is initially secreted as full length protein. Processing was first detected during mid-exponential growth (Figure 16). It might be hypothesized that ProA-processing of PlaA occurs not before a critical density of bacteria is reached. Thus, ProA-processing of PlaA might act as a form of quorum sensing. Quorum sensing allows the regulation of gene expression patterns as a function of cell density and functions via the secretion of so called autoinducers. The concentration of these molecules increases with increasing cell density. When a critical cell density, indicated by a critical concentration of the autoinducer, is reached differential regulation of gene expression is stimulated (Miller and Bassler, 2001). *L. pneumophila* expresses the Lsq quorum sensing system which is important for the induction of virulence traits (Tiaden et al., 2008). A similar mechanism might be responsible for the ProA processing of PlaA. That way, processing of PlaA, which is accompanied by the activity switch, would only occur when a critical density of *L. pneumophila* inside the LCV is reached. It may be assumed that the increased LPLA activity of ProA processed PlaA would then prepare the LCV membrane for exit of *L. pneumophila*. The importance of PlaA for exit of *L. pneumophila* from the LCV will be discussed in the next chapter.

4.1.5 PlaA and SdhA adversely affect LCV integrity

Interestingly, it was shown that PlaA is responsible for the destabilization of the LCV in the absence of the T4BSS secreted effector SdhA which is associated with the LCV (Creasey and Isberg, 2012). SdhA deficient *L. pneumophila* is unable to replicate in murine bone-marrow derived macrophages due to impairment of the LCV with subsequent induction of host cell death pathways (Creasey and Isberg, 2012; Laguna et al., 2006). This phenotype was rescued by the additional deletion of PlaA (Creasey and Isberg, 2012). The mechanism of interaction between SdhA and PlaA and whether this interaction is direct or indirect is not known so far. It is conceivable that SdhA stabilizes the LCV membrane from the cytoplasmic side while PlaA acts from the inside of the LCV to destabilize the membrane resulting in maintenance of the LCV integrity. A similar mechanism occurs in *Salmonella enterica* spp. *enterica* serovar Typhimurium where SseJ, which shows homology to PlaA, destabilizes the vacuolar membrane in the absence of SifA (Ruiz-Albert et al., 2002). In general, it is important for intracellular pathogens to maintain the integrity of the vacuole to avoid detection by the immune system of the host (Roy, 2012). However, for the exit of the pathogen and the initiation of a new infection cycle, the vacuole needs to be disrupted (Flieger et al., 2018). Assuming that the opposing functions of SdhA and PlaA are balanced for maintaining the integrity of the LCV it can be supposed that a change of abundance or activity of either factor could result in exit of *L. pneumophila* from the LCV and subsequently the host cell. Both *sdhA* and *plaA* are expressed throughout bacterial replication (Bruggemann et al., 2006; Laguna et al., 2006). Additionally, the intact catalytic triad of PlaA is required for destabilization of the LCV (Creasey and Isberg, 2012). In this thesis it was shown that processing of rPlaA by rProA results in increased LPLA activity and decreased GCAT activity (Figure 12). It may be hypothesized that this switch of PlaA activity could disturb the balance between SdhA and PlaA in an infection and might thus lead to destabilization of the LCV. Unfortunately, to date, it is not known whether the activity and activation of PlaA in infection are comparable to that of the recombinant protein. To test this hypothesis, infection experiments could be performed with *L. pneumophila* expressing either inactive or hyperactive PlaA such as catalytic triad mutants or the loop deletion mutant. However, it is also possible that another, so far unknown, factor might be responsible for disturbing the balance between SdhA protection and PlaA destabilization of the LCV. Moreover, PlaA might also be involved in modification of the LCV membranes towards easier expansion or fusion with membrane vesicles (Lang et al., 2017).

4.1.6 Despite structural similarity *L. pneumophila* PlaA and *P. aeruginosa* EstA show distinct activities

Database searches for proteins with structural similarity towards rPlaA identified the *P. aeruginosa* esterase EstA and a putative lipolytic protein of GDSL family from *D. hafniense* DCB-2. Both enzymes belong to the family of GDSL hydrolases (Wilhelm et al., 2007). Thus, structural similarity might be expected to some degree. Unfortunately, no detailed characterization of the latter protein has been published to date. Therefore, PlaA is compared here only with EstA. EstA is an autotransporter and is divided into a β-barrel domain that is essential for transport and a passenger domain (van den Berg, 2010). This passenger domain is a catalytically active esterase which belongs to the family of GDSL hydrolases (van den Berg, 2010) and shows structural homology to PlaA. In contrast, the β-barrel domain of EstA shows no homology to PlaA. Both enzymes show predominantly alpha/beta folds. The passenger domain of EstA is not cleaved off after transport and thus remains bound to the outer membrane of *P. aeruginosa* (van den Berg, 2010) while PlaA is secreted into the external space by the T2SS of *L. pneumophila* (Lang et al., 2017). Interestingly, the active site of EstA is located on the surface of the protein at the entrance of a hydrophobic pocket that is supposed to be involved in substrate binding (van den Berg, 2010). In contrast to PlaA, the active site is not covered by a lid and thus a constitutive activity could be supposed. Indeed, no indication towards an activation mechanism for EstA is found in the literature. EstA is necessary for establishment of full virulence of *P. aeruginosa*, was found to be involved in rhamnolipid formation and affects motility and biofilm formation (Wilhelm et al., 2007). In contrast, an *L. pneumophila plaA*$^{-}$ mutant shows no defect in surface translocation and is indistinguishable from the wild type in single infections (Flieger et al., 2002; Stewart et al., 2009). However, in this thesis it was shown that the *plaA*$^{-}$ mutant has a disadvantage compared to the wild type strain in competitive infections (Figure 6). Taken together, although *L. pneumophila* PlaA and *P. aeruginosa* EstA both belong to the family of GDSL hydrolases and show structural similarities there are no indications towards similar activities of these enzymes.

4.2 Characterization of PlaD

4.2.1 rPlaD degrades during or after purification

Production and purification of rPlaD was performed according to the same protocol that was used for rPlaA. The achieved protein concentrations were high. However, the stability of rPlaD was distinctly lower than that of rPlaA. In addition to the 60 kDa protein bands representing rPlaD further protein bands were visible at approximately 38 kDa in Coomassie-stained SDS-PAGEs (Figure 21). The observed band patterns of purified rPlaD could be explained in different ways. First, the 38 kDa

protein bands might be caused by co-purified proteins. However, the co-purification of *E. coli* proteins is described especially for the purification of His-tagged proteins via immobilized metal affinity chromatography (Bolanos-Garcia and Davies, 2006; Mateo et al., 2001) while the specificity of the Strep-tactin purification system is very high and thus minimizes the binding of untagged *E. coli* proteins (Schmidt and Skerra, 2007). Another cause might be the direct interaction of the co-purified proteins with the recombinant target protein. This is especially observed for chaperones and often indicates problems regarding the correct folding of the recombinant protein (Bolanos-Garcia and Davies, 2006). Western blot analyses of the purified rPlaD with an antibody directed against the N-terminal Strep-tag confirmed the 60 kDa protein band as rPlaD. Moreover, also the smaller protein band observed at 38 kDa in the Coomassie-stained SDS-PAGEs was identified as fragment of rPlaD (Figure 21). Merely, the faint bands with sizes above 100 kDa that were observed in the Coomassie-stained SDS-PAGEs were not detected in the Western blot and might thus represent minor contaminations with co-purified proteins. Thus, the observation of multiple protein bands with distinct sizes for rPlaD indicates degradation of the protein. Such a pattern of rPlaD degradation may be indicative for premature termination of translation (Chroboczek, 1985). This hypothesis was tested in the master thesis of Christine Busching. There, rPlaD was purified via a C-terminally attached Strep-tag. Thus, only full length rPlaD, without premature termination of translation, should have been purified. However, Coomassie-stained SDS-PAGEs of rPlaD purified via a C-terminal Strep-tag showed similar instability as the N-terminally Strep-tagged rPlaD (Busching, 2018). Thus, it should be concluded that rPlaD degrades during or after purification.

4.2.2 The predicted PlaD 3D structure resembles the crystal structure of rPlaA

It might be desirable to optimize the purification conditions as pure protein could be used for the generation of an rPlaD crystal structure which could not be obtained during this thesis. Instead, a prediction of the PlaD 3D structure was performed with the “Phyre 2 server” (Kelley et al., 2015) and revealed a high degree of similarity with the structure of rPlaA (Figure 26). However, as PlaD is larger than PlaA, only a part of the PlaD model superimposed with the crystal structure of rPlaA. This region of structural similarity agrees with the sequence similarity of PlaA and PlaD. Thus it was shown that the N-terminal half of PlaD most likely adopts a classical lipase fold which was also shown for PlaA and the structurally similar *P. aeruginosa* esterase EstA (van den Berg, 2010). The C-terminal half of PlaD, which is not present in PlaA, was modeled *ab initio* which is highly unreliable (Kelley et al., 2015). Most of this part was rather unstructured. Interestingly, lipid-protein overlay assays showed that the C-terminal half of rPlaD is essential for binding to the lipids PI, PI(4)P and PI(3,4,5)P_3 (Figure 23). It can be assumed that the conformation of PlaD or at least the C-terminal half of the protein is

altered after binding. The induction of conformational changes in response to ligand binding is very common and might even affect enzymatic activities (Koshland Jr., 1995).

4.2.3 rPlaD exhibits only weak enzymatic activity

A comparison of the modeled PlaD structure with the crystal structure of rPlaA revealed that the predicted catalytic triads of both proteins are localized at the same position (Figure 26). However, while the predicted catalytic site of rPlaA is covered by a disulfide-loop, no such lid structure is present in the PlaD structure model. As described above, the active site of the *P. aeruginosa* esterase EstA is also not covered by any lid structure and is constitutively active (van den Berg, 2010; Wilhelm et al., 2007). Therefore, a constitutive activity of PlaD without the need for activation could be expected. Indeed, in this thesis it was demonstrated that rPlaD shows LPLA and lysophospholipid-dependent GCAT activity (Figure 22). Additionally, the master thesis of Christine Busching demonstrated that, unlike the activity of rPlaA, the activity of rPlaD is not altered by the addition of culture supernatant from an *L. pneumophila plaACD*$^{-}$ mutant or rProA. Moreover, the addition of metal ions did not alter the activity of rPlaD (Busching, 2018). However, all activities of rPlaD were only observed when huge amounts of approximately 50 µg protein were applied for the assays. In contrast, the activities of rPlaA are observed after application of as little as 25 ng of recombinant protein (Figure 9) (Lang et al., 2017). Thus, it remains unclear, whether the weak activity observed for rPlaD is relevant for *L. pneumophila*. It may also be conceivable that PlaD needs a so far unidentified activator for exhibition of strong enzymatic activity. It may be possible that the interaction of PlaD with the eukaryotic 14-3-3 proteins or its binding to PI(4)P would result in activation and should be investigated. Moreover, it might be possible that PlaD performs a function which is independent of lipolytic activity during infection. Such a behavior has been shown for the *L. pneumophila* patatin-like protein VipD which interferes with the Golgi-to-vacuole trafficking in yeast. Interestingly, although this protein exhibits enzymatic activity, it was reported that the interference of VipD with Golgi-to-vesicle trafficking in yeast was independent of the N-terminal patatin domain (Shohdy et al., 2005). Thus it may be possible that also PlaD has a function during *L. pneumophila* infection that is independent of its active site.

Additionally, a weak phosphatase activity was indicated for rPlaD. However, this activity did not depend on the predicted catalytic triad of rPlaD (Figure 24). This might hint towards a phosphatase activity of rPlaD that is independent of the predicted catalytic triad serin suggesting that there might be an additional active site. However, it can not be excluded that the observed phsophatase activity is caused by impurity of the purified protein. The potential phosphatase activity of rPlaD in

combination with its binding to PI, PI(4)P and PI(3,4,5)P_3 (Figure 23, Figure 24) was particularly interesting as the LCV membrane is characterized by an enrichment in PI(4)P (Weber et al., 2018; Weber et al., 2014; Weber et al., 2006). Several *L. pneumophila* effector proteins have been shown to be involved in the generation or recruitment of PI(4)P. Thus, it was speculated that PlaD might also be involved in modulating the phosphorylation status of PIPs. However, incubation of rPlaD with PIPs and subsequent thin layer chromatography revealed that rPlaD does not alter the phosphorylation status of these lipids (Figure 24).

4.2.4 PlaD might bind to the cytoplasmic side of the LCV and the plasma membrane

In total seven different phosphoinositides occur in eukaryotic cells which are characterized by distinct localizations in subsets of cell membranes. PI(3,4,5)P_3 is found exclusively in the plasma membrane. PI(4)P can also be detected at the plasma membrane but is mainly enriched in the Golgi complex (Di Paolo and De Camilli, 2006). Moreover, the recruitment to and enrichment at the LCV membrane was demonstrated for PI(4)P (Weber et al., 2018; Weber et al., 2014; Weber et al., 2006). Many T4BSS secreted effector proteins of *L. pneumophila* are anchored to the cytoplasmic side of the LCV membrane via binding to PI(4)P. Overall, phosphoinositides are essential for eukaryotic membranes and involved in various signaling cascades. Importantly, phosphoinositides do not occur in the membranes of *L. pneumophila* but only in host cells. The ability of rPlaD to bind PI(4)P and PI(3,4,5)P_3 might thus indicate that PlaD gets access to the host cell cytoplasm. Indeed, the translocation of PlaD into the host cell cytoplasm via the Dot/Icm T4BSS was demonstrated during this thesis (Figure 27). Other phospholipases of *L. pneumophila* have also been found as substrates of the Dot/Icm T4BSS. The patatin-like protein VipD as well as its paralogues VpdA, VpdB and VpdC, the PLC PlcC/CegC1 and the PLD LpdA (Altman and Segal, 2008; VanRheenen et al., 2006; Viner et al., 2012). Interestingly, LpdA localizes to the cytoplasmic side of the LCV membrane and the plasma membrane and is involved in the hydrolysis of PI, PI(3)P, PI(4)P and PG and leads to the generation of PA (Schroeder et al., 2015; Viner et al., 2012). Taken together, it may be hypothesized that PlaD might as well interact with the plasma membrane or the cytoplasmic side of the LCV membrane after injection into the host cell cytoplasm.

Further experiments revealed that the secretion of PlaD relies on the distal C-terminus of the protein (Figure 27). This is very common for T4BSS secreted effector proteins of *L. pneumophila*. Kubori et al. even described the properties of typical translocation signals which allowed them to predict T4BSS effector proteins (Kubori et al., 2008). These translocation signals are characterized by the presence of a hydrophobic amino acid residue close to the C-terminus. Moreover, in relation to the

hydrophobic residue, the -8 to -2 positions are enriched with amino acids with tiny side chains and the -13 to +1 positions are enriched with polar amino acids (Kubori et al., 2008; Nagai et al., 2005a). These characteristics are met by PlaD (data not shown). Other studies also described the enrichment of glutamic acid at the -17 to -5 positions and an enrichment of serine and threonine at the -10 to -5 positions in relation to the C-terminus of the protein (Burstein et al., 2009). However, these characteristics are not met by PlaD (data not shown). Interestingly, based on the aforementioned characteristics, the Dot/Icm dependent secretion of the PlaD ortholog in *L. longbeachae* has been predicted (Lifshitz et al., 2013). Thus, it can be assumed that the translocation of PlaD via the T4BSS is not exclusively found in *L. pneumophila* but is conserved in other *Legionella* species.

4.2.5 *Legionella pneumophila* PlaD interacts with eukaryotic 14-3-3 proteins

Proximity ligation and pull down assays revealed an interaction of PlaD with eukaryotic 14-3-3 proteins (Figure 28, Figure 29). An interaction of other proteins from *L. pneumophila* with 14-3-3 proteins has not been described so far. However, 14-3-3 proteins have been detected in proteome analyses of LCVs isolated from *D. discoideum* or RAW264.7 mouse macrophages (Shevchuk et al., 2009; Urwyler et al., 2009). Interestingly, a higher amount of 14-3-3 proteins is detected on LCVs isolated from *D. discoideum* infected with *L. hackeliae* than on LCVs isolated from *D. discoideum* infected with *L. pneumophila* (Shevchuk et al., 2009). A presence of individual isoforms of the 14-3-3 proteins has also been described for the inclusion membrane formed by *Chlamydia trachomatis* as well as the membrane of the parasitophorous vacuole formed by *Coxiella burnetii* (MacDonald et al., 2014; Scidmore and Hackstadt, 2001). In contrast, 14-3-3 proteins are not detected in proteome analyses of latex bead phagosomes (Gotthardt et al., 2006).

The 14-3-3 proteins are a family of proteins that contains seven isoforms that are encoded by separate genes and the isoforms are denoted by Greek letters (β, ε, γ, η, σ, τ and ζ) (Ichimura et al., 1988; Toker et al., 1992). 14-3-3 proteins are highly abundant in the nervous system where they account for approximately 1 % of total protein. However, 14-3-3 proteins are generally present in all tissues. Only the isoforms σ and τ are mainly present in epithelia and T-cells respectively (Aitken, 2006). The 14-3-3 isoforms are redundant to some extent as the knockout of individual isoforms does not affect normal cell metabolism. However, a knockout of 14-3-3 σ is lethal to cells (Chan et al., 1999). During this thesis, the interaction of PlaD with six of the seven 14-3-3 isoforms was demonstrated (Figure 28, Figure 29). Interestingly, the only isoform for which no binding towards PlaD was observed is 14-3-3 σ. It might thus be assumed that PlaD does not influence the function of 14-3-3 σ but only those of the other isoforms. The functions of the 14-3-3 proteins are described in the next chapter. Orthologues of the 14-3-3 proteins are also present in amoebae. In *D. discoideum* one gene which is designated as *fttB* is expressed. A knockout of *fttB* is lethal to *D. discoideum* within

a few generations (Zhou et al., 2010). Indeed, PlaD interacts not only with the 14-3-3 proteins of RAW264.7 mouse macrophages but also with the orthologues from A549 lung epithelial cells and *A. castellanii* amoebae (Figure 29). This most likely indicates a conserved binding mechanism.

The interaction of the 14-3-3 proteins with their manifold target proteins occurs via conserved binding motifs. These classical binding motifs contain either a phosphorylated serine or a phosphorylated threonine residue which is essential for the interaction (Muslin et al., 1996; Yaffe et al., 1997). Due to the high conservation of these binding motifs the interaction of a specific protein with the 14-3-3 proteins can be predicted from its amino acid sequence (Madeira et al., 2015). Seven potential binding sites were predicted for PlaD and it was shown that the mutation of individual sites was not sufficient to prevent the interaction with the 14-3-3 proteins completely (Figure 30). Such a behavior is very common. Often interacting proteins bind to the 14-3-3 proteins via multiple binding sites. This allows the modulation of interaction strengths (Fu et al., 2000; Yaffe et al., 1997). In case of PlaD the mutation of three predicted binding sites was sufficient to block interaction (Figure 30). This mutant might be helpful for further analyses of the importance of the PlaD/14-3-3 interaction during *L. pneumophila* infection.

4.2.6 What are 14-3-3 proteins and what do they do?

14-3-3 proteins are mainly found in the cytoplasm but association with membranes has also been observed. Moreover, the proteins usually form homo- or heterodimers where each monomer can bind to one ligand (Chaudhri et al., 2003; Jones et al., 1995). As a result, 14-3-3 dimers can either bind a single ligand with stronger affinity or two identical or two different ligands at the same time. The binding of ligands can result in multiple outcomes (Fu et al., 2000). For one thing it might act as a scaffold and induce conformational changes in the ligand which might affect for example enzymatic activities (Fu et al., 2000). During this thesis only very weak LPLA, lysophospholipid dependent GCAT activity, phosphatase activity and minor deacetylase activity was detected for rPlaD (Figure 22, Figure 24, Figure 25). It might thus be speculated that binding to 14-3-3 proteins would increase or alter the enzymatic activity of rPlaD. A similar behavior has been demonstrated for the cytotoxin ExoS from *P. aeruginosa*. The activity of ExoS is activated only after binding to 14-3-3 proteins (Fu et al., 1993). Moreover, binding to 14-3-3 proteins may protect post-translational modifications such as phosphorylation of the ligand from being removed. For example, the kinases Raf-1 and phosphatidylinositol 4 kinase III β (PI4KIIIβ) require phosphorylation for their activity and these phosphorylations are protected by 14-3-3 binding (Hausser et al., 2006; Thorson et al., 1998). At the same time 14-3-3 proteins can also block post-translational modifications for example by hiding or

presenting ubiquitination sites (Cornell and Toyo-oka, 2017). Analysis of the PlaD amino acid sequence with the UbPred online tool (Radivojac et al., 2010) predicted three possible ubiquitination sites with medium confidence (data not shown). Thus, it might be hypothesized that the interaction with 14-3-3 proteins would protect PlaD from being degraded. Additionally, 14-3-3 proteins might block binding sites for other proteins or DNA or hide localization signals and sequester the ligand in the cytoplasm (Cornell and Toyo-oka, 2017). That way, 14-3-3 proteins are involved in controlling the cell cycle. The cell cycle control involves multiple checkpoints and entry into mitosis requires among others the activity of the phosphatase Cdc25c. This protein shuttles between the nucleus and the cytoplasm. During interphase Cdc25c is sequestered in an inactive form in the cytoplasm by binding to 14-3-3 proteins. It has been shown that prevention of 14-3-3/Cdc25c binding results in accumulation of Cdc25c in the nucleus and dysregulation of the cell cycle (Dalal et al., 1999; Muslin and Xing, 2000; Telles et al., 2009). Moreover, as mentioned before, 14-3-3 proteins may bind two different ligands at the same time and thus facilitate their interaction. Additionally, the complex consisting of a 14-3-3 dimer with two distinct ligands might be recruited to a specific subcellular compartment by one of the ligands resulting in the recruitment of the other ligand to the place of action. As binding of PlaD to PI(4)P (Figure 23), a lipid which is enriched in the LCV, was shown and the presence of 14-3-3 proteins at the LCV was described as well (Shevchuk et al., 2009; Urwyler et al., 2009), it may be hypothesized that PlaD is involved in the recruitment of the 14-3-3 proteins to the LCV membrane. This could be verified by immunofluorescence microscopy as had been performed for *C. trachomatis* (Scidmore and Hackstadt, 2001). 14-3-3 proteins have also been shown to bind the PI4KIIIβ an enzyme that is responsible for the generation of PI(4)P which is enriched in the LCV membrane (Hausser et al., 2006). It had been proposed that PI4KIIIβ might be indirectly recruited to the LCV membrane via the *L. pneumophila* T4BSS secreted effector protein Arf1 (Hilbi et al., 2011b). However, this has not been confirmed yet. Instead, it might also be hypothesized that PI4KIIIβ is recruited to the LCV via binding to 14-3-3 proteins which interact with PI(4)P-bound PlaD. To verify this theory it would be helpful to check whether blocking of the PlaD/14-3-3 interaction would prevent the recruitment of the 14-3-3 proteins as well as the recruitment of PI4KIIIβ to the LCV. To this end, immunofluorescence microscopy and proteomics analyses of purified LCVs might be performed. A similar approach was used for the identification of the importance of the 14-3-3/Cdc25 interaction for cell cycle control (Muslin and Xing, 2000). As mentioned above, 14-3-3 proteins are more abundant on LCVs from *D. discoideum* infected with *L. hackeliae* than from those infected with *L. pneumophila* (Shevchuk et al., 2009). BLAST analyses show that PlaD from *L. pneumophila* and *L. hackeliae* are 71 % identical. However, less 14-3-3 binding sites are predicted for the PlaD orthologue from *L. hackeliae* than for *L. pneumophila* PlaD (data not shown). Under the assumption that PlaD is responsible for the recruitment of the 14-3-3 proteins to the LCV membranes, it might

thus be speculated that the PlaD orthologue from *L. hackeliae* would show a higher affinity towards the 14-3-3 proteins than *L. pneumophila* PlaD.

4.2.7 14-3-3 proteins regulate multiple metabolic pathways

The 14-3-3 proteins are involved in multiple metabolic pathways and interact with a plethora of cellular proteins but they do not have any intrinsic enzymatic activity (Cornell and Toyo-oka, 2017). 14-3-3 proteins contribute among others to cell cycle control via sequestration of Cdc25c in the cytoplasm as described above (Dalal et al., 1999; Muslin and Xing, 2000; Telles et al., 2009). Moreover, the MAPK signaling pathway and the PKB/akt signaling pathway are affected by 14-3-3 protein binding (Roberts et al., 1997; Tzivion et al., 2011; Xing et al., 2000). Interestingly, it has been shown that multiple pathogens exploit the regulatory functions of the 14-3-3 proteins. Among others, the core protein of Hepatitis C virus activates the Raf-1 kinase via interaction with 14-3-3 proteins and thus interferes with hepatocyte growth regulation (Aoki et al., 2000). Moreover, it was shown that infection with *C. burnetii* leads to an increase in phosphorylation of the pro-apoptotic Bcl-2 protein Bad which, together with the adaptor protein 14-3-3 β, is then recruited to the parasitophorous vacuole and results in inhibition of host cell apoptosis. This process depends on phosphorylation of Bad after activation of the cAMP dependent protein kinase A (MacDonald et al., 2014). Similarly, it has been shown that 14-3-3 proteins bind to proteins that have been phosphorylated by the protein kinase B (PKB) which is activated downstream of PI3K in response to extracellular signals (Tzivion et al., 2011). The induction of PKB is involved in the induction of growth response and cell survival (Duronio, 2008). Some of the phosphorylated PKB targets that are sequestered by 14-3-3 proteins are FOXO transcription factors, the transcriptional regulator YAP65 and the pro-apoptotic Bcl-2 protein Bad. Interestingly, these ligands are either directly or indirectly involved in the induction of apoptosis and their sequestration by 14-3-3 proteins leads to inhibition of apoptosis (Basu et al., 2003; Downward, 2004; Masters et al., 2001; Tzivion et al., 2011; Zha et al., 1996).

4.2.7.1 PlaD contributes to the inhibition of host cell apoptosis during *L. pneumophila* infection

The induction of apoptosis is, among others, used as a defense mechanism of cells (Elmore, 2007; Pistritto et al., 2016). However, many intracellular pathogens have evolved mechanisms to prevent the induction of host cell apoptosis as described above for *C. burnetii* (MacDonald et al., 2014). Some Mycobacteria even induce apoptosis at later stages of infection for exit from the host cell (Flieger et al., 2018; Friedrich et al., 2012). For *L. pneumophila*, the induction or inhibition of host cell apoptosis

has been discussed controversially. On the one hand, the activation of caspase-3, a hallmark of apoptosis, was described for early stages of infection (Gao and Abu Kwaik, 1999a; Gao and Abu Kwaik, 1999b). However, on the other hand, multiple T4BSS secreted effector proteins have been described to inhibit apoptosis (Abu-Zant et al., 2007; Banga et al., 2007; Creasey and Isberg, 2012; Losick and Isberg, 2006). The consensus is that *L. pneumophila* actively inhibits the induction of host cell apoptosis via multiple T4BSS secreted effector proteins but induces inflammasome dependent pyroptosis (Flieger et al., 2018; Katagiri et al., 2012). Among other, SidF and SdhA have been described as anti-apoptotic proteins. It has been shown that SidF mediates its anti-apoptotic properties via targeting the pro-apoptotic Bcl-2 proteins BNIP3 and Bcl-rambo (Banga et al., 2007; Creasey and Isberg, 2012). However, in most cases the underlying mechanisms have not been elucidated. In this thesis, the ability of *L. pneumophila* to inhibit host cell apoptosis has been reproduced (Figure 32). In contrast, the *plaD*$^{-}$ mutant showed increased caspase-3 induction (Figure 31), a hallmark of apoptosis (Nafis et al., 2015), already 24 h post infection and was unable to prevent staurosporine-induced host cell apoptosis (Figure 32). In fact, staurosporine-induced host cell apoptosis was even increased in cells that had been infected with *L. pneumophila plaD*$^{-}$ before. Taken together, these observations point towards an anti-apoptotic activity of PlaD. So far, the mechanism of how PlaD is involved in inhibition of host cell apoptosis has not been elucidated. However, as the 14-3-3 proteins, which are among others involved in inhibition of apoptosis (Masters and Fu, 2001), are the only detected eukaryotic interaction partners of PlaD it can be speculated that this interaction is essential for the execution of the anti-apoptotic activity of PlaD. As described above, it is known that the inhibition of apoptosis by 14-3-3 proteins is among others mediated via the sequestration of the pro-apoptotic Bcl-2 protein Bad (Masters et al., 2001; Zha et al., 1996). This interaction is blocked by acetylation of the 14-3-3 proteins (Pennington et al., 2018a). Thus, it was suspected that PlaD might be involved in the deacetylation of the 14-3-3 proteins and would thus stabilize the sequestration of Bad. During this thesis only minor deacetylase activity of PlaD was observed (Figure 25). Therefore, it should next be examined whether the anti-apoptotic activity of PlaD is indeed mediated via the interaction with the 14-3-3 proteins. To test this hypothesis, complementation of the *L. pneumophila plaD*$^{-}$ mutant with intact *plaD* or a variant of *plaD* that does not bind to the 14-3-3 proteins and subsequent analysis of apoptosis induction or inhibition would be crucial. The basis for such experiments was laid in this thesis, as a PlaD variant was identified that no longer interacted with the 14-3-3 proteins in pull down assays (Figure 32).

4.2.8 Proposed model for PlaD during infection

In summary, the following model is proposed for the importance of PlaD during infection with *L. pneumophila*. Upon infection, PlaD is injected into the host cell cytoplasm in a Dot/Icm dependent manner. There, it interacts with 14-3-3 proteins and most likely binds to the cytoplasmic side of the LCV membrane and the plasma membrane via PI(4)P and PI(3,4,5)P_3 respectively. Additionally, PlaD might be involved in the recruitment of PI4KIIIβ to the LCV membrane via interaction with the 14-3-3 proteins. Thus, PlaD might indirectly be involved in the enrichment of PI(4)P in the LCV membrane. Moreover, PlaD inhibits the induction of host cell apoptosis via a yet unknown mechanism.

4.3 *L. pneumophila plaA*$^-$ is outcompeted by the wild type strain in competitive infections while the *plaD*$^-$ mutant prevails

During this thesis it was demonstrated that the individual deletion of *plaA* or *plaD* did not affect growth of *L. pneumophila* in intracellular replication during standard infections of *A. castellanii* amoebae or RAW264.7 mouse macrophages (Figure 6, Figure 19). The lack of phenotypes resulting from the knockout of single genes has been described multiple times for *L. pneumophila* and is usually assigned to redundancy (Ghosh and O'Connor, 2017). *L. pneumophila* secretes a multitude of more than 25 proteins via the T2SS and more than 300 effector proteins via the T4BSS (Cianciotto, 2009; Ensminger and Isberg, 2009). Moreover, *L. pneumophila* possesses 19 phospholipases and secretion via the T2SS or the T4BSS has been shown for most of them (Hiller et al., 2018). Thus it might be conceivable that the deletion of a single phospholipase gene, *plaA* or *plaD*, would be compensated by other phospholipases. This has been shown for example for the patatin-like protein VipD whose deletion is compensated by its homologues (VanRheenen et al., 2006). In contrast, the *L. pneumophila plaA*$^-$ and *plaD*$^-$ mutants showed strong phenotypes when competitive infections with the wild type strain were performed.

During infection of host cells with *L. pneumophila* wild type and the *plaA*$^-$ mutant at the same time in a competitive infection assay the mutant was outcompeted by the wild type strain (Figure 6). A similar behavior in competition assays was shown for example for components of the T2SS as well as for deletion of the *feoAB* operon which is involved in the uptake of ferrous iron and promotes intracellular infection (Robey and Cianciotto, 2002; Rossier et al., 2004). It can be assumed that the absence of PlaA conferred a disadvantage to *L. pneumophila*. As stated above, PlaA might have a function in the lysis of the LCV membrane during later time points of *L. pneumophila* infection (Creasey and Isberg, 2012). Thus, it may be hypothesized that the lack of PlaA might result in delayed exit of *L. pneumophila* from the host cell.

Interestingly, deletion of *plaD* resulted in increased replication of the mutant as compared to the wild type strain during intracellular competition assays. This phenotype was observed in both *A. castellanii* amoebae and RAW264.7 mouse macrophages (Figure 20). Such a behavior of *L. pneumophila* mutants is rather unusual. Mostly the mutant strains are outcompeted by *L. pneumophila* wild type as observed for the *L. pneumophila plaA*$^{-}$ mutant. So far, it was not elucidated why the *plaD*$^{-}$ mutant outcompetes the wild type strain during competitive infections. However, during this thesis it was shown that presence PlaD confers anti-apoptotic properties to *L. pneumophila* wild type while the *plaD*$^{-}$ mutant is characterized by increased and earlier induction of host cell apoptosis (Figure 31, Figure 32). Some bacteria such as *Mycobacterium avium* use apoptotic bodies for the spread to uninfected macrophages (Flieger et al., 2018; Friedrich et al., 2012). That way, detection by the immune system of the host cell is avoided as apoptotic bodies are anti-inflammatory (Lamkanfi and Dixit, 2010). The spread of *L. pneumophila* via apoptotic bodies has neither been described nor disproven so far but it may be possible. Thus, it may be conceivable that the *L. pneumophila plaD*$^{-}$ mutant, which induces increased and faster apoptosis, spreads and infects naïve bystander macrophages via apoptotic bodies faster than the wild type. This hypothesis could be analyzed via the application of an apoptosis-inhibitor during infection. If the increased induction of host cell apoptosis would be responsible for the replication advantage of the *L. pneumophila plaD*$^{-}$ mutant, inhibition of apoptosis should diminish this advantage.

4.4 Concluding remarks

In infection experiments it was shown that both PlaA and PlaD are dispensable for intracellular replication of *L. pneumophila*. However, in competitive infection assays the *plaA*$^{-}$ mutant was outcompeted by the wild type strain while the *plaD*$^{-}$ mutant replicated better than the wild type strain. Moreover, both proteins differ with regard to their mode of secretion and enzymatic activity. PlaA is secreted via the T2SS resulting in its presence inside the LCV during infection and its strong LPLA activity might be important for exit of *L. pneumophila* from the host cell. In contrast, PlaD exhibits only minor enzymatic activity and is injected into the host cell cytoplasm via the T4BSS where it is involved in the inhibition of host cell apoptosis. Taken together, the data generated during this thesis indicate that, although PlaA and PlaD both belong to the family of GDSL hydrolases, they probably have distinct functions during host cell infections.

5 References

Abdelaziz, D.H., Gavrilin, M.A., Akhter, A., Caution, K., Kotrange, S., Khweek, A.A., Abdulrahman, B.A., Grandhi, J., Hassan, Z.A., Marsh, C., 2011. Apoptosis-associated speck-like protein (ASC) controls Legionella pneumophila infection in human monocytes. J. Biol. Chem. 286, 3203-3208.

Abu-Zant, A., Jones, S., Asare, R., Suttles, J., Price, C., Graham, J., Kwaik, Y.A., 2007. Anti-apoptotic signalling by the Dot/Icm secretion system of L. pneumophila. Cell. Microbiol. 9, 246-264.

Abu-Zant, A., Santic, M., Molmeret, M., Jones, S., Helbig, J., Abu Kwaik, Y., 2005. Incomplete activation of macrophage apoptosis during intracellular replication of Legionella pneumophila. Infect. Immun. 73, 5339-5349.

Abu Khweek, A., Amer, A., 2010. Replication of Legionella pneumophila in human cells: why are we Susceptible? Front. Microbiol. 1, 133.

Aitken, A., 2006. 14-3-3 proteins: A historic overview. Semin. Cancer Biol. 16, 162-172.

Akhter, A., Gavrilin, M.A., Frantz, L., Washington, S., Ditty, C., Limoli, D., Day, C., Sarkar, A., Newland, C., Butchar, J., 2009. Caspase-7 activation by the Nlrc4/Ipaf inflammasome restricts Legionella pneumophila infection. PLoS Pathog. 5, e1000361.

Akoh, C.C., Lee, G.-C., Liaw, Y.-C., Huang, T.-H., Shaw, J.-F., 2004. GDSL family of serine esterases/lipases. Prog. Lipid Res. 43, 534-552.

Albert-Weissenberger, C., Cazalet, C., Buchrieser, C., 2007. Legionella pneumophila - a human pathogen that co-evolved with fresh water protozoa. Cell Mol Life Sci 64, 432-448.

Allewelt, M., Coleman, F.T., Grout, M., Priebe, G.P., Pier, G.B., 2000. Acquisition of expression of the Pseudomonas aeruginosa ExoU cytotoxin leads to increased bacterial virulence in a murine model of acute pneumonia and systemic spread. Infect. Immun. 68, 3998-4004.

Allombert, J., Fuche, F., Michard, C., Doublet, P., 2013. Molecular mimicry and original biochemical strategies for the biogenesis of a Legionella pneumophila replicative niche in phagocytic cells. Microbes Infect 15, 981-988.

Altman, E., Segal, G., 2008. The response regulator CpxR directly regulates expression of several Legionella pneumophila icm/dot components as well as new translocated substrates. J. Bacteriol. 190, 1985-1996.

Ambrose, J., Hampton, L.M., Fleming-Dutra, K.E., Marten, C., McClusky, C., Perry, C., Clemmons, N.A., McCormic, Z., Peik, S., Mancuso, J., Brown, E., Kozak, N., Travis, T., Lucas, C., Fields, B., Hicks, L., Cersovsky, S.B., 2014. Large outbreak of Legionnaires' disease and Pontiac fever at a military base. Epidemiol. Infect. 142, 2336-2346.

Aoki, H., Hayashi, J., Moriyama, M., Arakawa, Y., Hino, O., 2000. Hepatitis C Virus Core Protein Interacts with 14-3-3 Protein and Activates the Kinase Raf-1. J. Virol. 74, 1736-1741.

Aragon, V., Kurtz, S., Cianciotto, N.P., 2001. Legionella pneumophila major acid phosphatase and its role in intracellular infection. Infect. Immun. 69, 177-185.

Aragon, V., Rossier, O., Cianciotto, N.P., 2002. Legionella pneumophila genes that encode lipase and phospholipase C activitiesa. Microbiology 148, 2223-2231.

Aurass, P., Gerlach, T., Becher, D., Voigt, B., Karste, S., Bernhardt, J., Riedel, K., Hecker, M., Flieger, A., 2016. Life Stage-specific Proteomes of Legionella pneumophila Reveal a Highly Differential Abundance of Virulence-associated Dot/Icm effectors. Mol. Cell. Proteomics 15, 177-200.

Aurass, P., Schlegel, M., Metwally, O., Harding, C.R., Schroeder, G.N., Frankel, G., Flieger, A., 2013. The Legionella pneumophila Dot/Icm-secreted effector PlcC/CegC1 together with PlcA and PlcB promotes virulence and belongs to a novel zinc metallophospholipase C family present in bacteria and fungi. J. Biol. Chem. 288, 11080-11092.

Banerji, S., Aurass, P., Flieger, A., 2008. The manifold phospholipases A of Legionella pneumophila - identification, export, regulation, and their link to bacterial virulence. Int. J. Med. Microbiol. 298, 169-181.

Banerji, S., Bewersdorff, M., Hermes, B., Cianciotto, N.P., Flieger, A., 2005. Characterization of the major secreted zinc metalloprotease- dependent glycerophospholipid:cholesterol acyltransferase, PlaC, of Legionella pneumophila. Infect. Immun. 73, 2899-2909.

Banga, S., Gao, P., Shen, X., Fiscus, V., Zong, W.-X., Chen, L., Luo, Z.-Q., 2007. Legionella pneumophila inhibits macrophage apoptosis by targeting pro-death members of the Bcl2 protein family. Proceedings of the National Academy of Sciences 104, 5121-5126.

Bangsborg, J.M., 1997. Antigenic and genetic characterization of Leaionella proteins: Contribution to taxonomy, diagnosis and pathogenesis. APMIS 105, 5-53.

Basu, S., Totty, N.F., Irwin, M.S., Sudol, M., Downward, J., 2003. Akt phosphorylates the Yes-associated protein, YAP, to induce interaction with 14-3-3 and attenuation of p73-mediated apoptosis. Mol. Cell 11, 11-23.

Beauté, J., Zucs, P., Jong, B.d., 2013. Legionnaires' disease in Europe, 2009-2010.

Bellinger-Kawahara, C., Horwitz, M.A., 1990. Complement component C3 fixes selectively to the major outer membrane protein (MOMP) of Legionella pneumophila and mediates phagocytosis of liposome-MOMP complexes by human monocytes. J. Exp. Med. 172, 1201-1210.

Bergsbaken, T., Fink, S.L., Cookson, B.T., 2009. Pyroptosis: host cell death and inflammation. Nature Reviews Microbiology 7, 99.

Bligh, E.G., Dyer, W.J., 1959. A RAPID METHOD OF TOTAL LIPID EXTRACTION AND PURIFICATION. Can. J. Biochem. Physiol. 37, 911-917.

Bolanos-Garcia, V.M., Davies, O.R., 2006. Structural analysis and classification of native proteins from E. coli commonly co-purified by immobilised metal affinity chromatography. Biochimica et Biophysica Acta (BBA) - General Subjects 1760, 1304-1313.

Bozue, J.A., Johnson, W., 1996. Interaction of Legionella pneumophila with Acanthamoeba castellanii: uptake by coiling phagocytosis and inhibition of phagosome-lysosome fusion. Infect. Immun. 64, 668-673.

Brieland, J., Freeman, P., Kunkel, R., Chrisp, C., Hurley, M., Fantone, J., Engleberg, C., 1994. Replicative Legionella pneumophila lung infection in intratracheally inoculated A/J mice. A murine model of human Legionnaires' disease. The American journal of pathology 145, 1537-1546.

Bruggemann, H., Hagman, A., Jules, M., Sismeiro, O., Dillies, M.A., Gouyette, C., Kunst, F., Steinert, M., Heuner, K., Coppee, J.Y., Buchrieser, C., 2006. Virulence strategies for infecting phagocytes

deduced from the in vivo transcriptional program of Legionella pneumophila. Cell. Microbiol. 8, 1228-1240.

Buckley, J.T., Halasa, L.N., MacIntyre, S., 1982. Purification and partial characterization of a bacterial phospholipid: cholesterol acyltransferase. J. Biol. Chem. 257, 3320-3325.

Burstein, D., Zusman, T., Degtyar, E., Viner, R., Segal, G., Pupko, T., 2009. Genome-scale identification of Legionella pneumophila effectors using a machine learning approach. PLoS Pathog. 5, e1000508.

Busching, C., 2018. Analyse der Aktivität und Lokalisierung der Phospholipase PlaD aus Legionella pneumophila. Technischen Universität Carolo-Wilhelmina zu Braunschweig.

Byrne, B., Swanson, M.S., 1998. Expression of Legionella pneumophila virulence traits in response to growth conditions. Infect. Immun. 66, 3029-3034.

Cerqueira, D.M., Pereira, M.S., Silva, A.L., Cunha, L.D., Zamboni, D.S., 2015. Caspase-1 but Not Caspase-11 Is Required for NLRC4-Mediated Pyroptosis and Restriction of Infection by Flagellated Legionella Species in Mouse Macrophages and In Vivo. J. Immunol. 195, 2303-2311.

Chan, T.A., Hermeking, H., Lengauer, C., Kinzler, K.W., Vogelstein, B., 1999. 14-3-3σ is required to prevent mitotic catastrophe after DNA damage. Nature 401, 616-620.

Chaudhri, M., Scarabel, M., Aitken, A., 2003. Mammalian and yeast 14-3-3 isoforms form distinct patterns of dimers in vivo. Biochem. Biophys. Res. Commun. 300, 679-685.

Chroboczek, J., 1985. Incomplete polypeptides are formed in vitro by premature chain termination. Eur. J. Biochem. 149, 565-569.

Cianciotto, N.P., 2005. Type II secretion: a protein secretion system for all seasons. Trends Microbiol. 13, 581-588.

Cianciotto, N.P., 2009. Many substrates and functions of type II secretion: lessons learned from Legionella pneumophila. Future Microbiol. 4, 797-805.

Cianciotto, N.P., Eisenstein, B.I., Mody, C.H., Engleberg, N.C., 1990. A mutation in the mip gene results in an attenuation of Legionella pneumophila virulence. J. Infect. Dis. 162, 121-126.

Cirillo, J.D., Falkow, S., Tompkins, L.S., 1994. Growth of Legionella pneumophila in Acanthamoeba castellanii enhances invasion. Infect. Immun. 62, 3254-3261.

Cornell, B., Toyo-oka, K., 2017. 14-3-3 Proteins in Brain Development: Neurogenesis, Neuronal Migration and Neuromorphogenesis. Front. Mol. Neurosci. 10.

Correia, A.M., Ferreira, J.S., Borges, V., Nunes, A., Gomes, B., Capucho, R., Gonçalves, J., Antunes, D.M., Almeida, S., Mendes, A., 2016. Probable person-to-person transmission of Legionnaires' disease. N. Engl. J. Med. 374, 497-498.

Creasey, E.A., Isberg, R.R., 2012. The protein SdhA maintains the integrity of the Legionella-containing vacuole. Proc. Natl. Acad. Sci. U. S. A. 109, 3481-3486.

Cunha, B.A., Burillo, A., Bouza, E., 2016. Legionnaires' disease. Lancet 387, 376-385.

D'Auria, G., Jiménez-Hernández, N., Peris-Bondia, F., Moya, A., Latorre, A., 2010. Legionella pneumophila pangenome reveals strain-specific virulence factors. BMC Genomics 11, 181.

Dalal, S.N., Schweitzer, C.M., Gan, J., DeCaprio, J.A., 1999. Cytoplasmic localization of human cdc25C during interphase requires an intact 14-3-3 binding site. Mol. Cell. Biol. 19, 4465-4479.

Dalebroux, Z.D., Svensson, S.L., Gaynor, E.C., Swanson, M.S., 2010. ppGpp conjures bacterial virulence. Microbiol. Mol. Biol. Rev. 74, 171-199.

Datta, S.R., Katsov, A., Hu, L., Petros, A., Fesik, S.W., Yaffe, M.B., Greenberg, M.E., 2000. 14-3-3 proteins and survival kinases cooperate to inactivate BAD by BH3 domain phosphorylation. Mol. Cell 6, 41-51.

de Felipe, K.S., Glover, R.T., Charpentier, X., Anderson, O.R., Reyes, M., Pericone, C.D., Shuman, H.A., 2008. Legionella Eukaryotic-Like Type IV Substrates Interfere with Organelle Trafficking. PLoS Pathog. 4, e1000117.

Di Paolo, G., De Camilli, P., 2006. Phosphoinositides in cell regulation and membrane dynamics. Nature 443, 651-657.

Diaz, M.H., Hauser, A.R., 2010. Pseudomonas aeruginosa cytotoxin ExoU is injected into phagocytic cells during acute pneumonia. Infect. Immun. 78, 1447-1456.

Diaz, M.H., Shaver, C.M., King, J.D., Musunuri, S., Kazzaz, J.A., Hauser, A.R., 2008. Pseudomonas aeruginosa induces localized immunosuppression during pneumonia. Infect. Immun. 76, 4414-4421.

Downward, J., 2004. PI 3-kinase, Akt and cell survival, Semin. Cell Dev. Biol. Elsevier, pp. 177-182.

Duronio, V., 2008. The life of a cell: apoptosis regulation by the PI3K/PKB pathway. Biochem. J. 415, 333-344.

ECDC, 2019. Legionnaires' disease Annual Epidemiological Report 2017.

Elmore, S., 2007. Apoptosis: a review of programmed cell death. Toxicol. Pathol. 35, 495-516.

Ensminger, A.W., Isberg, R.R., 2009. Legionella pneumophila Dot/Icm translocated substrates: a sum of parts. Curr. Opin. Microbiol. 12, 67-73.

Escoll, P., Rolando, M., Gomez-Valero, L., Buchrieser, C., 2013. From amoeba to macrophages: exploring the molecular mechanisms of Legionella pneumophila infection in both hosts, Molecular Mechanisms in Legionella Pathogenesis. Springer, pp. 1-34.

Feeley, J.C., Gibson, R.J., Gorman, G.W., Langford, N.C., Rasheed, J.K., Mackel, D.C., Baine, W.B., 1979. Charcoal-yeast extract agar: primary isolation medium for Legionella pneumophila. J. Clin. Microbiol. 10, 437.

Fields, B.S., Benson, R.F., Besser, R.E., 2002. Legionella and Legionnaires' disease: 25 years of investigation. Clin. Microbiol. Rev. 15, 506-526.

Fischer, S.F., Vier, J., Muller-Thomas, C., Hacker, G., 2006. Induction of apoptosis by Legionella pneumophila in mammalian cells requires the mitochondrial pathway for caspase activation. Microbes Infect 8, 662-669.

Flieger, A., Frischknecht, F., Hacker, G., Hornef, M.W., Pradel, G., 2018. Pathways of host cell exit by intracellular pathogens. Microb Cell 5, 525-544.

Flieger, A., Gong, S., Faigle, M., Deeg, M., Bartmann, P., Neumeister, B., 2000a. Novel phospholipase A activity secreted by Legionella species. J. Bacteriol. 182, 1321-1327.

Flieger, A., Gong, S., Faigle, M., Mayer, H.A., Kehrer, U., Mußotter, J., Bartmann, P., Neumeister, B., 2000b. Phospholipase A secreted by Legionella pneumophila destroys alveolar surfactant phospholipids. FEMS Microbiol. Lett. 188, 129-133.

Flieger, A., Gong, S., Faigle, M., Neumeister, B., 2000c. Critical evaluation of p-nitrophenylphosphorylcholine (p-NPPC) as artificial substrate for the detection of phospholipase C☆. Enzyme Microb. Technol. 26, 451-458.

Flieger, A., Gong, S., Faigle, M., Northoff, H., Neumeister, B., 2001a. In vitro secretion kinetics of proteins from Legionella pneumophila in comparison to proteins from non-pneumophila species. Microbiology 147, 3127-3134.

Flieger, A., Gong, S., Faigle, M., Stevanovic, S., Cianciotto, N.P., Neumeister, B., 2001b. Novel lysophospholipase A secreted by Legionella pneumophila. J. Bacteriol. 183, 2121-2124.

Flieger, A., Neumeister, B., Cianciotto, N.P., 2002. Characterization of the gene encoding the major secreted lysophospholipase A of Legionella pneumophila and its role in detoxification of lysophosphatidylcholine. Infect. Immun. 70, 6094-6106.

Flieger, A., Rydzewski, K., Banerji, S., Broich, M., Heuner, K., 2004. Cloning and characterization of the gene encoding the major cell-associated phospholipase A of Legionella pneumophila, plaB, exhibiting hemolytic activity. Infect. Immun. 72, 2648-2658.

Flores-Diaz, M., Monturiol-Gross, L., Naylor, C., Alape-Giron, A., Flieger, A., 2016. Bacterial Sphingomyelinases and Phospholipases as Virulence Factors. Microbiol. Mol. Biol. Rev. 80, 597-628.

Fraser, D.W., Tsai, T.R., Orenstein, W., Parkin, W.E., Beecham, H.J., Sharrar, R.G., Harris, J., Mallison, G.F., Martin, S.M., McDade, J.E., Shepard, C.C., Brachman, P.S., 1977. Legionnaires' disease: description of an epidemic of pneumonia. N Engl J Med 297, 1189-1197.

Freeman, J.A., Ohl, M.E., Miller, S.I., 2003. The Salmonella enterica serovar typhimurium translocated effectors SseJ and SifB are targeted to the Salmonella-containing vacuole. Infect. Immun. 71, 418-427.

Friedrich, N., Hagedorn, M., Soldati-Favre, D., Soldati, T., 2012. Prison break: pathogens' strategies to egress from host cells. Microbiology and molecular biology reviews : MMBR 76, 707-720.

Fu, H., Coburn, J., Collier, R.J., 1993. The eukaryotic host factor that activates exoenzyme S of Pseudomonas aeruginosa is a member of the 14-3-3 protein family. Proceedings of the National Academy of Sciences 90, 2320-2324.

Fu, H., Subramanian, R.R., Masters, S.C., 2000. 14-3-3 Proteins: Structure, Function, and Regulation. Annu. Rev. Pharmacol. Toxicol. 40, 617-647.

Funk, C.D., 2001. Prostaglandins and leukotrienes: advances in eicosanoid biology. Science 294, 1871-1875.

Furugen, M., Higa, F., Hibiya, K., Teruya, H., Akamine, M., Haranaga, S., Yara, S., Koide, M., Tateyama, M., Mori, N., Fujita, J., 2008. Legionella pneumophila infection induces programmed cell death, caspase activation, and release of high-mobility group box 1 protein in A549 alveolar epithelial cells: inhibition by methyl prednisolone. Respir. Res. 9, 39.

Gao, L.-Y., Abu Kwaik, Y., 1999a. Activation of Caspase 3 during Legionella pneumophila-Induced Apoptosis. Infect. Immun. 67, 4886-4894.

Gao, L.Y., Abu Kwaik, Y., 1999b. Apoptosis in macrophages and alveolar epithelial cells during early stages of infection by Legionella pneumophila and its role in cytopathogenicity. Infect. Immun. 67, 862-870.

Ghosal, D., Chang, Y.W., Jeong, K.C., Vogel, J.P., Jensen, G.J., 2017. In situ structure of the Legionella Dot/Icm type IV secretion system by electron cryotomography. EMBO reports 18, 726-732.

Ghosal, D., Kim, K.W., Zheng, H., Kaplan, M., Vogel, J.P., Cianciotto, N.P., Jensen, G.J., 2019. In vivo structure of the Legionella type II secretion system by electron cryotomography. bioRxiv, 525063.

Ghosh, S., O'Connor, T.J., 2017. Beyond paralogs: the multiple layers of redundancy in bacterial pathogenesis. Frontiers in cellular and infection microbiology 7, 467.

Gjellesvik, D.R., 1991. Fatty acid specificity of bile salt-dependent lipase: enzyme recognition and super-substrate effects. Biochim. Biophys. Acta 1086, 167-172.

Gomez-Valero, L., Rusniok, C., Cazalet, C., Buchrieser, C., 2011. Comparative and functional genomics of legionella identified eukaryotic like proteins as key players in host-pathogen interactions. Front. Microbiol. 2, 208.

Gomez-Valero, L., Rusniok, C., Rolando, M., Neou, M., Dervins-Ravault, D., Demirtas, J., Rouy, Z., Moore, R.J., Chen, H., Petty, N.K., Jarraud, S., Etienne, J., Steinert, M., Heuner, K., Gribaldo, S., Médigue, C., Glöckner, G., Hartland, E.L., Buchrieser, C., 2014. Comparative analyses of Legionella species identifies genetic features of strains causing Legionnaires' disease. Genome Biol. 15.

Gordon, V.M., Leppla, S.H., 1994. Proteolytic activation of bacterial toxins: role of bacterial and host cell proteases. Infect. Immun. 62, 333-340.

Gotthardt, D., Dieckmann, R., Blancheteau, V., Kistler, C., Reichardt, F., Soldati, T., 2006. Preparation of intact, highly purified phagosomes from Dictyostelium. Methods Mol. Biol. 346, 439-448.

Grun, D., Unger, M.M., Kauffmann, J., Zimmer, V., Fassbender, K., Fousse, M., 2019. Legionnaire's-disease-associated meningoencephalitis: A case report. Pulmonology.

Hagele, S., Hacker, J., Brand, B.C., 1998. Legionella pneumophila kills human phagocytes but not protozoan host cells by inducing apoptotic cell death. FEMS Microbiol. Lett. 169, 51-58.

Hales, L.M., Shuman, H.A., 1999. Legionella pneumophila contains a type II general secretion pathway required for growth in amoebae as well as for secretion of the Msp protease. Infect. Immun. 67, 3662-3666.

Hamilton, K.A., Hamilton, M.T., Johnson, W., Jjemba, P., Bukhari, Z., LeChevallier, M., Haas, C.N., Gurian, P.L., 2019. Risk-Based Critical Concentrations of Legionella pneumophila for Indoor Residential Water Uses. Environ. Sci. Technol.

Hammer, B.K., Swanson, M.S., 1999. Co-ordination of Legionella pneumophila virulence with entry into stationary phase by ppGpp. Mol. Microbiol. 33, 721-731.

Hausser, A., Link, G., Hoene, M., Russo, C., Selchow, O., Pfizenmaier, K., 2006. Phospho-specific binding of 14-3-3 proteins to phosphatidylinositol 4-kinase III β protects from dephosphorylation and stabilizes lipid kinase activity. J. Cell Sci. 119, 3613-3621.

Hayek, I., Berens, C., Lührmann, A., 2019. Modulation of host cell metabolism by T4SS-encoding intracellular pathogens. Curr. Opin. Microbiol. 47, 59-65.

Heidtman, M., Chen, E.J., Moy, M.Y., Isberg, R.R., 2009. Large-scale identification of Legionella pneumophila Dot/Icm substrates that modulate host cell vesicle trafficking pathways. Cell. Microbiol. 11, 230-248.

Hengartner, M.O., 2000. The biochemistry of apoptosis. Nature 407, 770-776.

Hilbi, H., Hoffmann, C., Harrison, C.F., 2011a. Legionella spp. outdoors: colonization, communication and persistence. Environ. Microbiol. Rep. 3, 286-296.

Hilbi, H., Jarraud, S., Hartland, E., Buchrieser, C., 2010. Update on Legionnaires' disease: pathogenesis, epidemiology, detection and control. Mol. Microbiol. 76, 1-11.

Hilbi, H., Weber, S., Finsel, I., 2011b. Anchors for Effectors: Subversion of Phosphoinositide Lipids by Legionella. Front. Microbiol. 2.

Hiller, M., Lang, C., Michel, W., Flieger, A., 2018. Secreted phospholipases of the lung pathogen Legionella pneumophila. Int. J. Med. Microbiol. 308, 168-175.

Hollie, N.I., Cash, J.G., Matlib, M.A., Wortman, M., Basford, J.E., Abplanalp, W., Hui, D.Y., 2014. Micromolar changes in lysophosphatidylcholine concentration cause minor effects on mitochondrial permeability but major alterations in function. Biochim. Biophys. Acta 1841, 888-895.

Horwitz, M.A., Maxfield, F.R., 1984. Legionella pneumophila inhibits acidification of its phagosome in human monocytes. The Journal of cell biology 99, 1936-1943.

Horwitz, M.A., Silverstein, S.C., 1980. Legionnaires' disease bacterium (Legionella pneumophila) multiplies intracellularly in human monocytes. The Journal of clinical investigation 66, 441-450.

Ichimura, T., Isobe, T., Okuyama, T., Takahashi, N., Araki, K., Kuwano, R., Takahashi, Y., 1988. Molecular cloning of cDNA coding for brain-specific 14-3-3 protein, a protein kinase-dependent activator of tyrosine and tryptophan hydroxylases. Proceedings of the National Academy of Sciences 85, 7084-7088.

Jeong, K.C., Ghosal, D., Chang, Y.-W., Jensen, G.J., Vogel, J.P., 2017. Polar delivery of Legionella type IV secretion system substrates is essential for virulence. Proceedings of the National Academy of Sciences 114, 8077-8082.

Jepras, R., Fitzgeorge, R., Baskerville, A., 1985. A comparison of virulence of two strains of Legionella pneumophila based on experimental aerosol infection of guinea-pigs. Epidemiol. Infect. 95, 29-38.

Jones, D.H., Ley, S., Aitken, A., 1995. Isoforms of 14-3-3 protein can form homo- and heterodimers in vivo and in vitro: implications for function as adapter proteins. FEBS Lett. 368, 55-58.

Katagiri, N., Shobuike, T., Chang, B., Kukita, A., Miyamoto, H., 2012. The human apoptosis inhibitor NAIP induces pyroptosis in macrophages infected with Legionella pneumophila. Microbes and infection 14, 1123-1132.

Kelley, L.A., Mezulis, S., Yates, C.M., Wass, M.N., Sternberg, M.J., 2015. The Phyre2 web portal for protein modeling, prediction and analysis. Nat. Protoc. 10, 845-858.

Khan, F.I., Lan, D., Durrani, R., Huan, W., Zhao, Z., Wang, Y., 2017. The Lid Domain in Lipases: Structural and Functional Determinant of Enzymatic Properties. Frontiers in bioengineering and biotechnology 5, 16-16.

Koshland Jr., D.E., 1995. The Key–Lock Theory and the Induced Fit Theory. Angewandte Chemie International Edition in English 33, 2375-2378.

Krinos, C., High, A.S., Rodgers, F.G., 1999. Role of the 25 kDa major outer membrane protein of Legionella pneumophila in attachment to U-937 cells and its potential as a virulence factor for chick embryos. J. Appl. Microbiol. 86, 237-244.

Ku, B., Lee, K.H., Park, W.S., Yang, C.S., Ge, J., Lee, S.G., Cha, S.S., Shao, F., Heo, W.D., Jung, J.U., Oh, B.H., 2012. VipD of Legionella pneumophila targets activated Rab5 and Rab22 to interfere with endosomal trafficking in macrophages. PLoS Pathog. 8, e1003082.

Kubori, T., Hyakutake, A., Nagai, H., 2008. Legionella translocates an E3 ubiquitin ligase that has multiple U-boxes with distinct functions. Mol. Microbiol. 67, 1307-1319.

Kuhle, K., Krausze, J., Curth, U., Rossle, M., Heuner, K., Lang, C., Flieger, A., 2014. Oligomerization inhibits Legionella pneumophila PlaB phospholipase A activity. J. Biol. Chem. 289, 18657-18666.

Kurmanova, A., Llorente, A., Polesskaya, A., Garred, Ø., Olsnes, S., Kozlov, J., Sandvig, K., 2007. Structural requirements for furin-induced cleavage and activation of Shiga toxin. Biochem. Biophys. Res. Commun. 357, 144-149.

Kwaik, Y.A., 1996. The phagosome containing Legionella pneumophila within the protozoan Hartmannella vermiformis is surrounded by the rough endoplasmic reticulum. Appl. Environ. Microbiol. 62, 2022-2028.

Labbe, K., Saleh, M., 2008. Cell death in the host response to infection. Cell Death Differ. 15, 1339.

Laguna, R.K., Creasey, E.A., Li, Z., Valtz, N., Isberg, R.R., 2006. A Legionella pneumophila-translocated substrate that is required for growth within macrophages and protection from host cell death. Proceedings of the National Academy of Sciences 103, 18745-18750.

Laivier, C., Bleuze, M.O., Hantson, P., Devos, J., 2019. Extreme Rhabdomyolysis, Acute Renal Failure, and Protracted Ileus in a Case of Legionella Pneumonia. Case Rep Crit Care 2019, 3472627.

Lambert, J.P., Tucholska, M., Go, C., Knight, J.D., Gingras, A.C., 2015. Proximity biotinylation and affinity purification are complementary approaches for the interactome mapping of chromatin-associated protein complexes. J. Proteomics 118, 81-94.

Lamkanfi, M., Dixit, V.M., 2010. Manipulation of Host Cell Death Pathways during Microbial Infections. Cell Host & Microbe 8, 44-54.

Lang, C., Hiller, M., Flieger, A., 2017. Disulfide loop cleavage of Legionella pneumophila PlaA boosts lysophospholipase A activity. Sci. Rep. 7, 16313.

Lang, C., Rastew, E., Hermes, B., Siegbrecht, E., Ahrends, R., Banerji, S., Flieger, A., 2012. Zinc metalloproteinase ProA directly activates Legionella pneumophila PlaC glycerophospholipid:cholesterol acyltransferase. J. Biol. Chem. 287, 23464-23478.

Lawley, T.D., Chan, K., Thompson, L.J., Kim, C.C., Govoni, G.R., Monack, D.M., 2006. Genome-wide screen for Salmonella genes required for long-term systemic infection of the mouse. PLoS Pathog. 2, e11.

Leung, Y.M., Xion, Y., Ou, Y.J., Kwan, C.Y., 1998. Perturbation by lysophosphatidylcholine of membrane permeability in cultured vascular smooth muscle and endothelial cells. Life Sci. 63, 965-973.

Levental, I., Veatch, S., 2016. The Continuing Mystery of Lipid Rafts. J. Mol. Biol. 428, 4749-4764.

Lifshitz, Z., Burstein, D., Peeri, M., Zusman, T., Schwartz, K., Shuman, H.A., Pupko, T., Segal, G., 2013. Computational modeling and experimental validation of the Legionella and Coxiella virulence-related type-IVB secretion signal. Proceedings of the National Academy of Sciences 110, E707-E715.

Lin, M.-E., Herr, D.R., Chun, J., 2010. Lysophosphatidic acid (LPA) receptors: signaling properties and disease relevance. Prostaglandins Other Lipid Mediat. 91, 130-138.

Lordan, R., Tsoupras, A., Zabetakis, I., 2017. Phospholipids of Animal and Marine Origin: Structure, Function, and Anti-Inflammatory Properties. Molecules 22.

Losick, V.P., Isberg, R.R., 2006. NF-κB translocation prevents host cell death after low-dose challenge by Legionella pneumophila. J. Exp. Med. 203, 2177-2189.

Losick, V.P., Stephan, K., Smirnova, I.I., Isberg, R.R., Poltorak, A., 2009. A hemidominant Naip5 allele in mouse strain MOLF/Ei-derived macrophages restricts Legionella pneumophila intracellular growth. Infect. Immun. 77, 196-204.

Lossi, N.S., Rolhion, N., Magee, A.I., Boyle, C., Holden, D.W., 2008. The Salmonella SPI-2 effector SseJ exhibits eukaryotic activator-dependent phospholipase A and glycerophospholipid : cholesterol acyltransferase activity. Microbiology 154, 2680-2688.

MacDonald, L.J., Graham, J.G., Kurten, R.C., Voth, D.E., 2014. Coxiella burnetii exploits host cAMP-dependent protein kinase signalling to promote macrophage survival. Cell. Microbiol. 16, 146-159.

Machado, G.-B.S., de Assis, M.-C., Leão, R., Saliba, A.M., Silva, M.C., Suassuna, J.H., de Oliveira, A.V., Plotkowski, M.-C., 2010. ExoU-induced vascular hyperpermeability and platelet activation in the course of experimental Pseudomonas aeruginosa pneumosepsis. Shock 33, 315-321.

MacIntyre, S., Trust, T.J., Buckley, J.T., 1979. Distribution of glycerophospholipid-cholesterol acyltransferase in selected bacterial species. J. Bacteriol. 139, 132-136.

Madeira, F., Tinti, M., Murugesan, G., Berrett, E., Stafford, M., Toth, R., Cole, C., MacKintosh, C., Barton, G.J., 2015. 14-3-3-Pred: improved methods to predict 14-3-3-binding phosphopeptides. Bioinformatics 31, 2276-2283.

Marion, C.R., Dela Cruz, C.S., Niederman, M.S., 2016. What is Legionnaires' Disease? Am. J. Respir. Crit. Care Med. 193, P5-6.

Masters, S.C., Fu, H., 2001. 14-3-3 proteins mediate an essential anti-apoptotic signal. J. Biol. Chem. 276, 45193-45200.

Masters, S.C., Yang, H., Datta, S.R., Greenberg, M.E., Fu, H., 2001. 14-3-3 inhibits Bad-induced cell death through interaction with serine-136. Mol. Pharmacol. 60, 1325-1331.

Mateo, C., Fernandez-Lorente, G., Pessela, B.C.C., Vian, A., Carrascosa, A.V., Garcia, J.L., Fernandez-Lafuente, R., Guisan, J.M., 2001. Affinity chromatography of polyhistidine tagged enzymes: New dextran-coated immobilized metal ion affinity chromatography matrices for prevention of undesired multipoint adsorptions. J. Chromatogr. A 915, 97-106.

Mehta, D., 2005. Lysophosphatidylcholine: an enigmatic lysolipid. American Journal of Physiology-Lung Cellular and Molecular Physiology 289, L174-L175.

Miao, E.A., Miller, S.I., 2000. A conserved amino acid sequence directing intracellular type III secretion by Salmonella typhimurium. Proceedings of the National Academy of Sciences 97, 7539-7544.

Miller, M.B., Bassler, B.L., 2001. Quorum sensing in bacteria. Annu. Rev. Microbiol. 55, 165-199.

Molmeret, M., Kwaik, Y.A., 2002. How does Legionella pneumophila exit the host cell? Trends Microbiol. 10, 258-260.

Molofsky, A.B., Swanson, M.S., 2004. Differentiate to thrive: lessons from the Legionella pneumophila life cycle. Mol. Microbiol. 53, 29-40.

Murugesan, G., Rani, M.S., Gerber, C.E., Mukhopadhyay, C., Ransohoff, R.M., Chisolm, G.M., Kottke-Marchant, K., 2003. Lysophosphatidylcholine regulates human microvascular endothelial cell expression of chemokines. J. Mol. Cell. Cardiol. 35, 1375-1384.

Muslin, A.J., Tanner, J.W., Allen, P.M., Shaw, A.S., 1996. Interaction of 14-3-3 with signaling proteins is mediated by the recognition of phosphoserine. Cell 84, 889-897.

Muslin, A.J., Xing, H., 2000. 14-3-3 proteins: regulation of subcellular localization by molecular interference. Cell. Signal. 12, 703-709.

Nafis, S., Kalaiarasan, P., Brojen Singh, R.K., Husain, M., Bamezai, R.N., 2015. Apoptosis regulatory protein-protein interaction demonstrates hierarchical scale-free fractal network. Brief Bioinform 16, 675-699.

Nagai, H., Cambronne, E.D., Kagan, J.C., Amor, J.C., Kahn, R.A., Roy, C.R., 2005a. A C-terminal translocation signal required for Dot/Icm-dependent delivery of the Legionella RalF protein to host cells. Proc. Natl. Acad. Sci. U. S. A. 102, 826-831.

Nagai, H., Cambronne, E.D., Kagan, J.C., Amor, J.C., Kahn, R.A., Roy, C.R., 2005b. A C-terminal translocation signal required for Dot/Icm-dependent delivery of the Legionella RalF protein to host cells. Proceedings of the National Academy of Sciences 102, 826-831.

Neumeister, B., Faigle, M., Lauber, K., Northoff, H., Wesselborg, S., 2002. Legionella pneumophila induces apoptosis via the mitochondrial death pathway. Microbiology 148, 3639-3650.

Newton, H.J., Ang, D.K.Y., van Driel, I.R., Hartland, E.L., 2010. Molecular Pathogenesis of Infections Caused by Legionella pneumophila. Clin. Microbiol. Rev. 23, 274-298.

Nogueira, C.V., Lindsten, T., Jamieson, A.M., Case, C.L., Shin, S., Thompson, C.B., Roy, C.R., 2009. Rapid pathogen-induced apoptosis: a mechanism used by dendritic cells to limit intracellular replication of Legionella pneumophila. PLoS Pathog. 5, e1000478.

Nomura, M., Shimizu, S., Sugiyama, T., Narita, M., Ito, T., Matsuda, H., Tsujimoto, Y., 2003. 14-3-3 Interacts directly with and negatively regulates pro-apoptotic Bax. J. Biol. Chem. 278, 2058-2065.

Ogata, M., Fryling, C., Pastan, I., FitzGerald, D., 1992. Cell-mediated cleavage of Pseudomonas exotoxin between Arg279 and Gly280 generates the enzymatically active fragment which translocates to the cytosol. J. Biol. Chem. 267, 25396-25401.

Ohlson, M.B., Fluhr, K., Birmingham, C.L., Brumell, J.H., Miller, S.I., 2005. SseJ deacylase activity by Salmonella enterica serovar Typhimurium promotes virulence in mice. Infect. Immun. 73, 6249-6259.

Oliva, G., Sahr, T., Buchrieser, C., 2018. The life cycle of L. pneumophila: cellular differentiation is linked to virulence and metabolism. Frontiers in cellular and infection microbiology 8, 3.

Ourisson, G., Albrecht, P., Rohmer, M., 1979. The hopanoids: palaeochemistry and biochemistry of a group of natural products. Pure Appl. Chem. 51, 709-729.

Padilla-Carlin, D.J., McMurray, D.N., Hickey, A.J., 2008. The guinea pig as a model of infectious diseases. Comp. Med. 58, 324-340.

Payne, N.R., Horwitz, M.A., 1987. Phagocytosis of Legionella pneumophila is mediated by human monocyte complement receptors. The Journal of Experimental Medicine 166, 1377-1389.

Pennington, K., Chan, T., Torres, M., Andersen, J., 2018a. The dynamic and stress-adaptive signaling hub of 14-3-3: emerging mechanisms of regulation and context-dependent protein–protein interactions. Oncogene 37, 5587.

Pennington, K.L., Chan, T.Y., Torres, M.P., Andersen, J.L., 2018b. The dynamic and stress-adaptive signaling hub of 14-3-3: emerging mechanisms of regulation and context-dependent protein-protein interactions. Oncogene 37, 5587-5604.

Pistritto, G., Trisciuoglio, D., Ceci, C., Garufi, A., D'Orazi, G., 2016. Apoptosis as anticancer mechanism: function and dysfunction of its modulators and targeted therapeutic strategies. Aging (Albany NY) 8, 603-619.

Radivojac, P., Vacic, V., Haynes, C., Cocklin, R.R., Mohan, A., Heyen, J.W., Goebl, M.G., Iakoucheva, L.M., 2010. Identification, analysis, and prediction of protein ubiquitination sites. Proteins 78, 365-380.

Ragaz, C., Pietsch, H., Urwyler, S., Tiaden, A., Weber, S.S., Hilbi, H., 2008. The Legionella pneumophila phosphatidylinositol-4 phosphate-binding type IV substrate SidC recruits endoplasmic reticulum vesicles to a replication-permissive vacuole. Cell. Microbiol. 10, 2416-2433.

Rahme, L.G., Ausubel, F.M., Cao, H., Drenkard, E., Goumnerov, B.C., Lau, G.W., Mahajan-Miklos, S., Plotnikova, J., Tan, M.-W., Tsongalis, J., 2000. Plants and animals share functionally common bacterial virulence factors. Proceedings of the National Academy of Sciences 97, 8815-8821.

Ren, T., Zamboni, D.S., Roy, C.R., Dietrich, W.F., Vance, R.E., 2006. Flagellin-deficient Legionella mutants evade caspase-1- and Naip5-mediated macrophage immunity. PLoS Pathog. 2, e18.

RKI, 2013. Ausbruch von Legionärskrankheit in Warstein, Landkreis Soest. Epidemiologisches Bulletin 35.

RKI, 2018. Aktuelle Statistik meldepflichtiger Infektionskrankheiten, Deutschland. Epidemiologisches Bulletin 19.

RKI, 2019a. Aktuelle Statistik meldepflichtiger Infektionskrankheiten, Deutschland. Epidemilogisches Bulletin 14.

RKI, 2019b. Infektionsepidemiologisches Jahrbuch für 2018.

Roberts, R.L., Mösch, H.-U., Fink, G.R., 1997. 14-3-3 proteins are essential for RAS/MAPK cascade signaling during pseudohyphal development in S. cerevisiae. Cell 89, 1055-1065.

Robey, M., Cianciotto, N.P., 2002. Legionella pneumophila feoAB Promotes Ferrous Iron Uptake and Intracellular Infection. Infect. Immun. 70, 5659-5669.

Rossier, O., Cianciotto, N.P., 2005. The Legionella pneumophila tatB gene facilitates secretion of phospholipase C, growth under iron-limiting conditions, and intracellular infection. Infect. Immun. 73, 2020-2032.

Rossier, O., Starkenburg, S.R., Cianciotto, N.P., 2004. Legionella pneumophila Type II Protein Secretion Promotes Virulence in the A/J Mouse Model of Legionnaires' Disease Pneumonia. Infect. Immun. 72, 310-321.

Rowbotham, T., 1986. Current views on the relationships between amoebae, legionellae and man. Isr. J. Med. Sci. 22, 678-689.

Roy, C.R., 2012. Vacuolar pathogens value membrane integrity. Proc. Natl. Acad. Sci. U. S. A. 109, 3197-3198.

Rubin, B., 1994. Grease pit chemistry exposed. Nat. Struct. Biol. 1, 568.

Ruiz-Albert, J., Yu, X.J., Beuzón, C.R., Blakey, A.N., Galyov, E.E., Holden, D.W., 2002. Complementary activities of SseJ and SifA regulate dynamics of the Salmonella typhimurium vacuolar membrane. Mol. Microbiol. 44, 645-661.

Saliba, A., Nascimento, D., Silva, M., Assis, M., Gayer, C., Raymond, B., Coelho, M., Marques, E., Touqui, L., Albano, R., 2005. Eicosanoid-mediated proinflammatory activity of Pseudomonas aeruginosa ExoU. Cell. Microbiol. 7, 1811-1822.

Salte, R., Norberg, K., Arnesen, J., Ødegaard, O., Eggset, G., 1992. Serine protease and glycerophospholipid: cholesterol acyltransferase of Aeromonas salmonicida work in concert in thrombus formation; in vitro the process is counteracted by plasma antithrombin and α2-macroglobulin. J. Fish Dis. 15, 215-227.

Santic, M., Asare, R., Doric, M., Kwaik, Y.A., 2007. Host-dependent trigger of caspases and apoptosis by Legionella pneumophila. Infect. Immun. 75, 2903-2913.

Sato, H., Frank, D.W., 2004. ExoU is a potent intracellular phospholipase. Mol. Microbiol. 53, 1279-1290.

Savill, J., Dransfield, I., Gregory, C., Haslett, C., 2002. A blast from the past: clearance of apoptotic cells regulates immune responses. Nature Reviews Immunology 2, 965.

Schmidt, T.G.M., Skerra, A., 2007. The Strep-tag system for one-step purification and high-affinity detection or capturing of proteins. Nat. Protoc. 2, 1528.

Schmiel, D.H., Miller, V.L., 1999. Bacterial phospholipases and pathogenesis. Microbes and Infection 1, 1103-1112.

Schroeder, G.N., Aurass, P., Oates, C.V., Tate, E.W., Hartland, E.L., Flieger, A., Frankel, G., 2015. Legionella pneumophila Effector LpdA Is a Palmitoylated Phospholipase D Virulence Factor. Infect. Immun. 83, 3989-4002.

Schunder, E., Adam, P., Higa, F., Remer, K.A., Lorenz, U., Bender, J., Schulz, T., Flieger, A., Steinert, M., Heuner, K., 2010. Phospholipase PlaB is a new virulence factor of Legionella pneumophila. Int. J. Med. Microbiol. 300, 313-323.

Scidmore, M., Hackstadt, T., 2001. Mammalian 14-3-3β associates with the Chlamydia trachomatis inclusion membrane via its interaction with IncG. Mol. Microbiol. 39, 1638-1650.

Segal, G., Purcell, M., Shuman, H.A., 1998. Host cell killing and bacterial conjugation require overlapping sets of genes within a 22-kb region of the Legionella pneumophila genome. Proc. Natl. Acad. Sci. U. S. A. 95, 1669-1674.

Shevchuk, O., Batzilla, C., Hagele, S., Kusch, H., Engelmann, S., Hecker, M., Haas, A., Heuner, K., Glockner, G., Steinert, M., 2009. Proteomic analysis of Legionella-containing phagosomes isolated from Dictyostelium. Int. J. Med. Microbiol. 299, 489-508.

Shevchuk, O., Jäger, J., Steinert, M., 2011. Virulence properties of the legionella pneumophila cell envelope. Front. Microbiol. 2, 74.

Shohdy, N., Efe, J.A., Emr, S.D., Shuman, H.A., 2005. Pathogen effector protein screening in yeast identifies Legionella factors that interfere with membrane trafficking. Proc. Natl. Acad. Sci. U. S. A. 102, 4866-4871.

Simons, K., Van Meer, G., 1988. Lipid sorting in epithelial cells. Biochemistry 27, 6197-6202.

Sohlenkamp, C., Geiger, O., 2016. Bacterial membrane lipids: diversity in structures and pathways. FEMS Microbiol. Rev. 40, 133-159.

Souza, L.T.A., Oliveira, J.S., dos Santos, V.L., Regis, W.C.B., Santoro, M.M., Resende, R.R., 2014. Lipolytic potential of Aspergillus japonicus LAB01: production, partial purification, and characterisation of an extracellular lipase. BioMed research international 2014, 108913-108913.

Steinert, M., Hentschel, U., Hacker, J., 2002. Legionella pneumophila: an aquatic microbe goes astray. FEMS Microbiol. Rev. 26, 149-162.

Stewart, C.R., Rossier, O., Cianciotto, N.P., 2009. Surface translocation by Legionella pneumophila: a form of sliding motility that is dependent upon type II protein secretion. J. Bacteriol. 191, 1537-1546.

Stone, B.J., Abu Kwaik, Y., 1998. Expression of multiple pili by Legionella pneumophila: identification and characterization of a type IV pilin gene and its role in adherence to mammalian and protozoan cells. Infect. Immun. 66, 1768-1775.

Stone, B.J., Kwaik, Y.A., 1999. Natural competence for DNA transformation by Legionella pneumophila and its association with expression of type IV pili. J. Bacteriol. 181, 1395-1402.

Szeto, L., Shuman, H.A., 1990. The Legionella pneumophila major secretory protein, a protease, is not required for intracellular growth or cell killing. Infect. Immun. 58, 2585-2592.

Takeshita, S., Inoue, N., Gao, D., Rikitake, Y., Kawashima, S., Tawa, R., Sakurai, H., Yokoyama, M., 2000. Lysophosphatidylcholine enhances superoxide anions production via endothelial NADH/NADPH oxidase. Journal of atherosclerosis and thrombosis 7, 238-246.

Telles, E., Hosing, A.S., Kundu, S.T., Venkatraman, P., Dalal, S.N., 2009. A novel pocket in 14-3-3ε is required to mediate specific complex formation with cdc25C and to inhibit cell cycle progression upon activation of checkpoint pathways. Exp. Cell Res. 315, 1448-1457.

Thorson, J.A., Lily, W., Hsu, A.L., Shih, N.-Y., Graves, P.R., Tanner, J.W., Allen, P.M., Piwnica-Worms, H., Shaw, A.S., 1998. 14-3-3 proteins are required for maintenance of Raf-1 phosphorylation and kinase activity. Mol. Cell. Biol. 18, 5229-5238.

Tiaden, A., Spirig, T., Carranza, P., Brüggemann, H., Riedel, K., Eberl, L., Buchrieser, C., Hilbi, H., 2008. Synergistic Contribution of the Legionella pneumophila lqs Genes to Pathogen-Host Interactions. J. Bacteriol. 190, 7532-7547.

Tielen, P., Rosenau, F., Wilhelm, S., Jaeger, K.-E., Flemming, H.-C., Wingender, J., 2010. Extracellular enzymes affect biofilm formation of mucoid Pseudomonas aeruginosa. Microbiology 156, 2239-2252.

Toker, A., Sellers, L.A., Amess, B., Patel, Y., Harris, A., Aitken, A., 1992. Multiple isoforms of a protein kinase C inhibitor (KCIP-1/14-3-3) from sheep brain. Amino acid sequence of phosphorylated forms. Eur. J. Biochem. 206, 453-461.

Tompkins, L.S., Roessler, B.J., Redd, S.C., Markowitz, L.E., Cohen, M.L., 1988. Legionella Prosthetic-Valve Endocarditis. N. Engl. J. Med. 318, 530-535.

TrinkwV, 2018. Trinkwasserverordnung in der Fassung der Bekanntmachung vom 10. März 2016 (BGBl. I S. 459), die zuletzt durch Artikel 1 der Verordnung vom 3. Januar 2018 (BGBl. I S. 99) geändert worden ist, in: Bundesgesundheitsministerium (Ed.).

Truchan, H.K., Christman, H.D., White, R.C., Rutledge, N.S., Cianciotto, N.P., 2017. Type II secretion substrates of Legionella pneumophila translocate out of the pathogen-occupied vacuole via a semipermeable membrane. MBio 8, e00870-00817.

Tzivion, G., Dobson, M., Ramakrishnan, G., 2011. FoxO transcription factors; Regulation by AKT and 14-3-3 proteins. Biochimica et Biophysica Acta (BBA)-Molecular Cell Research 1813, 1938-1945.

Upton, C., Buckley, J.T., 1995. A new family of lipolytic enzymes? Trends Biochem. Sci. 20, 178-179.

Urwyler, S., Nyfeler, Y., Ragaz, C., Lee, H., Mueller, L.N., Aebersold, R., Hilbi, H., 2009. Proteome analysis of Legionella vacuoles purified by magnetic immunoseparation reveals secretory and endosomal GTPases. Traffic 10, 76-87.

van den Berg, B., 2010. Crystal Structure of a Full-Length Autotransporter. J. Mol. Biol. 396, 627-633.

van Deurs, B., Sandvig, K., 1995. Furin-induced cleavage and activation of Shiga toxin. J. Biol. Chem. 270, 10817-10821.

van Meer, G., Voelker, D.R., Feigenson, G.W., 2008. Membrane lipids: where they are and how they behave. Nature Reviews Molecular Cell Biology 9, 112.

Vanaman, T.C., Bradshaw, R.A., 1999. Proteases in cellular regulation minireview series. J. Biol. Chem. 274, 20047-20047.

Vanden Bergh, P., Frey, J., 2014. Aeromonas salmonicida subsp. salmonicida in the light of its type-three secretion system. Microbial biotechnology 7, 381-400.

VanRheenen, S.M., Luo, Z.Q., O'Connor, T., Isberg, R.R., 2006. Members of a Legionella pneumophila family of proteins with ExoU (phospholipase A) active sites are translocated to target cells. Infect. Immun. 74, 3597-3606.

Viner, R., Chetrit, D., Ehrlich, M., Segal, G., 2012. Identification of two Legionella pneumophila effectors that manipulate host phospholipids biosynthesis. PLoS Pathog. 8, e1002988.

Vogel, J.P., Andrews, H.L., Wong, S.K., Isberg, R.R., 1998. Conjugative transfer by the virulence system of Legionella pneumophila. Science 279, 873-876.

Vogel, J.P., Isberg, R.R., 1999. Cell biology of Legionella pneumophila. Curr. Opin. Microbiol. 2, 30-34.

Voth, D.E., Broederdorf, L.J., Graham, J.G., 2012. Bacterial Type IV secretion systems: versatile virulence machines. Future Microbiol. 7, 241-257.

Warren, W.J., Miller, R.D., 1979. Growth of Legionnaires disease bacterium (Legionella pneumophila) in chemically defined medium. J. Clin. Microbiol. 10, 50-55.

Weber, M.M., Faris, R., 2018. Subversion of the endocytic and secretory pathways by bacterial effector proteins. Frontiers in cell and developmental biology 6, 1.

Weber, S., Steiner, B., Welin, A., Hilbi, H., 2018. Legionella-Containing Vacuoles Capture PtdIns(4)P-Rich Vesicles Derived from the Golgi Apparatus. mBio 9, e02420-02418.

Weber, S., Wagner, M., Hilbi, H., 2014. Live-cell imaging of phosphoinositide dynamics and membrane architecture during Legionella infection. MBio 5, e00839-00813.

Weber, S.S., Ragaz, C., Reus, K., Nyfeler, Y., Hilbi, H., 2006. Legionella pneumophila exploits PI (4) P to anchor secreted effector proteins to the replicative vacuole. PLoS Pathog. 2, e46.

Weissenmayer, B.A., Prendergast, J.G.D., Lohan, A.J., Loftus, B.J., 2011. Sequencing Illustrates the Transcriptional Response of Legionella pneumophila during Infection and Identifies Seventy Novel Small Non-Coding RNAs. PLoS One 6.

White, R.C., Gunderson, F.F., Tyson, J.Y., Richardson, K.H., Portlock, T.J., Garnett, J.A., Cianciotto, N.P., 2018. Type II Secretion-Dependent Aminopeptidase LapA and Acyltransferase PlaC Are Redundant for Nutrient Acquisition during Legionella pneumophila Intracellular Infection of Amoebas. MBio 9.

Wilhelm, S., Gdynia, A., Tielen, P., Rosenau, F., Jaeger, K.-E., 2007. The Autotransporter Esterase EstA of Pseudomonas aeruginosa Is Required for Rhamnolipid Production, Cell Motility, and Biofilm Formation. J. Bacteriol. 189, 6695-6703.

Wright Jr, E.K., Goodart, S.A., Growney, J.D., Hadinoto, V., Endrizzi, M.G., Long, E.M., Sadigh, K., Abney, A.L., Bernstein-Hanley, I., Dietrich, W.F., 2003. Naip5 affects host susceptibility to the intracellular pathogen Legionella pneumophila. Curr. Biol. 13, 27-36.

Xing, H., Zhang, S., Weinheimer, C., Kovacs, A., Muslin, A.J., 2000. 14-3-3 proteins block apoptosis and differentially regulate MAPK cascades. The EMBO journal 19, 349-358.

Yaffe, M.B., Rittinger, K., Volinia, S., Caron, P.R., Aitken, A., Leffers, H., Gamblin, S.J., Smerdon, S.J., Cantley, L.C., 1997. The structural basis for 14-3-3: phosphopeptide binding specificity. Cell 91, 961-971.

Young, J.S., Farber, B.F., Pupovac, S.S., Graver, L.M., 2019. Prosthetic Valve Legionella Endocarditis. Ann. Thorac. Surg.

Zha, J., Harada, H., Yang, E., Jockel, J., Korsmeyer, S.J., 1996. Serine phosphorylation of death agonist BAD in response to survival factor results in binding to 14-3-3 not BCL-XL. Cell 87, 619-628.

Zhou, Q., Kee, Y.-S., Poirier, C.C., Jelinek, C., Osborne, J., Divi, S., Surcel, A., Will, M.E., Eggert, U.S., Müller-Taubenberger, A., Iglesias, P.A., Cotter, R.J., Robinson, D.N., 2010. 14-3-3 coordinates microtubules, Rac, and myosin II to control cell mechanics and cytokinesis. Current biology : CB 20, 1881-1889.

Zhu, W., Banga, S., Tan, Y., Zheng, C., Stephenson, R., Gately, J., Luo, Z.Q., 2011. Comprehensive Identification of Protein Substrates of the Dot/Icm Type IV Transporter of Legionella pneumophila. PLoS One 6.

Zhu, W., Hammad, L.A., Hsu, F., Mao, Y., Luo, Z.Q., 2013. Induction of caspase 3 activation by multiple Legionella pneumophila Dot/Icm substrates. Cell. Microbiol. 15, 1783-1795.

Zink, S.D., Pedersen, L., Cianciotto, N.P., Abu-Kwaik, Y., 2002. The Dot/Icm type IV secretion system of Legionella pneumophila is essential for the induction of apoptosis in human macrophages. Infect. Immun. 70, 1657-1663.

6 Supplement

6.1 Listings of all proteins identified during mass spectrometry analysis of BioID assay

Table 37: List of proteins identified in the BioID assay when comparing BirA*-PlaD transfected with non-transfected cells without additional infection.
The values listed are only those that were significantly enriched via with a false discovery rate controlled t-tests. The list is sorted by increasing fold changes. Proteins printed in bold, italic letters have been identified in all four conditions that were applied for analysis of the BioID results.

Protein name	Gene name	Fold change	P-value
Tight junction protein ZO-1	TJP1	1,85	0,0007
14-3-3 protein eta	***YWHAH***	***3,88***	***0,0047***
14-3-3 protein epsilon	***YWHAE***	***11,72***	***0,0014***
14-3-3 protein theta	***YWHAQ***	***12,10***	***0,0015***
14-3-3 protein beta/alpha;14-3-3 protein beta/alpha, N-terminally processed	***YWHAB***	***12,44***	***0,0013***
14-3-3 protein gamma;14-3-3 protein gamma, N-terminally processed	***YWHAG***	***13,35***	***0,0006***
14-3-3 protein zeta/delta	***YWHAZ***	***14,70***	***0,0021***

Table 38: List of proteins identified in the BioID assay when comparing BirA*-PlaD transfected with non-transfected cells with additional *L. pneumophila* infection.
The values listed are only those that were significantly enriched via with a false discovery rate controlled t-tests. The list is sorted by increasing fold changes. Proteins printed in bold, italic letters have been identified in all four conditions that were applied for analysis of the BioID results.

Protein name	Gene name	Fold change	P-value
Ribosome-binding protein 1	RRBP1	2,05	0,0037
Sequestosome-1	SQSTM1	2,56	0,0012
14-3-3 protein eta	***YWHAH***	***2,56***	***0,0029***
14-3-3 protein epsilon	***YWHAE***	***3,20***	***0,0025***
14-3-3 protein beta/alpha;14-3-3 protein beta/alpha, N-terminally processed	***YWHAB***	***3,38***	***0,0040***
14-3-3 protein gamma;14-3-3 protein gamma, N-terminally processed	***YWHAG***	***3,55***	***0,0005***
14-3-3 protein zeta/delta	***YWHAZ***	***3,76***	***0,0028***
14-3-3 protein theta	***YWHAQ***	***4,92***	***0,0053***

Table 39: List of proteins identified in the BioID assay when comparing BirA*-PlaD transfected with BirA* transfected cells without additional infection.
The values listed are only those that were significantly enriched via with a false discovery rate controlled t-tests. The list is sorted by increasing fold changes. Proteins printed in bold, italic letters have been identified in all four conditions that were applied for analysis of the BioID results.

Protein name	Gene name	Fold change	P-value
Erythrocyte band 7 integral membrane protein	STOM	1,59	0,0005
14-3-3 protein eta	***YWHAH***	***2,46***	***0,0152***
Methylcrotonoyl-CoA carboxylase beta chain, mitochondrial	MCCC2	2,82	0,0115
Propionyl-CoA carboxylase alpha chain, mitochondrial	PCCA	2,88	0,0204
Propionyl-CoA carboxylase beta chain, mitochondrial	PCCB	2,89	0,0079
Dermcidin;Survival-promoting peptide;DCD-1	DCD	3,43	0,0040
14-3-3 protein gamma;14-3-3 protein gamma, N-terminally processed	***YWHAG***	***3,99***	***0,0022***
14-3-3 protein epsilon	***YWHAE***	***4,19***	***0,0007***
14-3-3 protein beta/alpha;14-3-3 protein beta/alpha, N-terminally processed	***YWHAB***	***4,60***	***0,0005***
14-3-3 protein zeta/delta	***YWHAZ***	***5,61***	***0,0003***
14-3-3 protein theta	***YWHAQ***	***5,84***	***0,0003***

Table 40: List of proteins identified in the BioID assay when comparing BirA*-PlaD transfected with BirA* transfected cells with additional *L. pneumophila* infection.
T The values listed are only those that were significantly enriched via with a false discovery rate controlled t-tests. The list is sorted by increasing fold changes. Proteins printed in bold, italic letters have been identified in all four conditions that were applied for analysis of the BioID results.

Protein name	Gene name	Fold change	P-value
4F2 cell-surface antigen heavy chain	SLC3A2	1.21	0.0019
Guanine nucleotide-binding protein G(s) subunit alpha isoforms short;Guanine nucleotide-binding protein G(s) subunit alpha isoforms XLas	GNAS	1.27	0.0078
ATP-dependent RNA helicase A	DHX9	1.28	0.0108
Ribosomal protein L19;60S ribosomal protein L19	RPL19	1.32	0.0250
60S ribosomal protein L31	RPL31	1.34	0.0231
40S ribosomal protein S3a	RPS3A	1.36	0.0026
ATP synthase subunit alpha, mitochondrial	ATP5A1	1.36	0.0241
60S ribosomal protein L7a	RPL7A	1.39	0.0113
78 kDa glucose-regulated protein	HSPA5	1.41	0.0400
60S ribosomal protein L5	RPL5	1.41	0.0112
Histone H1x	H1FX	1.41	0.0009

Protein name	Gene name	Fold change	P-value
60S ribosomal protein L13	RPL13	1.41	0.0041
ELAV-like protein 1	ELAVL1	1.44	0.0004
60S ribosomal protein L26	RPL26;KRBA2	1.44	0.0086
Eukaryotic translation initiation factor 1A, X-chromosomal;Eukaryotic translation initiation factor 1A, Y-chromosomal	EIF1AX;EIF1AY	1.46	0.0236
60S ribosomal protein L6	RPL6	1.47	0.0178
Voltage-dependent anion-selective channel protein 2	VDAC2	1.47	0.0196
Polypyrimidine tract-binding protein 1	PTBP1	1.48	0.0033
Cytochrome c oxidase subunit 5B, mitochondrial	COX5B	1.50	0.0399
Nicotinamide phosphoribosyltransferase	NAMPT	1.50	0.0041
Membrane-associated progesterone receptor component 1	PGRMC1	1.52	0.0614
Histone H2A.V;Histone H2A.Z;Histone H2A	H2AFV;H2AFZ	1.52	0.0562
40S ribosomal protein S16	RPS16	1.53	0.0258
Apoptosis-inducing factor 1, mitochondrial	AIFM1	1.54	0.0157
Neutral amino acid transporter B(0)	SLC1A5	1.55	0.0023
Heterogeneous nuclear ribonucleoprotein M	HNRNPM	1.56	0.0243
40S ribosomal protein S13	RPS13	1.57	0.0094
Alpha-enolase	ENO1	1.57	0.0014
Proliferating cell nuclear antigen	PCNA	1.58	0.0297
60S ribosomal protein L23a	RPL23A	1.58	0.0234
ADP-ribosylation factor 1;ADP-ribosylation factor 3;ADP-ribosylation factor 5	ARF1;ARF3;ARF5	1.58	0.0303
Prohibitin-2	PHB2	1.59	0.0087
Myoferlin	MYOF	1.59	0.0347
Puromycin-sensitive aminopeptidase	NPEPPS	1.59	0.0613
MICOS complex subunit MIC60	IMMT	1.59	0.0289
60S ribosomal protein L32	RPL32	1.60	0.0246
Tubulin beta-2A chain;Tubulin beta-2B chain	TUBB2A;TUBB2B	1.60	0.0267
Non-histone chromosomal protein HMG-17;High mobility group nucleosome-binding domain-containing protein 3	HMGN2;HMGN3	1.60	0.0507
Interleukin enhancer-binding factor 3	ILF3	1.60	0.0242
ATP synthase subunit beta, mitochondrial; ATP synthase subunit beta	ATP5B	1.60	0.0153

Protein name	Gene name	Fold change	P-value
Histone H1.5	HIST1H1B	1.60	0.0701
ATP-dependent RNA helicase DDX18	DDX18	1.61	0.0374
Integrin alpha-3;Integrin alpha-3 heavy chain; Integrin alpha-3 light chain	ITGA3	1.61	0.0263
Leukocyte elastase inhibitor	SERPINB1	1.62	0.0099
Guanine nucleotide-binding protein G(k) subunit alpha; Guanine nucleotide-binding protein G(i) subunit alpha-1; Guanine nucleotide-binding protein G(o) subunit alpha; Guanine nucleotide-binding protein G(i) subunit alpha-2	GNAI3;GNAI1;GNAO1;GNAI2	1.62	0.0673
Heterogeneous nuclear ribonucleoprotein A/B	HNRNPAB	1.62	0.0063
ATP-dependent 6-phosphofructokinase, platelet type	PFKP	1.62	0.0710
Nucleolar RNA helicase 2	DDX21	1.62	0.0313
Putative RNA-binding protein Luc7-like 2	LUC7L2	1.63	0.0160
Prohibitin	PHB	1.63	0.0006
Macrophage migration inhibitory factor	MIF	1.63	0.0474
Ras-related C3 botulinum toxin substrate 1;Ras-related C3 botulinum toxin substrate 3;Ras-related C3 botulinum toxin substrate 2	RAC1;RAC3;RAC2	1.64	0.0638
Heterogeneous nuclear ribonucleoprotein H3	HNRNPH3	1.65	0.0560
Peptidyl-prolyl cis-trans isomerase FKBP1A;Peptidyl-prolyl cis-trans isomerase	FKBP1A	1.66	0.0401
ATP-dependent RNA helicase DDX1	DDX1	1.67	0.0168
Adenylate kinase 2, mitochondrial; Adenylate kinase 2, mitochondrial; Adenylate kinase 2, mitochondrial, N-terminally processed	AK2	1.68	0.0539
D-3-phosphoglycerate dehydrogenase	PHGDH	1.69	0.0164
Histone H1.2	HIST1H1C	1.69	0.0034
Asparagine--tRNA ligase, cytoplasmic	NARS	1.70	0.0501
Acyl-CoA-binding protein	DBI	1.70	0.0590
THO complex subunit 4	ALYREF	1.70	0.0654
Copine-3	CPNE3	1.70	0.0723
Dynamin-2	DNM2	1.70	0.0073
Spermidine synthase	SRM	1.71	0.0628
ATP-binding cassette sub-family E member 1	ABCE1	1.71	0.0269
Acyl-coenzyme A thioesterase 1;Acyl-coenzyme A thioesterase 2, mitochondrial	ACOT1;ACOT2	1.73	0.0585
Histone H1.0;Histone H1.0, N-terminally processed	H1F0	1.73	0.0101

Protein name	Gene name	Fold change	P-value
Delta-1-pyrroline-5-carboxylate synthase; Glutamate 5-kinase;Gamma-glutamyl phosphate reductase	ALDH18A1	1.73	0.0449
Nucleoside diphosphate kinase; Nucleoside diphosphate kinase B	NME1-NME2;NME2;NME1	1.74	0.0347
Thioredoxin-dependent peroxide reductase, mitochondrial	PRDX3	1.74	0.0688
60S ribosomal protein L10a	RPL10A	1.74	0.0439
Trifunctional enzyme subunit beta, mitochondrial;3-ketoacyl-CoA thiolase	HADHB	1.74	0.0158
Glyceraldehyde-3-phosphate dehydrogenase	GAPDH	1.74	0.0080
Pyruvate kinase PKM;Pyruvate kinase	PKM	1.74	0.0102
Hsc70-interacting protein; Putative protein FAM10A4;Putative protein FAM10A5	ST13;ST13P4;ST13P5	1.75	0.0470
40S ribosomal protein S18	RPS18	1.75	0.0010
Triosephosphate isomerase	TPI1	1.75	0.0373
Inorganic pyrophosphatase	PPA1	1.75	0.0136
60S acidic ribosomal protein P0;60S acidic ribosomal protein P0-like	RPLP0;RPLP0P6	1.75	0.0069
40S ribosomal protein S10;Putative 40S ribosomal protein S10-like	RPS10;RPS10	1.76	0.0115
Heat shock protein HSP 90-beta;Putative heat shock protein HSP 90-beta-3	HSP90AB1;HSP90AB3P	1.76	0.0329
Glutamate--cysteine ligase regulatory subunit	GCLM	1.76	0.0021
Ubiquitin-conjugating enzyme E2 N; Putative ubiquitin-conjugating enzyme E2 N-like	UBE2N;UBE2NL	1.77	0.0644
Ras GTPase-activating-like protein IQGAP1	IQGAP1	1.78	0.0149
Integrin beta-1	ITGB1	1.78	0.0327
NADH-ubiquinone oxidoreductase 75 kDa subunit, mitochondrial	NDUFS1	1.79	0.0611
Actin, cytoplasmic 1;Actin, cytoplasmic 1, N-terminally processed	ACTB	1.80	0.0018
X-ray repair cross-complementing protein 5	XRCC5	1.80	0.0336
Putative heat shock protein HSP 90-beta 2	HSP90AB2P	1.81	0.0409
L-lactate dehydrogenase A chain	LDHA	1.82	0.0106
40S ribosomal protein S4, X isoform;40S ribosomal protein S4, Y isoform 1	RPS4X;RPS4Y1	1.82	0.0204
60S ribosomal protein L35	RPL35	1.82	0.0112
Proteasome subunit beta type-1	PSMB1	1.82	0.0761

Protein name	Gene name	Fold change	P-value
Lysosomal alpha-glucosidase;76 kDa lysosomal alpha-glucosidase;70 kDa lysosomal alpha-glucosidase	GAA	1.83	0.0169
Atlastin-3	ATL3	1.83	0.0167
C-1-tetrahydrofolate synthase, cytoplasmic; Methylenetetrahydrofolate dehydrogenase; Methenyltetrahydrofolate cyclohydrolase; Formyltetrahydrofolate synthetase; C-1-tetrahydrofolate synthase, cytoplasmic, N-terminally processed	MTHFD1	1.83	0.0557
Cytochrome b-c1 complex subunit 1, mitochondrial	UQCRC1	1.83	0.0870
60S ribosomal protein L17	RPL17	1.84	0.0494
Rho GDP-dissociation inhibitor 1	ARHGDIA	1.84	0.0479
Cytochrome c oxidase subunit 5A, mitochondrial	COX5A	1.84	0.0683
Eukaryotic peptide chain release factor subunit 1	ETF1	1.84	0.0247
Staphylococcal nuclease domain-containing protein 1	SND1	1.85	0.0572
Fatty acid-binding protein, epidermal	FABP5	1.85	0.0093
Transketolase	TKT	1.85	0.0343
Sodium/potassium-transporting ATPase subunit alpha-1	ATP1A1	1.85	0.0077
Heat shock 70 kDa protein 4	HSPA4	1.85	0.0225
Ras-related protein Rab-10	RAB10	1.86	0.0451
Flavin reductase (NADPH)	BLVRB	1.86	0.0279
Elongation factor 1-alpha 1;Putative elongation factor 1-alpha-like 3;Elongation factor 1-alpha 2	EEF1A1;EEF1A1P5;EEF1A2	1.86	0.0531
ATP synthase subunit O, mitochondrial	ATP5O	1.87	0.0227
Cytochrome c oxidase subunit NDUFA4	NDUFA4	1.87	0.0044
Peptidyl-prolyl cis-trans isomerase FKBP4;Peptidyl-prolyl cis-trans isomerase FKBP4, N-terminally processed	FKBP4	1.88	0.0343
Proliferation-associated protein 2G4	PA2G4	1.89	0.0561
Electron transfer flavoprotein subunit alpha, mitochondrial	ETFA	1.89	0.0114
Peroxisomal multifunctional enzyme type 2;(3R)-hydroxyacyl-CoA dehydrogenase; Enoyl-CoA hydratase 2	HSD17B4	1.89	0.0776
		1.89	0.0920
Threonine--tRNA ligase, cytoplasmic	TARS	1.91	0.0671
Isocitrate dehydrogenase [NADP] cytoplasmic	IDH1	1.91	0.0234
ATP synthase subunit g, mitochondrial	ATP5L	1.92	0.0096
Leucine-rich PPR motif-containing protein, mitochondrial	LRPPRC	1.92	0.0808
Transferrin receptor protein 1;Transferrin receptor protein 1, serum form	TFRC	1.93	0.0231

Protein name	Gene name	Fold change	P-value
Heat shock protein 75 kDa, mitochondrial	TRAP1	1.93	0.0470
Peroxiredoxin-6	PRDX6	1.93	0.0126
Sulfide:quinone oxidoreductase, mitochondrial	SQRDL	1.94	0.0563
Aldose reductase	AKR1B1	1.94	0.0822
Adenosylhomocysteinase	AHCY	1.96	0.0241
Voltage-dependent anion-selective channel protein 3	VDAC3	1.97	0.0306
Microsomal glutathione S-transferase 1	MGST1	1.98	0.0057
Thymosin beta-10	TMSB10	1.98	0.0723
Cullin-associated NEDD8-dissociated protein 1	CAND1	1.98	0.0878
WD repeat-containing protein 1	WDR1	1.99	0.0419
10 kDa heat shock protein, mitochondrial	HSPE1	1.99	0.0044
Putative RNA-binding protein 3	RBM3	2.00	0.0503
High mobility group protein B1;Putative high mobility group protein B1-like 1	HMGB1;HMGB1P1	2.00	0.0248
Dynein light chain roadblock-type 1;Dynein light chain roadblock-type 2	DYNLRB1;DYNLRB2	2.00	0.0051
ADP-ribosylation factor-like protein 1	ARL1	2.00	0.0602
Thiosulfate sulfurtransferase	TST	2.01	0.0347
Aldehyde dehydrogenase, mitochondrial	ALDH2	2.01	0.0241
14-3-3 protein sigma	SFN	2.01	0.0658
Sideroflexin-1	SFXN1	2.01	0.0085
Heat shock protein HSP 90-alpha	HSP90AA1	2.01	0.0327
Dolichyl-diphosphooligosaccharide--protein glycosyltransferase subunit 1	RPN1	2.01	0.0764
Reticulon-4 receptor-like 2	RTN4RL2	2.02	0.0511
Endoplasmin	HSP90B1	2.02	0.0097
Transitional endoplasmic reticulum ATPase	VCP	2.02	0.0230
Serum paraoxonase/arylesterase 2	PON2	2.03	0.0485
Leukotriene A-4 hydrolase	LTA4H	2.03	0.0403
Leucine-rich repeat-containing protein 59	LRRC59	2.04	0.0125
Retinal dehydrogenase 1	ALDH1A1	2.04	0.0345
Barrier-to-autointegration factor;Barrier-to-autointegration factor, N-terminally processed	BANF1	2.05	0.0290
NADH dehydrogenase [ubiquinone] 1 alpha subcomplex subunit 9, mitochondrial	NDUFA9	2.05	0.0555

Protein name	Gene name	Fold change	P-value
NADH dehydrogenase [ubiquinone] 1 alpha subcomplex subunit 13	NDUFA13	2.05	0.0398
Fumarate hydratase, mitochondrial	FH	2.05	0.0094
Tubulin-specific chaperone A	TBCA	2.06	0.0671
Retinol dehydrogenase 11	RDH11	2.06	0.0344
Carbonyl reductase [NADPH] 1	CBR1	2.07	0.0246
Very long-chain specific acyl-CoA dehydrogenase, mitochondrial	ACADVL	2.07	0.0103
Protein arginine N-methyltransferase 1	PRMT1	2.08	0.0729
Sterol-4-alpha-carboxylate 3-dehydrogenase, decarboxylating	NSDHL	2.08	0.0235
Isocitrate dehydrogenase [NAD] subunit alpha, mitochondrial	IDH3A	2.08	0.0247
Transmembrane emp24 domain-containing protein 10	TMED10	2.08	0.0517
Transaldolase	TALDO1	2.09	0.0236
Aldo-keto reductase family 1 member C2	AKR1C2	2.09	0.0763
L-lactate dehydrogenase B chain;L-lactate dehydrogenase	LDHB	2.09	0.0075
Peptidyl-prolyl cis-trans isomerase FKBP3	FKBP3	2.09	0.0442
Proteasome subunit alpha type-5	PSMA5	2.10	0.0609
Delta(3,5)-Delta(2,4)-dienoyl-CoA isomerase, mitochondrial	ECH1	2.10	0.0015
Parathymosin	PTMS	2.10	0.0204
SUMO-activating enzyme subunit 2	UBA2	2.11	0.0101
Far upstream element-binding protein 1	FUBP1	2.12	0.0019
60S ribosomal protein L38	RPL38	2.12	0.0307
Proteasome subunit alpha type;Proteasome subunit alpha type-4;Proteasome subunit beta type	PSMA4	2.12	0.0327
Chloride intracellular channel protein 1	CLIC1	2.12	0.0318
Ras-related protein Rab-11A;Ras-related protein Rab-11B	RAB11A;RAB 11B	2.13	0.0052
RNA-binding protein Raly	RALY	2.13	0.0848
Trifunctional enzyme subunit alpha, mitochondrial;Long-chain enoyl-CoA hydratase;Long chain 3-hydroxyacyl-CoA dehydrogenase	HADHA	2.13	0.0036
Persulfide dioxygenase ETHE1, mitochondrial	ETHE1	2.13	0.0289
Annexin A11	ANXA11	2.14	0.0118
Contactin-1	CNTN1	2.14	0.0383

Protein name	Gene name	Fold change	P-value
26S proteasome non-ATPase regulatory subunit 6	PSMD6	2.14	0.0292
Reticulon;Reticulon-4	RTN4	2.15	0.0185
40S ribosomal protein S19	RPS19	2.16	0.0041
40S ribosomal protein SA	RPSA	2.16	0.0133
Cytoskeleton-associated protein 4	CKAP4	2.17	0.0137
Valine--tRNA ligase	VARS	2.17	0.0817
Tricarboxylate transport protein, mitochondrial	SLC25A1	2.17	0.0340
Heterogeneous nuclear ribonucleoproteins A2/B1	HNRNPA2B1	2.18	0.0103
Proteasome subunit beta type-5	PSMB5	2.18	0.0369
DNA-(apurinic or apyrimidinic site) lyase;DNA-(apurinic or apyrimidinic site) lyase, mitochondrial	APEX1	2.19	0.0345
Glutathione S-transferase omega-1	GSTO1	2.19	0.0246
3-oxo-5-beta-steroid 4-dehydrogenase	AKR1D1	2.19	0.0239
Serine hydroxymethyltransferase, mitochondrial;Serine hydroxymethyltransferase	SHMT2	2.20	0.0595
39S ribosomal protein L12, mitochondrial	MRPL12	2.20	0.0911
Fructose-bisphosphate aldolase C	ALDOC	2.20	0.0595
Stress-induced-phosphoprotein 1	STIP1	2.21	0.0341
Proteasome subunit alpha type-7	PSMA7	2.21	0.0432
RNA-binding motif protein, X chromosome;RNA-binding motif protein, X chromosome, N-terminally processed;RNA binding motif protein, X-linked-like-1	RBMX;RBMX L1	2.21	0.0079
Dolichyl-diphosphooligosaccharide--protein glycosyltransferase subunit 2	RPN2	2.21	0.0213
Histidine triad nucleotide-binding protein 2, mitochondrial	HINT2	2.22	0.0005
40S ribosomal protein S7	RPS7	2.22	0.0357
Cytochrome b-c1 complex subunit 6, mitochondrial	UQCRH	2.23	0.0810
Citrate synthase;Citrate synthase, mitochondrial	CS	2.23	0.0368
Electron transfer flavoprotein subunit beta	ETFB	2.23	0.0199
Thymosin beta-4;Hematopoietic system regulatory peptide	TMSB4X	2.24	0.0551
Dolichyl-diphosphooligosaccharide--protein glycosyltransferase subunit DAD1	DAD1	2.24	0.0785
Aconitate hydratase, mitochondrial	ACO2	2.25	0.0468
Cytochrome c oxidase subunit 2	MT-CO2	2.25	0.0095
Glucosidase 2 subunit beta	PRKCSH	2.25	0.0171

Protein name	Gene name	Fold change	P-value
Sorting and assembly machinery component 50 homolog	SAMM50	2.25	0.0170
ATP synthase subunit delta, mitochondrial	ATP5D	2.26	0.0823
Cytochrome c1, heme protein, mitochondrial	CYC1	2.26	0.0050
Proteasome subunit alpha type;Proteasome subunit alpha type-6	PSMA6	2.27	0.0091
Mitochondrial import receptor subunit TOM40 homolog	TOMM40	2.28	0.0333
Aspartyl/asparaginyl beta-hydroxylase	ASPH	2.29	0.0085
Transportin-1	TNPO1	2.29	0.0362
Profilin-1	PFN1	2.29	0.0233
Purine nucleoside phosphorylase	PNP	2.31	0.0572
Nicalin	NCLN	2.31	0.0043
X-ray repair cross-complementing protein 6	XRCC6	2.34	0.0588
Malate dehydrogenase, mitochondrial;Malate dehydrogenase	MDH2	2.34	0.0249
Calreticulin	CALR	2.35	0.0131
Heterogeneous nuclear ribonucleoprotein A1;Heterogeneous nuclear ribonucleoprotein A1, N-terminally processed;Heterogeneous nuclear ribonucleoprotein A1-like 2	HNRNPA1;HNRNPA1L2	2.36	0.0237
Dolichyl-diphosphooligosaccharide--protein glycosyltransferase 48 kDa subunit	DDOST	2.37	0.0098
Prenylcysteine oxidase 1	PCYOX1	2.37	0.0014
Proteasome activator complex subunit 1	PSME1	2.37	0.0492
Translocon-associated protein subunit delta	SSR4	2.37	0.0418
GTP:AMP phosphotransferase AK3, mitochondrial	AK3	2.37	0.0190
NSFL1 cofactor p47	NSFL1C	2.38	0.0116
Annexin A6;Annexin	ANXA6	2.40	0.0424
Microsomal glutathione S-transferase 3	MGST3	2.41	0.0080
Obg-like ATPase 1	OLA1	2.41	0.0945
Annexin A1	ANXA1	2.41	0.0422
Lon protease homolog, mitochondrial	LONP1	2.43	0.0041
ADP-ribosylation factor 4	ARF4	2.44	0.0125
Adipocyte plasma membrane-associated protein	APMAP	2.44	0.0032
Alpha-actinin-4	ACTN4	2.46	0.0539
Neutral alpha-glucosidase AB	GANAB	2.47	0.0623
ERO1-like protein alpha	ERO1L	2.48	0.1055

Protein name	Gene name	Fold change	P-value
Malate dehydrogenase, cytoplasmic;Malate dehydrogenase	MDH1	2.48	0.0066
Rab GDP dissociation inhibitor beta	GDI2	2.50	0.0111
		2.50	0.0256
Prostaglandin reductase 1	PTGR1	2.52	0.0159
Dihydrolipoyl dehydrogenase, mitochondrial	DLD	2.53	0.0381
Thioredoxin domain-containing protein 17	TXNDC17	2.53	0.0305
Ubiquitin-like modifier-activating enzyme 1	UBA1	2.54	0.0815
Long-chain-fatty-acid--CoA ligase 3	ACSL3	2.54	0.0464
Cytochrome b5 type B	CYB5B	2.55	0.0697
Acyl-coenzyme A thioesterase 13;Acyl-coenzyme A thioesterase 13, N-terminally processed	ACOT13	2.55	0.0339
Epoxide hydrolase 1	EPHX1	2.56	0.0033
Protein disulfide-isomerase A6	PDIA6	2.56	0.0708
Cytochrome c oxidase subunit 4 isoform 1, mitochondrial	COX4I1	2.57	0.0081
40S ribosomal protein S5;40S ribosomal protein S5, N-terminally processed	RPS5	2.59	0.0386
Protein disulfide-isomerase	P4HB	2.59	0.0509
CD44 antigen	CD44	2.59	0.0240
B-cell receptor-associated protein 31	BCAP31	2.59	0.0154
Aldehyde dehydrogenase, dimeric NADP-preferring	ALDH3A1	2.60	0.0320
Thymidylate kinase	DTYMK	2.60	0.0238
DNA topoisomerase 1	TOP1	2.62	0.0212
Endoplasmic reticulum resident protein 29	ERP29	2.63	0.0338
Succinyl-CoA ligase [GDP-forming] subunit beta, mitochondrial	SUCLG2	2.63	0.0761
Ras-related protein Rap-1b;Ras-related protein Rap-1A;Ras-related protein Rap-1b-like protein	RAP1B;RAP1A	2.65	0.0526
Glutathione S-transferase P	GSTP1	2.65	0.0126
Fructose-bisphosphate aldolase A	ALDOA	2.66	0.0618
Mitochondrial import receptor subunit TOM70	TOMM70A	2.67	0.0458
Quinone oxidoreductase	CRYZ	2.68	0.0115
Glutamate dehydrogenase 1, mitochondrial;Glutamate dehydrogenase 2, mitochondrial	GLUD1;GLUD2	2.69	0.0714
Protein disulfide-isomerase A3	PDIA3	2.71	0.0158
14-3-3 protein gamma;14-3-3 protein gamma, N-	***YWHAG***	***2.72***	***0.0045***

Protein name	Gene name	Fold change	P-value
terminally processed			
Protein disulfide-isomerase A4	PDIA4	2.77	0.0419
Importin-5	IPO5	2.78	0.0301
Galectin-1	LGALS1	2.83	0.0129
Plastin-3	PLS3	2.84	0.0512
Annexin A5;Annexin	ANXA5	2.86	0.0965
Aldo-keto reductase family 1 member C3	AKR1C3	2.90	0.0543
6-phosphogluconate dehydrogenase, decarboxylating	PGD	2.91	0.0384
14-3-3 protein eta	***YWHAH***	***2.92***	***0.0014***
Glucose-6-phosphate isomerase	GPI	2.97	0.0961
Aspartate aminotransferase, mitochondrial	GOT2	2.98	0.0343
14-3-3 protein epsilon	***YWHAE***	***3.00***	***0.0088***
Aldo-keto reductase family 1 member B10	AKR1B10	3.03	0.0823
Peptidyl-prolyl cis-trans isomerase B	PPIB	3.08	0.0690
NAD(P)H dehydrogenase [quinone] 1	NQO1	3.09	0.0435
Anterior gradient protein 2 homolog	AGR2	3.23	0.0807
Bifunctional purine biosynthesis protein PURH;Phosphoribosylaminoimidazolecarboxamide formyltransferase;IMP cyclohydrolase	ATIC	3.23	0.0625
Voltage-dependent anion-selective channel protein 1	VDAC1	3.30	0.0216
Cytochrome c	CYCS	3.31	0.0561
Kynureninase	KYNU	3.40	0.1008
Annexin A4;Annexin	ANXA4	3.52	0.0438
Prothymosin alpha;Prothymosin alpha, N-terminally processed;Thymosin alpha-1	PTMA	3.57	0.1012
Phosphoglycerate kinase 1	PGK1	3.58	0.0731
14-3-3 protein beta/alpha;14-3-3 protein beta/alpha, N-terminally processed	***YWHAB***	***3.70***	***0.0005***
14-3-3 protein zeta/delta	***YWHAZ***	***5.97***	***0.0018***
14-3-3 protein theta	***YWHAQ***	***7.72***	***0.0002***

6.2 Listings of all proteins identified via mass spectrometry analysis of pull down assay

Table 41: List of proteins identified as significantly upregulated during pull down assay.

The listed proteins have been identified as significantly upregulated in a pull-down assay performed with rPlaD as bait and cell lysates from A549 human lung type II epithelial cells as prey. The list is sorted by increasing fold changes.

Protein name	Gene name	Fold change	P-value
14-3-3 protein beta/alpha;14-3-3 protein beta/alpha, N-terminally processed	YWHAB	156.8	0.0326
14-3-3 protein sigma	SFN	426.9	0.0004
14-3-3 protein theta	YWHAQ	645.5	0.0004
14-3-3 protein epsilon	YWHAE	652.1	0.0002
14-3-3 protein zeta/delta	YWHAZ	687.1	0.0000
14-3-3 protein gamma;14-3-3 protein gamma, N-terminally processed	YWHAG	2225.5	0.0000

Acknowledgments (German) / Danksagung

Bei Frau Prof. Dr. Antje Flieger möchte ich mich für die Bereitstellung des spannenden Themas und die gute Betreuung, sowie viele fachliche und persönliche Gespräche bedanken. Besonders für die Möglichkeit meine eigenen Ideen in die Arbeit einbringen zu können bin ich sehr dankbar.

Bei Frau Dr. Christina Lang bedanke ich mich ebenfalls für die gute Betreuung und dafür, dass ich zu jeder Zeit mit jeglichen Fragen zu ihr kommen konnte. Außerdem bin ich froh, dass sie sowohl für berufliche als auch private Dinge immer ein offenes Ohr und Unterstützung angeboten hat.

Wiebke Michel danke ich für eine tolle gemeinsame Doktorarbeitszeit als Büro- und Laborkolleginnen. Besonders über die gegenseitige Unterstützung im Laboralltag bin ich sehr froh. Außerdem werde ich viele gemeinsame Dienstreisen in guter Erinnerung behalten.

Bei unseren TAs Simone Dumschat, Susanne Karste, Ute Strutz und Christian Galisch möchte ich mich für die Organisation des Laboralltags und die Kultivierung der Zellkulturen bedanken. Außerdem bin ich sehr froh, bei Bedarf, immer unterstützt worden zu sein.

Erika Kleindienst danke ich für die Unterstützung bei und Übernahme von vielen organisatorischen Angelegenheiten.

Außerdem bedanke ich mich bei allen aktuellen und ehemaligen Kolleginnen und Kollegen aus Wernigerode für ihre Unterstützung und eine immer angenehme Arbeitsatmosphäre.

Bei Herrn Dr. Jörg Döllinger bedanke ich mich für die Durchführung aller in dieser Arbeit gezeigten Massenspektrometrie Analysen.

Bei Maurice Diwo und Herrn Prof. Dr. Wulf Blankenfeldt bedanke ich mich für die Kristallisation von PlaA und die zahlreichen Versuche PlaD zu kristallisieren. Bei Maurice Diwo bedanke ich mich zusätzlich für die Erstellung der in dieser Arbeit gezeigten Topologie-Diagramme.

Abschließend möchte ich mich bei meiner Familie und meinen Freunden bedanken, da sie mich gefördert und unterstützt haben und auch für stressige Phasen viel Verständnis hatten.